THE ROLE OF THE P2X7 RECEPTOR IN AUTOIMMUNE GLOMERULONEPHRITIS AND VASCULITIS

A thesis submitted to Imperial College London in candidature for the degree of Doctor of Philosophy by

Maria Prendecki

May 2018

Renal and Vascular Inflammation Section
Department of Medicine
Imperial College London
Commonwealth Building
Hammersmith Hospital
Du Cane Road
LONDON W12 0NN

Abstract

P2X7, an ionotropic receptor for extracellular ATP is expressed on immune cells including macrophages, dendritic cells and lymphocytes and is up-regulated on non-immune cells following injury. P2X7 is important in many biological processes including production of pro-inflammatory cytokines and both cell proliferation and death. Previous work by our laboratory and others has identified a potential role for P2X7 in the pathogenesis of glomerulonephritis (GN). However, studies of auto-immunity have generated conflicting results and existing lines of P2X7 knockout (KO) mice are incomplete with persistent splice variants. The aims of my project were to determine a role for P2X7 in the pathogenesis of GN and vasculitis and to investigate its importance at a cellular level in inflammatory responses of neutrophils and monocytes.

My project includes the first description of a novel P2X7 knockout rat showing that it is a true knockout with no functional P2X7 protein expressed. Using bone marrow derived cells from the knockout rat I show that different cell types have a differential requirement for P2X7 to cleave active IL-1β, with dendritic cells but not macrophages able to cleave IL-1β via an ATP/P2X7 independent pathway in response to stimulation with LPS alone. I have also investigated the effect of P2X7 KO on 3 different experimental models of glomerulonephritis and vasculitis and show that P2X7 KO rats are not protected from disease severity or the generation of autoimmunity. I next used a small molecule P2X7 antagonist in one of these models, nephrotoxic nephritis, showing that it protected both wild type and P2X7 KO rats from disease, suggesting it may be mediating its actions via off target effects.

I also investigated the potential role for P2X7 in human anti-neutrophil cytoplasm antibody (ANCA) associated vasculitis (AAV). I show that human neutrophils express functional P2X7 on the cell surface; this is a particularly interesting finding as this is a controversial area with previously conflicting results. P2X7 is up-regulated on neutrophils and peripheral blood mononuclear cells (PBMC) in patients with active AAV compared to patients in remission or healthy controls. Neutrophils and PBMC can produce IL-1β in response to stimulation with MPO-

ANCA IgG and ATP. In patients with active AAV, P2X7 mRNA is present on infiltrating leucocytes in the glomeruli and interstitium in renal biopsy tissue.

My data suggest that P2X7 is not a critical pathway in mediating glomerulonephritis and it is likely that the antagonist is acting via one or more off target effects. Further understanding of these mechanisms may lead to the identification of novel therapeutic targets and increase our understanding of the pathogenesis of glomerulonephritis and vasculitis.

Declaration of Originality

I, Maria Prendecki confirm that the work described in this thesis is my own. All experiments and data presented were performed by me unless otherwise stated.

Copyright Declaration

Acknowledgements

I am grateful to the UK Medical Research Council for awarding me the Clinical Research Training Fellowship which enabled me to undertake this project.

I would like to thank all of my colleagues in the renal lab who are too numerous to name but who have all provided endless help, support and friendship during my PhD. In particular, I would like to thank Steve McAdoo and Tabitha Turner-Stokes for their assistance with my *in vivo* work; Shenny Tempest-Roe for her expertise in P2X7; Fayaz Dudhyia, Anisha Tanna and Lina Nikolopoulou for their assistance with collecting clinical samples and data; Damilola Pinheiro for her advice on my cell culture work and her flow cytometry skills; Bynvant Sandhu for discussions of my work and late night company working in the lab; Gurjeet Bhangal for getting me started in the lab many years ago and Neil Galloway-Phillips for his endless patience with my many urgent ordering requests. I would like to thank Kevin Woollard who allowed me to conduct my *in vivo* work under his project license; Ana Garcia-Diaz for her role in the creation of the P2X7 KO rat and all the staff in CBS, particularly Jo, Phil and David for their help with my *in vivo* studies and the breeding colony.

Finally I would like to thank my supervisors, Fred Tam, Charles Pusey and Robert Unwin for giving me the opportunity to work on this project and their guidance throughout.

Table of Contents

List of Figures

List of Tables

List of Abbreviations

2MeSATP	methylthio adenosine triphosphate
4PL	4 parameter logistic
α3(IV)NC1	non-collagenous (NC1) domain of the alpha-3 chain of type IV collagen
AAV	ANCA associated vasculitis
ADAM17	disintegrin and metalloproteinase domain-containing protein 17
ADP	adenosine diphosphate
Ala	alanine
ALP	alkaline phosphatase
AMP	adenosine monophosphate
ANCA	anti-neutrophil cytoplasm antibody
ANO6	anoctamin 6
ANOVA	analysis of variance
APRIL	a proliferation inducing ligand
ASC	apoptosis-associated speck like protein
Asp	aspartic acid
ATG	anti-thymocyte globulin
ATP	adenosine 5' triphosphate
BBG	brilliant blue G
BCA	bicinchoninic acid
BCIP-NBT	5-bromo-4-chloro-3-indolyl phosphate/nitro blue tetrazolium
BLyS	B lymphocyte stimulator
BMDC	bone marrow derived dendritic cell
BMDM	bone marrow derived macrophage
BSA	bovine serum albumin
BzATP	2,3-O-(4-benzoylbenzoyl)-ATP
C.Elegans	Caenorhabditis elegans
CARD	C terminal caspase activation and recruitment domain
CD62L	L-selectin
CFA	complete Freund's adjuvant
CKD	Chronic kidney disease
CLL	chronic lymphocytic leukaemia
Cmax	maximal concentration

COX	cyclooxygenase
CT	computed tomography
DAB	3,3’-diaminobenzidine
DAPI	4',6-diamidino-2-phenylindole
DC	dendritic cell
DMEM	Dulbecco's modified Eagle medium
DMSO	dimethyl sulphoxide
DNA	deoxyribonucleic acid
DNase	deoxyribonuclease
DPPI	dipeptidyl peptidase I
dsDNA	double stranded deoxyribonucleic acid
DTH	delayed type hypersensitivity
EAE	experimental autoimmune encephalomyelitis
EAG	experimental autoimmune glomerulonephritis
EAV	experimental autoimmune vasculitis
ECL	enhanced chemiluminescence
ED50	half maximal effective dose
EGPA	eosinophilic GPA
ELISA	enzyme linked immunosorbent assay
ELISpot	enzyme linked immunosorbent spot assay
ENT	ear nose and throat
ERK	extracellular signal regulated kinases
ESRD	end stage renal disease
EULAR	European league against rheumatism
FADD	fas-associated protein with death domain
Fc	fragment, crystallisable
FcR	Fc receptor
FCS	foetal calf serum
FimH	type 1 fimbrin D-mannose specific adhesin
FITC	fluorescein isothiocyanate
FSC	forward scatter
GAPDH	Glyceraldehyde 3-phosphate dehydrogenase
GBM	glomerular basement membrane
GCS	glomerular cross sectional
Gly	glycine

GM-CSF	granulocyte macrophage colony stimulating factor
GN	glomerulonephritis
GPA	granulomatosis with polyangitis
GPCR	G protein coupled receptor
GSK	GlaxoSmithKline
GWAS	genome wide association study
H+E	haematoxylin and eosin
HBSS	Hank's balanced salt solution
HEK	human embryonic kidney
HEPES	4-(2-hydroxyethyl)-1-piperazineethanesulfonic acid
HLA	human leukocyte antigen
HMGB-1	high mobility group box 1
HRP	horse-radish peroxidase
Hsc	heat shock cognate protein
Hsp	heat shock protein
IC50	half maximal inhibitory concentration
ICAM	intracellular adhesion molecule
ICE	IL-1β converting enzyme
IHC	immunohistochemistry
IL-	interleukin
IL1Ra	IL-1 receptor antagonist
INF-γ	interferon γ
IP	intraperitoneal
IQR	interquartile range
KO	knockout
lacZ	β-galactosidase
LAMP-2	lysosome-associated membrane protein-2
LDH	lactate dehydrogenase
LPS	lipopolysaccharide
LRR	leucine rich repeat
MAGUK	membrane-associated guanylate kinases
MAPK	mitogen activated protein kinase
MCP-1	monocyte chemotactic protein-1
MCSF	macrophage colony stimulating factor
MFI	median fluorescence intensity

MHC	major histocompatibility complex
MMF	mycophenolate mofetil
MOG	myelin oligodendrocyte glycoprotein
MOPS	3-(N-morpholino)propanesulfonic acid
MPA	microscopic polyangiitis
MPO	myeloperoxidase
mRNA	messenger RNA
MTT	3-[4,5-dimethylthiazol-2-yl]-2,5 diphenyl tetrazolium bromide
MyD88	myeloid differentiation primary-response protein 88
NACHT	NAIP (neuronal apoptosis inhibitor protein), C2TA (MHC class 2 transcription activator), HET-E (heterokaryon incompatibility) and TP1 (telomerase-associated protein 1)
NAD	nicotinamide adenine dinucleotide
NC1	non-collagenous domain
NET	neutrophil extracellular trap
NFκB	nuclear factor kappa-light-chain-enhancer of activated B cells
NHS	national health service
NK	natural killer
NLRP3	NACHT, LRR and PYD domains containing protein 3
NMDG	N-methyl-D-glutamine
NO	nitric oxide
NOD	non-obese diabetic
NP40	nonidet P40
NTN	nephrotoxic nephritis
NTS	nephrotoxic serum
oATP	oxidised ATP
OCT	optimal cutting temperature
OD	optical density
OVA	ovalbumin
PAGE	polyacrylamide gel electrophoresis
PAS	periodic acid Schiff
PBMC	peripheral blood mononuclear cell
PBS	phosphate buffered saline
PCR	polymerase chain reaction
PGK1	phosphoglycerate kinase 1

PI4K	phosphatidylinositol 4-kinase
PK	pharmacokinetic
PMSF	phenylmethylsulfonyl fluoride
PPADS	pyridoxal-phosphate-6-azophenyl-2',4'-disulfonate
PPIB	peptidyl-prolyl cis-trans isomerase B
PR3	proteinase-3
PS	phosphatidylserine
PYD	pyrin domain
RIPK	receptor-interacting serine/threonine-protein kinase
RNA	ribonucleic acid
RNase	ribonuclease
RNASeq	RNA sequencing
ROS	reactive oxygen species
RPGN	rapidly progressive glomerulonephritis
RPLP0	60S acidic ribosomal protein P0
rpm	revolutions per minute
RPMI	Roswell Park Memorial Institute
RPTPβ	receptor protein tyrosine phosphatase β
RT-qPCR	quantitative reverse transcription PCR
SAR	structure activity relationship
SCID	severe combined immunodeficiency
SDS	sodium dodecyl sulfate
SEM	standard error of mean
siRNA	silencing RNA
SNP	single nucleotide polymorphism
SSC	side scatter
STZ	streptozocin
Syk	spleen tyrosine kinase
Syk	spleen tyrosine kinase
t1/2	halflife
TAE	tris, acetic acid, EDTA
TBS	tris buffered saline
TLR	toll like receptor
TM	transmembrane
TMB	3,3',5,5'-tetramethylbenzidine

TNFR1	tumour necrosis factor receptor 1
TNF-α	tumour necrosis factor α
TRF	TIR-domain-containing adapter-inducing interferon-β
uPCR	urine protein:creatinine ratio
VCAM	vascular cell adhesion molecule
VEGF	vascular endothelial growth factor
WKY	wistar kyoto
WT	wild type
ZFN	zinc finger nuclease

Presentations arising from this work

P2X7 expression on human neutrophils and PBMC in ANCA associated vasculitis.

M Prendecki, S McAdoo, T Bhatt, F Dudhiya, CD Pusey, FWK Tam.

Oral presentation in the young investigator award session at the Renal Association annual conference. June 2018

P2X7 is expressed on human neutrophils and PBMC and is upregulated in patients with ANCA associated vasculitis

M Prendecki, S McAdoo, T Bhatt, F Dudhiya, CD Pusey, FWK Tam.

Oral presentation at the RSM Presidents prize day 2017

Chapter One: Introduction and Background

Anti neutrophil cytoplasm antibody (ANCA) associated vasculitis (AAV) and anti-glomerular basement membrane (GBM) disease are important causes of rapidly progressive glomerulonephritis and of disease in other organs, including life-threatening lung haemorrhage. Current treatments remain non-specific and are based on broad immunosuppression with toxic side effects, there is an unmet need for better targeted and safer therapies.

P2X7, an ionotropic receptor for extracellular ATP is expressed on immune cells including macrophages, dendritic cells and lymphocytes and is up-regulated on non-immune cells following injury. P2X7 is important in many biological processes including production of pro-inflammatory cytokines and both cell proliferation and death. P2X7 may have a role in the pathogenesis of glomerulonephritis and autoimmunity but this is not clearly defined.

In this introduction I aim to summarise current understanding of P2X7 structure and function as is relevant to this project. I review current understanding of the animal models used in the project; nephrotoxic nephritis (NTN), experimental autoimmune glomerulonephritis (EAG) and experimental autoimmune vasculitis (EAV); and the human diseases they mirror: AAV and anti-GBM disease.

1.1 Purinergic signalling and receptors

1.1.1 History and classification of purinergic signalling

Purine nucleotides and nucleosides were first reported to play a role in extracellular signalling nearly a century ago when Drury and Szent-Gyorgyi reported the effects of adenosine and adenosine monophosphate (AMP) on mammalian heart.[1] By 1970 Burnstock had identified adenosine triphosphate (ATP) to be the non-adrenergic, non-cholinergic neurotransmitter released from inhibitory neurones in mammalian gut.[2] He then went on to summarise the mechanisms of

purinergic nerve signalling including synthesis, storage, release and inactivation of ATP.[3] In 1978, purinergic receptors were classified as P1 which are preferentially activated by adenosine and AMP, and P2 which are activated by ATP or adenosine diphosphate (ADP). In addition to differential agonist sensitivity, P1 but not P2 receptors were antagonised by methylxanthines.[4] P2 receptors were then further divided into P2X and P2Y receptors on the basis of their pharmacology, with differing responses to ATP analogues and antagonists.[5] Identification of further P2 receptor subtypes followed, including P2T a receptor on platelets selective for ADP, P2U which is sensitive to both pyrimidines and purines, and P2Z which is present on macrophages.[6] A wide range of organ systems and cell types were identified as responsive to extracellular ATP including neurotransmission, vascular and visceral smooth muscle, platelets, neutrophils, macrophages, mast cells and endothelial cells.[7] P2Y, P2U and P2T receptors were shown to signal via G protein coupled receptors (GPCR) and P2X receptors via ligand gated ion channels. Initially P2Z and its signalling mechanism were less well understood.[8] Following cloning of both P1 and P2 receptors in the early 1990s, P2 receptors were classified according to their molecular structure and signalling mechanism. The P2 receptors which were G protein coupled such as P2U and P2T were reclassified as P2Y receptors.[9] P2Z has subsequently been identified as P2X7.[10]

Currently there are four P1 receptor subtypes, seven P2X receptors and eight P2Y receptors. The eight P2Y receptors are termed P2Y1, P2Y2, P2Y4, P2Y6, P2Y11, P2Y12, P2Y13 and P2Y14 and the P2X receptor subtypes are named 1-7. Non-neuronal cellular expression of purinergic receptors is summarised in table 1.

	P2Y 1	P2Y 2	P2Y 4	P2Y 6	P2Y 11	P2Y 12	P2Y 13	P2Y 14	P2X 1	P2X 2	P2X 3	P2X 4	P2X 5	P2X 6	P2X 7
Smooth Muscle	X	X							X	X		X			X
Cardiac Muscle		X							X	X	X	X	X	X	X
Skeletal Muscle	X	X	X	X					X	X	X	X	X	X	
Osteoblasts	X	X													X
Cartilage	X	X								X					
Keratinocytes	X	X	X							X	X		X		
Fibroblasts	X	X													X
Adipocytes	X	X	X						X						
Epithelial Cells	X	X		X	X							X	X	X	X
Hepatocytes	X	X	X	X	X	X	X								
Glial cells	X	X	X	X	X	X	X	X	X	X	X	X	X	X	X
Sperm		X								X					X
Endothelial cells	X	X	X	X					X						
Erythrocytes	X									X		X			X
Platelets	X					X			X						
Immune cells	X	X							X			X			X
Exocrine cells	X	X	X						X			X			X
Endocrine cells		X	X						X	X	X	X	X	X	X
Inner Ear		X	X						X	X	X				X
Eye		X								X					X
Tongue	X									X	X				
Olfactory organ	X	X								X		X			

Table 1.1 Cellular expression of P2 receptors Adapted from, G Burnstock. Purinergic signalling: Its unpopular beginning, its acceptance and its exciting future. BioEssays 2012; 34:218-225[11]

1.1.2 P2X receptors

P2X receptors (P2XR) are non selective cation channels which activate rapidly in response to extracellular ATP. The cDNA for the first P2X receptor subunit, P2X1 was identified in 1994 by injecting xenopus oocytes with a cDNA library isolated from rat vas deferens. P2X2 was identified the same year using similar techniques and the others were soon identified using homology based approaches.[12-14] The seven genes encoding the seven P2X receptor subunits vary significantly in length but all consist of 11-13 exons and share a common structure. P2X4 and P2X7 are adjacent in human (chromosome 12) and mouse (chromosome 5) genomes, which may be a result of gene duplication. P2X1 and P2X5 are also located close together on chromosome 13. P2X2, P2X3 and P2X6 are all located on different chromosomes[14]

All P2X receptor subunits share the same structure with two hydrophobic transmembrane domains, intracellular N and C termini and the bulk of the protein is made up from a large, heavily glycosylated ectodomain (Figure 1). There is 30-50% peptide sequence homology between the subunits with the C terminus representing the most heterologous region. P2X4 has the most sequence homology with the other subunits and P2X7 the least.[14] All subunits have 10 conserved cysteine residues, which form a series of disulphide bonds within the extracellular portion.[15] Functional P2X receptor proteins consist of trimers with three ATP binding sites; this has been shown by several techniques including gel electrophoresis, the use of reporter mutations and by single channel kinetics corresponding to binding of 3 ATP molecules.[16-19] A major breakthrough in confirming earlier work on P2X receptor structure was the crystallisation of zebrafish P2X4 receptor in 2009.[20] The crystal structure confirmed that P2X receptors exist as trimers and suggested a potential ATP binding site in the groove between subunits in the extracellular domain in keeping with previous mutagenesis studies.[20 21]

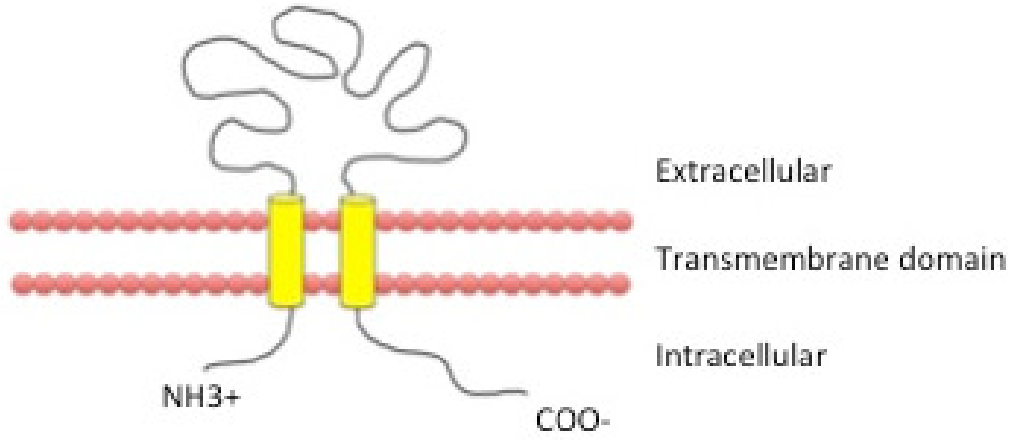

Figure 1.1 Schematic representation of the structure of P2X receptor subunits
Schematic representation of the common P2X receptor membrane topology with 2 transmembrane domains separated by a long extracellular loop and intracellular N and C termini.

All of the P2X receptor subunits, with the exception of P2X6 can assemble to form homotrimers.[22] [23] Subunits have also been shown to form heterotrimers; in co-immunoprecipitation studies by Torres all the subunits except for P2X7 were able to assemble as heterotrimers, in addition P2X4 did not oligomerise with P2X1, P2X2 or P2X3 and P2X3 would not oligomerise with P2X6.[22] Heterotrimers have also been shown to exist using other techniques including chemical cross-linking, native PAGE electrophoresis and functional co-expression studies.[17] [24-26] Despite initial evidence that P2X7 could form homotrimers only, it has subsequently been shown to co-immunoprecipitate with P2X4 from both transfected HEK293 cells and murine bone marrow derived macrophages (BMDM).[27] [28] Functional assays using acinar cells also suggested that P2X4 and P2X7 subunits exist as heterotrimers.[29] However other studies have shown that P2X7 and P2X4 preferentially oligomerise as homotrimers in several different cell types and that interactions may be due to close associations of homotrimers rather than the formation of heterotrimers. [30-32] There is evidence that P2X4 can have a regulatory effect on P2X7 function, Kawano et al. have shown

that in mouse bone marrow derived dendritic cells (BMDC) and in the mouse macrophage cell line RAW246.7, P2X4 may enhance P2X7 dependent cytokine release thus having a pro-inflammatory effect.[33 34]

1.2 P2X7 receptor

The previously named P2Z receptor, which was responsible for ATP dependent lysis of macrophages was shown to be the 7th member of the P2X receptor family using cDNA isolated from rat brain.[10] Human and mouse cDNA were subsequently cloned from monocyte and microglial cells. P2X7 has several features which make it distinct from other P2XR subtypes, it is relatively insensitive to ATP requiring mM rather than μM concentrations for activation and it is the only P2XR which is more sensitive to synthetic 2,3-O-(4-benzoylbenzoyl)-ATP (BzATP) than ATP.[35] P2X7 has an additional 200 amino acids at the C terminus and is characterised by two states of activation; brief agonist exposure leads to rapid opening of the nonselective cation channel and more prolonged agonist exposure leads to pore formation and the passage of large cations such as N-methyl-D-glutamine (NMDG) and high molecular weight dyes such as Yo-Pro-1.

1.2.1 P2X7 tissue expression

P2X7 was originally thought to mainly be expressed on immune cells, however, its more ubiquitous expression has become apparent in recent years. In human haematopoietic cells expression is highest on macrophages but it is also present on dendritic cells, monocytes, natural killer (NK) cells, B lymphocytes, T lymphocytes and erythrocytes in descending order. Mast cells and eosinophils also express P2X7.[36 37] The expression of functional P2X7 on neutrophils is a controversial area. Neutrophils have been shown to be a source of IL-1β in some models of

inflammatory arthritis but there is conflicting evidence as to whether cleavage of IL-1β to its active form is caspase-1 and inflammasome dependent or not. Some studies suggest a role for neutrophil proteases in the cleavage of IL-1β to its bioactive form.[38-40] Some groups have not detected P2X7 mRNA or protein in human neutrophils or in HL-60 promyelocytic leukaemia cell line differentiated into neutrophils and one report found evidence of non-functional cytosolic receptors but no cell surface receptor.[36 41 42] However others have both detected mRNA and shown cell surface P2X7 to be present with characteristic membrane potentials and passage of Yo-Pro-1 in response to extracellular BzATP.[43] Human and murine neutrophils have also been shown to secrete IL-1β in response to ATP in a P2X7 dependent manner. In this study there was considerable variation between donors with differing P2X7 dependent calcium flux and P2X7 antagonist sensitivity, which seemed to be independent of ethnicity. This suggests there may be variation in P2X7 neutrophil cell surface expression or differing P2X7 polymorphisms between individuals.[44]

P2X7 is detected at low levels in the kidney but has been shown to be upregulated in rat models of renal injury.[45 46] In cultured mesangial cells P2X7 mRNA expression was increased in response to TNFα.[47] P2X7 is present on osteoblasts and osteoclasts and plays a role in bone mineralisation and mechanotransduction, one study using P2X7 deficient mice showed decreased bone mineral content, however other studies using rat osteoblasts have shown conflicting results.[48-50] P2X7 is expressed on microglia and Schwann cells within the central nervous system although the expression of receptors on neurones is another controversial area with conflicting results.[51 52] P2X7 protein was detected in brain from both of the available P2X7 deficient mouse strains using immunoprecipitation and immunohistochemistry techniques, leading Sim et al to conclude that antibodies were recognising a P2X7 like protein.[51] However more recent studies using PCR have raised the possibility that this represents the presence of P2X7 splice variants.[53] P2X7 is also expressed on epithelial cells including from renal, skin and exocrine gland tissue. The physiological role of P2X7 on endothelium is yet to be fully understood.[54]

1.2.2 P2X7 pore formation

One of the defining characteristics of P2X7 activation is the formation of non-selective pores permeable to large molecules of up 900 Daltons following the prolonged application of ATP. Initially it was thought that the P2X7 channel itself dilated to form pores.[55] More recently, studies have shown that either by using low concentrations of inhibitor or by using mutagenesis it was possible to block P2X7 ion channel activation independently of pore formation.[56 57] This suggests the mechanism of pore formation is by activation of P2X7 causing opening of a distinct accessory protein; this interacting protein is likely to be pannexin 1, a hemichannel protein.[58] Prior to the identification of P2X7, early studies suggested that connexin hemichannels themselves were the P2Z receptor.[59] However this was disproven as in P2X7 negative cells which endogenously expressed or over-expressed connexin, stimulation with ATP did not lead to dye uptake.[60] Pannexin-1 has ubiquitous tissue expression and is responsible for ATP efflux in a variety of cell types.[61] When pannexin-1 was overexpressed in P2X7 expressing HEK293 cells, pannexin-1 localised to the cell membrane and could be co-immunoprecipitated with P2X7.[58] When pannexin-1 was inhibited using siRNA or a panexin-1 inhibitory peptide, ethidium bromide dye uptake was inhibited in both HEK293 and THP-1 cells. Overexpression of pannexin-1 in P2X7 negative cells resulted in constitutive dye uptake whereas overexpression in P2X7 positive cells resulted in no constitutive dye uptake but exaggerated uptake in response to ATP stimulation, suggesting that unstimulated P2X7 has a negative regulatory effect on pannexin-1.[58]

In contrast to these results other studies have not proven a role for pannexin 1 in P2X7 pore formation. Use of pannexin-1 siRNA in mouse macrophages did not affect dye uptake in response to ATP in one study and BMDM from pannexin-1 deficient mice had normal uptake of Yo-Pro-1 dye after stimulation in another. [62 63] Another possible candidate protein is anoctamin 6 (ANO6), a calcium dependent phospholipid scramblase and calcium activated non-selective cation channel. Use of ANO6 inhibitors or ANO6 siRNA in xenopous oocytes or HEK293 cells expressing P2X7

resulted in blockage of P2X7 pore currents. Yo-pro-1 uptake in response to ATP was inhibited by ANO6 inhibitors in both HEK293 and THP-1 cells.[64] It may be that these different results are due to P2X7 being able to associate with different pore forming proteins dependent on cell and species specificity.

1.2.3 P2X7 channel and signalling

Brief exposure of P2X7 to agonist causes opening of a non-selective cation channel which is permeable to monovalent and divalent cations leading to Ca^{2+} and Na^{+} influx and K^{+} efflux from the cell. There is subsequent cell membrane depolarisation and downstream calcium signalling. Mutagenesis studies on P2X2 have provided information regarding the structure function relationship of P2X receptors and have shown that the second transmembrane domain (TM2) forms the channel pore and the external half of TM2 is a channel gating domain.[65] The channel has unexpectedly high Ca^{2+} permeability (when compared to other ligand gated ion channels such as acetylcholine or glutamate gated channels), likely due to a selectivity filter involving the transmembrane domains.[66] Downstream signalling from activation of P2X7 is then coupled to several signalling cascades including, release of IL-1β, activation of other signalling cascades including MAPK, plasma membrane blebbing and cytoskeletal rearrangement, lymphoid cell proliferation, phosphatidylserine (PS) exposure, and apoptosis or necrosis.

1.2.4 Plasma membrane blebbing and cytoskeleton rearrangement

P2X7 has been shown to interact with cytoskeleton components. P2X7 expressed in HEK293 cells co-immunoprecipitates with 11 other proteins as a receptor-protein complex, including structural proteins (laminin α3; transmembrane, integrin β2 subunit, β-actin, α-actinin 4, supervillin, Hsp90,

Hsp70, Hsc71, MAGuK) and signalling proteins (PI4K and RPTPβ).[67] When HEK293 cells are stimulated with extracellular ATP there is rapid formation of membrane blebs which increase in number and begin to coalesce by 1-2 minutes.[55] This same process has been shown to occur in cells with endogenous P2X7 expression such as dendritic cells and macrophages.[68-70] In murine macrophages membrane blebbing was shown to be dependent on reorganisation of the actin cytoskeleton, incubation of cells with cytochalasin C which inhibits actin polymerisation decreases P2X7 induced membrane blebbing independently of other P2X7 functions.[68] Membrane blebbing has been shown to be dependent on the intracellular C terminus of P2X7 interacting with epithelia membrane proteins. [71] The significance of P2X7 induced blebbing is yet to be fully understood, however blebbing is known to have several roles in physiological processes including apoptosis, mitosis, cell movement and cell spreading.[72]

1.2.5 CD62L shedding

L-selectin, also known as CD62L is a C type lectin involved in leukocyte adhesion and rolling on endothelial cells. It is widely expressed on leukocytes including lymphocytes, monocytes, neutrophils, eosinophils and progenitor cells, with highest expression being on leukocytes.[73] Activation of P2X7 on human CD4+ and CD8+ T cells by extracellular ATP leads to rapid shedding of CD62L within seconds. The exact mechanism for this shedding is unknown although it may well be mediated by a metalloproteinase such as ADAM17. Mouse T cells also shed CD62L in response to stimulation of P2X7 with ATP and this is accompanied by PS exposure.[74] [75] Cells lacking in CD62L show impaired migration to lymph nodes and thus activation of P2X7 may promote homing of T cells to non-lymphoid sites.[75]

1.2.6 Phosphatidylserine exposure

PS is an aminophospholipid normally present on the inner leaflet of the plasma cell membrane, its translocation is regulated by enzymes including flippases, floppases and scramblases and its position on the inner leaflet is maintained by aminophospholipid translocase. [76 77] Translocation of PS and its exposure on the outer leaflet of the cell membrane is recognised by PS receptors on macrophages and other phagocytes and leads to clearance of apoptotic cells.[78] In HEK293 cells transfected with P2X7, activation of P2X7 by extracellular ATP has been shown to induce PS translocation. Prolonged activation (greater than a few minutes) led to irreversible PS exposure and cell death however brief stimulation led to reversible PS flip and microvesicle shedding independent of cell death.[79] Transient PS exposure may have a physiological role independent of cell death pathways and has previously been shown to have a role in skeletal muscle differentiation and neutrophil chemotaxis. [80 81] Elliott et al showed that in mouse T cells P2X7 dependent PS exposure has a role in physiological transduction mechanisms. PS translocation resulted in altered adhesion molecule expression, reduction in CD45 transmembrane tyrosine phosphatase and decreased P-glycoprotein activity.[75] In some cell types PS exposure has been shown to be dependent on Ca^{2+} influx into the cell.[82] In erythrocytes and mouse thymocytes PS exposure can occur independently of extracellular calcium and is dependent on Na^{+} influx. Na^{+} and Ca^{2+} may both be activating a phospholipid transporter and inhibiting aminophospholipid translocase directly. However an alternative theory postulated by Courageat et al is that Na^{+} influx may lead to depletion of intracellular ATP via the Na/K pump removing Na^{+} from cells. This ATP depletion in turn causes inhibition of aminophospholipid translocase.[82 83]

1.2.7 P2X7 and cell death

Stimulation of cells by extracellular ATP can result in activation of cell death pathways. In thymocytes stimulation with extracellular ATP results in a rise in intracellular Ca^{2+}, cell blebbing and classical features of apoptosis including cytoplasmic condensation and nuclear segmentation. This has been shown to be mediated by a mechanism independent of large pore formation as the use of perforin, which causes large, non-selective pores resulted in cell death but not apoptosis.[84] Apoptotic cell death has been shown to occur in response to extracellular ATP in many other cell types including macrophages, dendritic cells, T cells and microglia.[85-87] In human monocyte derived macrophages, this mechanism of cell death was shown to have the additional benefit of killing the intracellular organism, Bacillus Calmette-Guérin, whereas other cell death mechanisms left it intact.[85]

P2X7 dependent cell death has also been shown to occur via necrosis; in mouse microglia, cell death occurred both by caspase dependent apoptosis and by caspase independent necrosis.[86] Cultured rat mesangial cells also displayed features of both apoptosis and necrosis in response to extracellular ATP.[88] It is likely that both necrosis and apoptosis can occur in response to P2X7 stimulation, however the issue is clouded by the fact that markers may be shared between the two pathways, for example release of LDH and HMGB-1.[89] Cell volume changes have been thought to be a more reliable way to differentiate between apoptosis and necrosis; with cell swelling due to uptake of osmolytes indicating necrosis and cell shrinking indicating apoptosis. However both cell shrinking and swelling have been reported to be associated with P2X7 dependent cell death.[86] Taylor et al demonstrated that murine lymphocytes, in response to stimulation with extracellular ATP, underwent initial cell shrinkage and PS translocation, followed within minutes by cell swelling, lysis and collapse of the remnant cell body. They suggest that cell death via P2X7 stimulation results from a novel pathway of mixed apoptosis/necrosis.[89]

Caspases were first postulated to play a role in cell death when CED-3, the gene product responsible for cell death in *C.Elegans* was identified and found to be related to caspase-1.[90] All caspases are pro-enzymes and require cleavage for activation. Caspases participate in mediating cell death via several mechanisms including: inactivating proteins that protect cells from apoptosis, destroying cell structures, and cleaving proteins which are involved in cytoskeletal regulation.[91-93] Caspase -3,-6,-7,-2,-8,-9,-10 have been shown to play a role in apoptosis whereas caspase -1,-4,-5,-11 and -12 (caspase-11 is only present in rodents and caspase -4 and -5 are its human counterparts) are termed inflammatory caspases.[94] Caspase-1 and 4/5/11 have been shown to have a role in cell death via pyroptosis- a form of programmed necrosis. In keeping with the finding that both apoptosis and necrosis can occur in response to P2X7 activation by ATP, caspases from both the 'apoptosis' and 'inflammatory' groups have been implicated in cell death mechanisms. In one study of mouse BMDM, ATP stimulation resulted in cell death and an up-regulation of caspase 3/7. This was independent of caspase-1 and a pan caspase inhibitor did not completely abolish cell death.[95] Other studies have also shown that P2X7 mediated cell death occurs by both caspase-1 dependent and independent mechanisms.[96-98]

1.2.8 Cell proliferation

Although P2X7 has classically been associated with cell death via apoptosis and necrosis, in some cell types such as T lymphocytes and microglia it has also been associated with cell proliferation. One study has shown that T cell receptor stimulation leads to autocrine release of ATP, activation of P2X7 and secretion of IL-2, the T cell growth factor.[99] The same was true when T cells were stimulated by hypertonic stress and the stimulatory effects were downregulated by use of apyrase or P2 receptor antagonists.[100] Activation of P2X7 has been shown to be able to trigger signalling via MAPK/ERK pathways. MAPK are a highly conserved family of serine/threonine protein kinases and activation can induce cell growth and proliferation via de novo synthesis of pyrimidine

nucleotides in the nucleus.[101 102] In keeping with a role for P2X7 in cell proliferation, increased P2X7 expression has been shown in several tumours such as chronic lymphocytic leukaemia (CLL), skin or prostate cancer.[103-105]

1.2.9 IL-1β release

IL-1 (IL-1α and IL-1β) is a major mediator of inflammation and has been shown to cause accumulation of arachidonic acid metabolites, up-regulate nitric oxide production (NO), increase adhesion molecule expression on endothelial cells, enhance extravasation of leukocytes and induce fever. It also causes bone resorption via activation of osteoclasts. [106] IL-1α and IL-1β are members of the IL-1 superfamily and in keeping with other members of the group have low sequence similarity but high structural homology. In response to signalling via TLR stimulation and the NFκB transcription factor, IL-1α and IL-1β are translated and accumulate in the cytoplasm as 31kDa secretory proteins.[107] IL-1α is active in this form but IL-1β requires proteolytic cleavage to its 17.5 kDa active form.[106] In the extracellular compartment IL-1β can be cleaved by several proteases but intracellular processing is mediated by the IL-1β converting enzyme (ICE). [108] ICE was identified to be a cysteine protease which functioned as a heterodimer with two subunits, p10 and p20 which are derived from a full length p45 proenzyme. ICE has now been identified to be caspase-1.[109]

The site for IL-1β processing is evolutionarily conserved and is located at Asp116-Ala117.[110] In human monocytes and THP-1 cells it has been shown that cleavage can occur at an additional site, Asp27-Gly28 leading to two products of 17.5kDa and 28kDa. Caspase-1 has also been shown to activate IL-18 and IL-33, two other members of the IL1 superfamily.[111 112] IL-33 acts at the ST2 receptors and is an 'alarm signal' cytokine shown to be important as an immune modulator and is involved in allergy, fibrosis and chronic inflammation.[113] IL-18 is synthesised as an inactive 24kDa precursor protein which is constitutively expressed in monocytes, macrophages and dendritic cells.

Active IL-18 is also pro-inflammatory and leads to increases in cell adhesion molecules such as ICAM-1 and VCAM-1, increased NO synthesis and synthesis of other pro-inflammatory cytokines such as IL-6, IL-8, TNF-α and INF-γ. It also acts to promote angiogenesis via increased expression of VEGF.[114]

Caspase-1 is activated through assembly of the NLRP3 inflammasome (NACHT, LRR and PYD domains containing protein 3). NLRP3 contains a C terminal caspase activation and recruitment domain (CARD) and an N terminus pyrin domain (PYD) and binds to ASC (apoptosis-associated speck like protein) via the PYD of both proteins. These proteins oligomerise on cell activation and ASC recruits caspase-1 through CARD-CARD interactions.[115] Relatively few molecules of NLRP3 are needed to cause polymerisation and activation of large numbers of ASC and caspase-1; recruitment of multiple caspsase-1 molecules then leads to proximity induced dimerization and polymerisation of caspase-1 which in turn leads to autocatalytic activation of the biologically active p10 and p20 subunits.[116] Caspase-1 polymerisation and activation is summarised in Figure 1.2.

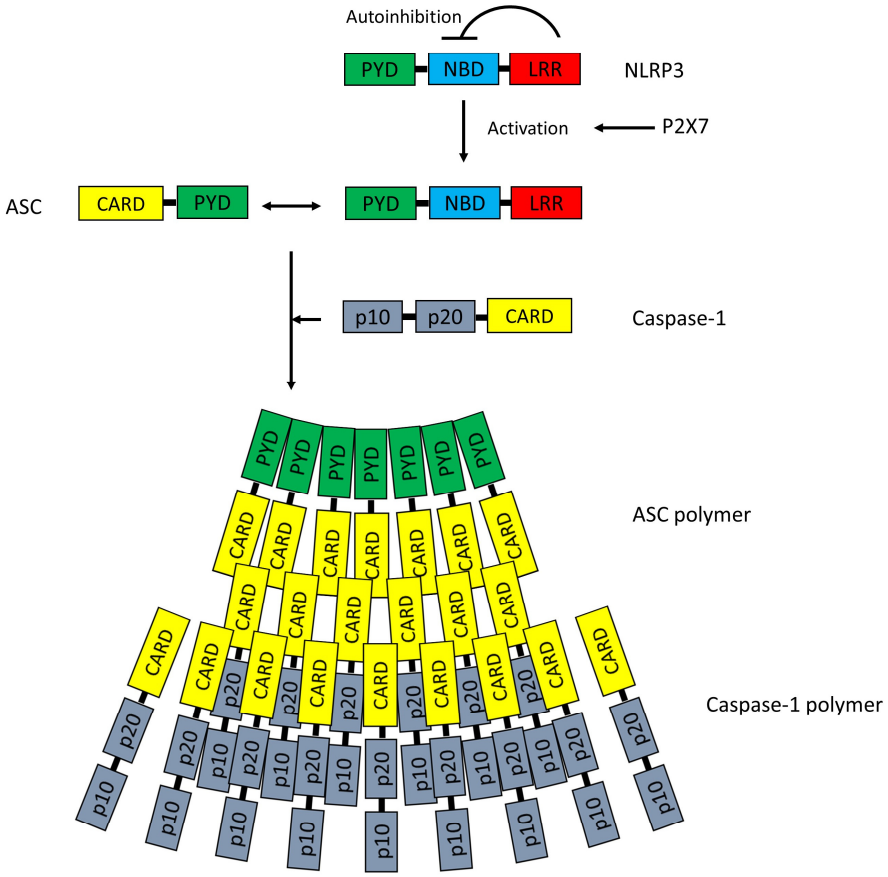

Figure 1.2 Assembly of the NLRP3 inflammasome
In unstimulated cells NLRP3 exists in an autoinhibited state. Activation of NLRP3 for example via P2X7 signalling pathways allows the PYD of NLRP3 to interact with the PYD of ASC. This results in polymerisation of ASC into long fibres which recruit caspase-1 via CARD-CARD interactions. Proximity induced caspase-1 polymerisation results in autocatalyitic activation of the p10 and p20 subunits. Adapted from Ruland J. Inflammasome:Putting the pieces together. Cell 2014;156:1127-29[116]

ATP stimulation and K+ efflux after TLR priming have been shown to be sufficient to act as a second signal to induce caspase-1 activation, IL-1β cleavage and release from the cell.[96 117] It has been shown, using P2X7 antagonists and knockout mice, that ATP is acting via P2X7 receptors to mediate this signalling.[118 98 119] The C terminus of P2X7 is required for release of IL-1β; in individuals with a single nucleotide polymorphism (SNP) of glutamine to alanine at position 496 within the C terminus, IL-1β release following cell stimulation was reduced.[120] The ability of P2X7

to form pores may be linked to its ability to induce maturation of IL-1β; P2X7 with the SNP described above could not form large pores in addition to defective cytokine production. There are conflicting results as to whether pannexin-1 is required for ATP/P2X7 induced released of mature IL-1β from cells. Inhibition of pannexin-1 with siRNA inhibited caspase-1 activation and IL-1β cleavage in transfected HEK293 cells.[58] However, another study using pannexin-1 deficient mice found no effect on cytokine release in response to LPS/ATP stimulation of BMDM. [62] K+ efflux from cells is also thought to be a necessary step in IL-1β release, increasing extracellular K+ impairs IL-1β release and stimulating cells in a sucrose containing media which potentiates K+ efflux causes increased release.[117] [121] The mechanism of release of bioactive IL-1β from cells is incompletely understood with many postulated mechanisms including secretory lysosomes, shedding of microvesicles or loss of plasma membrane integrity associated with pyroptosis.[122] The two signal mechanism for release of IL-1β is shown in Figure 1.3

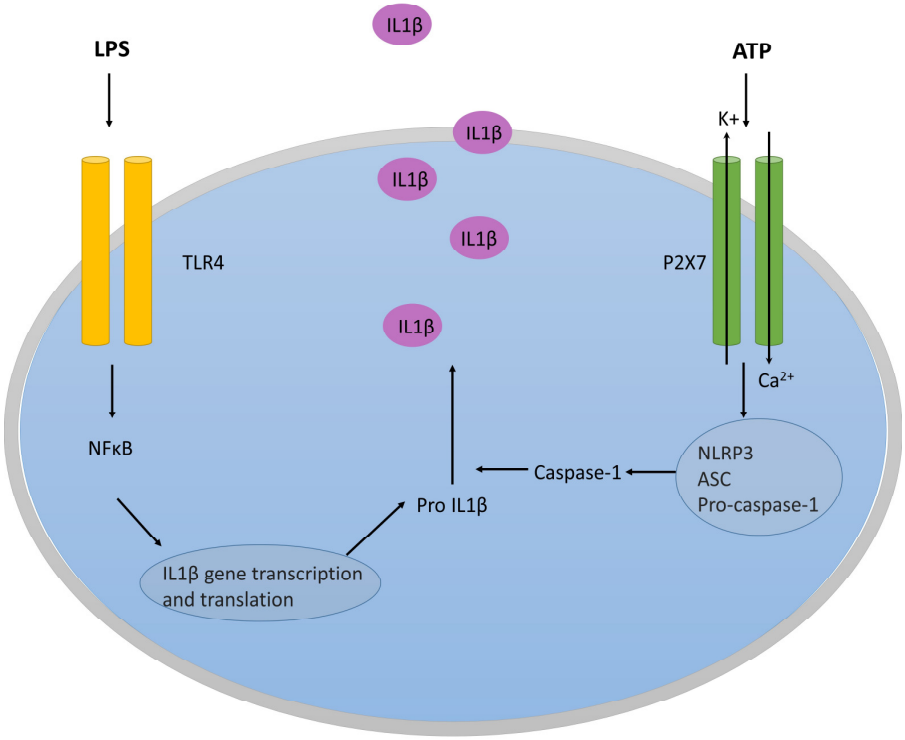

Figure 1.3 Two signal hypothesis for IL-1β release.
In macrophages two stages of signalling are required for release of mature IL-1β from the cell. Initial 'priming' via TLR4 stimulation results in kinase signalling cascades via NFκB resulting in synthesis of 31kDa pro IL-1β. Subsequent activation of P2X7 by ATP results in K+ efflux from the cell, activation of NLRP3 and caspase-1. Active caspase-1 now cleaves IL-1β to its 17kDa mature form which is released from the cell.

Several studies have reported that a second signal via ATP and P2X7 is not required for IL-1β maturation and release in some cell types. LPS stimulation alone has been shown to be sufficient for human but not murine monocytes to release mature IL-1β. [123-125] [126] Both human and rodent macrophages require the second signal of ATP and there are differing results in dendritic cells (DCs). Human monocyte derived DCs are reported to require ATP but murine bone marrow derived DC (BMDC) and splenic DCs have been shown to release mature IL-1β in response to LPS alone.[125] [127] Different mechanisms for LPS induced IL-1β release have been suggested. Netea et al reported that IL-1β release was dependent on canonical inflammasome activation. They showed that human monocytes have constitutively active caspase-1 due to release of ATP from the cells even at basal

conditions. IL-1β release was dependent on ASC and NLRP3 and blocking the action of P2X7 with oATP significantly decreased mature IL-1β production.[125] Parzych et al also showed that IL-1β release from human monocytes could occur in response to LPS alone and was caspase-1 dependent. However, they found that this was independent of P2X7 and pannexin-1 but was dependent on the MaxiK potassium channel suggesting that LPS activation of MaxiK channels leads to potassium efflux and assembly of the inflammasome. In a detailed paper by Gaidt et al it is also shown that IL-1β release is caspase-1 dependent but that this occurs via an alternative inflammasome pathway with upstream signalling via TRF-RIPK-FADD-Caspase-8 leading to activation of NLRP3 and caspase-1. They showed that this pathway has a more gradual response that canonical inflammasome activation and it is not dependent on K+ efflux from the cell.[126] In contrast Vigano et al demonstrated that IL-1β release was not caspase-1 dependent. They showed caspase-1 was not active in resting monocytes and conclude that caspase-4 and 5 activation by LPS mediates TLR4 derived IL-1β release independently of caspase-1/the inflammasome. They also implicate Spleen tyrosine kinase (Syk) in this mechanism, showing that LPS induces phosphorylation of Syk and using a selective Syk inhibitor (R406) leads to a reduction in active caspase-5 and mature IL-1β release.[123] In murine dendritic cells, LPS alone or a variety of other TLR ligands were sufficient to induce IL-1β release; this was dependent on caspase-1 and NLRP3 but independent of K+ efflux. LPS was shown to be acting independently of P2X7 in P2X7 deficient mice (Pfizer). There was no reduction of IL-1β release from BMDC in response to LPS in vitro and serum levels of IL-1β in vivo following IP LPS were equivalent to those in WT mice.[127] The mechanism demonstrated in this study could possibly be equivalent to the one elucidated by Gaidt et al in human monocytes.

1.2.10 Other inflammatory pathways

P2X7 activation can lead to activation of other pro-inflammatory intracellular pathways which are different but often linked to activation of the inflammasome. In several studies, ATP acting at P2X7 has been shown to activate the transcription factor NFκB via the MAPK signalling cascade.[128 129] NFκB, via translocation to the nucleus, mediates the expression of pro-inflammatory genes including TNFα, COX-2 and IL-1β. One study suggested that P2X7 interacts with myeloid differentiation primary-response protein 88 (MyD88) in a shared pathway with TLR activation and this may occur via the P2X7 C terminus.[130] P2X7 activation has also been shown to be associated with activation of phospholipases including phospholipase A2 and D.[131 132]

1.2.11 P2X7 C terminus

One distinct feature of P2X7 is its long C terminus, 200 amino acids longer than other P2X receptor subtypes; as such its function has been extensively studied both through endogenous and induced mutation. Delinger et al performed an alignment comparison of the C terminus and showed there was a lipid interaction domain at residues 573-590 which was homologous to the LPS binding domain of LPS binding protein. The LPS binding domain has been shown to have an essential role in P2X7 function; mutations induced in this domain led to decreased ion channel activity and pore formation. This domain is also involved in trafficking of P2X7 to the cell membrane; mutations at residues 578 and 579 led to normal total protein expression but decreased cell surface localisation. This was thought to be due to a defect in receptor recycling as slowing this process by incubating cells at lower temperature restored normal cell surface expression.[133]

There was also an SH3 domain at residues 441-460 homologous to the TNFR1 death domain.[134] A naturally occurring P451L mutation in C57Bl/6 mice has been shown to impair P2X7 induced cell death and pore formation but had no effect on ion channel function.[135 136] In humans the glutamine

to alanine polymorphism at position 496 that was discussed previously, along with other naturally occurring polymorphisms within this domain, decreased leukocyte pore formation and decrease of P2X7 function. [137-139]

1.2.12 P2X7 polymorphisms

P2X7 is highly polymorphic with many SNPs and splice variants reported in both rodents and humans. In 2014 it was reported there were over 1500 SNPs although most were intronic with around 150 exonic non-synonymous SNPs.[140] As discussed above several loss of function SNPs have been described in the C terminus and gain of function mutations have also been reported.[141] [142]

Several SNPs have been associated with human disease although often with conflicting results. SNPs have been associated with susceptibility to tuberculosis with a 1513 A/C polymorphism which replaces glutamine with alanine at amino acid 496 identified on meta-analysis to increase susceptibility to both pulmonary and extra-pulmonary tuberculosis in an Asian population.[143] This allele has also been associated with other diseases including Crohns disease and CLL, although in CLL it does not seem to correlate with clinical outcomes of the disease.[139] [144] [145] Impaired intracellular killing in patients with this polymorphism is thought to underlie their susceptibility to tuberculosis, with macrophages from patients homozygous for this allele unable to kill intracellular mycobacterium in response to ATP stimulation.[143] Other SNPs have also been associated with mood disorders, increased bone loss in post-menopausal women, increased risk of age-related macular degeneration and protection from toxoplasma gondii infection.[146-149]

1.2.13 Human P2X7 splice variants

Nine splice variants of human P2X7 have been described to date; the full length receptor is termed P2X7A and the nine variants B-J (Figure 1.4). P2X7 B-H were identified first, P2X7B contains an intron between exon 10 and 11 resulting in loss of the last 171 amino acids and an alternate region of 18 amino acids after the second transmembrane domain. P2X7 C and E contain this same intron but are also lacking exon 4 and 7 and 8 respectively. P2X7 D and F lack exons which form part of the extracellular domain with D missing 5 and F 4 and 8. P2X7 G and H contain a new exon termed N3 between exon 2 and 3, which contains a new start codon; this could potentially lead to translation of a protein missing the first transmembrane domain. P2X7G also contains an intron between exon 10 and 11 as described previously.[150] Subsequently P2X7 I and J have been described. P2X7I contains a point mutation between exon 1 and 2 which results in a null allele, this has been shown to be present in 1-2% of the Caucasian population.[151] P2X7J lacks exon 8 resulting in a truncated protein ending after the first 2/3 of the intracellular domain.[152]

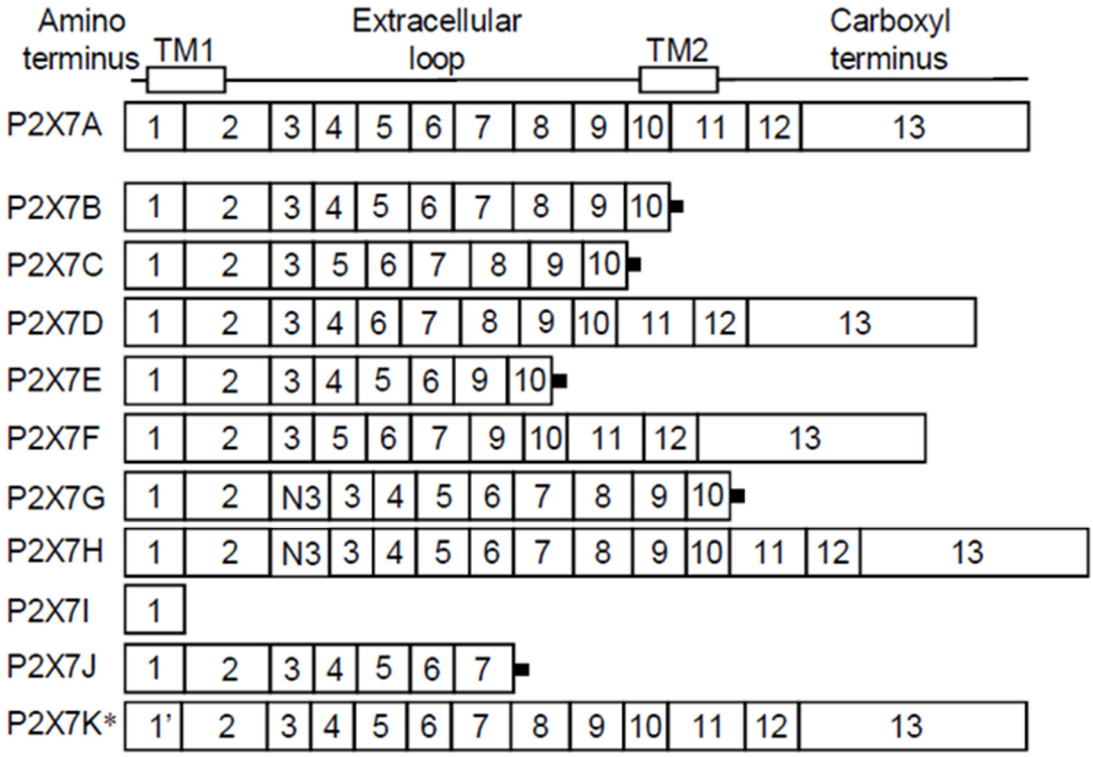

Figure 1.4 Human and rat splice variants of P2X7.
The top line shows a schematic representation of P2X7 topology and how it corresponds to exons of the full length receptor, P2X7A. P2X7B-K are splice variants. Numbered boxes represent exons and solid lines represent alternate coding regions. Image from Sluyter R and Stokes L. Significance of P2X7 receptor variants to human health and disease. Recent Pat DNA Gene Seq 2011;5:41-54[153]

P2X7B expressed in HEK293 cells has been shown to lack pore formation but retain ion channel functionality in response to extracellular ATP although it was 5 times less sensitive to BzATP. When it was co-expressed with P2X7A it co-assembled with P2X7A and potentiated P2X7A function. P2X7B has similar tissue distribution to P2X7A and in brain, spinal cord, lymphocytes and spleen, expression was higher than that of the full length receptor.[154] Human osteosarcomas have been shown to express both P2X7A and B.[155] The expression of P2X7H was found to be very low when compared to full length P2X7 and was shown to be non-functional when transfected into HEK293 cells.[150] P2X7J has been shown to be present in cervical tissue, with higher expression in patients with malignancy than those without. When expressed in HEK293 cells P2X7J was shown

to be non-functional and when co-expressed with P2X7A it exerted a dominant negative effect, it is thought that possibly this splice variant is protecting cancer cells against apoptosis via this mechanism.[152]

The native protein expression of these splice variants in cells and tissues is yet to be ascertained due to lack of available exon specific antibodies. The significance of splice variants to human disease is largely uncertain. It is possible that, as in the case of P2X7H, even non-functional receptor subunits could form heterotrimers with the full length subunit and exert modulatory effects. Differential expression of splice variants may explain some of the many conflicting reports of P2X7 function between cell and tissue types.

1.2.14 Rodent P2X7 splice variants

In addition to the full length P2X7A a splice variant P2X7K has been identified in rodents but not humans. P2X7K contains an additional exon termed 1' in between exon 1 and 2; this results in an alternate start codon and a protein with an alternative N terminus and first transmembrane domain. P2X7K has increased sensitivity to BzATP, more membrane blebbing and increased propensity to form large pores.[156] The P2X7K transcript was found to be widely expressed in rat tissues with particularly high expression in liver, thymus and spleen, at the protein level the spleen was the main site of expression.[156] [157] P2X7K on T lymphocytes is activated by an additional agonist, nicotinamide adenine dinucleotide (NAD), which is a substrate for ADP ribosylation.[157]

Three further P2X7 splice variants have been identified in mice but not in rats. P2X7 2, 3 and 4 all have a truncated C terminal, 2 and 3 are identical to P2X7A at amino acids 1-430 with v2 then terminating at reside 431 and v3 containing an alternative further 11 amino acids.[53] [158] P2X7 v4 is missing not only the C terminus but also the second transmembrane domain. When expressed in

HEK293 cells P2X7v2 and v3 can form homotrimers but were not efficiently trafficked to the cell membrane, had low cell surface expression and were essentially non-functional. When P2X7A was co-expressed with P2X7v3 the splice variant was found to have a dominant negative effect.[53]

1.2.15 P2X7 deficient mice

There are two available strains of P2X7 deficient mice; the first generated by Pfizer utilises a neomycin cassette inserted into exon 13 which deletes the region from amino acid 506 to 532 in the C terminus.[118] The alternative strain was generated by GlaxoSmithKline (GSK) using a LacZ reporter gene and neomycin resistance cassette inserted into exon 1.[51 159] Both in vitro and in vivo experiments using these knockout mouse strains have generated conflicting results. The P2X7 deficient mouse line generated by Pfizer has decreased cytokine production from macrophages and lymphocytes in response to ATP and has a bone phenotype with lower cortical bone mass[160].[50 118] However in the GSK mouse, lymphocytes were in fact shown to have exaggerated responses to BzATP although both peritoneal macrophages and BMDC were unresponsive.[160] Additionally, in the mouse model of multiple sclerosis, experimental autoimmune encephalomyelitis (EAE), disease was worsened in the Pfizer mouse strain but improved in the GSK mice.[161 162] Some of these results are explained by the fact that both mouse strains escape full knockout and exhibit persistent splice variants with P2X7K escaping knockout in the GSK mouse and P2X7v2 and v3 escaping knockout in the Pfizer strain.[53 156]

1.2.16 P2X7 agonists

Compared to other P2X receptors, P2X7 has a low sensitivity to ATP requiring mM rather than μM concentrations for activation. BzATP is the most potent agonist at human, rat and mouse P2X7. When assessing pore formation BzATP is most potent against human P2X7, with 10 times greater activity than at rat receptors and 100 fold greater than mouse.[163] ATP is 17 fold less potent than BzATP at human P2X7 and again shows weaker agonist activity at mouse and rat P2X7. 2-methylthio adenosine triphosphate (2MeSATP) and ATPγS exhibit weak or no agonist activity at rat or mouse P2X7 and 2MeSATP can stimulate channel formation but not dye uptake at human P2X7.[163] There are also reported differences in receptor kinetics between species. Repeated application of BzATP leads to current growth (a progressive increase in the magnitude of the current across the receptor) at mouse and human P2X7 but this phenomenon does not occur in rat P2X7.[164] ADP and AMP act as very weak agonists of P2X7 but possibly can prime human microglial cells to be more sensitive to ATP.[165] It may be that differences in P2X7 agonist sensitivity between species can be explained by differences in amino acid sequence. Two amino acid residues within the extracellular domain are proposed to be responsible for the differences in ATP sensitivity and mutating these residues at 127 and 284 from their mouse amino acid to the rat amino acid increased the sensitivity of P2X7 to BzATP 30 fold.[166]

There have been several reports of compounds which can act as allosteric modulators at P2X7 increasing its sensitivity to extracellular ATP. The first of these to be described was tenidap, an anti-inflammatory drug. In cell culture it was shown to increase ATP induced cytotoxicity and pore formation on mouse macrophages, this effect was not seen in the J774 macrophage cell line which does not express native P2X7.[167] Geldanamycin, an ansamycin antibiotic, specifically inhibits heat shock protein 90 (HSP90) and decreases the levels of tyrosine phosphorylated HSP90 that co-immunoprecipitate with P2X7. Geldanamycin alone did not act as an agonist for P2X7 but resulted in enhanced P2X7 responses to ATP. It is suggested that dephosphorylation of HSP90 with

geldanamycin decreases the suppressor function of HSP90 on P2X7.[168] Polymixin B, another antibiotic also potentiates P2X7 agonist sensitivity, with increased ATP induced pore formation and cytotoxicity and increased IL-1β production by macrophages. It is thought that polymixin mediates its modulatory effects by binding directly to P2X7 itself.[169] The human cathelicidin derived peptide, LL-37, has also been reported to be able to induce IL-1β release from LPS primed monocytes although there are conflicting results as to whether this is via a P2X7 dependent mechanism or not. One group reported that the effect of LL-37 on IL-1β release was P2X7 dependent as it was inhibited by P2X7 antagonists, oxidised ATP (oATP) and KN-62.[170] Another study reported that LL-37 enhanced pore and channel functions of P2X7 in response to extracellular ATP. Furthermore LL-37 restored the pore forming ability of P2X7 with a truncated C terminus which would usually be deficient in this function.[171] However others have reported that a porcine cathelicidin peptide can mediate IL-1β release via a direct effect on cell membrane permeability, leading to K+ efflux from cells and activation of caspase-1.[172] It is possible that the mM concentrations of ATP required for P2X7 activation *in vitro* are not achieved *in vivo* meaning that allosteric modulation would be required. Historically measurement of extracellular ATP in vivo has been difficult due to a lack of molecular probes. Novel techniques which enable direct measurement of extracellular ATP concentrations in vivo using a luciferase system have been developed and studies using this method in models of inflammation will help answer this question.[173 174]

1.2.17 P2X7 antagonists

Historically there were 5 main classes of P2X7 antagonist.[14] The first group consists of ions such as calcium, magnesium, zinc, copper and protons all of which can inhibit ATP-evoked currents.[14] [57] P2X7 is distinct from other P2X receptors in that zinc and copper exhibit an inhibitory effect

whereas ATP induced currents at other P2X receptors are potentiated by similar concentrations of these cations.[175] It is known that decreasing divalent cation concentration in cell culture can potentiate P2X7 responses to ATP and in an inflammatory state dilution of these extracellular ions by release of cytoplasmic contents from damaged cells could lead to exaggerated P2X7 responses.[176] The second class are generic, non-selective antagonists such as suramin, pyridoxal-phosphate-6-azophenyl-2',4'-disulfonate (PPADS), Brilliant Blue G (BBG) and oATP. BBG is fairly specific and inhibits rat and human P2X7 at nM concentrations compared to μM range at other P2X receptors.[177] oATP is an irreversible blocker but requires 1-2 hours pre-incubation prior to application of agonist. It is also non-selective and can act at other P2X receptors at equivalent concentrations.[178] The third group is two large organic cations, calmidazolium and KN-62. KN-62 was the first drug like P2X7 antagonist to be identified and is extremely potent at human P2X7 although ineffective at rat P2X7.[179] [180] The fourth class is 17β-estradiol which reversibly inhibited ATP-evoked currents at human P2X7 in one study.[181] The final group is a mouse monoclonal antibody, which is effective in blocking human P2X7.[182]

KN-62 was used as a basis for several structure activity relationship (SAR) studies with the aim of identifying novel P2X7 antagonists. In 2003, 2 novel groups of competitive antagonists with activity at P2X7 in vitro were described, cyclic imides and adamantine amides.[183] [184] Both of these groups of molecules have greater potency at human over rat P2X7. In 2006 two further groups of P2X7 antagonists were described by Abbott Laboratories, cynoguanidines and disubstituted tetrazoles, again these were identified using an SAR approach.[185] [186] These antagonists are competitive and reversible and show similar potency across human, rat and mouse P2X7.[163] The antagonist A740003 is a member of the cynoguanidine family; in vitro it was shown to have IC_{50} of 40 nM at human P2X7 and 18 nM for rat. It was selective with IC_{50} of >10 μM at other P2 receptors and a variety of other ion channels and enzymes. It was effective at inhibiting IL-1β release and pore formation in THP-1 cells with IC_{50} of 156 nM and 92 nM respectively. It was also effective in vivo in a rat model of nociception with an ED_{50} for IP dosing of 38-54 mg/kg.[186]

A438079, the antagonist used in this thesis, is a member of the disubstituted tetrazole family. It is specific for P2X7 in vitro with IC_{50} 1000 fold smaller at P2X7 than at other P2X receptors (IC_{50} 100nM and 300nM for human and rat P2X7 respectively, 100 μM for other P2X and P2Y receptors). When tested against a panel of 75 different GPCR, ion channels and enzymes in a cell free system IC_{50} was >5 μM.[186] [187] A438079 inhibited IL-1β production from murine peritoneal macrophage at doses of 1 μM and 3 μM. In vivo a dose of 10μmol/kg IP in rats was shown to have a C_{max} of 0.45 μg/ml at 15 minutes and $t_{1/2}$ of 1 hour. It is 84% plasma protein bound and localises 2:1 in brain over plasma. In rats it had dose dependent nociceptive effects at doses of 100-300 μmol/kg IP.[187]

Most recently a nanobody antagonist of P2X7 has been developed. Nanobodies are based on the smallest antigen binding domain of naturally occurring heavy chain only antibodies. They are reported to have several advantages over conventional antibodies. In this study two nanobodies were developed one with activating and one with antagonist properties at P2X7. The antagonist nanobody was shown to decrease P2X7 channel and pore formation and decrease severity of a mouse contact dermatitis model in vivo. [188]

1.2.18 P2X7 antagonists in vivo

Using P2X7 blockade in vivo has been shown to be effective in a wide range of rodent models of disease although due to publication bias there is the potential that studies in which P2X7 antagonist was not efficacious have not been published. Historically many early studies have utilised the non-specific P2X7 antagonists discussed above such as BBG, PPADS or oATP. BBG in particular has been widely used in neurological studies due to its ability to cross the blood brain barrier. In recent years the more selective antagonists have become more widely used, particularly A438079. Studies using A438079 in in vivo models of renal disease are summarised in Table 1.2.

A438079 has been extensively used in nociceptive models in both rats and mice and has been shown to be effective when given IP at decreasing pain in a dose-dependent manner.[185-187] It has also been used in several seizure models but has generated conflicting results with some studies showing decreased and some increased seizure severity.[189-191] In cigarette smoke and LPS induced lung injury, A438079 has been shown to be effective in decreasing airway neutrophil infiltration and cytokine production.[192 193] In kidney disease A438079 decreased severity of a rat model of glomerulonephritis with fewer crescents and improved renal function in antagonist treated rats.[194] Immediate treatment with A438079 also protected against renal dysfunction in an ischaemia reperfusion model of acute kidney injury whereas delayed treatment had no effect. Mice treated at time of injury or within 6 hours afterwards had decreased renal tubular injury and cell death and suppression of renal expression of monocyte chemotactic protein-1(MCP-1).[195] It was also used in two studies of hypertension in rats. In angiotensin-II induced hypertension there were beneficial effects of A438079 treatment on arteriolar resistance and glomerular flow suggesting a role for P2X7 in microvascular dysfunction.[196] In Dahl salt sensitive rats there was a decrease in renal injury in rats treated with A-438079 with decreased renal macrophage and T cell infiltration and less proteinuria.[197]

1.2.19 P2X7 antagonists in human clinical trials

The use of P2X7 modulation in clinical trials is summarised in Table 1.2. Two antagonists have published reports on their safety and efficacy in rheumatoid arthritis. AZD9056 is an adamantine amide which has been evaluated in phase IIa and IIb clinical trials. It was well tolerated with no reported serious adverse events. In IIa studies it was reported to decrease joint swelling and tenderness however in a more appropriately powered phase IIb study these results were not substantiated.[198] CE -224,535 was also used in a phase IIA study in patients with rheumatoid arthritis and active disease despite methotrexate. There were no serious adverse events but no

improvement in symptoms when compared to placebo.[199] AZD9056 was used in a phase IIa trial in patients with moderate to severe Crohns disease. Again it was well tolerated with no significant adverse events reported but there was no decrease in inflammatory markers in patients receiving the drug compared to placebo. There were numerically higher numbers of patients who experienced remission but this was not significant.[200]

A novel P2X7 polyclonal antibody directed against an epitope on a non-functional form of P2X7 that is upregulated in certain cancers has been used as a topical treatment for basal cell carcinoma in a phase 1 clinical trial with an acceptable safety profile.[201]

Reference	Disease model	Species	Strain	Dose and route	Regimen	Outcome
Martins et al 2012[202]	Cyclophosphamide-induced hemorrhagic cystitis	Mice	Swiss and C57BL/6	50-200 µmol/kg	30 min before and 4 hours after cyclophosphamide	Reduced nociceptive behavior scores. Decreased haemorrhage indices, decreased tissue IL1B
Taylor et al 2009[194]	Nephrotoxic nephritis	Rats	WKY	100-300 µmol/kg IP	At time of nephrotoxic serum and bd for 7 days	Decreased severity of glomerulonephritis with 300 but not 100 umol/kg
Ji et al 2012[197]	Salt-sensitive hypertension and renal injury	Rats	Dahl salt sensitive	100 mg/kg IP	OD for 7 days	Decreased macrophage and T cell infiltration in renal tissue, decreased proteinuria
Franco et al 2017[196]	Angiotensin II induced hypertension	Rats	Sprague-Dawley	80 µmol/kg IV	Aortic infusion 1 hour before study	Decreased Ang-II induced arteriolar resistance leading to increased glomerular blood flow
Yan et al 2015[195]	Ischaemic acute kidney injury	Mice	NS	80 mg/kg IP	0, 6 and 24 hours after ischeamia reperfusion injury	0 and 6 hours protect against renal dysfuntion. 24 hours- no effect
Zhang et al 2014[203]	Cisplatin induced nephropathy	Mice	C57BL/6	300 µmol/kg IP	6 hours prior to cisplatin	Decreased cisplatin induced renal injury, decreased renal NLRP3, p53, caspase-3

Table 1.2 Summary of published studies using A438079 in *in vivo* models of kidney disease

Reference	Type of study	N	Antagonist used and protocol	Entry Criteria	Outcome
Gilbert et al 2017	Phase 1 open label	21	Antibody directed against non-functional P2X7. Topical application twice daily for 28 days.	Histologically confirmed basal cell carcinoma suitable for surgical excision	11 patients reported treatment site adverse events 1 serious adverse event (death) unrelated to treatment
Eser et al 2015	Phase 2A	34 24 treated, 10 placebo	AZD9056, 200mg bd for 28 days	Moderate to severely active Crohn's disease	Numerically higher rates of remission in treated patients but not statistically significant Acceptable safety profile.
Stock et al 2012	Phase 2A	100 53 treated, 47 placebo	CE-224,535, 500 mg bd for 12 weeks	Active rheumatoid arthritis despite treatment with methotrexate	No difference in activity of rheumatoid arthritis between treatment and placebo. Acceptable safety profile.
Keystone et al 2012	Phase 2B	319 65 placebo 63 50 and 200mg 64 100 and 400mg	AZD9056, 50mg, 100mg 200mg or 400mg od for 6 months	Active rheumatoid arthritis despite treatment with methotrexate or sulphasalazine	No difference in activity of rheumatoid arthritis between treated groups and placebo

Table 1.3 Summary of published clinical trials using P2X7 antagonists

1.2.20 P2X7 and kidney disease

P2X7 is expressed at low levels in the normal kidney but has been detected at the mRNA level in whole kidney, podocytes and mesangial cells.[47 88 204 205] P2X7 protein has been shown to be present on murine collecting duct epithelium although its role on these cells is unclear with isolated mouse collecting ducts insensitive to BzATP in vitro.[206] However there is good evidence that P2X7 is up-regulated in inflammation or injury. In cultured rat mesangial cells, P2X7 is up-regulated in response to stimulation with LPS, IFNγ or TNFα.[47 88 204] P2X7 expression in renal disease was first described in rat models of diabetes and hypertension. In keeping with previous results P2X7 was expressed at low levels in normal rat glomeruli but was up-regulated by week 12 in transgenic hypertensive rats and by week 6 in rats with streptozocin induced diabetes. This expression was shown to be mainly in glomerular podocytes although there was also some up-regulation in mesangial and endothelial cells.[205]

There is evidence that P2X7 has a role in diabetic kidney disease, likely through its pro-inflammatory mechanisms. In patients with type 2 diabetes their PBMC had higher cell surface P2X7 expression and this correlated with serum CRP and IL-1β.[207] In rats with streptozocin induced diabetes there was increased glomerular P2X7 and in renal biopsy tissue from patients with diabetes, interstitial P2X7 staining correlated with fibrosis and degree of CKD.[46 205] In one study of P2X7 deficient mice there was no difference in the degree of streptozocin (STZ) induced diabetes but the mice were protected from the associated glomerular damage with decreased glomerular macrophage infiltration.[46] In another study P2X7 deficient mice were protected from the development of hyperglycaemia itself with decreased β cell death in the pancreas; renal histology was not looked at in this study but there was decreased macrophage, DC and lymphocyte infiltration into the pancreas of STZ treated P2X7 deficient mice compared to STZ treated WT. [208] In rats which underwent unilateral nephrectomy plus STZ induced diabetes there was again no difference in degree of hyperglycaemia between rats receiving P2X7 antagonist and those not treated, but

there was decreased glomerular macrophage infiltration.[46] When fibroblasts from diabetic patients were cultured at normal glucose concentration they showed enhanced P2X7 responses including apoptosis, shape changes and IL-6 release in response to extracellular ATP. Even in the absence of the addition of exogenous ATP, fibroblasts from patients with diabetes released IL-6 and fibronectin. The authors propose this occurs through higher basal release of ATP and increased P2X7 sensitivity in cells from diabetic patients.[209]

P2X7 may also be involved in renal fibrosis. Unilateral ureteric obstruction (UUO) in mice induces up-regulation of P2X7 in renal tubular epithelial cells and in P2X7 deficient mice compared to wild type there was decreased myofibroblast number, collagen deposition and inflammatory cell infiltration.[210] In another study P2X7 was shown to play a role in inflammatory renal damage due to hypertension. When Dahl salt sensitive rats were fed a high salt diet (thus inducing hypertension) there was up-regulation of renal P2X7 mRNA and protein. Treatment with a P2X7 antagonist (BBG) in rats fed a high salt diet resulted in decreased proteinuria, decreased interstitial fibrosis and glomerular sclerosis and decreased interstitial macrophage infiltration. These results were also corroborated with the more selective antagonist A438079.[197]

1.2.21 P2X7 and glomerulonephritis

There are several studies providing evidence for the involvement of P2X7 in glomerulonephritis both in rodents and humans. In a mouse model of accelerated nephrotoxic nephritis there was increased glomerular expression of P2X7 protein and an increase of glomerular apoptotic cells as demonstrated by double labelling with P2X7 and caspase-3. There was also a significant increase in renal IL-1β mRNA.[45] In another study utilising the same model P2X7 deficient mice had decreased disease severity with decreased proteinuria, fewer infiltrating glomerular macrophages and decreased glomerular necrosis when compared to wild type mice.[194]

In rat nephrotoxic nephritis there was increased glomerular P2X7, IL-1β and pro-apoptotic genes coinciding with onset of proteinuric disease at day 4.[45] There was also an increase in P2X7 protein expression, active caspase-1, IL-1β and IL-18 in nephritic glomeruli cultured ex vivo from rats with NTN.[211] WKY rats are uniquely susceptible to NTN when compared to Lewis (LEW) rats and even at basal conditions macrophages from WKY rats express more P2X7 and NLRP3 protein and mRNA than LEW macrophages and this difference may in part underlie their susceptibility.[211] When rats with NTN were treated with A438079 there was significant decrease in disease severity with decreased proteinuria and glomerular macrophage infiltration, fewer crescents and improved renal function.[194] In another study of spontaneous lupus mice there was up-regulation of P2X7 and NLRP3 in the kidney when compared to control mice. Blockade of P2X7 resulted in decreased severity of lupus nephritis and decreased circulating dsDNA antibodies. This study used the less selective antagonist BBG but similar results were generated with the use of P2X7 siRNA in vivo.[212] P2X7 was also shown to be up-regulated in renal biopsy tissue from patients with lupus nephritis.[45] These results suggest a role for P2X7 in the pathogenesis of glomerulonephritis however, the mechanism of how P2X7 is involved in these models of glomerulonephritis is yet to be elucidated. These models are independent of endotoxin yet priming of cells by LPS is a key initial stage in the release of IL-1β from macrophages stimulated with ATP.

1.2.22 P2X7 and autoimmunity

The study previously discussed using a P2X7 antagonist in spontaneous lupus mice showed that one consequence of treatment was decreased dsDNA autoantibody levels suggesting a role for P2X7 in antigen presentation and autoimmunity.[212] However previous studies in the mouse model of multiple sclerosis, EAE, have generated conflicting results. Treatment with P2X7 antagonist in EAE resulted in decreased severity of disease and decreased neuronal demyelination.[213] However experiments utilising P2X7 deficient mouse strains have generated conflicting results. In one study,

using GSK P2X7 $^{(-/-)}$ mice there was decreased incidence of EAE, although the mice that did develop disease had similar disease course to WT mice.[161] When splenocytes were re-stimulated with MOG, the protein used for immunisation ex vivo the amount of cytokine (IL-17 and IFNγ) produced was greater from P2X7 knockout mice (that did not show clinical signs of EAE) than from wild type.[161] This finding is in keeping with the finding by Taylor et al that lymphocytes from GSK P2X7 deficient mice show exaggerated responses due to the persistence of the P2X7K splice variant. In another study using the Pfizer P2X7 $^{(-/-)}$ mice there was greater severity of disease in the P2X7 $^{(-/-)}$ mice. Splenocytes from P2X7 $^{(-/-)}$ mice proliferated more and underwent decreased apoptosis in response to stimulation with MOG protein. Possibly this loss of apoptotic activity underlies increased disease severity in these mice.[162] Neither of these studies looked directly at the role of P2X7 on antigen presentation or autoantibody production.

1.3 Anti-glomerular basement membrane disease

Anti-GBM disease is characterised by deposited and circulating antibodies against the GBM with clinical features of rapidly progressive glomerulonephritis (RPGN) and pulmonary haemorrhage. The clinical syndrome was first described by Stanton and Tange in 1957 who described 9 cases of glomerulonephritis (GN) associated with lung haemorrhage.[214] They termed this Goodpasture syndrome after Ernest Goodpasture who had described a case of fatal GN and lung haemorrhage in 1919.[215] When the technique of direct immunofluorescence was developed in the 1960s it was shown that renal biopsy tissue had characteristic linear deposition of IgG along the GBM. These antibodies were directly pathogenic as they could be eluted from the GBM and used to passively transfer disease to primates.[216 217]

Anti-GBM disease is a rare condition with a recent nationwide Irish study reporting an incidence of 1.67 per million population/year.[218-220] Anti-GBM disease affects all racial groups although it

seems to be commoner in white patients and rare in African populations. There are 2 peaks of incidence, one in the third decades of life and one in the sixth and seventh decades.[221] Pulmonary haemorrhage is more common in the first peak as is male preponderance; renal limited disease is more common in the second peak along with a slight female preponderance.[218 222-224]

1.3.1 Aetiology

Anti GBM disease has a strong HLA DR2 allele association; HLA *DRB1*1501* is positively associated in around 80% of cases and is consistent in Caucasian and Asian populations.[225 226] HLA *DRB*03* and HLA *DRB*04* have also been reported to be positively associated, and HLA *DRB1*01* and HLA *DRB1*07* have been reported to be negatively associated.[227] Non-HLA genes have also been associated with disease such as copy number polymorphisms in Fcγ- receptors.[228] Despite these genetic associations HLA *DRB1*1501* is common in the general population and has also been associated with other autoimmune diseases, making it likely there must be a role for environmental triggers in those who have an underlying genetic susceptibility. There have been several reports of infectious associations with anti-GBM disease particularly respiratory tract infection.[229 230] In animal models, LPS has been shown to worsen disease severity.[231] There are clear associations between lung haemorrhage and inhaled hydrocarbons or smoking.[232 233] Anti-GBM disease has been described as a secondary phenomenon following other forms of GN, including vasculitis, IgA nephropathy, membranous nephropathy and lupus nephritis.[234 235] It may be that inflammation from smoking, infection or a primary GN causes damage to the basement membrane leading to exposure of previously sequestered epitopes and development of pathogenic autoantibodies.

1.3.2 α3(IV)NC1- the Goodpasture antigen

There are 6 subunit chains of type 4 collagen (α1- α6) which assemble to form to 3 different triple helices, known as protomers. The normal adult GBM contains the protomer formed from α3.α4.α5. A network of type 4 collagen is formed by 2 triple helices forming a hexamer via a sulfilimine bond at the C terminus which results in the formation of the non collagenous (NC1) domain (Figure 1.5). Binding between protomers at the 7S domain in the N terminus stabilises the quaternary structure of the hexamer.[236] The main autoantigen in anti-GBM disease is the NC1 domain of the α3 chain (α3(IV)NC1). α3(IV)NC1 present in the glomerular and alveolar basement membrane accounts for the clinical features of anti-GBM disease. It is also present in the cochlea, testes, choroid plexus and Bruchs membrane in the retina, but does not usually cause clinical disease at these sites.[237-239] Two target epitopes, EA and EB have been identified using epitope mapping, these epitopes are normally sequestered within the quaternary structure of the hexamer.[240] It has been shown that in the presence of inflammatory stimuli such as reactive oxygen species (ROS), conformational change can occur unmasking these epitopes.[241] Antibodies to α4 and α5 chains can also be detected in some patients, presumably due to epitope spreading.

Autoantibodies against α3(IV)NC1 have been shown to be directly pathogenic. When eluted from the kidneys of patients with disease they transfer disease to primates, and in rodent models of disease autoimmune responses to either collagenase digested or recombinant forms of α3(IV)NC1 are sufficient to induce disease.[216] Clinical findings confirm the pathogenicity of the antibody, in that antibody titre and avidity correlate with disease severity and outcome, and renal transplantation, in the face of persistent antibody results in recurrence of disease.[242 243] Additionally, removal of pathogenic antibodies by plasma exchange is one of the main principles of treatment of anti GBM disease. Natural autoantibodies directed against the same epitopes are also found in healthy individuals but with lower titre and affinity than in those with disease. In addition the

antibodies in healthy individuals are, generally restricted to IgG2 and IgG4 subclass, whereas in patients with anti GBM disease IgG1 predominates.[244-246] It is not clear what induces an increase in antibody titre or change in antibody subclass to lead to clinical disease.

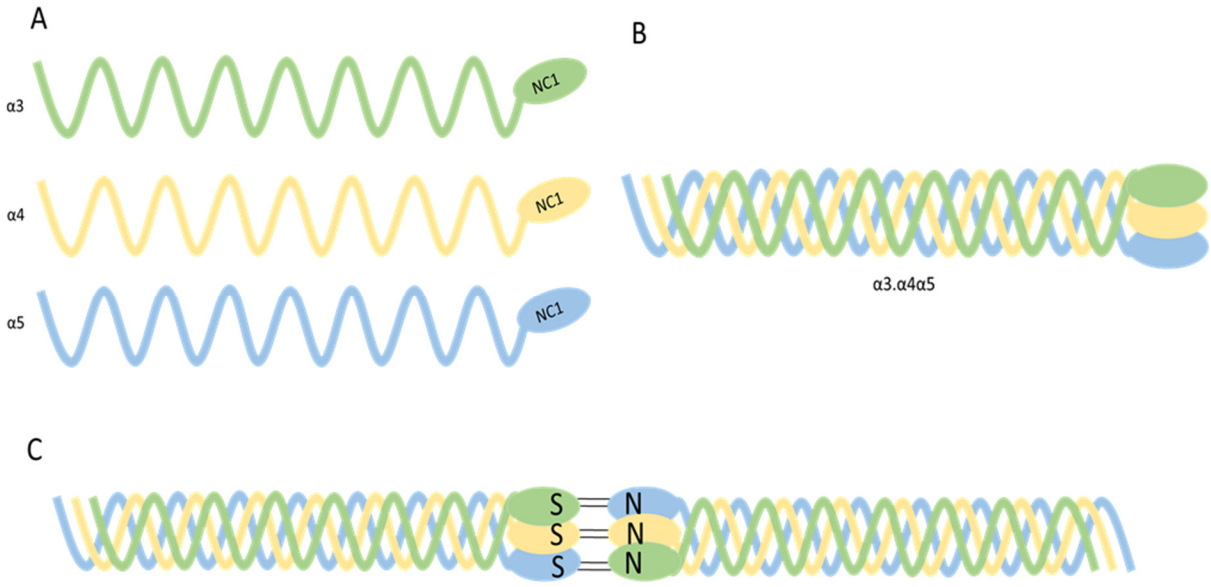

Figure 1.5 Structure of the glomerular basement membrane
(A) The individual α3, α4 and α5 chains of type 4 collagen assemble to form a triple helical protomer shown in (B). (C) The C terminal domains of the chains form a cap and association of 2 triple helices via a sulfilimine bond forms the hexameric non-collagenous domain (NC1). Adapted from McAdoo SP, Pusey CD Anti-glomerular basement membrane disease. In: Encyclopedia of Medical Immunology: Autoimmune Diseases, edited by Mackay IR, Rose NR, Diamond B, Davidson A, New York, NY, Springer New York, 2014, pp 50–56[247]

1.3.3 Cell mediated immunity

T cell mechanisms also contribute to disease pathogenesis in anti-GBM disease. In experimental models of anti-GBM disease, T cells have been shown to be sufficient to induce disease in the absence of autoantibody and treatment with anti-T cell therapies decreases disease severity.[248-250] In patients with anti-GBM disease, T cells can be seen in the glomeruli on renal biopsy and peripheral CD4+ cells proliferate when exposed to α3(IV)NC1 ex vivo.[251 252] Additionally the auto-antibodies in anti-GBM disease are class switched between those with natural antibodies and those with disease, implying T cell help is needed.[244 253] As α3(IV)NC1 is present in the normal thymus, some auto-reactive T cells may be eliminated by central tolerance; however even in healthy

individuals CD4+ T cells reacting with α3(IV)NC1 escape deletion and are present in the circulation.[254 255] Although the pathogenic T cell epitopes have been identified in experimental anti-GBM disease they have not been conclusively defined in humans.[256-258]

1.3.4 Clinical features

Anti-GBM disease presents with the features of RPGN in most patients and around half will also have features of lung disease. A small proportion (<10%) will have isolated pulmonary haemorrhage, although these patients usually also have histological evidence of renal involvement.[259 260] Circulating antibodies against GBM are detectable in most patients' serum using immuno-assays which utilise purified or recombinant GBM. Although most patients with anti-GBM disease have antibodies of IgG_1 or IgG_3 subclass a small number may have atypical antibody such as IgA or IgG_4, which may not be detected by routine testing.[261 262] Western blot using collagenase solubilised GBM is more sensitive but not used in most clinical practice. Light microscopy of renal tissue will show crescent formation in nearly all patients and many will have >50% of glomeruli with crescents.[263] Direct immunofluorescence on frozen kidney sections is highly sensitive for linear staining of the GBM with anti-IgG antibodies. Paraffin embedded tissue and immunoperoxidase techniques will give the same result but is less sensitive. In most biopsies the staining is strong and has a ribbon like appearance. Co-staining is common, with C3 alone being commonest followed by C3+IgM then C3+IgM +C1q.[224]

1.3.5 Treatment and prognosis

The protocol for treatment of anti-GBM disease using plasma exchange was first described in 1976 and current treatment protocols have changed little from the one described.[264] The main aims of treatment are to rapidly remove circulating antibodies using plasma exchange and suppress further antibody production and inflammation using cyclophosphamide and corticosteroids. Untreated anti-GBM disease has a poor prognosis; patients will not recover renal function and progress to end stage renal disease (ESRD), and the risk of mortality from pulmonary haemorrhage is high. Current treatment strategies have improved this prognosis particularly in patients not yet requiring dialysis. In a large published series from Hammersmith Hospital, London, renal survival was 94% and patient survival 94% at 5 years in patients presenting with a creatinine <500µmol/L, and renal survival was 50% and patient survival 80% at 5 years in patients presenting with a creatinine >500 µmol l/L but not requiring dialysis.[222] Patients who required renal replacement therapy at presentation had very low rates of renal recovery, 8% in this series.

1.4 Animal models of anti-GBM disease

1.4.1 Nephrotoxic nephritis

Nephrotoxic nephritis (NTN) was first described in 1900 when Lindemann immunised rabbits with heterologous antiserum against rabbit kidney raised in guinea pigs.[265] NTN has subsequently been demonstrated in several species including rabbits, mice, rats, hamsters and dogs. Induction of disease is by an injection of nephrotoxic serum (NTS) raised in rabbits or sheep immunised with rodent glomeruli, animals then develop co-localisation of alloantibody and an inflammatory renal lesion (heterologous phase) followed by host response to the foreign antigen (autologous phase). The use of pre-immunisation with immunoglobulin from the species in which the NTS is raised

accelerates the development of glomerular inflammation (accelerated NTS).[266] In Wistar Kyoto (WKY) rats NTN is characterised by early leucocyte infiltration, mesangial proliferation and crescent formation, and clinically the animals develop proteinuria and haematuria. Subsequently there is the development of tissue destruction, scarring and renal failure with glomerulosclerosis.[267] Disease histology resembles anti-GBM disease with linear deposition of IgG along the GBM on immunofluorescence. WKY rats are uniquely susceptible to NTN compared to the MHC identical Lewis rats.[268] The F2 generation of a cross between WKY and Lewis rats demonstrated a range of phenotypes along a spectrum between the Lewis and WKY parenteral strains.[268] A genome wide linkage study of these F2 rats identified two major loci for crescentic GN on chromosome 13 (Crgn1) and 16 (Crgn2).[269] Both loci were linked to crescent formation and proteinuria, and infiltration of macrophages was linked to Crgn1.[269] Deletion of the rat gene Fcgr3-related sequence (Fcgr3-rs) was identified as the molecular basis for Crgn1 and analysis across rat strains identified that loss of Fgcr3-rs results in macrophage over activity.[268] Congenic rat strains were used to identify the AP-1 transcription factor, JunD, as the likely identity of Crgn2. Jund siRNA knockdown in macrophages was shown to decrease macrophage cytokine production in response to stimulation.[269]

NTN has historically been thought to be due to T_{H1} dependent delayed type hypersensitivity (DTH) leading to macrophage and other mononuclear cell infiltrate.[270] Various cytokines have been shown to be important at the effector level in rat NTN, with antagonism of pro-inflammatory cytokines or administration of anti-inflammatory cytokines such as IL-4 and IL-11 having a protective effect.[271-273] IL-11 treatment also downregulated glomerular NFκB.[274] NFκB inhibition was shown in another study to down regulate expression of glomerular pro-inflammatory cytokines and decrease proteinuria.[275]

NTN in mice has a more variable phenotype and is often more thrombotic on renal pathology; however more studies have been done into pathogenesis of disease. Development of disease in mice has been shown to be dependent on CD4 but not CD8 T cells and in antibody deficient mice

anti-CD4 antibody protected them from disease.[276 277] Administration of (CD4+, CD25+) T_{regs} was also shown to decrease severity of NTN, again without an effect on antibody deposition suggesting that regulatory T cells effect cell mediated organ damage and not the initial humoral immune response.[278] The IL-17 subset of T cells, $T_{H17,}$ have been shown to have a pathogenic role in disease, IL-23 p19 deficient mice (which have decreased numbers of T_{H17} cells) and IL-17 deficient mice both have decreased severity of disease.[279] However bone marrow chimeras between WT and IL-17 deficient mice have shown IL-17 deficient mice reconstituted with WT bone marrow have worse disease severity suggesting a potentially protective role of IL-17 from intrinsic renal cells.[280]

The IL-1β/NLRP3/caspase-1 axis has been shown in several studies to be involved in the pathogenesis of NTN. Administration of IL-1β prior to induction of NTN in rats resulted in increased disease severity with more glomerular leukocyte infiltration.[281] IL-1β deficient mice have preserved humoral responses but decreased glomerular infiltration of T cells and macrophages with consequent decrease in crescents and improvement in renal disease. In keeping with NTN being T_{H1} mediated there was a decrease in T_{H1} dependent and an increase in T_{H2} dependent IgG subclasses. IL-1R1 deficient mice had a similar degree of reduction in cellular injury but also had a decrease in immunoglobulin deposition suggesting a role for IL-1α in the development of humoral responses.[282] A further study using bone marrow chimeras suggests that IL-1β on leucocytes and IL-1R1 on intrinsic renal cells are required for development of disease.[283] Despite the seemingly key role for IL-1β in the pathogenesis of disease, Lichtenkert et al showed there was no change in severity of the heterologous phase of NTN in mice deficient for either NLRP3, ASC or caspase-1.[284] In contrast, in the autologous phase of murine NTN, Andersen et al showed increased expression of NLRP3, ASC and IL-1β mRNA with detection of mature IL-1β protein within the kidney during disease. Deficiency of NLRP3 and ASC improved renal function and glomerular injury although there was no difference in antibody deposition. Deficiency of ASC resulted in no detection of mature IL-1β in the kidney although NLRP3 deficient mice had levels comparable with WT mice.[285] Renal dendritic cells (DC) have been shown to be pathogenic in the later,

autologous phases of NTN possibly due to an increase in expression of DC co-stimulatory molecules leading to greater T_{H1} and T_{H17} responses.[286] These results together may suggest a role for DC derived IL-1β in autologous NTN. As discussed previously, results published by our group suggest a role for P2X7 activation in mediating disease with decreased severity of NTN in mice deficient in P2X7 and in rats treated with antagonist (A438079) (Figure 1.6).[194] TLR4 signalling has also been shown to exacerbate disease with LPS administration at time of induction of disease resulting in greater number of crescents, increased macrophage infiltration and no effect on glomerular CD4 cell infiltration.[287]

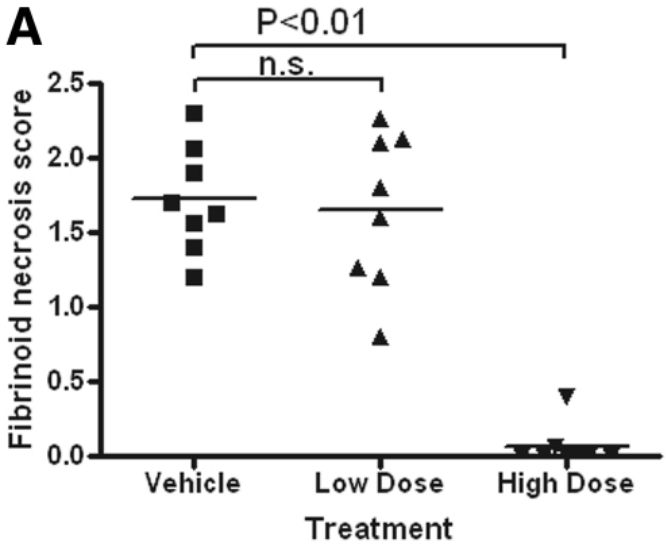

Figure 1.6 Decreased glomerular injury in rats with NTN treated with A438079
Rats with NTN treated with A438079 300 µmol/kg bd (high dose) from onset of disease for 7 days had significant decrease in glomerular fibrinoid necrosis compared to vehicle treated animals. Rats treated with 100 µmol/kg showed a trend to lower severity of disease. From Taylor et al. P2X7 deficiency attenuates renal injury in experimental glomerulonephritis. J Am Soc Nephrol 2009;20:1275-1281

1.4.2 Experimental Autoimmune Glomerulonephritis

Experimental Autoimmune Glomerulonephritis (EAG) was first demonstrated in 1962 by Steblay who immunised sheep with human GBM in complete Freund's adjuvant and described the development of circulating anti-GBM antibodies and crescentic glomerulonephritis.[288] Since then EAG has been reproduced in several species particularly in susceptible strains of rats and mice by immunisation with solubilised bovine, rat or human GBM, or with recombinant human or rat α3(IV)NC1.[289-291] EAG in WKY rats closely mirrors human disease with circulating and deposited anti-GBM antibodies and severe crescentic nephritis. As in human disease antibodies are directly pathogenic and can be used to transfer disease.[292 293] Transfer of serum from mice with EAG into RAG-1 knockout mice which lack adaptive immunity has been shown to induce disease, indicating that humoral immunity alone can induce disease.[249] However, there is also a role for T cells in disease pathogenesis. T cells may be important in initiation of disease and it has been shown that T cell infiltration into glomeruli precedes glomerular injury.[294] Splenic T cells from animals with disease proliferate in response to α3(IV)NC1 and can be used to induce crescentic disease in naïve recipients in the absence of antibody deposition in the glomerulus.[295] In murine EAG, mice which do not have a functional T cell receptor are protected from disease even in passive transfer experiments.[296] Additionally, T cell therapies such as anti-CD4 and anti-CD8 monoclonal antibodies can reduce severity of disease.[297 298] It has also been shown that nasal administration of α3(IV)NC1 or an immunodominant peptide can induce tolerance and decrease severity of EAG possibly through the induction of T_{reg}.[299 300] As in NTN, T_{H17} cells also play a role with IL-23p19 deficient mice protected from disease.[301] The role of IL-1β and the inflammasome has not been identified in these models.

1.5 ANCA associated vasculitis

AAV is a group of systemic autoimmune diseases, which can involve a variety of organs including the kidney, lung, ear nose and throat, nerves and gut. Autoantibodies directed against granulocytes were first identified in patients with rheumatoid arthritis and Feltys syndrome.[302] Subsequently anti-neutrophil cytoplasm autoantibodies were shown to be associated with crescentic glomerulonephritis and the two main ANCA antigens were identified as proteinase-3 (PR3) and myeloperoxidase (MPO), which are present in the granules of neutrophils and monocytes. There are differing clinical syndromes associated with ANCA, granulomatosis with polyangiitis (GPA), microscopic polyangiitis (MPA), eosinophilic GPA (EGPA) and renal limited vasculitis. Around 10% of patients are ANCA negative but will have a similar clinical course to those who are ANCA positive.[303]

AAV is an uncommon condition with incidence of AAV in Europe reported as 13-20 cases/million.[304] From the 1980s-90s incidence seemed to be increasing although this may have been due to increased detection rates following increased availability of ANCA testing. There is a slight male preponderance and incidence increases with age, although peak incidence has been reported at 55-64, 65-74 and >75 years in different studies.[305-307] AAV is relatively rarer in non-Caucasian populations and there are also differences in the incidence of the differing clinical phenotypes. When a Japanese and UK population were directly compared the overall incidence of AAV was similar but GPA was much less common in Japan.[308] There is certainly a genetic basis for AAV and this may explain some of the population differences. A large GWAS showed an association between AAV and genetic factors with a stronger genetic association with ANCA specificity than with clinical syndrome. In anti P3R AAV there were associations with HLA-DP, PRTN3 (the gene encoding proteinase-3) and SERPINA1 (the gene encoding a1-antitrypsin a circulating inhibitor of PR3).[309] There are also reports of an association between HLA-*DRB1*15*

with PR3-ANCA in African-Americans and HLA *DPB1*0401* has also been associated with PR3-ANCA disease.[310]

There are several reported environmental associations with AAV. Infection may precede disease relapse, and nasal carriage of staphylococci correlates with disease relapse in patients with anti-PR3 AAV and ENT disease.[311] A mechanism of molecular mimicry whereby an immune response against microbial antigens cross reacts with self has been proposed. An atypical ANCA, anti-human lysosome-associated membrane protein-2 (anti-LAMP-2) antibody was first identified in patients with pauci-immune GN in 1995 and has 100% sequence homology with FimH a bacterial adhesin on gram negative bacteria. Rats immunised with FimH develop GN and antibodies which react to human and rat LAMP-2.[312] However, these results have not been reproduced in other laboratories.[313] Patients with anti-PR3 AAV have been shown to have circulating antibodies to both PR3 and anti-sense complementary PR3 peptides (cPr3) suggesting that an initial immune response may be against the anti-sense peptide leading to the development of anti-idiotype antibodies which recognise both cPr3 and PR3.[314] In a mouse model of anti-MPO AAV administration of TLR4 agonist (LPS) worsened disease severity and TLR4 deficient mice were protected from disease. Bone marrow chimeras showed that TLR4 on both immune cells and intrinsic renal cells was required for disease.[315] Other environmental risk factors identified include silica, heavy metal exposure and drugs which can induce ANCA including propylthiouracil, hydralazine and levamisole contaminated cocaine.[316-318]

The pathogenesis of AAV is summarised in Figure 1.7 and discussed in detail in 1.5.1-1.5.5

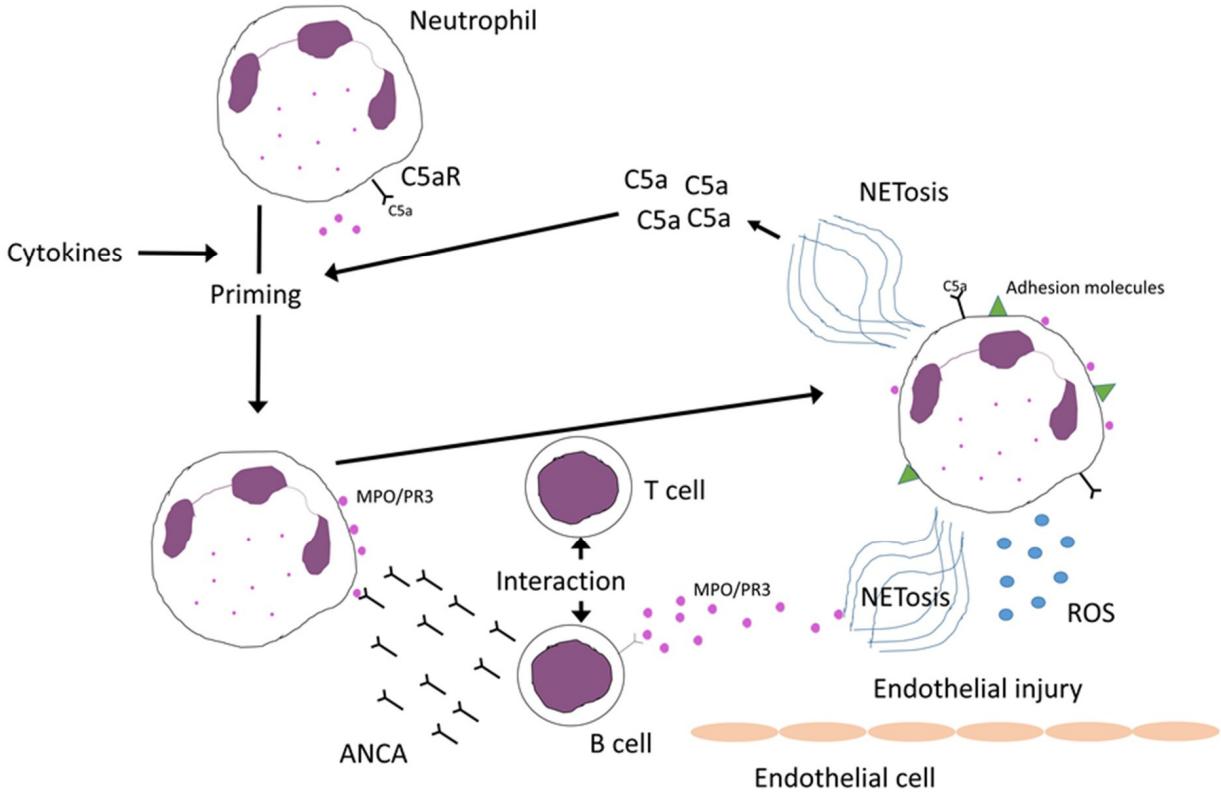

Figure 1.7 The pathogenesis of AAV

Neutrophils are primed by C5a or cytokines such as LPS and TNFα leading to up-regulation of MPO and PR3 at the cell surface. ANCA activate primed neutrophils leading to NETosis, production of reactive oxygen species and other inflammatory mediators causing endothelial cell damage. Activated neutrophils also cause activation of the alternative complement pathway leading to further neutrophil priming and an amplification loop. Adapted from Furuta S and Jayne D. Antineutrophil cytoplasm antibody–associated vasculitis: recent developments. Kidney Int 2013;84:244-249.[319]

1.5.1 Pathogenicity of ANCA

There are several clinical observations suggesting the pathogenicity of ANCA. There is a reported case of maternal-foetal transfer of MPO-ANCA resulting in neonatal renal disease and pulmonary haemorrhage shortly after birth.[320] This is however the only report of this phenomenon and another case report describes no clinical disease in a neonate despite trans-placental transfer of MPO-ANCA.[321] 90% of patients with AAV have circulating ANCA and generally ANCA titres correlate

with disease activity although this is not always the case.[303] Removal of antibodies with plasma exchange has been shown to improve prognosis in AAV and depletion of B cells has been shown to be effective in induction and maintenance of remission.[322 323]

There are several in vitro studies showing that ANCA can activate neutrophils and monocytes. Incubation of MPO-ANCA or PR3-ANCA with neutrophils which have been primed with TNFα, LPS or complement (C5a) results in neutrophil activation, degranulation and endothelial cell damage.[324-326] ANCA binding to neutrophils has also been shown to activate other intracellular signalling pathways leading to altered adhesion molecule expression and conformational changes which promote neutrophil adhesion and transmigration at the vascular endothelium.[327] Both the ANCA antigen binding site and binding to Fcγ receptors on the surface of primed neutrophils and monocytes have been identified as the mechanism by which ANCA activates these cells. One study has shown that ANCA Fab could bind to ANCA antigen on neutrophils but this was not sufficient to induce activation but cross-linked Fab fragments or F(ab)2 fragments could induce generation of ROS.[328] Another study confirmed this result in monocytes showing that F(ab)2 ANCA fragments were sufficient to induce respiratory burst and had similar activating potential as intact ANCA IgG.[329] Several studies have shown the importance of ANCA binding to FcγRIIa (CD32A) and blockage of this receptor decreased ANCA mediated neutrophil activation.[330] Further evidence for the role of FcγRIIa in ANCA mediated neutrophil activation was shown by comparing responses of individuals with the 'high responder' allelic variant for the receptor to those with the 'low responder' receptor. Those who were homozygous for the high responder variant had threefold greater ROS production in response to stimulation with ANCA.[331] Human neutrophils also express FcγRIIIb (Cd16B) which is present at 10 times higher levels than FcγRIIa.[332] Genotype of FcγRIIIb was shown in one study to predict degree of renal involvement in patients with GPA.[333] The role of ANCA binding to FcγRIIIb is more controversial but it has been shown that human anti-MPO and anti-PR3 ANCA can bind to FcγRIIIb and this increases neutrophil activation and adhesion.[334]

ANCA have also been shown to be mediators of NETosis, a form of neutrophil cell death with release of neutrophil extracellular traps (NETs). NETs have a DNA backbone with a variety of pro-inflammatory proteins including histones, high-mobility group box 1(HMGB-1), neutrophil elastase, calprotectin, MPO and PR3.[335] NETs have been shown to be present at sites of tissue damage in AAV and patients also have increased levels of NETs in the circulation.[336] NETs may play a pathogenic role in AAV as they can cause activation of dendritic cells and autoreactive B cells, endothelial damage and complement activation.[337] [338] NETs may also play a role in the loss of tolerance to ANCA antigens, one study has shown that dendritic cells activated by NETs undergo loss of tolerance to both MPO and PR3.[339] Neutrophils from patients with AAV undergo more spontaneous NETosis than healthy controls but ANCA can also induce this process. The exact mechanism by which ANCA induces NETosis is unclear but it is thought to require binding of both Fcγ receptors and the ANCA antigen on the cell surface.[328]

There is good evidence for the pathogenicity of ANCA from animal models of disease. When MPO deficient mice are immunised with murine MPO they produce high titres of anti-MPO antibodies Transfer of purified anti-MPO IgG into WT or Rag2 mice (which lack B and T cells) results in a severe necrotising vasculitis including crescentic glomerulonephritis and haemorrhagic pulmonary capillaritis, demonstrating anti-MPO antibodies alone are sufficient to induce disease.[340] ANCA have also been shown to be pathogenic in an autoimmune rat model of AAV, experimental autoimmune vasculitis (EAV) in the susceptible WKY rat strain. WKY rats immunised with human MPO develop polyclonal anti-MPO antibodies with pauci-immune vasculitis and pulmonary haemorrhage. Intra-vital imaging in this model showed increased leucocyte adhesion and transmigration at the endothelium in response to CXCL1 and this could also be observed in healthy animals following infusion of anti-MPO IgG isolated from rats with disease, supporting a role for the pathogenicity of ANCA.[341] The pathogenic role of PR3-ANCA is less well defined, at least in part due to the difficulty in developing animal models of anti-PR3 AAV.

Although there is much evidence for the pathogenicity of ANCA, the relationship between ANCA and active vasculitis is complex and ANCA are not always pathogenic. ANCA can persist in remission, have been identified in healthy individuals and can recur without clinical relapse. Natural anti-MPO antibodies are of lower avidity and titre than those with AAV.[342] IgG subclass of ANCA may also be important. In vitro, IgG3-ANCA has been shown to be more effective at activating neutrophils than other IgG subclasses although in other clinical studies IgG subclass of ANCA did not correlate with disease severity.[330 343] Epitope mapping to identify the pathogenic epitopes of both PR3 and MPO have been carried out. One study identified a linear epitope on MPO at residue 447-459 that was limited to patients with disease; interestingly when the 3D structure of MPO was visualised this was close to epitopes seen in those with natural antibodies leading the authors to suggest that pathogenic ANCA arise by a process of epitope spreading.[344] In this study IgG purified from patients with ANCA negative vasculitis were able to bind an MPO epitope and it was suggested that competition for binding in immunoassays by a fragment of caeruloplasmin may be why ANCA cannot be detected in these patients. [344]

1.5.2 Neutrophils and monocytes as effector cells in AAV

As discussed, there are many studies demonstrating the ability of ANCA to activate neutrophils and monocytes. Neutrophils have been shown in several studies to be effector cells mediating damage in AAV. In renal biopsies from patients with AAV neutrophils are present within the glomerulus and the number of activated neutrophils (defined by measuring hydrogen peroxide production in situ) correlated with degree of renal impairment in one study.[345] When mice are depleted of circulating neutrophils using an anti-neutrophil monoclonal antibody they were protected from developing anti-MPO IgG induced GN.[346] Many studies have focussed on neutrophils and their interactions with ANCA in the pathogenesis of disease but there is increasing evidence that monocytes also play a role in mediating AAV. Monocytes express ANCA antigens

and stimulation of monocytes in vitro with ANCA leads to cytokine production and generation of ROS.[329 347] Monocytes from patients with AAV have been shown to express higher levels of CD14, the LPS receptor than monocytes from patients in remission or healthy controls suggesting an increased cell activation state in patients with AAV.[348] Circulating monocytes from patients with active AAV have been shown to express higher levels of cell surface markers which are essential for interaction between leucocytes and the endothelium.[349] Recent studies have shown that monocytes and macrophages are the predominant cells in glomeruli in renal biopsies from patients with AAV.[350 351] In one study using the passive transfer model of mouse anti-MPO AAV, depleting monocytes decreased glomerular crescent formation although had no effect on proteinuria.[352]

1.5.3 Complement and AAV

Complement is increasingly recognised to play a role in the pathogenesis of AAV. Using the mouse model of anti-MPO AAV described above, C5 deficient and factor B deficient mice are protected from disease whereas C4 knockout has no effect, suggesting a role for the alternative pathway of complement activation.[353] Mice deficient in C5aR are protected from disease and mice with knock-in of the human C5a receptor treated with an antagonist of human C5a also showed decreased disease severity.[354 355] There is evidence of complement such as C3d and B at sites of tissue inflammation in patients with AAV and, in the kidney, deposition of Bb correlated with pathological severity of disease.[356] Plasma levels of C3a, C5a, soluble C5b-9 and Bb were higher in patients with active AAV than in remission.[357] In one study patients with lower circulating C3 levels were shown to have poorer outcomes both in terms of patient and renal survival.[358] It has been shown in vitro that C5a can prime neutrophils to respond to stimulation with ANCA resulting in degranulation and NETosis, this may be due to its actions at C5aR.[359] The other receptor for C5a is C5L2 and interactions at this receptor are more complex with some conflicting results. Some

studies suggest it has a pro-inflammatory role in vitro but in mouse anti-MPO AAV knockout of C5L2 resulted in more severe disease.[355 360]

1.5.4 B cells and AAV

B cells have a central role in AAV in that they produce ANCA and levels of activated B cells have been shown to correlate with disease activity.[361] Depletion of B cells with rituximab has been shown to be effective in inducing and maintaining disease remission.[323 362] Several studies have shown differences in B cell subsets between patients with AAV and healthy controls. One study reported a memory B cell subset with higher CD19 expression in patients with AAV, suggesting that these may represent autoreactive B cells.[363] Regulatory B cells skew T cell differentiation towards T_{regs} and away from T_{H1} and T_{H17} phenotypes and decrease B cells which are producing ANCA.[364] Several studies have shown decreased Bregs in patients with AAV as defined by cell surface markers such as CD5, CD24 and CD38. [365 366] In vitro, neutrophils stimulated with ANCA release B cell survival factors such as B lymphocyte stimulator (BLyS) and a proliferation inducing ligand (APRIL). In one study, incubating B cells both with supernatant from ANCA stimulated neutrophils and with recombinant BlyS resulted in increased B cell survival.[367] Several studies have reported higher levels of BLyS in patients with AAV and some have shown that levels correlated with disease activity and ANCA titre and decreased following treatment.[368 369] Following rituximab treatment serum BLyS levels have been shown to increase, both in patients with AAV and other auto-immune diseases.[367 370]

1.5.5 T cell immunity and AAV

T cells are present in glomeruli and the tubulointerstitium in renal biopsy tissue from patients with AAV and in granulomas in patients with GPA. One study has identified that patients with AAV had defective T_{reg} suppressive function and had increased frequency of a CD4+ T cell subset that was resistant to the suppressor effects of T_{regs}.[371] In a small group of patients anti-thymocyte globulin (ATG) was used as successful treatment for refractory GPA.[372] Additionally, differential T_H cell polarisation has been described in AAV, such that patients with active and systemic disease are more likely to have a T_{H2} response.[373]

In a model of anti-MPO AAV whereby mice are immunised with anti-MPO followed by a subnephritogenic dose of anti-GBM globulin depletion of CD4+ cells decreased disease severity with no effect on ANCA titres.[374] Mouse models of AAV have provided further evidence for the pathogenicity of T cells in AAV and this is discussed further in section 1.6.1.

The IL-17 axis may also be involved in the development of ANCA, serum IL-23 and IL-17 are raised in the serum of patients with acute AAV and ANCA can induce IL-17 production from neutrophils. IL-17 deficient mice are protected from MPO ANCA induced disease.[375] [376]

1.5.6 Clinical features, treatment and prognosis

AAV is a multi-system disease and clinical presentation varies widely in both severity and organ involvement. Typically patients with GPA may have evidence of ENT or upper respiratory tract disease and patients with MPA often have more severe renal involvement. EGPA is typified by asthma, nasal polyps and peripheral eosinophilia.

Current European League Against Rheumatism (EULAR)/European renal association (ERA) guidelines stratify treatment depending on severity and phase of disease. For acute presentations they recommend methotrexate or MMF with corticosteroids for non-organ threatening disease and cyclophosphamide or rituximab plus corticosteroids for patients with organ or life threatening disease. They suggest the addition of plasma exchange for patients with RPGN or pulmonary haemorrhage.[377] AAV is a relapsing disease so once remission is induced patients requires maintenance therapy with azathioprine, methotrexate, MMF or rituximab. Survival rates in AAV have improved significantly with effective immunosuppressive strategies however one study estimated that 59% of early deaths were caused by treatment associated adverse events and only 15% as a direct consequence of vasculitis.[378] Novel therapies are currently being evaluated in clinical trials including C5aR inhibitors and anti-BLyS antibodies.

1.6 Animal models of AAV

1.6.1 Mouse anti-MPO vasculitis

1.6.1.1 Passive disease models

MPO deficient mice immunised with mouse MPO in Freunds adjuvant develop anti-MPO antibodies. When these antibodies are transferred to naïve mice they develop paucimmune crescentic GN and pulmonary capillaritis.[340] As discussed previously this model established a key pathogenic role for ANCA and neutrophils in mediating disease. There are strain differences in susceptibility to this model of disease which may be explained in part by different neutrophil sensitivity to activation. 129S6/SvEv mice are more susceptible to disease and in vitro neutrophils from these mice showed increased responses to stimulation with TNFα and ANCA.[379]

Another passive transfer model is that of splenocytes from MPO deficient mice immunised with MPO although in this model disease is not pauci-immune, as in humans, as immune complex deposition does occur.[340] CD4+ and CD8+ T cells have also been used to transfer disease and to demonstrate a role for T cells in pathogenesis. Mice pre-immunised with CD4+ T cells from MPO immunised, B cell deficient, MPO deficient mice developed greater severity of GN after induction of disease with MPO-ANCA compared to mice immunised with OVA sensitised CD4+ cells.[380] A major limitation to these passive transfer models is that they are not truly autoimmune; MPO is a novel antigen to the immunised mice and ANCA may have different characteristics to those in humans.

1.6.1.2 Autoimmune anti-MPO models

Models of active autoimmunity have been developed using a subnephritogenic dose of anti-GBM globulin to boost disease and 'plant' MPO in the glomerulus. In this model mice are immunised with mouse MPO, anti-MPO antibodies develop at low titre and are not sufficient to result in GN. A subsequent injection of sheep anti-mouse GBM globulin (at a dose which would itself not result in GN) results in transient neutrophil recruitment to the glomerulus. This 'planting' of the autoantigen results in recruitment of MPO specific CD4+ cells.[381] The advantage of this model as it allows two distinct phases of disease to be studied; the autoimmune response to MPO and the cellular responses. The disease triggered by immunisation with anti-GBM is due to autoimmunity against MPO and disease does not occur in MPO deficient mice.[374] However a limitation to this model is that it is induced by anti-GBM globulin, and after around 4 days the mice develop a nephritogenic immune response to the anti-GBM antibody which leads to a second phase of disease. As such, study of anti-MPO mediated disease is limited to earlier time points.[381] Nonetheless this model has furthered our understanding of the importance of cellular responses in

mediating disease and pathogenic epitopes for both CD4+ and CD8+ T cells have been identified and used to induce disease.[382 383]

MPO deficient mice immunised with MPO develop high titres of anti-MPO antibodies but of course do not develop disease as the antibodies have no target. When mice subsequently undergo bone marrow transplant from WT mice they develop necrotising GN and pulmonary capillaritis.[384] This model identified a key role for neutrophil serine proteases in development of disease; bone marrow transplant from mice deficient in DPPI (an enzyme required for proteolytic activation of serine proteases, also known as cathepsin C) did not result in disease. Mice had decreased infiltration of inflammatory cells and decreased glomerular cytokine levels. The cytokine for which there was the greatest reduction was IL-1β, which was 15 fold lower than in mice transplanted with WT bone marrow. In vitro, MPO-ANCA stimulation of monocytes resulted in production of active IL-1β which was dependent on both serine protease and caspase-1 dependent mechanisms.[385] Mice treated with the IL-1-receptor antagonist anakinra had significantly lower urinary abnormalities and glomerular leucocyte infiltration than controls.[385]

Another model of AAV was induced by immunising mice deficient in MHC class II and transgenic for HLA-DRB1*15:01 with a pathogenic B cell epitope of MPO that was identified in humans. Mice developed a mild proliferative glomerular lesion, and transfer of IgG from these mice into naïve recipients resulted in greater disease severity than in the initial immunised animals, albeit still with a proliferative rather than necrotising lesion.[344]

1.6.2 Experimental autoimmune vasculitis in the WKY rat

Our laboratory has developed a model of experimental autoimmune vasculitis (EAV) in the susceptible WKY rat strain. Rats are immunised with human MPO in complete Freunds adjuvant

(CFA) and also receive two doses of intraperitoneal pertussis toxin as an immune adjuvant. Rats develop polyclonal anti-MPO antibodies, small vessel vasculitis, pauci-immune glomerulonephritis and haemorrhagic pulmonary capillaritis.[386] As discussed this model shows a directly pathogenic role for ANCA. It has also been used to identify a potential therapeutic role for anti-TNFα treatment in AAV. The main limitation to this model is that disease can be mild and unlike human disease eventually undergoes spontaneous resolution.[387]

1.6.3 Models of anti-PR3 AAV

Generation of models of anti-PR3 AAV has been more complex than for anti- MPO AAV. An attempt to create a passive transfer model analogous to the one using anti-MPO antibodies resulted in no features of vasculitis and only a very mild inflammatory response to TNF in the skin.[388] This could potentially be due to lack of PR3 expression on the surface of unstimulated mouse neutrophils and a lesser degree of sequence homology between mouse and human PR3 than there is for MPO.[389] A series of chimeric PR3 molecules were developed and used to immunise mice and rats, and again although animals developed antibodies no clinical disease resulted.[390] A splenocyte transfer model was successful in causing severe necrotising GN when splenocytes were transferred into immunodeficient NOD/SCID mice.[391] When mice are reconstituted with a humanised immune system human PR3-ANCA and low dose LPS they develop pulmonary haemorrhage and proliferative GN.[392]

1.7 Experimental questions and aims

P2X7 has been shown to play a role in inflammatory cytokine production and through its effect on mechanisms of cell death and proliferation may play a role in the generation of the autoimmune response. Glomerular P2X7 and NLRP3-inflammasome are up-regulated in rodent models of passive antibody-mediated glomerulonephritis, and renal expression of P2X7 is up-regulated in biopsy tissue from patients with lupus nephritis. In NTN, the expression of MCP-1, glomerular macrophage infiltration, and severity of glomerulonephritis, were all reduced in mice lacking P2X7, and also in rats treated with a P2X7 antagonist (A438079). NTN relies on passive transfer of antibody that acts as an alloantigen meaning it is not truly an autoimmune disease limiting translation to clinical disease. Other researchers have shown that treatment with a P2X7 antagonist decreases severity of renal injury and levels of dsDNA antibodies in lupus mice. These results may indicate that P2X7 has a role in antigen presentation and autoantibody production. However, studies of EAE and other studies of spontaneous lupus mice have generated conflicting results. This may be due to the difficulties in interpreting results from the two available P2X7 knockout mice, both mice strains are incomplete knockouts and express splice variant forms of P2X7. In addition, C57BL/6 mice which are the background strain express a naturally mutated P451L low sensitivity P2X7R allele. Moreover, early P2X7R antagonists, such as oATP, have significant off target effects.

In order to characterise the role of P2X7 in auto-immune kidney disease further a global P2X7 knockout has been developed by Professor Tim Aitman in collaboration with Professor Frederick Tam (detailed further in the methods section).

I hypothesise that P2X7R is important in autoantibody production and leucocyte activation, leading to glomerular injury and lung haemorrhage in anti-GBM disease and AAV.

The aims of my project are;

1. To demonstrate whether P2X7 is involved in renal inflammation in anti-GBM disease and AAV, and to study at a cellular level the importance of P2X7 in inflammatory response of neutrophils and monocytes.
2. To investigate the role of P2X7 in the development of autoimmunity in anti-GBM disease and EAV.

1. Characterisation of the P2X7 knockout rat

As this is a newly generated rat line, its characterisation is an important part of my project. I have investigated expression of P2X7 at the protein and RNA level, and defined the role for P2X7 in IL-1β production from bone marrow derived cells.

2. The role of P2X7 in NTN, EAG and EAV

I have investigated the effect of P2X7 knockout in all three models of disease. By using all three models my aim was to further define the role for P2X7 in either initiation or effector mechanisms of disease. EAG and EAV are truly autoimmune models whereas NTN allows us to further localise the effect of treatment or genetic modification to the downstream effects of anti-GBM antibody by eliminating any effect interventions may have on the production of antibodies.

3. The role of P2X7 on human neutrophils and PBMC

The expression of P2X7 on neutrophils is a controversial area and there is limited evidence for the role of P2X7, the inflammasome and IL-1β in EAV and AAV. I have investigated the expression of P2X7 on both human neutrophils and PBMC. I have used a cell culture based approach to study the functionality of P2X7 on these cell types and whether stimulation of cells with ANCA can have a role in P2X7 dependent production of IL-1β.

Chapter 2: Materials and Methods

2.1 General reagents and buffers

Unless otherwise stated laboratory chemicals were obtained from Sigma-Aldrich (Poole, UK), plasticware from ThermoFisherScientific (London, UK), tissue culture plasticware from Greiner Bio-one (Stonehouse, UK) and tissue culture media from Life Technologies (London, UK). Microcentrifuge tubes were supplied by Eppendorf (Hamburg, Germany).

Buffers

Phosphate Buffered Saline (PBS)- NaCl 137 mM, KCl 2.7 mM, Na_2HPO_4 8.1 mM, KH_2PO_4 1.47 mM, pH 7.2-7.4

Tris Buffered Saline (TBS)- 20 mM Tris, 150 mM NaCl, pH 7.5

Carbonate Buffer- 15 mM Na_2CO_3, 35 mM $NaHCO_3$, pH 9.6

Tris, acetic acid, EDTA (TAE)- 40 mM Tris acetate, 1 mM EDTA, pH 8.0

Enzyme-linked immunosorbent assay (ELISA)

Wash buffer- 0.05% Tween-20 in PBS

Block buffer- 1% bovine serum albumin (BSA) in PBS

Reagent diluent- 1% BSA in PBS or 0.1% BSA, 0.05% Tween-20 in TBS

Western blot

Lysis buffer- 1% Nonidet P40 (NP40) buffer (Invitrogen, California, USA) with Phenylmethylsulfonyl fluoride (PMSF) 2mM and 1% Protease inhibitor stock (Santa-Cruz, Dallas, USA)

5x laemelli buffer- 4% SDS, 20% Glycerol, 10% β-mercaptoethanol, 0.004% Bromophenol blue, 0.125M Tris HCl

Transfer buffer- 10% Methanol, 25 mM Tris Base, 190 mM Glycine

TBS with Tween (TBS/T)- 0.1% Tween-20 in TBS, 0.4 mM

Block buffer- 5% Marvel milk powder (Marvel, Dublin, Ireland) in TBS/T

Stripping buffer- 200mM Glycine, 3.5mM SDS, 1% Tween-20, pH 2.2

Flow cytometry

Cell staining buffer- 0.5% BSA in PBS

Cell fixation buffer- 2% Paraformaldehyde (PFA) in PBS

NaCl buffer- 140 mM NaCl, 2mM $CaCl_2$, 10 mM 4-(2-hydroxyethyl)-1-piperazineethanesulfonic acid (HEPES), 25 mM Glucose, 1mM $MgCl_2$

2.2 Animal methods

2.2.1 Animal study approval

All animal procedures were carried out under the Home Office Project License 70/8026 (Holder Dr Kevin Woollard) and Personal License I7B68292E and in accordance with the regulations of the UK Animals (Scientific Procedures) Act (1986).

2.2.2 Animal husbandry

P2X7 KO rats were provided by Professor Tim Aitman and bred in house and WKY WT were purchased from an Imperial College colony maintained at Charles River (Saffron Walden, UK). All rats were maintained in a pathogen free animal facility at the Central Biomedical Services unit, Hammersmith Hospital Campus, Imperial College London. Rats were housed in individually ventilated cages with cage occupancy of 2-5 rats dependent on body weight and had free access to water and standard laboratory diet.

2.2.3 P2X7 KO rat

A global P2X7 KO on a WKY background was created using zinc finger nuclease (ZFN) technology by Professor Tim Aitman's group. ZFN mRNA targeting exon 10 of P2X7 (Target sequence CATTGGATCCACCCTGTCCTATTTCGGTTTGGTAAGAG) were designed and validated by Sigma-Aldrich. 2.5ng of ZFN mRNAs were injected into the pronucleus of single cell WKY WT embryos and embryos transferred into the oviduct of pseudopregnant rats. Offspring were screened using PCR of genomic DNA extracted from ear clippings using primers F AGTGACTGCGAGTTGGTGTG and R ACGAGATGTCTCTCCCCAAA and a 2 base pair

insertion in exon 10 confirmed using direct automated fluorescent sequencing. Heterozygous animals carrying the 2 bp insertion were crossed with WT rats and selectively bred to homozygosity. The ZFN target and sequencing of DNA from a rat carrying the mutation are shown in Figure 2.1.

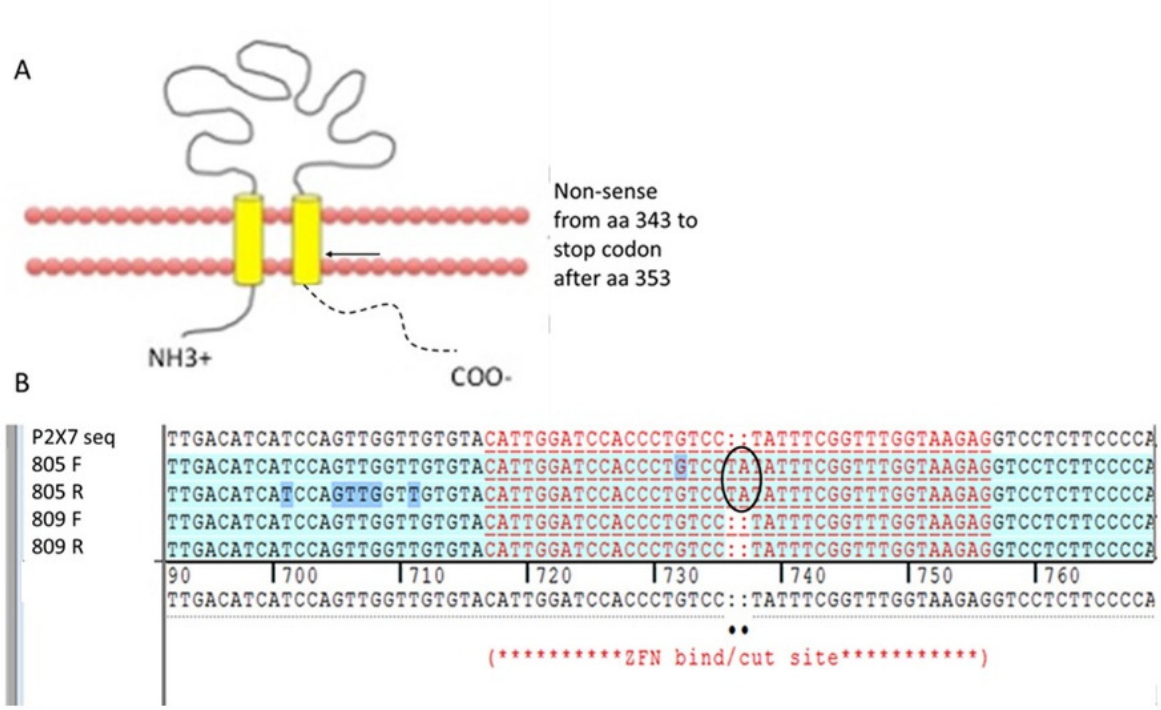

Figure 2.1 P2X7 KO rat creation

A global P2X7 KO was created by insertion of two base pairs (bp) in Chr12:4125199-4125200 positions of the 10th exon of P2X7R in WKY rats to create an early stop codon, using zinc-finger nuclease technology. (a) This mutation results in complete deletion of the cytoplasmic domain of P2X7R. (b) This electropherogram of the P2X7 gene sequences in pup 805 with the 2bp insertion (ringed), and in another WT pup 809 without the 2bp insertion.

2.2.4 Collection of tissue samples for protein and RNA

For tissue samples P2X7 KO and WKY WT rats were sacrificed using overdose of CO_2 and cervical dislocation. Tissue samples were snap frozen in cryovials in liquid nitrogen and stored at -80°C for later RNA and protein extraction.

2.3 Western blot analysis

2.3.1 Cell and tissue homogenisation

Approximately 5mg of tissue was homogenised using a Dounce homogeniser on ice in 300µL of ice cold lysis buffer. For cell lysis, $2x10^6$ cells either pelleted or grown in monolayer were washed with ice cold PBS and 300µL of lysis buffer added for 10 minutes on ice. Lysates were transferred to microcentrifuge tubes and clarified by centrifugation at 13,000 rpm (16200g) for 10 minutes at 4°C. Supernatants were transferred to fresh tubes and stored at -20°C until use.

2.3.2 Protein quantification

The Pierce™ BCA protein assay kit (ThermoFisher) was used to quantify total protein in lysates. BSA standards provided were diluted in lysis buffer (without PMSF and protease inhibitors) and used to prepare a standard curve. Standards and samples were tested in duplicate and 10µl of each added to 96 well microplates. Working reagent was prepared as per the manufacturer's instructions and 200µl added per well. Plates were incubated at 37°C for 30 minutes then allowed to cool to room temperature and absorbance measured at 562nm on a ELx800 absorbance reader (Biotek, Vermont, USA).

2.3.3 Sample preparation and electrophoresis

Samples containing 50µg of protein were prepared in 1x laemelli buffer and boiled on a heating block at 95°C for 3 minutes to denature and reduce proteins. Samples and 10µl of protein ladder (Full range rainbow molecular weight marker, GE Healthcare Life Sciences, Amersham, UK) were loaded onto 4-12% NuPage® Novex® Bis-Tris minigels (ThermoFisher) in Novex Bis-Tris gel

apparatus. Lower chambers were filled with 1x NuPage® MPOS running buffer (ThermoFisher) and upper chambers filled with 1x NuPage® MOPS running buffer supplemented with 2.5% antioxidant (ThermoFisher) to maintain proteins in a reduced state. The gel tank was connected to a power supply and proteins electrophoresed at 100 V for 2 hours.

2.3.4 Transfer to nitrocellulose membrane

Prior to halting electrophoresis adequate separation of proteins was confirmed by inspection of the ladder markers. The mini Trans-blot® electrophoretic transfer cell (BioRad, London, UK) was used to transfer proteins to 0.45µM nitrocellulose membrane which had been activated by soaking in 100% methanol. A 'sandwich' was formed in the cassette of 1 foam pad, 2 sheets of filter paper, gel, nitrocellulose membrane, 2 sheets of filter paper and 1 foam pad all soaked in cold transfer buffer. The gel cassette was inserted into the transfer tank adjacent to a cooling unit filled with ice and proteins were transferred at 100V for 75 minutes.

2.3.5 Blocking and antibody application

Membranes were blocked to prevent non-specific binding in 5% skimmed milk powder (Marvel) in TBS/T for one hour at room temperature. Blocking solution was poured off and primary antibody in 5% milk powder in TBS/T added (as detailed in Table 2.1). Membranes were incubated in primary antibody overnight at 4°C on a rocker. The membrane was then washed in TBS/T 3x1 minutes, 1x 15 minutes and 3x 5 minutes and species specific horse-radish peroxidase (HRP) conjugated secondary antibody diluted 1:5000 in 5% milk powder in TBS/T added (Table 2.1) for one hour at room temperature. Membranes were then washed as previously prior to signal detection.

For detection of subsequent proteins, membranes previously probed were incubated in stripping buffer for 2x 10 minutes at room temperature on a rocker then washed for 2x 10 minutes in PBS followed by 2x 10 minutes in TBS/T. Membranes were then blocked and incubated with antibody as above.

Primary antibodies				
	Dilution	**Isotype**	**Source**	**Catalogue reference**
GAPDH	1:1000	Polyclonal goat IgG	R+D	AF5718
P2X7 004	1:2000	Polyclonal rabbit IgG	Alomone	APR004
IL-1β	1:1000	Polyclonal goat IgG	R+D	AF-501
IL-18	1:1000	Polyclonal goat IgG	R+D	AF-521
Caspase-1	1:2000	Monoclonal rabbit IgG	Abcam	Ab179515
Secondary antibodies				
HRP-conjugated anti-goat IgG	1:5000	Polyclonal rabbit IgG	R+D	HAF017
HRP-conjugated anti-rabbit IgG	1:5000	Polyclonal mouse IgG	R+D	HAF005

Table 2.1 Western blot antibodies

2.3.6 Chemiluminescence and signal detection

Chemiluminescent reaction was used for detection of antibody bound to the nitrocellulose membrane. The enhanced chemiluminescence kit (ECL, GE Healthcare) consists of hydrogen peroxide and luminol which are mixed in a 1:1 ration and applied directly to the membrane. Membranes were incubated in ECL for 1 minute then excess solution blotted off and the membrane wrapped in cellophane. The membrane was exposed to photographic film (Hyperfilm ECL, GE

Healthcare) and film developed using an automatic film processor (SRX-10A, Konica Minolta, Osaka, Japan).

2.4 Immunoprecipitation

2.4.1 Preparation of spleen lysate and protein G slurry

Spleen lysates were prepared and protein quantified as in section 2.3.1 and 2.3.2. Protein G beads (Protein G Sepharose™, GE Healthcare) were washed three times with 1ml ice cold lysis buffer by centrifuging at 12000g for 20 seconds and removing supernatant. A 50% bead slurry was prepared by mixing equal volumes of beads and lysis buffer. This step and all subsequent steps were performed on ice and using pre-chilled microcentrifuge tubes.

2.4.2 Pre-clearing of lysate

To remove antibody present in tissue lysates 50µl of Protein G beads (50% slurry) were added to 250µl of spleen lysate and tumbled end to end for one hour at 4°C. Samples were centrifuged at 12000g for 20 seconds, supernatant transferred to a new tube and beads discarded.

2.4.3 Antigen/antibody binding and precipitation of immune complexes

4µg of either 004 or 008 P2X7 antibody or of polyclonal rabbit IgG isotype control was added to each sample and tubes tumbled end to end for two hours at 4°C. 50µl of Protein G beads (50% slurry) were added and the mixture incubated overnight at 4°C to allow binding of immune

complexes. Samples were then centrifuged at 12000g for 20 seconds to recover beads and the pellet washed 3 times with 1ml cold lysis buffer as before.

2.4.4 Dissociation and protein electrophoresis

The final bead pellet was re-suspended in 40µl of 1x laemelli buffer and boiled for 3 minutes at 95°C on a heat block. Samples were centrifuged at 12000g for 20 seconds and supernatant carefully removed from the beads and collected in a new centrifuge tube. Samples were then used for gel electrophoresis as described in 2.3.3.

2.4.5 Coomassie stain of gel

Sufficient electrophoresis was assessed by inspecting the ladder markers. Gels were then removed from cassettes and protein bands stained using Coomassie stain. Gels were fixed for 1 hour at room temperature using 50% Methanol, 10% Glacial acetic acid, followed by approximately 2 hours of Coomassie staining in 0.1% Coomassie blue, 50% Methanol, 10% Glacial acetic acid until the gel was no longer distinguishable from the staining liquid. Gels were then de-stained for 3 hours using 40% Methanol and 10% Glacial acetic acid with changes of solution approximately every 30 minutes. To improve clarity of bands, gels were then de-stained using dH_2O for 1 hour prior to photography.

2.5 PCR and RT-qPCR

2.5.1 Extraction of RNA

Approximately 5mg of tissue was homogenised in 750µl of trizol using a Dounce homogeniser. Cells were homogenised in 750µl of trizol for up to $5x10^6$ cells. To remove particulate matter from tissue homogenates samples were centrifuged at 12,000g for 1 minute at room temperature and supernatant transferred to fresh tubes. RNA extraction was carried out using the Direct-zol™ mini-prep kit (Zymo Research, Irvine, USA) according to the manufacturers instructions with an in-column DNase digestion step. RNA samples were eluted from spin columns using 25µl of RNase free water and quantity and purity of RNA assessed using A260:A280 ratio and A260:A230 ratio respectively using a Nanodrop 2000c Spectrophotometer (ThermoFisher).

2.5.2 Reverse transcription

Reverse transcription was performed using 1µg of total RNA per sample with iScript™ reverse transcription supermix (BioRad, Hertfordshire, UK). The reaction is primed at 25°C for 5 minutes, reverse transcription occurs at 46°C for 20 minutes and the enzyme inactivated for 1 minute at 95°C. The protocol was carried out using a DNA Engine® thermal cycler (BioRad) and cDNA was stored at -20°C until use.

2.5.3 RT-qPCR

RT-qPCR was performed using qPCRBIO SyGreen mix (PCR Biosystems, London, UK) using an Eppendorf Mastercycler RealPlex^2. Each sample was performed in duplicate and primer pairs and thermal cycling parameters are detailed in Table 2.2. All primers were synthesised by Sigma-

Aldrich. Melt curve analysis was performed for every reaction. Housekeeping genes for RPLP0 (human) and PGK1 (rat) were used as positive controls. The housekeeping genes selected were validated in our laboratory previously to have stable expression across many experimental conditions including inflammation. Negative controls were performed using RNase free water or total RNA. Quantification of target gene compared to housekeeping gene was calculated using the comparative Ct method and where appropriate fold change calculated using the $2^{-\Delta\Delta CT}$ method.

2.5.4 PCR

Traditional PCR was carried out using goTaq green mastermix (Promega, Wisconsin, USA) using primer pairs as detailed in Table 2.2. Thermal cycling parameters were 2 minutes at 95°C, (15 seconds at 95°C, 20 seconds at 57.7°C, 70 seconds at 72°C)x35 cycles, 5 minutes at 72°C and cooling to 4°C using a DNA Engine thermal cycler (BioRad).

2.5.5 Gel electrophoresis

Agarose gel electrophoresis of PCR products was performed using 1.5% agarose gels using 1xTAE buffer to make the gel and as running buffer. 7µl of ethidium bromide was added to each 150ml gel after cooling and before pouring into the gel mould. Samples were mixed with 6x DNA gel loading dye (ThermoFisher) and loaded into the agarose gel. A 1kb Hyperladder DNA ladder (BioLine, London, UK) was used as a DNA size marker. Samples were electrophoresed for 40 minutes at 150V and gels visualised using an ultra-violet transilluminator (Bio-Rad) and photographed using a gel doc system (Bio-Rad).

2.5.6 Sequencing PCR products

The QIAquick PCR purification kit (Qiagen, Valencia, CA) was used to clean up PCR products for sequencing analysis. Purified cDNA was sequenced with relevant primers by the MRC CSC Genomics Core Laboratory (Imperial College, London). Sequencing data was analysed with ApE A plasmid editor software (USA).

Name	Species	Forward	Reverse	Primer Concentration	Melting temperature (Tm) (°C)
RT-qPCR					
P2X7A	Rat	ACCGTCTTTTCCTACGTTAGCTT	GAGTTCCCCTGCAAAGGGAGG	400nM	63.0
P2X7K	Rat	TCGGAGAGCCTTCTCACCAT	CGCTCATCAAAGCAAAGCAGATA	400nM	66.2
IL-1β	Rat	CCTTGTGCAAGTGTCTGAAGC	CAGGTCATTCTCCTCACTGTCG	400nM	63.5
IL-18	Rat	AATGGAGACTTGGAATCAGACC	GGGATTCGTTGGCTGTTCG	400nM	63.1
NLRP3	Rat	CTGCAGAGCCTACAGTTGGG	GTCCTGCTTCCACACCTACC	400nM	63.5
Caspase-1	Rat	TGCCGTGGAGAGAAACAAGG	CCAGGACACATTATCTGGTGTTG	300nM	65.2
PGK1[393]	Rat	ATGCAAAGACTGGCCAAGCTAC	AGCCACAGCCTCAGCATATTTC	400nM	61.0
P2X7	Human	CCCTTTGCAGGGGAACTCTT	TCCGGTCTGAATTCCTTTGCT	400nM	66.4
IL-1β	Human	TCATTGCTCAAGTGTCTGAAGC	GCACTTCATCTGTTTAGGGCCA	400nM	64.4
IL-18	Human	GCTGAAGATGATGAAAACCTGGA	GAGGCCGATTTCCTTGGTCA	400nM	66.3
NLRP3[394]	Human	TGAAGAAAGATTACCGTAAGAAGTACAGA	GCGTTTGTTGAGGCTCACACT	400nM	64.0
Caspase-1	Human	GAAAAGCCATGGCCGACAAG	TGTACCTTCACCCATGGAACG	400nM	66.8
RPLP0	Human	GGCAGCATCTACAACCCTGA	AGGACTCGTTTGTACCCGTTG	400nM	65.0
PCR					
P2X7	Rat	CCGTCTTTTCCTACGTTAGCTTT	AGAAGTCCGTCTGGGGTCT	1µM	59.0

Table 2.2 Primer pairs and conditions

Where applicable reference is provided. RPLP0 primer sequence was kindly provided by Miss Bahire Kalfoglu.

2.6 Culture of bone marrow derived cells

2.6.1 Culture of L929 cell line

L929 cells are a murine fibroblast cell line which secrete macrophage colony stimulating factor (M-CSF). Cells were grown to confluence in Dulbecco's Modified Eagle Medium (DMEM; Life Technologies) supplemented with 10% FCS (Biosera, Nuaille, France), 2mM L-glutamine and 2% penicillin and streptomycin. Cell culture media was collected, passed through a 0.2 μM filter (Corning, Flintshire, UK) and stored at -20°C until use.

2.6.2 Bone marrow isolation

WKY WT and P2X7 KO rats were sacrificed and femurs and tibias excised. Excess soft tissue was removed and bones were washed twice in 70% ethanol. The ends were cut from the cleaned bones and bone marrow cells flushed into a 50ml centrifuge tube using a 20 gauge needle attached to a syringe containing 10mls cold Hank's balanced salt solution (HBSS; Life Technologies). Cells were kept on ice until all cells were isolated and were then passed through a 100μM cell strainer (Corning) and centrifuged at 1500 rpm (350g) for 5 minutes at 4°C. Cells were re-suspended in 10ml HBSS and the centrifuge tube placed in the CO_2 incubator in a horizontal position for 10 minutes. The cells were then centrifuged at 1500 rpm (350g) for 5 minutes at 4°C, cells re-suspended in full culture media and counted using a haemocytometer.

2.6.3 Bone marrow derived macrophage culture

Bone marrow cells were seeded at $50x10^6$ cells per 140mm non-treated cell culture dish (Sterilin, Newport, UK) in DMEM containing 25mM HEPES, 25% L929 cell line conditioned medium, 25% FCS, 2mM L-glutamine, and 2% penicillin and streptomycin. Cells were cultured for 7 days at 37°C in 5% CO_2 and media supplemented at 4 days. At day 7 non-adherent cells were washed away and adherent cells collected by incubating with non-enzymatic cell dissociation buffer (Sigma-Aldrich) for 30 minutes.

2.6.4 Bone marrow derived dendritic cell culture

Bone marrow cells were re-suspended in Roswell Park Memorial Institute media (RPMI; Life Technologies) containing 10% FCS, 2mM L-glutamine, and 2% penicillin and streptomycin, 10ng/ml recombinant rat granulocyte macrophage colony stimulating factor (GM-CSF) (Peprotech, London, UK) and 10ng/ml recombinant rat IL-4 (Peprotech) and seeded at $4x10^6$ cells per well in tissue culture treated 6 well plates. Wells were supplemented with fresh full culture media on day 3 and day 5 and non-adherent cells collected for use at day 7.

2.6.5 Stimulation of BMDM and BMDC

Bone marrow derived macrophages (BMDM) and bone marrow derived dendritic cells (BMDC) were differentiated and harvested as described in 2.6.3 and 2.6.4. Cells were plated at $1x10^6$ cell/ml into either 6 or 12 well plates and incubated for 24 hours in media without FCS or growth factors (BMDM, DMEM with 2mM L-glutamine, and 2% penicillin and streptomycin and BMDC, RPMI with 2mM L-glutamine, and 2% penicillin and streptomycin). Cells were washed with HBSS and cells re-suspended in serum free culture media with 1µg/ml LPS (ultrapure LPS from E.Coli

0111:B4, Invivogen, California, USA) followed by ATP (Sigma) 5mM for 30 minutes. 5mM concentration of ATP was selected as it is well established that P2X7 requires mM rather than µM concentrations of ATP for activation and this concentration is widely used in other published studies.[14 35 211] Selected cultures also contained 10 units/ml apyrase (Sigma). For P2X7 antagonist studies cells were pre-incubated with vehicle (0.01% DMSO) or 5µM or 10µM A438079 (Tocris, Bristol, UK) in vehicle for 30 minutes. For studies using ATP, A438079 was added after LPS and before ATP, for studies using LPS alone, A438079 was added prior to LPS. For studies using caspase-1 inhibition cells were pre-incubated with vehicle (0.1% DMSO) or 10µM, 25µM or 50µM Ac-YVAD-cmk (Invivogen) added at the same time points as for the P2X7 antagonist. For experiments in the presence of excess potassium, KCl was added to media to raise K+ to the indicated concentration. At the end of the experiment supernatant was collected and stored at -80°C until use. Cells were collected for Western blot or RT-qPCR as described in 2.3.1 and 2.5.1.

2.6.6 MTT assay

MTT (3-[4,5-dimethylthiazol-2-yl]-2,5 diphenyl tetrazolium bromide) assay was performed at the end of each cell culture experiment to assess cell viability. Cell culture was carried out in 96 well plates with $1x10^5$ cells per well with an identical experimental protocol but scaled appropriately. At the end of the experimental protocol media was removed, cells re-suspended in 100µl media containing 0.5mg/ml MTT and incubated overnight at 37°C, 5% CO_2. The following day 100µl of solubilisation solution (10% SDS in 0.01M HCl) was added and gently pipetted to mix. After incubation at 37°C for 4 hours the solution was again mixed by pipetting gently and OD read at 562nm using an ELx800 absorbance reader (Biotek).

2.7 Cytokine analysis

2.7.1 Preparation of supernatants for Western blotting

Supernatant was mixed with 4 volumes of ice cold acetone and incubated for 12 hours at -20°C for protein to precipitate. Tubes were then centrifuged at 3220g for 10 minutes at 4°C and supernatant discarded. Protein pellets were air dried for 5 minutes and re-suspended in 60µl sterile ddH_20. Samples were stored at -20°C until required and used for Western blotting as described in 2.3

2.7.2 ELISA

To quantify secreted cytokines supernatants were analysed using sandwich ELISA kits as detailed in Table 2.3 according to the manufacturers instructions. Half well 96 well ELISA plates (Greiner) were coated with 50µl of capture antibody in PBS and plates incubated overnight at room temperature. Wells were washed three times using 0.05% PBS/T and 150 µl of blocking buffer added per well for one hour at room temperature. Plates were again washed three times and 50µl of samples or standards added in duplicate and plates incubated for 2 hours at room temperature. After 3 further washes 50µl of detection antibody was added and plates incubated for 2 hours at room temperature. Plates were washed and streptavidin-HRP conjugate added for 20 minutes. Plates were then washed 5 times and 3,3',5,5'-tetramethylbenzidine (TMB; Biolegend, California, USA) added for a maximum of 20 minutes. The reaction was stopped by adding 50 µl of 1M H_2SO_4. Optical density was measured at 450 nm using an ELx800 absorbance reader (Biotek). A standard curve was constructed of mean 450nm absorbance on the y-axis and log concentration on the x-axis and unknown concentrations determined using a four parameter logistic curve fit. The rat MCP-1 ELISA differed slightly from others in that capture antibody was diluted in carbonate buffer

not PBS and incubated at 4°C not room temperature. Standards and samples were incubated for 1 hour and there is a combined detection antibody and strepdavidin-HRP incubation step for 1 hour.

ELISA	Source	Blocking buffer	Reagent Diluent
Rat MCP-1	BD	10% FCS in PBS	10% FCS in PBS
Rat IL-1β	R+D	1% BSA in PBS	1% BSA in PBS
Rat IL-6	R+D	1% BSA in PBS	1% BSA in PBS
Human IL-1β	R+D	1% BSA in PBS	1% BSA in PBS
Human IL-8	R+D	1% BSA in PBS	0.1% BSA, 0.05% Tween-20 in TBS

Table 2.3 Summary of ELISA kits used

2.8 Flow cytometry

2.8.1 Cell surface staining

BMDM and BMDC were isolated as above and re-suspended in 0.5% BSA-PBS. Cells were incubated on ice with flurochrome conjugated antibodies directed against cell surface markers as detailed in Table 2.4. Cells were washed in PBS and centrifuged at 1500 rpm for 5 minutes twice and fixed using 2% PFA in PBS. Cells were analysed on the BD Accuri C6 flow cytometer (BD Biosciences, Oxford, UK) and gating strategy and analysis performed using FlowJo v10 software.

Name (Clone)	Species	Isotype	Flurochrome	Source	Catalogue reference
P2X7	Rat/Human	Rabbit polyclonal	FITC	Alomone	APR-008F
CD11b/c (OX-42)	Rat	Mouse IgG2a κ	PE	BioLegend	201801
MHC II (HIS-19)	Rat	Mouse IgG1	APC	eBioscience	17-0920-82
CD80 (3H5)	Rat	Mouse IgG1a κ	PE	BioLegend	200205
CD86 (24F)	Rat	Mouse IgG1 κ	PE	BioLegend	200307
CD103 (OX-62)	Rat	Mouse IgG1	Alexa Fluor® 488	BioLegend	205507
CD14 (63D3)	Human	Mouse IgG1 κ	APC	BioLegend	367118
CD15 (HI98)	Human	Mouse IgM κ	PE	BioLegend	301906
7AAD				eBioscience	00-6993-50
OneComp beads Compensation beads				eBioscience	01-111-42

Table 2.4 Flow cytometry antibodies

2.8.2 Yo-pro-1/To-pro-3 uptake

Cells were plated into 12 well plates at 1 x10^6 cells per well and primed with LPS 1µg/ml for 4 hours. For Yo-pro-1 assay cells were harvested, washed with PBS and re-suspended in 1ml NaCl buffer. Cells were kept warm at 37°C and a final concentration of 10µM Yo-pro-1 Iodine (491/509) (Molecular probes™, Invitrogen) was added to cell suspensions 5 minutes prior to analysis. Baseline fluorescence was measured for 1 minute, 150µM BzATP added and dye uptake recorded over 5 minutes on the BD Accuri C6 flow cytometer (BD Biosciences). For To-pro-3 assay after

LPS priming, cells were washed with PBS and re-suspended in NaCl buffer with 10µM To-pro-3 Iodine (642/661) (Molecular Probes™) and 5mM ATP. After 30 minutes the reaction was stopped with ice cold NaCl buffer containing 20mM $MgCl_2$. Cells were harvested and fixed in 2% PFA prior to analysis on the BD Accuri C6 flow cytometer (BD Biosciences). Further analysis was done using FlowJo v10 software.

2.8.3 Cell viability assay with 7AAD

7-amino-actinomycin D (7AAD, ebioscience) was used as a live/dead cell discrimination assay. At the end of experimental protocols cells were harvested and re-suspended in 100µl cell staining buffer per $1x10^6$ cells. 0.25µg of 7AAD was added per $1x10^6$ cells and cells incubated at room temperature for 10 minutes. Cells were analysed on the BD Accuri C6 flow cytometer (BD Biosciences) without washing.

2.9 ATP luciferase assay

For quantitative analysis of ATP in supernatants the Molecular Probes™ ATP determination kit was used (Molecular Probes). The assay was carried out in a white 96 well plate in order to reduce background and enhance luminescent signal. An ATP standards curve was prepared from the ATP stock solution provided. 90µl of a reaction solution prepared according to the manufacturer's instructions was added to each well and 10µl of standards or samples added. The plate was read using a FLUOstar Omega plate reader (BioTek), and ATP concentrations of samples interpolated from the standards curve using 4PL regression.

2.10 Production of α3(IV)NC1

2.10.1 α3(IV)NC1-FLAG fusion protein cell line

A HEK-293 cell line stably transfected with genes encoding the amino-terminal fragment of rat α3(IV)NC1 and a FLAG signal peptide was kindly provided by Dr John Reynolds. The cell line is also transfected with a neomycin resistance gene ensuring that when cells are grown in the presence of G418 disulphate, an aminoglycoside antibiotic that would be toxic to eukaryotic cells, the cells transfected with the α3(IV)NC1 construct are grown selectively.

Cells were grown to confluence in 15x2.5cm cell culture treated dishes in DMEM with 4500mg/l glucose and L-glutamine 580mg/ml with 10% FCS (Biosera), 2% penicillin and streptomycin and G418 disulphate 600mg/l (Sigma). Once confluent media was changed to serum free media (DMEM with 2% penicillin and streptomycin) and cells cultured for up to 5 days or until loss of confluence was observed. Supernatant was then collected and stored at -20°C until required. Complete media was added to the cells, they were grown until confluent again and the process repeated.

2.10.1 Purification of α3(IV)NC1

α3(IV)NC1 was purified using an anti-FLAG affinity column. A 10ml polypropylene column (ThermoFisher) was flushed with TBS and a porous disc floated to the bottom of the column on top of the liquid. The column was then washed with 0.5% Triton X-100 Surfactant-Amps Solution (ThermoFisher) in TBS followed by 3 washes with TBS. 5ml of anti-FLAG affinity gel (Sigma) was added to the column and allowed to settle, the column was then washed with 3 column volumes of TBS to remove glycerol. The column was activated by washing with 3 column volumes of acid

elution buffer (Glycine HCl, 11.1g/L, pH 3.5) with a maximum time of 20 minutes contact of acid buffer with the column. The column was then washed again with 5 column volumes of TBS.

Cell culture supernatant was centrifuged at 1500rpm for 5 minutes at 4°C and 500ml of supernatant pooled and diluted 2:1 with TBS. The solution was passed through the column at 1-2ml/min using a peristaltic pump (Masterflex, Oldham, UK) and was maintained at 4°C. Bound protein was then eluted using acid elution buffer, 1ml fractions were eluted into microcentrifuge tubes containing 50µl of Tris-Base, pH 9 to neutralise acid. Protein concentrations of eluted fractions were measured using a spectrophotometer (Cecil Instruments, Cambridge, UK) at 280nm. Eluted fractions with the highest OD were pooled and dialysed using a dialysis cassette with molecular weight cut off 10,000 Daltons (ThermoFisher). The α3(IV)NC1 preparation was dialysed against sterile water overnight followed by sterile PBS for 8 hours, all dialysis was carried out at 4°C. Protein content was again quantified by spectrophotometry at 280 nm and the preparation aliquoted and stored at -20°C.

2.10.3 Characterisation of α3(IV)NC1

Western blotting was carried out using serum from an animal from a historical EAG experiment and from a patient with anti-GBM disease. α3(IV)NC1 was diluted in laemelli buffer without β-mercaptoethanol and electrophoresis and blotting carried out as in section 2.3.3 and 2.3.4, electrophoresis was carried out in non-reducing conditions (without the addition of antioxidant to the upper chamber). The blot was then blocked with 5% milk power in TBS/T for one hour then incubated with either rat serum at a dilution of 1:10 or human serum at a dilution of 1:100 for one hour. After washing as previously described either ALP-conjugated anti-rat IgG (Sigma) or HRP-conjugated anti-human IgG were added at a dilution of 1:5000 for one hour. The blot using HRP conjugated antibody was then developed as described in 2.3.6. The ALP-conjugated antibody blot was washed as previously described and developed using 5-bromo-4-chloro-3-indolyl

phosphate/nitro blue tetrazolium (Sigma) dissolved in 10ml of distilled water. When signal was developed the blot was briefly washed in distilled water. Blots showed two bands between 30 and 45kDa representing the two isoforms of the α3(IV)NC1 and a single band at 67kDa representing the dimer form.

2.11 Animal models

Animal husbandry and study approval are summarised in Section 2.1.Rats used for induction of the different in vivo studies included in this thesis are summarised in Table 2.5. Additional rats were used for cell culture experiments and phenotyping of the P2X7 KO rat as required.

Experiment	N	Strain	Sex	Approximate Age	Mean Weight (range)	Duration
NTN 1	11	WKY=6 P2X7 KO=5	M	8-10 weeks	275g (255-2 90) 233g (223-250)	28 days
NTN 2	10	WKY=5 P2X7 KO=5	M	8-9 weeks	209g (196-235) 192g (180-201)	28 days
EAG 1	12	WKY=6 P2X7 KO=6	F	6-7 weeks	141g (132-148) 112g (103-118)	28 days
EAG 2	12	WKY=6 P2X7 KO=6	F	6-7 weeks	135g (131-140) 120g (118-124)	28 days
EAG 3- time course	12	WKY	F	6-7 weeks	130g (110-140)	14 days, 18 days, 21 days, 28 days (n=3 at each time point)
EAG 4- Nephritic glomeruli	12	WKY=8 P2X7 KO=4	F	6-7 weeks	123g (114-131) 127g (112-140)	28 days
EAV 1	12	WKY=6 P2X7 KO=6	F	6-8 weeks	120g (96-150) 126g (120-135)	42 days
NTN 3- P2X7 antagonist	19	WKY=10 P2X7 KO=9	M	8-9 weeks	207g (190-245) 227g (195-260)	7 days

Table 2.5 Summary of animals used for in vivo studies

2.11.1 Induction of NTN

Disease was induced in male rats aged 8-10 weeks by injection of a single dose of 0.1ml of NTS (rabbit anti-rat GBM anti-serum) given by dorsal penile vein injection.[267]

2.11.2 Induction of EAG

Female rats were immunised with recombinant rat α3(IV)NC1 dissolved in PBS, emulsified with an equal volume of complete Freund's adjuvant (CFA; Sigma). A dose of 100μg α3(IV)NC1 per animal was used.[290]

For emulsification CFA and α3(IV)NC1 in PBS were layered in a glass vial and a 20 gauge needle used to aspirate from the interface with rapid expulsion and re-aspiration until there was full emulsification. Sufficient emulsification was confirmed by placing a drop of the mixture in a beaker of water and checking that it had sufficient surface tension to remain globular rather than disperse.

2.11.3 Induction of EAV

Female rats were immunised with purified human myeloperoxidase (MPO; Calbiochem, Merck Millipore, Darmstadt, Germany) reconstituted in sterile water for injection emulsified with an equal volume of CFA. CFA was supplemented with additional killed *Mycobacterium butyricum* to a final concentration of 4mg/ml. A dose of 1600μg/kg of MPO was administered to each rat. Animals also received 500ng of pertussis toxin (Invitrogen) in PBS intraperitoneally on day 0 and day 2.[386]

2.11.4 Preparation and administration of P2X7 antagonist for *in vivo* studies

A438079 was synthesised by Sai Life Sciences (Turkapally, India). For *in vivo* studies it was reconstituted in sterile water for injection. The antagonist was readily soluble in water but was noted to precipitate out of solution after approximately 4 hours at room temperature therefore a fresh batch of antagonist was prepared for each dose. Based on a previous study using this antagonist in NTN and the initial paper reporting development of this antagonist,[187 194] a dose of 275µmol/kg administered twice a day by intraperitoneal injection was selected. Control animals received equivalent injections of vehicle (sterile water for injection).

2.11.5 Collection of biological specimens from rats

2.11.5.1 Urine collection

Rats were housed overnight in individual metabolism cages with free access to water and standard laboratory diet. At the end of the collection period the total urine volume was measured, samples centrifuged at 1500rpm for 5 minutes, aliquoted and stored at -80°C until use. There was a minimum period of 48 hours in between urine collections.

2.11.5.2 Serum collection

For non-terminal serum collection rats were placed in a warming chamber at 30°C to promote vasodilation. The rat was then gently restrained by one operator and a second operator made a superficial nick to a lateral tail vein using a 10A surgical blade. Blood was collected using a plain

microvette tube (Sarstedt, Numbrecht, Germany) up to a maximum volume of 500µl. Samples were centrifuged at 1500rpm for 5 minutes, serum aliquoted and stored at -80°C until use.

2.11.5.3 Terminal processing of blood and tissues

At the end of each study animals were sacrificed under terminal anaesthesia for collection of blood and tissues. Animals were anaesthetised using inhaled isoflourane and exsanguinated by transecting the great vessels. Blood was collected for serum into a plain collection tube.

After sacrifice tissues were dissected out. If severity of lung haemorrhage was being assessed this was done prior to dissection to avoid inadvertent damage to the organs. A coronal pole of kidney was collected in a tissue cassette along with samples of liver, spleen and lung and immersed in 10% neutral buffered formalin. One kidney pole was fixed to cork discs using optimal cutting temperature (OCT) embedding matrix (ThermoFisher), placed in cold isopentane and transferred to liquid nitrogen. Samples were frozen at -80°C until use. Remaining kidney and samples of lung and spleen were snap frozen in cryovials in liquid nitrogen and frozen at -80°C until use.

2.12 Analysis of experimental disease severity

2.12.1 Haematuria

Haematuria was quantified by dipstick testing (Multistix 8 SG, Siemens Healthcare Diagnostics, Tarrytown, New York) of fresh urine and quantified as 0 (negative), 0.5 (trace), 1+, 2+ or 3+.

2.12.2 Serum and urine biochemistry

Proteinuria was quantified using the sulphosalicylic acid method. Bovine serum albumin (BSA; Sigma) was diluted in water to construct a standards curve and urine samples were diluted in water at ratios between 1:2 and 1:100. 100µl of each sample or standard were added in triplicate to a 96 well microplate and 10µl of 25% sulfosalicylic acid was added to two of three replicates and 10µl of water added to the third replicate to provide a blank for each sample. Absorbance was read at 405nm on a microplate reader (Biotek EL800). 24 hour protein excretion was calculated by multiplying protein concentration by total urine volume. Urinary protein creatinine ratio was calculated by dividing urinary protein concentration by the urinary creatinine concentration.

Urine and serum urea and creatinine concentration were measured by Dr John Morris and Ms Ela Biegun-Laroy in the Clinical Biochemistry Department, Hammersmith Hospital, UK using an AU700 analyser (Olympus, Southend, UK). Urinary clearance was calculated using (urinary concentration x urine volume)/(serum concentration x time).

2.12.3 Assessment of glomerular histology

Renal tissue was fixed overnight in 10% neutral buffered formalin then transferred to 70% ethanol. Tissue was processed to paraffin blocks and 4µM sections cut using a rotary microtome and stained with periodic acid Schiff (PAS) and haematoxylin and eosin (H+E). Processing of tissues and staining was performed by Ms Lorraine Lawrence, Department of Leucocyte Biology, Imperial College London.

Renal histology was quantified in a blinded fashion by assessing 50 consecutive glomeruli by light microscopy. For EAG and day 7 NTN glomeruli were graded as severely abnormal (>50% of glomerular tuft with necrosis, sclerosis or crescent formation), abnormal (any other abnormality) or normal. For EAV and day 28 NTN glomeruli were graded as normal or abnormal.

2.12.4 Immunohistochemistry for ED-1

Staining for rat ED-1 was carried out on formalin fixed paraffin embedded tissue sections. Sections were dewaxed by immersion in two sequential baths of xylene followed by graded ethanol concentrations and to water. De-waxed sections then underwent antigen retrieval for 30 minutes in a 95°C water bath in pre-warmed 0.1M sodium citrate buffer, pH 6.0. After antigen retrieval sections were encircled using a wax pen (Dako, Santa Clara, USA) to prevent run-off and dilution of solutions. Endogenous peroxidase activity was blocked by incubating section in 0.3% hydrogen peroxide solution for 10 minutes followed by washing in PBS. Non-specific antibody binding was blocked using 20% goat serum for 30 minutes. Serum block was tapped off the sections and mouse anti-rat ED-1 antibody (Biorad) added at a dilution of 1:500 in PBS. Two methods were then used for detection of primary antibodies.

1. For tissue from animals with NTN a commercial secondary antibody detection system (EnVision, Dako) was used. Primary antibody was tapped off slides followed by 2 consecutive 5 minute washes in PBS. Polymer reagent was added to tissue sections, this is a peroxidase conjugated polymer which carries secondary antibodies raised in goat and directed against mouse immunoglobulin. Slides were incubated with polymer for 30 minutes followed by 3 further 5 minute washes in PBS

2. For EAV and EAG kidney there is extensive glomerular background with use of the EnVision detection system. For tissue sections from these animals a biotinylated rabbit anti-mouse secondary antibody (Sigma) diluted 1:100 in PBS was added to slides for 1 hour. Slides were then washed twice in PBS and an Extravadin-HRP conjugate (Sigma) diluted 1:100 in PBS added to sections for 30 minutes. Slides were then washed 3 times in PBS.

Slides were developed using a 3,3'-diaminobenzidine (DAB) solution. DAB solution was prepared immediately prior to use by mixing DAB chromogen with DAB substrate buffer, 1:50. Sections were incubated with DAB chromagen for 1 minute and the reaction stopped by placing slides in PBS. Cells were counterstained using filtered Harris haematoxylin (SLS, Nottingham, UK) and excess stain removed by immersing for 1 second in acid-alcohol solution (1% HCl in 70% ethanol). Sections were dehydrated from water through graded alcohols to xylene. Slides were mounted using pertex mounting media (CellPath, Powys, UK) and glass cover slips.

Staining was quantified using ImagePro Plus software (Media Cybermetics, Maryland, USA) to measure percentage staining in 20 consecutive glomeruli. Staining was expressed as mean percentage stain per glomerular cross sectional (GCS) area per animal.

2.12.5 Assessment of lung injury

2.12.5.1 Macroscopic assessment of lung injury

In EAG and EAV severity of lung injury was graded at time of sacrifice after opening the chest cavity but prior to dissection of the lungs using a semi-quantitative scoring system. Lungs were graded as; 0 points- normal macroscopic appearance, 1 point- less than 10 petechiae, 2 points- 10-20 petechiae and 3 points if greater than 20 petechiae were seen. Representative lung images are shown in Figure 2.2.

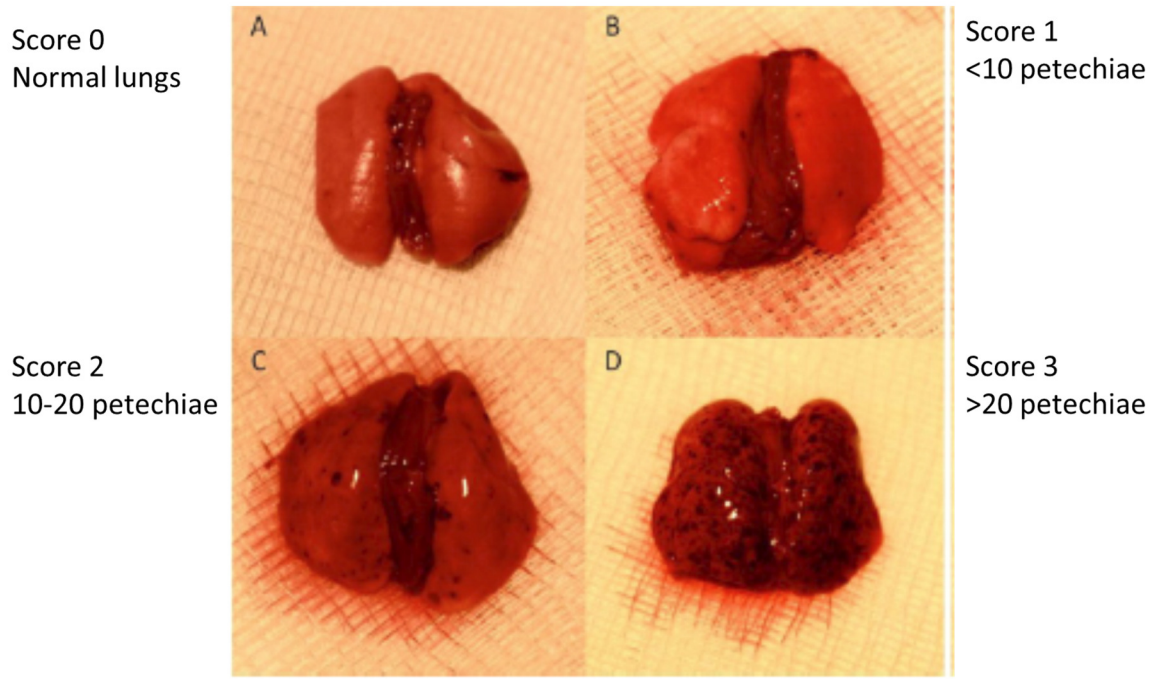

Figure 2.2 Macroscopic scoring of lung haemorrhage

Representative images of scoring system for lung haemorrhage.(A) Normal lung, (B) Mild severity, <10 petechiae, (C) Moderate severity 10-20 petechiae, (D) Severe lung haemorrhage >20 petechiae. Images courtesy of Dr Stephen McAdoo.

2.12.5.2 Microscopic assessment of lung injury

Lung tissue was collected, paraffin embedded and sectioned as for kidney tissue in 12.2.3. Perls Prussian blue staining was carried out by Mrs Lorraine Lawrence. Haemosiderin laden macrophages were quantified using ImagePro software by measuring proportion of blue stained cells in 5 high powered fields and expressed as mean percentage positive staining for each animal.

2.13 Assessment of humoral responses

2.13.1 Direct immunofluorescence for deposited glomerular antibody

Presence of deposited rat IgG (all models) and rabbit IgG (NTN only) was assessed using direct immunofluorescence of frozen kidney sections. Frozen kidney sections were cut using a cryostat (Bright, Luton, UK) at a thickness of 5µM onto poly-L-Lysine coated slides. Slides were left to air dry overnight and fixed in ice cold acetone for 10 minutes. If slides were not used immediately they were stored at -80°C in a sealed box with desiccant. For immunofluorescence staining slides were blocked for 30 minutes at room temperature with 20% goat serum (Dako) then washed in PBS twice for 5 minutes. Slides were then incubated for one hour at room temperature with either FITC conjugated goat anti-rabbit IgG (Sigma) or FITC conjugated goat anti-rat IgG (Sigma) diluted 1:100 in PBS. Slides were then washed three times in PBS and mounted with glass coverslips using vectorshield hard set mounting media with DAPI (Vector labs, Peterborough, UK). Immunofluorescence was assessed by examining 20 glomeruli using a fluorescence microscope and scoring each as 0-3+.

2.13.2 Anti-α3(IV)NC1 antibody ELISA in EAG

Serum antibodies against α3(IV)NC1 were measured by direct ELISA. Recombinant α3(IV)NC1 was diluted in carbonate buffer and a 96 well microplate (ThermoFisher) coated with 5µg/well in duplicate with a third well left uncoated to act as a 'blank' for each sample. Plates were incubated overnight at 4°C then washed 3 times with PBS/0.1% Tween-20. 300µl of 3% BSA in PBS was added per well as a blocking step and the plate was incubated at 37°C for 1 hour. A standard curve was constructed by pooling sera from rats from a previous experiment and an initial ELISA carried out using a serial dilution. Dilutions for future standard curves were selected which included the

linear part of a hyperbolic standard curve when OD was plotted against log dilution. Rat sera and standards were diluted in PBS and added in triplicate and plates incubated at 37°C for 1 hour. Plates were again washed 3 times, ALP-conjugated goat anti-rat IgG (Sigma) diluted 1:1000 in PBS added to each well and plates incubated for 1 hour at 37°C. The plate was washed and then developed with p-nitrophenyl phosphate solution (Sigma), the reaction was stopped with 3N NaOH and the plate read at 405 nm using a microplate reader. For each sample the blank well was subtracted from the mean of the duplicate and antibody titre calculated as arbitrary units from the standard curve.

2.13.3 anti-MPO antibody ELISA in EAV

Anti-MPO antibody levels were measured using direct ELISA with a similar method to that for anti- α3(IV)NC1. Purified human MPO (Calbiochem) was diluted to 1.33µg/ml in carbonate buffer and used to coat wells in duplicate with a third well left blank. Plates were washed three time using 0.1% PBS/T and blocked for 1 hour at 37°C with 1% BSA. After washing, 100µl of samples diluted in PBS/T with 1% BSA or standards (with a standard curve developed in the same way as described in 2.13.2) were added in triplicate and plates incubated at 37°C for one hour. Plates were washed 3 times in PBS/T and 100µl of ALP conjugated rabbit anti-rat IgG diluted 1:1000 in PBS/T with 1% BSA added. Plates were incubated for 1 hour at 37°C, washed then developed and read as described in 2.13.2.

2.13.4 Culture of nephritic glomeruli ex vivo

Nephritic glomeruli were cultured from animals with EAG. After sacrifice kidneys were dissected, kept on ice in sterile PBS and transferred to the tissue culture hood. The kidney capsule was removed, kidney cortex cut away from the medulla and hilum and cut into small pieces in ice cold

PBS. The pieces of cortex were passed through a 250µm stainless steel sieve using the plunger of a 10ml syringe and the sieved material passed through two further sieves of 150µm and 75µm. connective tissue and tubules should be retained by the first two sieves and glomeruli retained by the third sieve. Glomeruli were washed from the final sieve into a 50ml centrifuge tube using a Pasteur pipette and ice cold PBS. Glomeruli were washed 3 times in ice cold PBS by centrifuging at 500rpm for 5 minutes at 4°C. Glomeruli were then re-suspended in complete media (RPMI supplemented with 10% FCS, 2% penicillin and streptomycin, 2mM L-glutamine) and counted by pipetting three 10µl droplets of glomerular suspension onto a coverslip and counting total number of glomeruli in each drop. As yield of glomeruli was variable between animals the total number of glomeruli was divided into two wells of a 12 well plate and cytokine production normalised to the number of glomeruli present. Glomeruli were incubated for 48 hours at 37°C in 5% CO_2 and supernatant collected and used for analysis of cytokine production as described in 2.7.2.

2.13.5 Indirect immunofluorescence with anti-MPO antibodies

Rat anti-MPO IgG and control IgG were isolated from serum of rats with EAV and control rats using a 5ml protein G HiTrap® column (GE Life Sciences). Serum was centrifuged at 1500rpm for 5 minutes at 4°C, passed through a 0.45µm filter and diluted 1:1 with binding buffer (20mM Na_3PO_4 pH 7). The column was washed using 50ml binding buffer at 5ml/minute and then the diluted serum passed through the column. The column was again washed with 50ml binding buffer or until the effluent cleared. IgG was eluted from the column with 25ml elution buffer (0.1M Glycine-HCl, pH 2.7) into 1ml aliquots containing 120µl of 1M Tris-HCl, pH 9. Total IgG was quantified using a spectrophotometer at 280nm, the best aliquots pooled and dialysed using a dialysis cassette with molecular weight cut off 10,000 Daltons (ThermoFisher). The IgG preparation was dialysed against sterile water overnight followed by sterile PBS for 8 hours, all

dialysis was carried out at 4°C. Protein content was again quantified by spectrophotometry at 280 nm and the preparation aliquoted and stored at -20°C.

Bone marrow cells were prepared as in 2.6.2, resuspended at 1x106 cells/ml and 100µl of cell suspension applied to superfrost slides (ThermoFisher) using a cytospin (Cytospin 2, Shandon, ThermoFisher) at 400rpm for 3 minutes. Slides were dried at room temperature and fixed in cold acetone for 5 minutes. Slides were rinsed in PBS, blocked in 20% goat serum for 30 minutes and rat anti-MPO IgG (dilution 1:100) and control rat IgG (dilution 1:40) applied for 1 hour. Slides were washed three times in PBS, mounted in PBS/glycerol (Citiflour) and visualised using fluorescence microscopy.

2.13.6 B Cell ELISpot assay in EAV

The B cell ELISpot was used to quantify antigen-specific antibody producing cells, the method for rat B cell ELISpot assay was adapted in our laboratory from a commercially available kit designed for use in mice.[395] ELISpot filter plates (Multiscreen HTS 96 well filter plates, Merck Millipore) were activated using 70% ethanol and washed 5 times using sterile water, they were then coated with human MPO diluted at 50µg/ml in PBS and incubated at 4°C overnight. Plates were washed 5 times and blocked with 10% FCS in RPMI (Gibco) for one hour. After sacrifice of animals, spleens were dissected and kept on ice in cold HBSS, spleen was passed through a 100µm cell strainer with cold, sterile PBS. Red blood cells were lysed using a commercially available red cell lysis buffer (ebioscience), lysis buffer was neutralised using culture media (RPMI with 10% FCS, 2% penicillin and streptomycin, 2mM L-glutamine) and cells centrifuged at 1500rpm (350g) for 5 minutes. Cells were re-suspended to a concentration of $5x10^6$/ml. After removing block buffer and washing the plate 100µl of cell suspension was added per well and plates incubated at 37°C in 5% CO_2 for 48 hours. Wells were washed 5 times with PBS, biotinylated rabbit anti-rat immunoglobulin antibody (Dako) diluted 1:250 in PBS added and plates incubated for 2 hours at

room temperature. After further washes extravadin-ALP conjugate (Sigma) diluted 1:1000 in PBS was added and plates incubated at room temperature for one hour. Following further washes plates were developed in 5-bromo-4-chloro-3-indolyl phosphate/nitro blue tetrazolium (BCIP-NBT) solution (Sigma) and the reaction stopped with distilled water. Plates were dried and spots per well quantified using an ELISpot plate reader and software (ELISpot 4.0, Autoimmun Diagnostika, Strassberg, Germany).

2.14 Human in vitro methods

2.14.1 Study approval for use of human cells and tissue

Human renal tissue samples were obtained from patients using the Imperial College Healthcare NHS Trust Tissue Bank (Application R10015). Blood samples and plasma exchange fluid were obtained from patients under local ethics committee approval (04/Q0406/25 NHS National Research Ethics Committee London - West London & GTAC).

2.14.2 Neutrophil and PBMC isolation

Neutrophils and PBMC were isolated using dextran sedimentation and Percoll® density gradient. Up to 20mls of EDTA blood was taken from patients with AAV and healthy controls. Blood was used as soon as possible after venesection up to a maximum of one hour. Blood was mixed with 6% dextran (Sigma)/0.9% NaCl solution in a 1:2 ratio in a 50ml centrifuge tube and the tube gently inverted to mix. Blood/dextran mix was then poured into 15ml falcon tubes, the lids placed on loosely and left to sediment for 30mins at room temp. Percoll® gradient was prepared. 9ml of Percoll® was made isotonic by adding 1ml of 10 x PBS, then 3 layers prepared; ‘bottom’ 81%

layer, ‘middle’ 68% and ‘top’ 55%. 3mls of the bottom layer was placed in a 15ml centrifuge tube and 3mls of the middle layer carefully layered on top. After dextran sedimentation the supernatant was removed to a new centrifuge tube and centrifuged at 350g for 6 minutes at 20°C. Supernatant was aspirated and discarded and the cell pellet re-suspended in 3mls of 55% Percoll and carefully layered on top of the 81/68 layered gradient. Gradients were centrifuged at 700g for 20 minutes at room temperature with brake and acceleration at 0. PBMC were harvested from the 68/55 interface and granulocytes from the 68/81 interface using a Pasteur pipette and cells placed in a fresh 15ml centrifuge tube. 1xPBS was added to PBMC samples up to 15mls. Red blood cells were lysed in the neutrophil sample by adding 6mls of sterile ddH_20 for 20 seconds followed by 2ml of 0.6M KCl to restore tonicity and mixing then topping up samples to 15mls with 1xPBS. Samples were centrifuged at 250g for 6 minutes at 20°C with brake 9 and acceleration 5. If necessary red cell lysis was repeated once more. Cells were re-suspended in RPMI supplemented with 10% FCS, 2mM L-glutamine, and 2% penicillin and streptomycin, counted using a haemocytometer and adjusted to a concentration of $5x10^6$ cells/ml.

2.14.3 Flow cytometry

$0.25x10^6$ cells per antibody were re-suspended in 0.5% BSA in PBS and incubated with fluorochrome conjugated antibodies directed against P2X7 or neutrophil cell surface markers as detailed in Table 2.4. Cells were washed in PBS and centrifuged at 250g for 5 minutes twice and fixed using 2% PFA in PBS. Yo-pro-1 Iodine (491/509) and To-pro-3 Iodine (642/661) uptake assays were performed as described in 2.8.3. Cells were analysed on the BD Accuri C6 flow cytometer (BD Biosciences, Oxford, UK) and gating strategy and analysis performed using FlowJo v10 software.

2.14.4 Kwikdiff staining

Cells were re-suspended in PBS at a concentration of $5x10^4$ cells/ml and 100µl of cells applied to poly-L-Lysine coated slides using a cytospin centrifuge (Cytospin 2, Shandon, ThermoFisher) at 450rpm for 3 minutes. Slides were dried at room temperature for 1 hour then stained with KwikDiff™ (ThermoFisher) by immersing slides in solution 1 (methanol- fixative) for 30 seconds, solution 2 (Eosin) for 1 minute and solution 3 (Methylene blue) for 2 minutes. Slides were allowed to air dry before imaging using light microscopy to assess cytoplasmic and nuclear morphology.

2.14.5 Isolation of MPO-ANCA IgG

MPO ANCA IgG was isolated from plasma exchange fluid from patients with AAV and healthy control IgG from serum from healthy controls using a protein G sepharose column with the same method as described for rat serum in 2.13.5.

2.14.6 Anti-MPO ELISA

Anti-MPO antibody titre in IgG preparations was measured using a commercially available human anti-MPO antibody direct ELISA (AssayPro, St Charles, USA). The microplate provided is pre-coated with myeloperoxidase and a standards curve prepared from anti-MPO IgG. Samples were diluted between 1:2 and 1:50 in provided assay diluent and 50µl of samples or standards added in duplicate to the plate and incubated at room temperature for 6 hours. Plates were washed 5 times and 50µl of HRP-conjugate added per well and plates incubated for 1 hour at room temperature. Plates were washed again and 50µl stabilized peroxidase chromogen substrate tetramethylbenzidine added, plates incubated for 20 minutes and 50µl stop solution added. Plates were read using a microplate reader at 450nm, a standard curve constructed of mean 450nm

absorbance on the y-axis and log concentration on the x-axis and unknown concentrations determined using a four parameter logistic curve fit.

2.14.7 Neutrophil and PBMC stimulation

Cells were divided into 96 well round bottom cell culture plates with $0.25x10^6$ cells/well. Two stimulation protocols were used, some cells were stimulated with LPS 1µg/ml for 4 hours followed by ATP 5mM for 30 minutes with either 10µM P2X7 antagonist (A438079, Tocris) or vehicle (0.01% DMSO) added for 30 minutes prior to ATP. Alternatively cells were stimulated with MPO-ANCA IgG. Cells were primed with TNFα 2ng/ml (Peprotech) for 30 minutes, then MPO-ANCA IgG or control IgG 100µg/ml for 4 hours and finally ATP 5mM for 30 minutes. If P2X7 antagonist was used it (or vehicle) was added for 30 minutes prior to ATP stimulation as in the experiment using LPS and ATP. At the end of the experiment plates were centrifuged at 1500rpm for 5 minutes and supernatant collected and stored at -20°C until use. Cytokine production was analysed using IL-8 and IL-1β ELISAs (R+D) as described in 2.7.2.

2.14.8 RNAscope

Detection of P2X7 mRNA in tissue sections was carried out using RNAscope® (ADCBio, Newark USA). Formalin fixed, paraffin embedded human renal biopsy tissue surplus to clinical requirements was retrieved from the histology archive at Hammersmith Hospital, London, UK. Fresh sections were cut at 4µm thickness using a microtome (Anglia Scientific) onto poly-L-Lysine coated slides, slides were always used within 24 hours of sectioning. Slides were baked for one hour at 60°C then de-waxed in 2 consecutive baths of xylene followed by 2 consecutive baths of ethanol and allowed to dry at room temperature for 5 minutes. Endogenous peroxidases were

blocked by incubating sections with H_2O_2 for 10 minutes. Antigen retrieval was performed by boiling slides in TR reagent (ADCBio) at 98-102°C on a hotplate. Slides were washed in dH_2O twice followed by 100% ethanol and air drying slides at room temperature. Sections were encircled using wax pen to prevent run-off of solutions and allowed to dry completely at room temperature. 4 drops of Protease Plus (ADCBio) was added to each section and slides were incubated in a HybEZ™ oven at 40°C for 30 minutes followed by washing twice in dH_2O. Probes were warmed to 40°C and allowed to cool to room temperature before use and amplification reagents warmed to room temperature. 4 drops of probe were added to each section and slides returned to the HybEZ™ over for 2 hours. For each sample, one slide was incubated with a P2X7 probe and one with a PPIB probe as a positive control to check integrity of RNA, one slide per run was incubated with DapB, a bacterial gene as a negative control. Slides were then washed twice in wash buffer and a series of 6 amplification probes added with 2 washes in wash buffer after each step. Probes 1, 3 and 5 were incubated for 30 minutes and 2, 4 and 6 for 15 minutes, steps 1-4 were incubated in the HybEZ oven at 40°C and 5-6 at room temperature. After the 6th amplification steps slides were washed twice more, 80µl of red detection reagent added to each section and slides incubated in a covered tray for 10 minutes at room temperature. Slides were washed 5 times in dH_2O and counterstained for 30 seconds in Mayer's haematoxylin. Slides were washed in dH2O, dried at 60°C for 45 minutes, slides dipped briefly in xylene and mounted using Vectamount™ (Vector Labs) and glass cover slips

2.15 Statistical analysis

Statistical analysis was carried out and graphs constructed using Prism 7 (GraphPad Software Inc., San Diego, California). Where statistical tests are used this is detailed in the text or figure legend. Statistical tests used are indicated in the text. Normally distributed variables were compared using

t test for two variables or one way analysis of variance (ANOVA) for multiple variables with Dunnett's post-hoc correction to compare groups to a control group or Bonferroni post-hoc correction for multiple comparisons. For non-parametric data (or with small number of replicates) Mann Whitney U test was used for two variables or Kruskall-Wallis test for multiple variables with Dunn's post-hoc test to compare individual groups. For linear correlation Pearson correlation coefficient was used. Power calculations were used to select the number of animals per group used, for example in the EAG experiments comparing WKY WT and P2X7 KO , 6 rats per group would be sufficient to detect a 20% change in the number of severely abnormal glomeruli with 80% power.

Chapter 3: Characterisation of the P2X7 knockout rat and P2X7 responses in bone marrow derived cells

3.1 Introduction

The P2X7 knockout (KO) rat is a novel strain which has not yet been described in the literature, therefore a detailed characterisation of P2X7 deficient rats is an important part of my project. The P2X7 KO strain had no issues with breeding, with normal litter sizes and pregnancies. They were observed to be smaller in size and weight than age matched WKY WT rats. P2X7 is known to play a role in osteoclast function and bone development and one study has shown P2X7 deficient mice have decreased bone mineral density.[50] It is possible that the P2X7 KO rats have defects in bone development; however observations regarding their size and body weight is not in comparison to littermate controls and the WKY WT rats have been bred at an external facility.

3.1.1 P2X7 protein expression

P2X7 KO and WKY WT controls were sacrificed for tissue donation. Western blotting of protein and cell lysates from different tissue and cell types using the Alomone 004 antibody (which binds to the C terminus of P2X7) did not show any P2X7 protein in the cells or tissue from the knockout rat except for brain tissue where a double band is observed. The expression of P2X7 in the brain is a controversial area which has been addressed by others and it is unclear if this band represents a P2X7 related protein or a P2X7 splice variant.[51] No P2X7 protein was detected in heart or liver tissue from either P2X7 KO or WKY WT rats despite P2X7 being reported to be expressed by cardiac muscle.[54] (Figure 3.1)

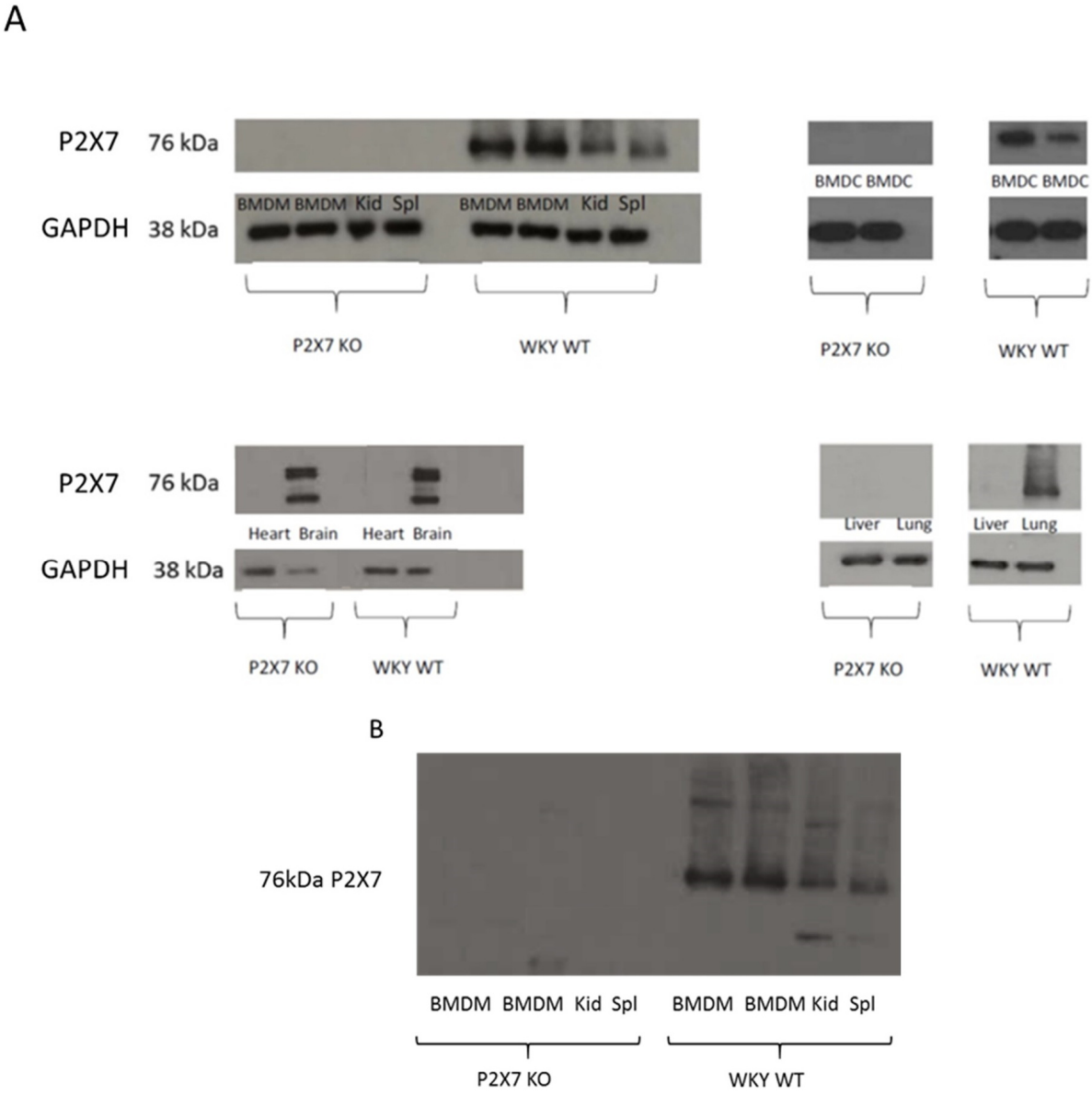

Figure 3.1 Expression of protein extracted from tissues and cells from the P2X7 KO and WKY WT rats.

(A) Tissue homogenates and cell lysates from different tissues and cell types were used for Western blotting with an antibody directed against the C terminus of P2X7. No protein was detected in tissue and cells from the P2X7 deficient rat except for in brain where a double band is detected in both P2X7 KO and WKY WT tissue. The double band has one band slightly larger and one slightly smaller than P2X7 detected in other tissues. No P2X7 was detected in liver or heart from either WKY WT or P2X7 deficient rats. This is representative of ≥3 biological replicates for each tissue and cell type.
(B) Representative whole western blot for P2X7 using an antibody directed against the C terminus
BMDM: Bone marrow derived macrophages, BMDC: Bone marrow derived dendritic cells, Kid: Kidney, Spl: Spleen

The 004 antibody would detect both P2X7A and P2X7K the two known isoforms of P2X7 in the rat. However there are splice variants in mice and humans which are missing the C terminus or have an alternative C terminus that would not be detected by this antibody. Attempts to detect protein using an antibody directed against the extracellular domain of the protein (008), were not successful due to high levels of non-specific binding. This antibody could be used with greater success for immunoprecipitation, spleen homogenate was used for this experiment as spleen is known to have high P2X7 expression. Both the 004 and 008 (extracellular domain) antibodies identified a band corresponding to P2X7 in spleen from WKY WT rats which was not present when a control antibody was used or in P2X7 KO rat spleen (Figure 3.2).

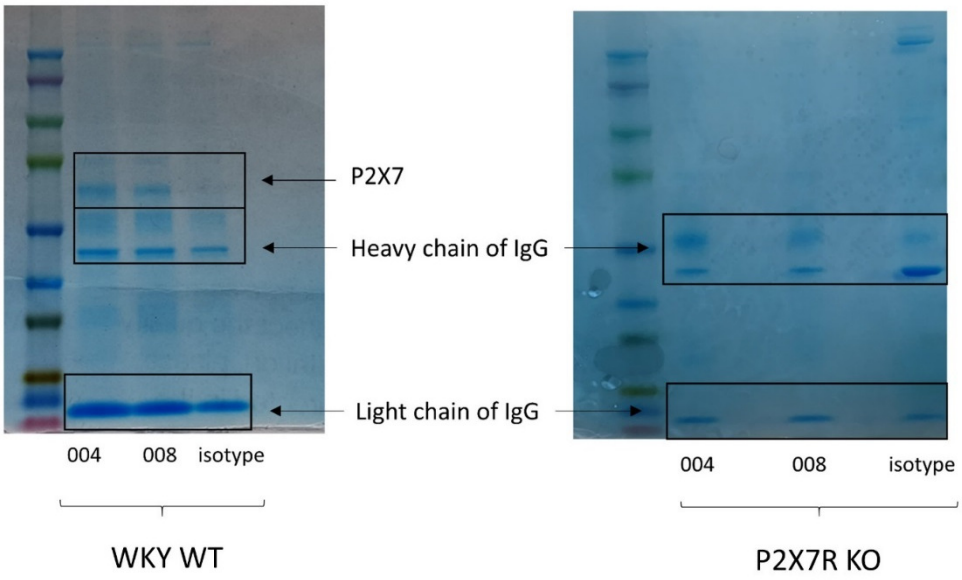

Figure 3.2 Immunoprecipitation of spleen homogenate from P2X7 KO and WKY WT rats. Spleen homogenate was used for IP with P2X7 004 (C terminus), P2X7 008 (extracellular) or isotype control (polyclonal rabbit IgG) antibody. Coomassie staining of gels run of the eluted antibody/protein complexes shows a 70kDa band corresponding to P2X7 when both 004 and 008 antibodies were used with WKY WT spleen homogenate. This band was absent when P2X7 KO rat spleen was used or when the isotype control antibody was used. The gels are representative of 2 biological replicates

3.1.2 P2X7 mRNA expression

Next I investigated the expression of P2X7 at the RNA level using RT-qPCR and could detect similar levels in cells and tissues from both P2X7 KO and WKY WT rats. RT-qPCR does not differentiate between mutated mRNA (in the KO) and un-mutated mRNA (in the WT) and when standard PCR was performed using primers to produce a PCR product of sufficient length for sequencing (carried out by the CSC genomics lab, MRC, Imperial College London) the 2 base pair insertion was present in mRNA from the KO rat. This insertion results in mis-sense and a premature stop codon which should not be translated into protein (Figure 3.3). As shown I could not detect any P2X7 protein in the P2X7 KO rat and so despite the presence of mRNA by RT-qPCR this does not seem to be translated to protein.

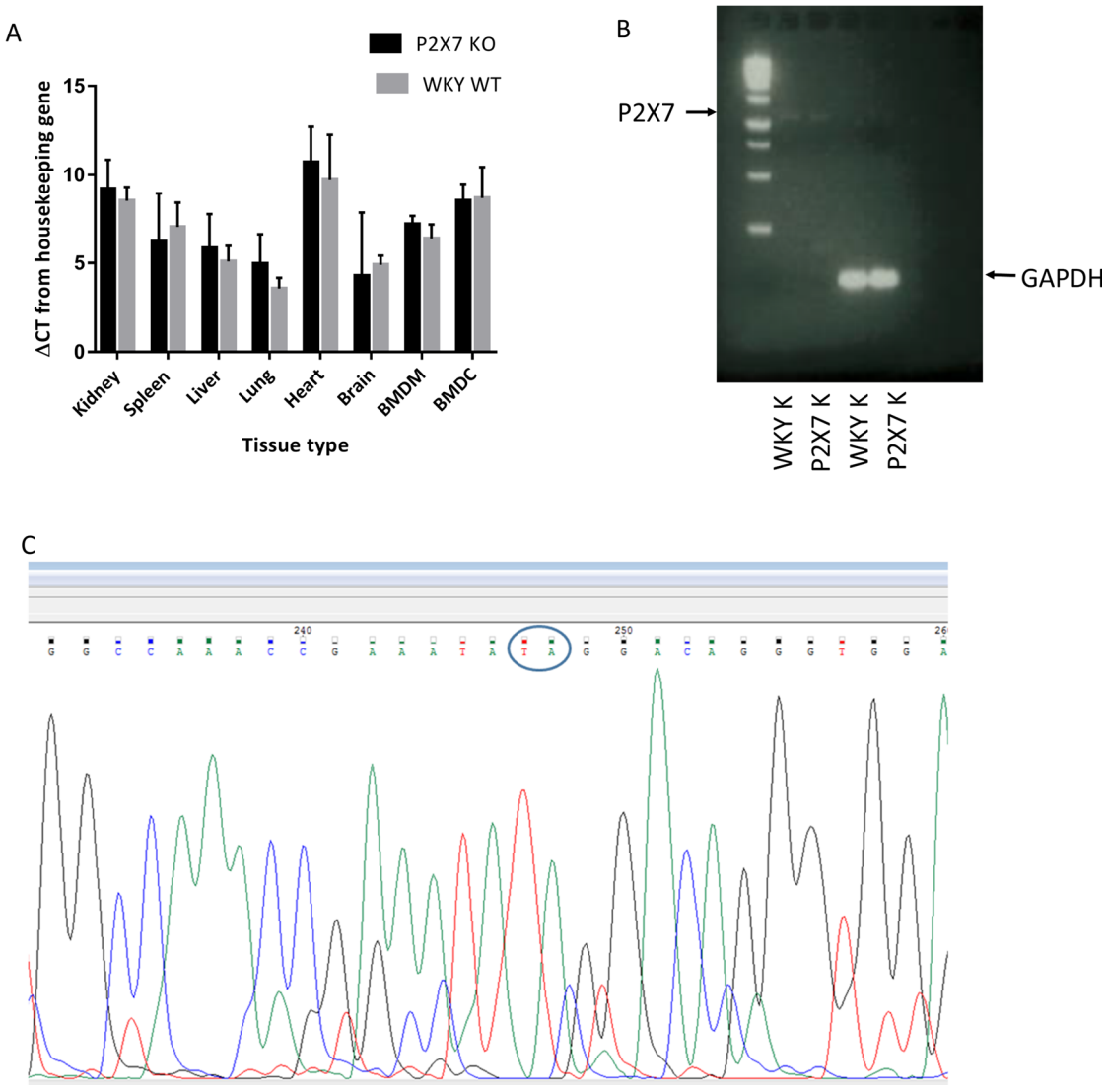

Figure 3.3 Expression of P2X7 RNA in tissues and cells from P2X7 KO and WKY WT rats.
(A) RT-qPCR for P2X7 in various tissues and cells from WKY WT and P2X7 KO expressed as mean ΔCT with SEM. (B) PCR products separated by gel electrophoresis showing a band corresponding to P2X7 in both WKY and P2X7 KO kidney. (C) Example of Sanger sequencing result of PCR products from P2X7 KO rat with two base pair insertion within circle.

BMDM: Bone marrow derived macrophages, BMDC: Bone marrow derived dendritic cells, K: Kidney

3.2 Bone marrow derived cells

BMDM and BMDC were differentiated from unsorted bone marrow cells as described in Chapter 2.6. Cells were used for cell surface staining and analysed using flow cytometry, demonstrating that both cell types express Cd 11b/c but that BMDC have higher cell surface expression of MHC class II and the DC co-stimulatory markers CD80 and CD86. (Figure 3.4)

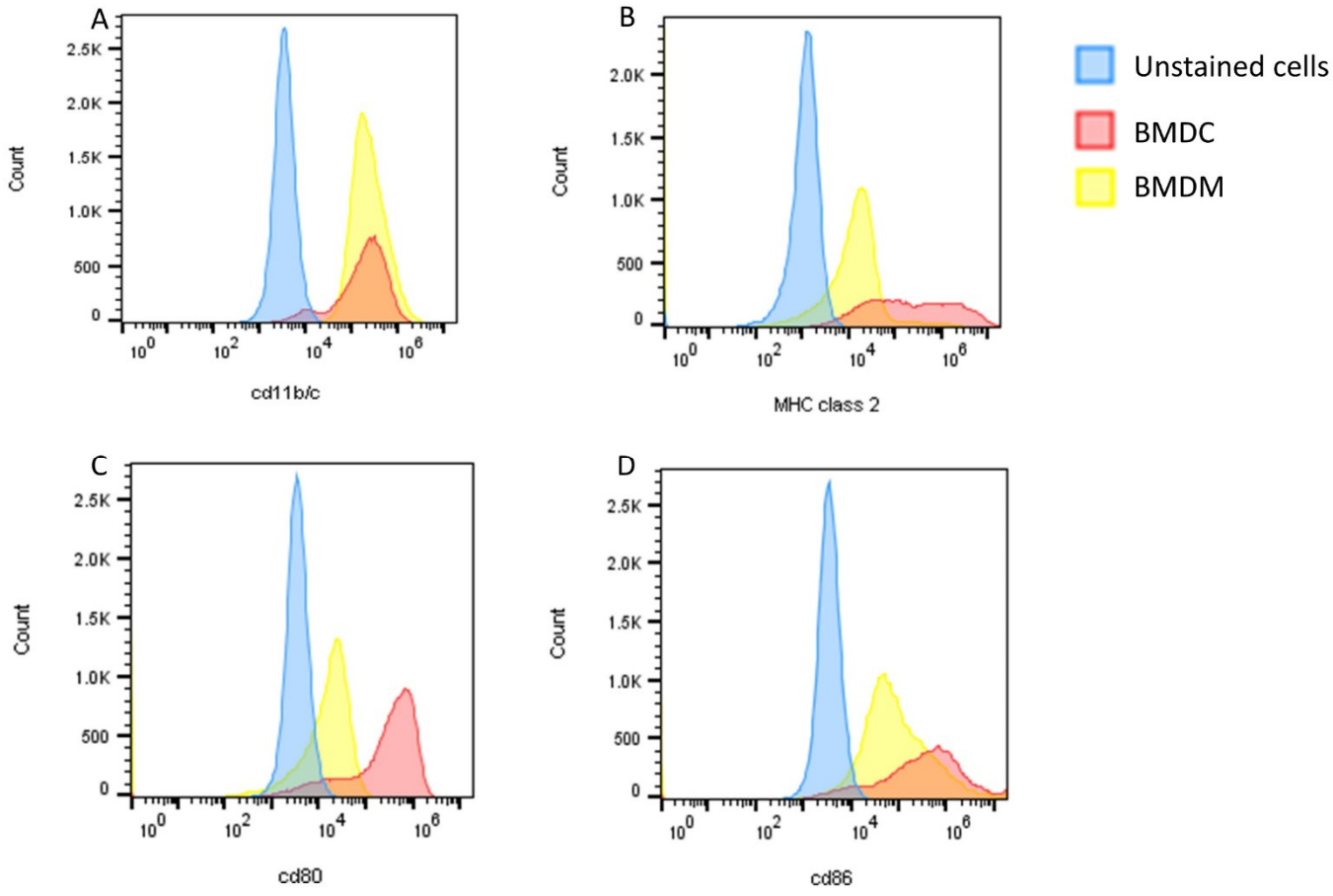

Figure 3.4 Cell surface staining of BMDM and BMDC
Cell surface staining of BMDM and BMDC for (A) CD11b/c, (B) MHC class II, (C) CD80 and (D) CD86.

3.2.1 P2X7 pore formation in bone marrow derived cells

In order to investigate the presence of functional P2X7 receptors on BMDM and BMDC I used the fluorescent dye Yo-pro-1 to assess P2X7 related pore formation in response to stimulation of cells with BzATP. BzATP is a more potent agonist at P2X7 than ATP and as such results in rapid pore formation than can be measured in real time. As expected, cells from WKY WT rats rapidly formed pores and took up Yo-pro-1 fluorescent dye in response to stimulation with BzATP and P2X7 KO cells did not. LPS priming of cells did not alter the uptake of dye (Figure 3.5).

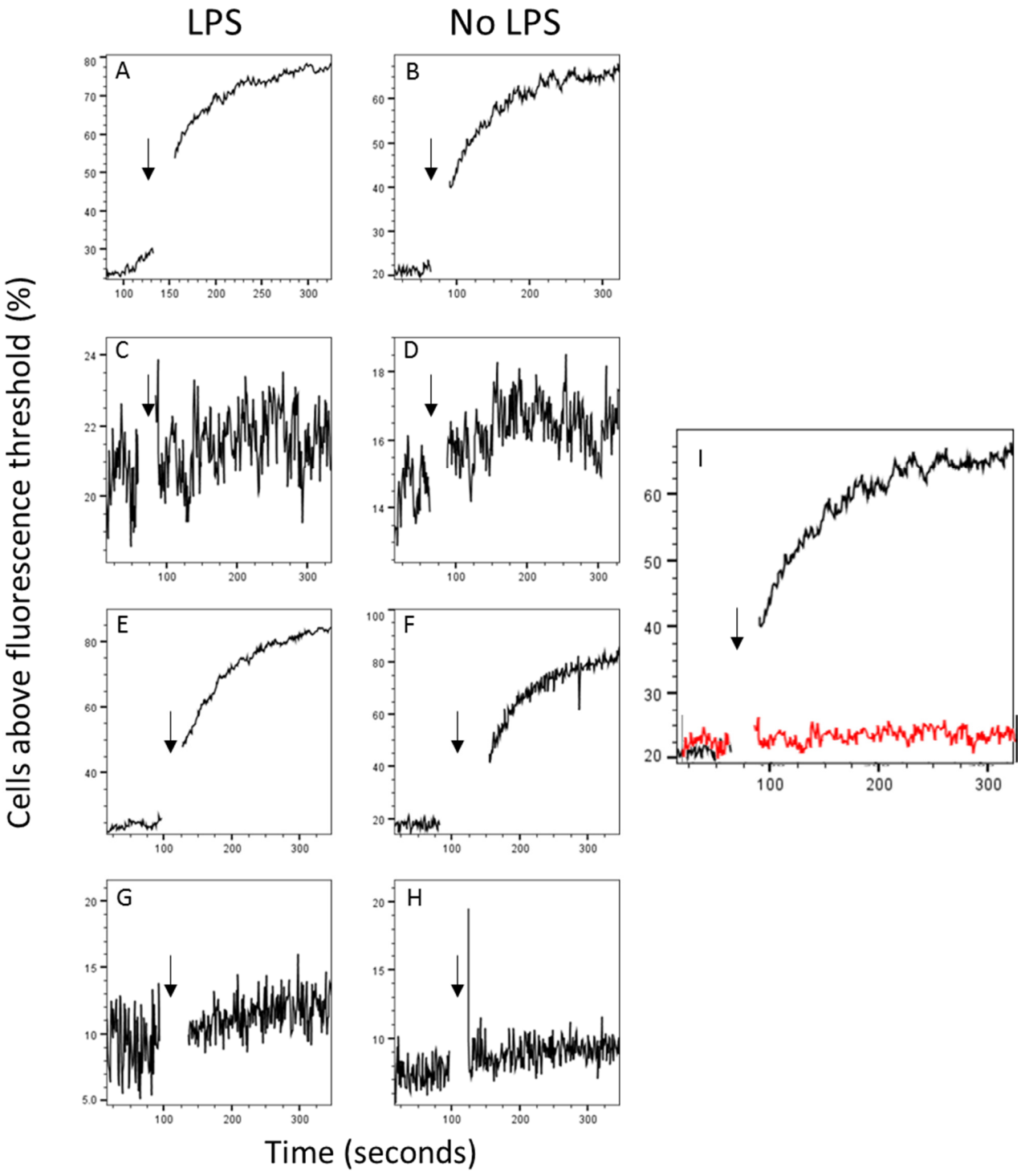

Figure 3.5 P2X7 pore formation in BMDC and BMDM

Cells were primed with and without 1µg/ml LPS for 4 hours prior to analysis of Yo-pro-1 fluorescent dye uptake. Following determination of baseline fluorescence 150µM BzATP was added to cells at the arrows. (A) and (B) WKY WT BMDC, (C) and (D) P2X7 KO BMDC, (E) and (F) WKY WT BMDM, (G) and (H) P2X7 KO BMDM. Please note differing y axis scales between graphs meaning an irregular baseline is seen in panels with no dye uptake. For clarity panel (I) represents an overlay of (B) and (D) with WKY WT BMDC in black and P2X7 KO BMDC in red. Images are representative of 3 biological replicates.

3.2.2 IL-1β release from bone marrow derived macrophages

I also assessed P2X7 functionality on cells from P2X7 KO and WKY WT by investigating cytokine production from BMDM in response to extracellular ATP. As expected WKY WT BMDM produced significant amounts of IL-1β when primed with 1µg/ml LPS and stimulated with 5mM ATP when compared to cells stimulated with LPS alone, ATP alone or media. BMDM from P2X7 KO rats did not produce significant amounts of IL-1β under any of these conditions. (Figure 3.6)

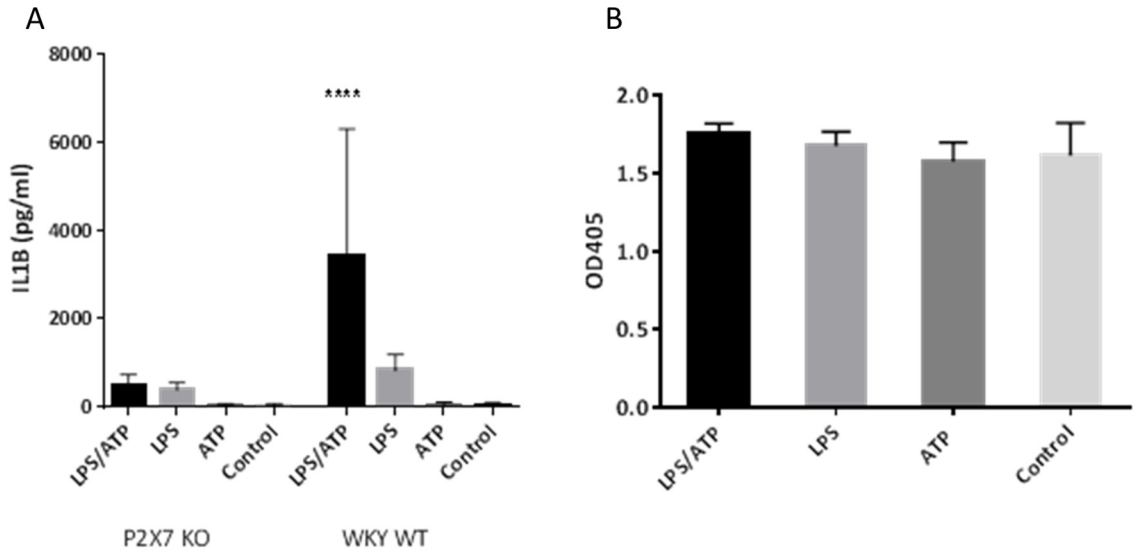

Figure 3.6 IL-1β production from BMDM stimulated with LPS and ATP
(A) BMDM from WKY WT rats but not P2X7 KO produce IL-1β following stimulation with 1µg/ml LPS for 4 hours followed by 5mM ATP for 30 minutes. (B) MTT assay results show that this method of stimulation is not toxic to cells with similar levels of cell proliferation between different assay conditions. Data shown are mean with SEM. Statistical analysis was performed using one-way ANOVA followed by Dunnetts post-hoc analysis to compare to WKY WT control cells. ***p<0.001

Although the IL-1β ELISA should preferentially detect bioactive IL-1β it is possible that the presence of pro IL-1β could be causing a false positive results and so western blotting using protein precipitated from supernatants was performed to confirm the presence of the 17.5 kDa cleaved protein. Cleaved IL-18 and cleaved caspase-1 were also detected in supernatants from WKY WT BMDM stimulated with LPS and ATP. As expected, LPS stimulation caused an up-regulation of pro IL-1β in cell lysates from both P2X7 KO and WKY WT BMDM, Full length caspase-1 and pro-IL-18 are constitutively expressed (Figure 3.7).

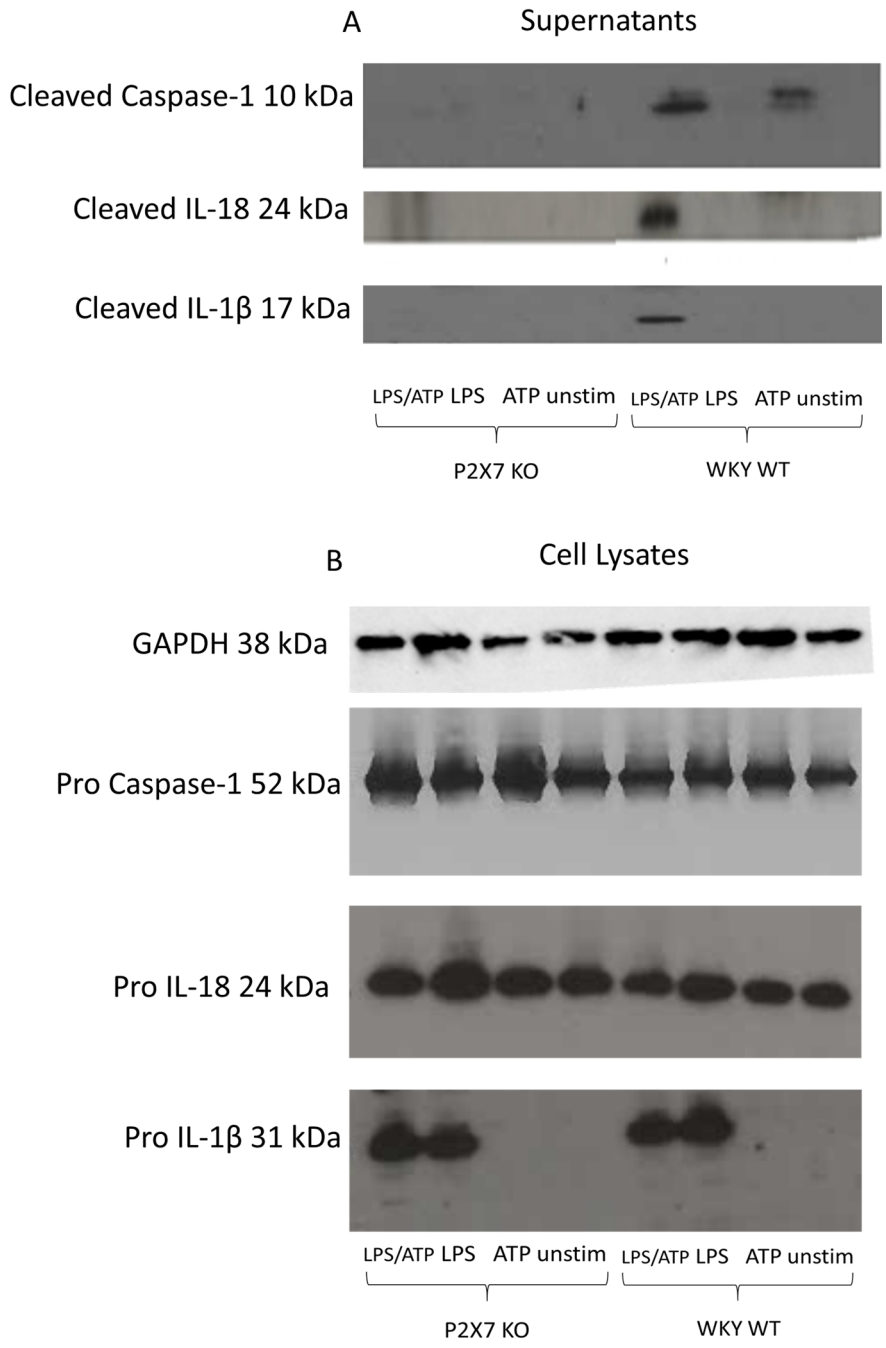

Figure 3.7 IL-1β, IL-18 and caspase-1 production from BMDM stimulated with LPS and ATP
(A) Supernatants and (B) Cell lysates. In response to stimulation 1µg/ml LPS for 4 hours followed by 5mM ATP for 30 minutes there is release of mature IL-1β and IL-18 and caspase-1 into supernatant from WKY WT but not P2X7 KO BMDM. In cell lysates Pro caspase-1 and pro IL-18 are constitutively expressed. Pro IL-1β is up-regulated in both WKY WT and P2X7 KO BMDM in response to LPS stimulation both with and without ATP. Western blot image is representative of >3 biological replicates.

To confirm that release of IL-1β from WKY BMDM was P2X7 dependent I also used a P2X7 antagonist, A438079, incubated with cells for 30 minutes prior to addition of ATP. 10μM of antagonist was sufficient to completely inhibit release of cleaved IL-1β and cleaved caspase-1 in response to LPS and ATP stimulation. There was no effect on intracellular pro IL-1β in cell lysates (Figure 3.8). MTT assay showed that the antagonist was not toxic to cells at any of the concentrations used (data not shown).

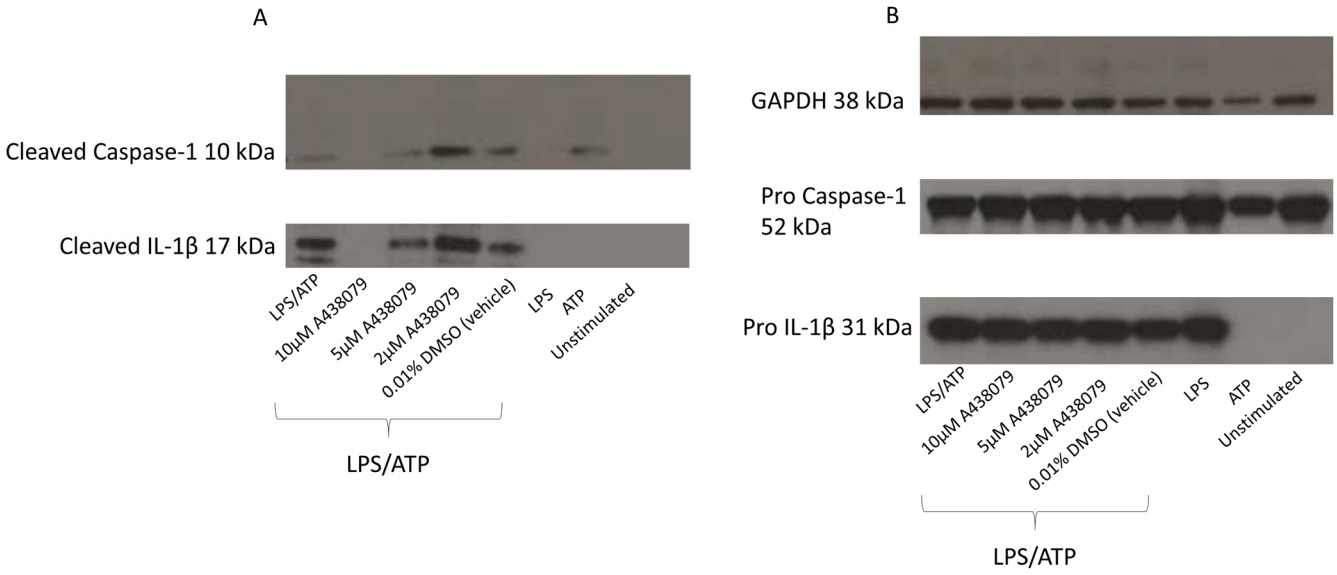

Figure 3.8 IL-1β and caspase-1 production from WKY WT BMDM stimulated with LPS and ATP with P2X7 antagonist

(A) Supernatants and (B) Cell lysates. In response to stimulation with 1μg/ml LPS for 4 hours followed by 5mM ATP for 30 minutes there is release of mature IL-1β and caspase-1 into supernatant from BMDM. This is inhibited when cells were incubated with 10μM of P2X7 antagonist (A438079) for 30 minutes prior to addition of ATP. In cell lysates Pro caspase-1 is constitutively expressed. Pro IL-1β is up-regulated in response to LPS stimulation both with and without ATP and the addition of P2X7 antagonist had no effect on this. Western blot image is representative of >3 biological replicates.

IL-1β production by BMDM was associated with caspase-1 activation downstream of P2X7 and cleaved caspase-1 was released into supernatant in response to stimulation of cells with ATP. To confirm this mechanism I used a competitive, irreversible caspase-1 inhibititor, Ac-YVAD-cmk, which was added to cells for 30 minutes prior to addition of ATP. 50μM and 10μM concentrations of inhibitor were both sufficient to completely inhibit release of cleaved IL-1β; as expected there

was no effect on release of caspase-1 (Figure 3.9). Again, MTT assay showed the drug had no significant cytotoxicity at these doses.

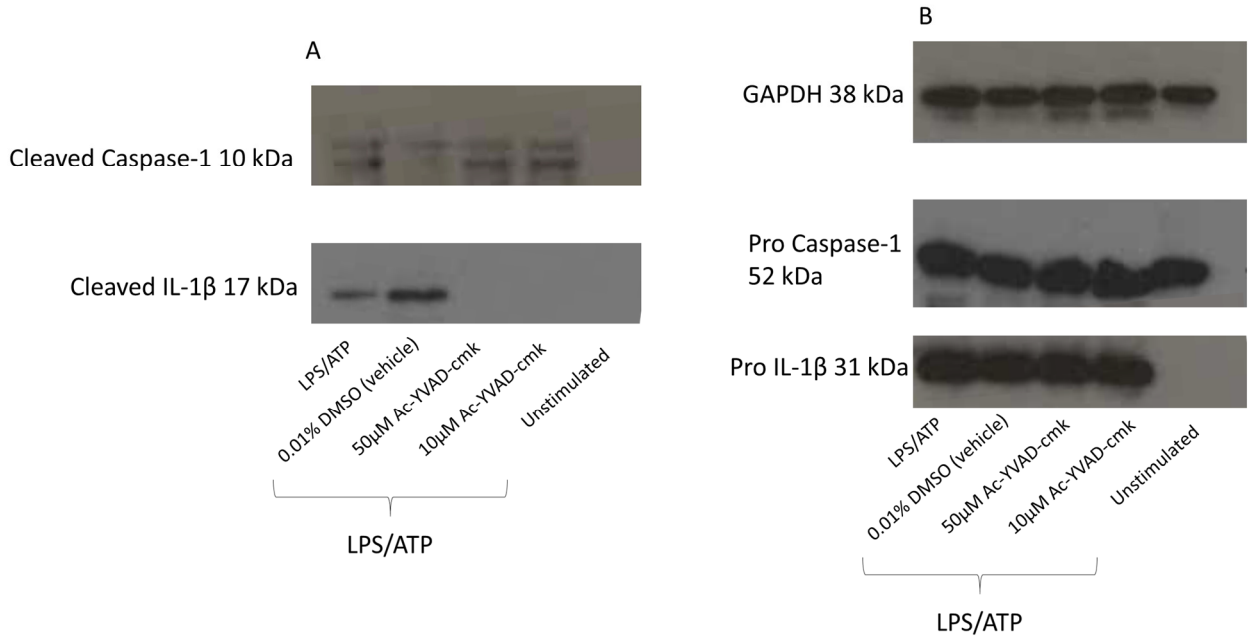

Figure 3.9 IL-1β and caspase-1 production from WKY WT BMDM stimulated with LPS and ATP with caspase-1 inhibitor

(A) Supernatants and (B) Cell lysates. In response to stimulation with 1μg/ml LPS for 4 hours followed by 5mM ATP for 30 minutes there is release of mature IL-1β and caspase-1 into supernatant from BMDM. This is inhibited when cells were incubated with 50 μM or 10μM of caspase-1 inhibitor (Ac-YVAD-Cmk) for 30 minutes prior to addition of ATP. It had no effect on release of caspase-1 into supernatant. In cell lysates Pro caspase-1 is constitutively expressed. Pro IL-1β is up-regulated in response to LPS stimulation both with and without ATP and the addition of caspase-1 inhibitor had no effect on this. Western blot image is representative of 3 biological replicates.

3.2.3 IL-1β release from bone marrow derived dendritic cells

I next investigated P2X7 function on BMDC. Cells were stimulated with 1µg/ml LPS for 4 hours followed by 5mM ATP for 30 minutes and supernatants used for Western blot. Both WKY WT and P2X7 KO BMDC could release cleaved IL-1β in response to stimulation with LPS with or without the addition of ATP. In cell lysates there was up-regulation of pro IL-1β in both P2X7 KO and WKY WT BMDC in response to stimulation with LPS with or without addition of ATP (Figure 3.10).

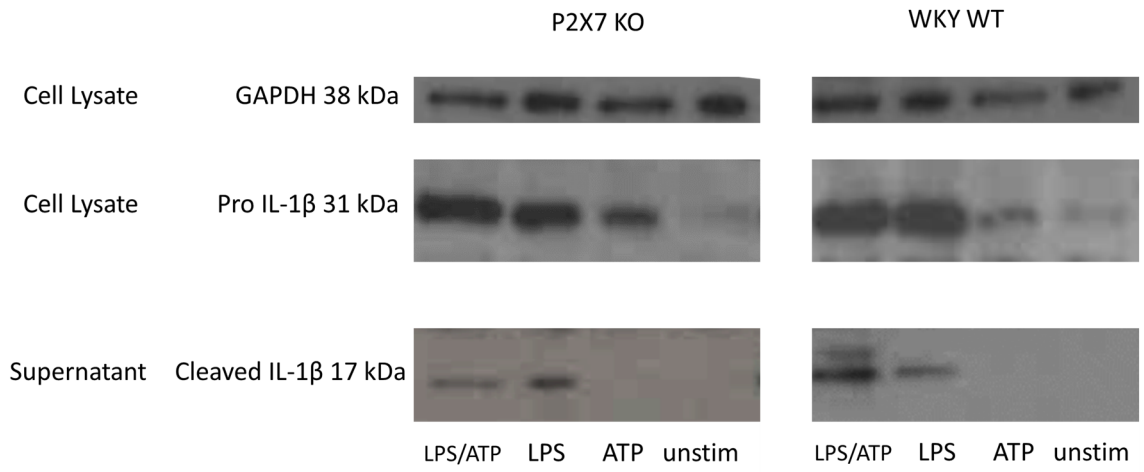

Figure 3.10 IL-1β production from BMDC stimulated with LPS and ATP
In response to stimulation with 1µg/ml LPS for 4 hours followed by 5mM ATP for 30 minutes or 1µg/ml LPS alone there is release of mature IL-1β into supernatant from WKY WT and P2X7 KO BMDC. In cell lysates pro IL-1β is up-regulated in both WKY WT and P2X7 KO BMDM in response to LPS stimulation both with and without ATP. Western blot image is representative of >3 biological replicates.

As one study reported that release of IL-1β in response to LPS alone in human monocytes was due to autocrine release of ATP acting at P2X7 receptors I wanted to ensure that the mechanism of IL-1β release was not via ATP signalling in my experiments.[125] Cells were cultured with LPS in the presence of 10U/ml of apyrase to hydrolyse any ATP produced. There was no effect on IL-1β production in either WKY WT or P2X7 KO BMDC (Figure 3.11).

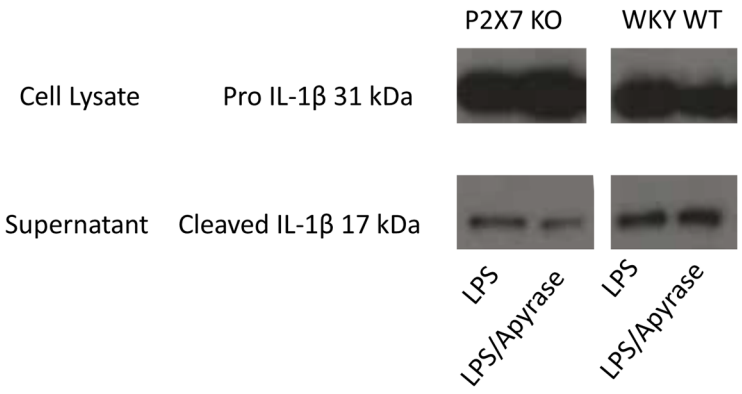

Figure 3.11 IL-1β production from BMDC stimulated with LPS in the presence of apyrase
In response to stimulation with 1µg/ml LPS for 4 hours in the presence of 10U/ml apyrase there is release of mature IL-1β into supernatant from WKY WT and P2X7 KO BMDC. In cell lysates pro IL-1β is up-regulated in both WKY WT and P2X7 KO BMDM in response to LPS stimulation. Western blot image is representative of 3 biological replicates.

ATP concentration was measured in supernatants from BMDC experiments to which no ATP had been added using the Molecular Probes^{TM} ATP determination kit. The assay is validated to detect down to 0.1 pmole of ATP and I constructed a standards curve ranging from 1mM to 0.1µM ATP. To ensure ATP had not been degraded by storage of samples prior to analysis, as a positive control I used supernatant to which ATP had been added then stored in the same manner. I could not detect any ATP in my LPS stimulated BMDC samples but positive control samples (in which 5mM ATP had been used to stimulate cells prior to storage) gave luminescent readings greater than my top standard of 1mM (results not shown).

When cell culture supernatant from BMDC experiments were used for IL-1β ELISA the results were inconsistent probably reflecting the detection of pro IL-1β (as seen on Western blot) in supernatant when cells were stimulated with LPS. It was clear however that significant amounts of IL-1β could be released from P2X7 KO and WKY WT BMDC in response to stimulation with LPS alone. In order to confirm that this IL-1β release was by P2X7 independent pathways cells were pre-incubated with 5 or 10µM of P2X7 antagonist (A438079) prior to the addition of 1µg/ml LPS.

In both WKY WT and P2X7 KO rats the antagonist had no effect on the production of IL-1β following stimulation with LPS (Figure 3.12).

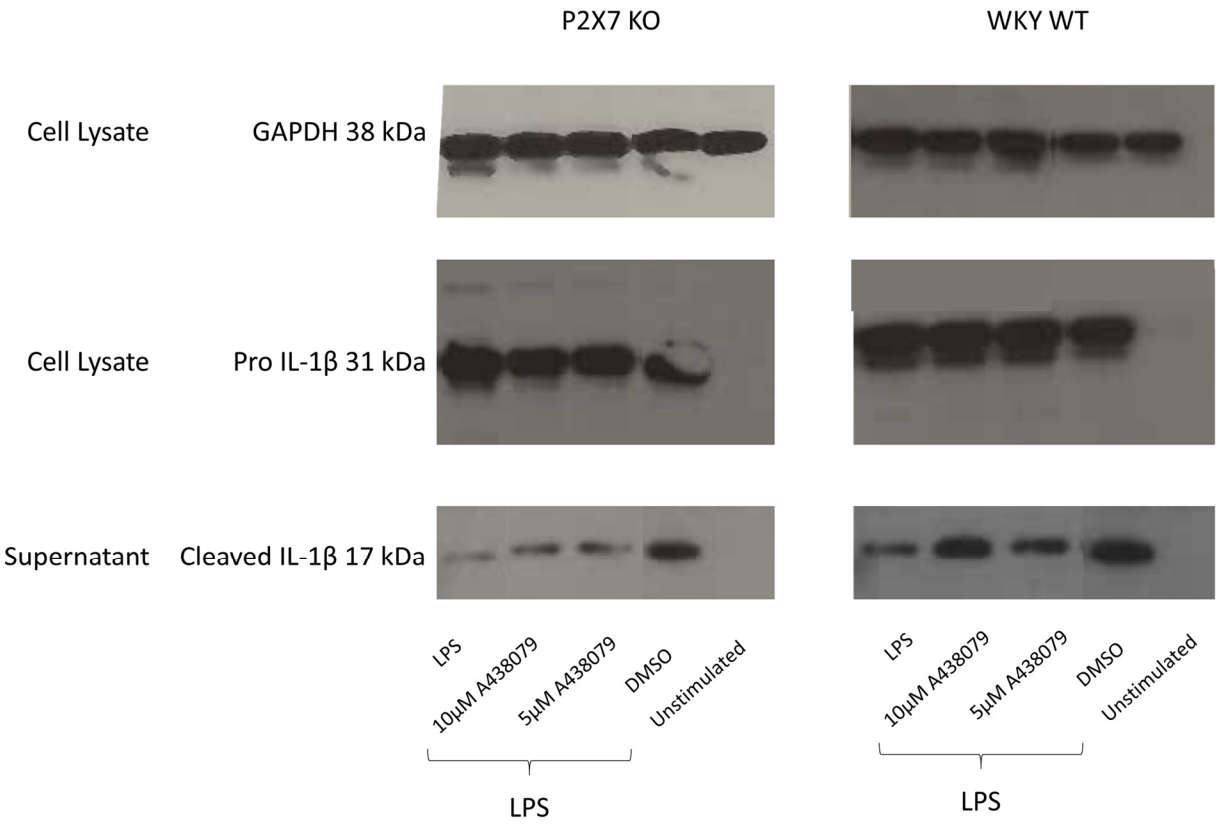

Figure 3.12 IL-1β production from BMDC stimulated with LPS and P2X7 antagonist
In response to stimulation with 1μg/ml LPS for 4 hours there is release of mature IL-1β and caspase-1 into supernatant from WKY WT and P2X7 KO BMDC. This is not inhibited when cells were incubated with 10μM of P2X7 antagonist (A438079) for 30 minutes prior to addition of LPS. In cell lysates Pro IL-1β is up-regulated in response to LPS stimulation and the addition of P2X7 antagonist had no effect on this. Western blot image is representative of 3 biological replicates.

Detection of active caspase-1 in supernatants or cell lysates from BMDC stimulated with LPS was inconsistent, possibly either due to it sometimes falling below the lower limit of detection or to it being rapidly used and cleared from supernatant and cell lysates. To determine if LPS mediated IL-1β release in BMDC was dependent on caspase-1 pathways despite being independent of P2X7 I

used the same caspase-1 inhibitor used in macrophages, Ac-YVAD-cmk, which was added to cells for 30 minutes prior to addition of LPS. Both 50µM and 10µM concentrations of inhibitor were sufficient to prevent release of cleaved IL-1β into supernatant in both WKY WT and P2X7 KO BMDC (Figure 3.13).

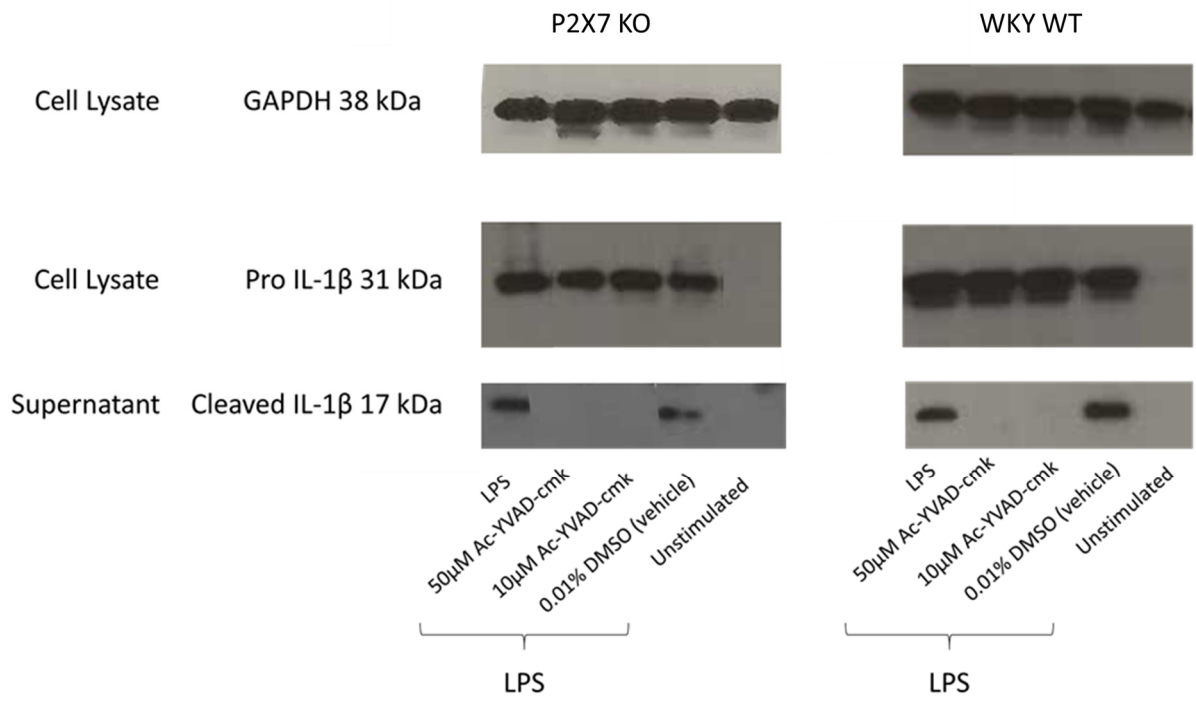

Figure 3.13 IL-1β production from BMDC stimulated with LPS with caspase-1 inhibitor
In response to stimulation with LPS (1µg/ml 4 hours) there is release of mature IL-1β into supernatant from BMDC. This is inhibited when cells were incubated with 50 µM or 10µM of caspase-1 inhibitor (Ac-YVAD-Cmk) for 30 minutes prior to addition of LPS. Pro IL-1β is up-regulated in response to LPS stimulation and the addition of caspase-1 inhibitor had no effect on this. Western blot image is representative of 3 biological replicates

As discussed in section 1.2.9, other studies in human monocytes and murine dendritic cells have shown a caspase-1 dependent, P2X7 independent pathway for cleavage of IL-1β. P2X7 dependent release of mature IL-1β has been well characterised to be dependent on K+ efflux from cells leading to activation of the inflammasome; however the role of K+ in P2X7 independent release of IL-1β

is less clearly defined with published studies generating conflicting results. In human monocytes, one group has shown that activation of the inflammasome in this pathway is by a K+ dependent process, possibly via MaxiK channels, whilst another showed this pathway was not K+ dependent but instead occurs via upstream signalling through caspase-8.[124 126] In order to determine whether rat BMDC IL-1β production is K+ dependent, I inhibited K+ efflux from cells by increasing the K+ concentration in cell culture media from 5mM (basal K+ concentration of RPMI cell culture media) to 25mM and 50mM. Normal extracellular K+ concentration is 5mM and intracellular 140mM. Several other published studies have shown that 25 and 50mM concentrations of potassium in cell culture media are sufficient to inhibit K+ efflux from cells.[126 396] Cells were allowed to equilibrate in media for 30 minutes prior to addition of 1µg/ml LPS. When K+ efflux was inhibited there was persistent release of IL-1β from both WKY WT and P2X7 KO BMDC following stimulation with LPS (Figure 3.14).

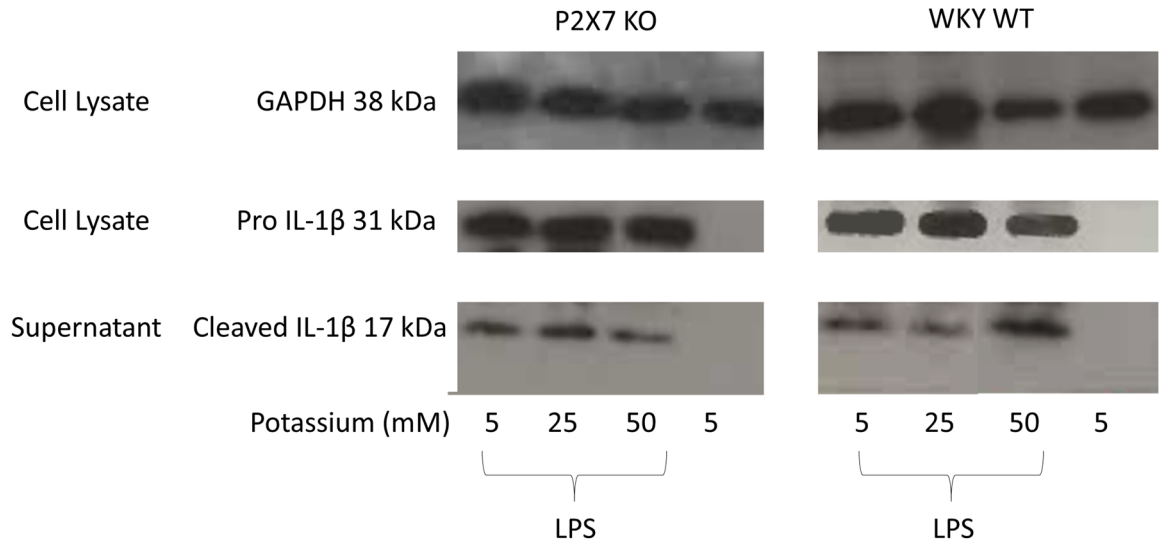

Figure 3.13 IL-1β production from BMDC stimulated with LPS with prevention of K+ efflux
BMDC were stimulated with LPS (1µg/ml 4 hours) in the presence of increasing concentrations of potassium. There is release of mature IL-1β into supernatant despite inhibiting potassium efflux from cells. Western blot is representative of two biological replicates.

My results show that BMDC can cleave active IL-1β via a P2X7 independent pathway to whereas BMDM do not seem to be able to utilise this pathway in response to stimulation with LPS. As other studies have suggested that cleavage of IL-1β in response to TLR4 stimulation alone is a much more gradual pathway, I incubated BMDM with LPS for longer time periods to see if these pathways could be engaged. Despite up to 12 hours incubation with LPS 1µg/ml, there was no release of mature IL-1β into supernatant. Pro IL-1β in cell lysates was present even with one hour LPS exposure and was significantly up-regulated from 2 hours LPS exposure (Figure 3.14).

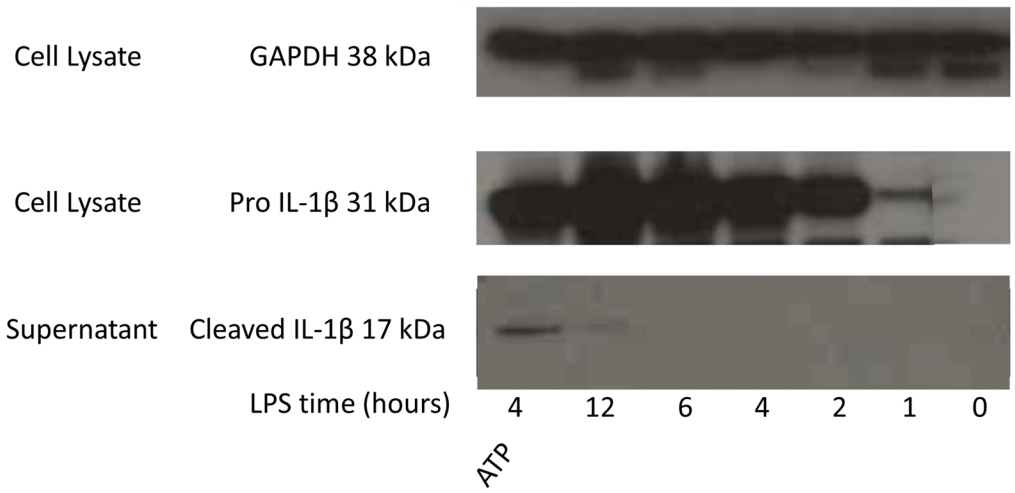

Figure 3.14 IL-1β production from WKY WT BMDM stimulated with LPS
BMDM were stimulated with LPS 1µg/ml for 1-12 hours without release of IL-1β into the supernatant. Pro IL-1β in cell lysates was significantly increased from 2 hours onwards. Western blot is representative of 2 biological replicates.

3.2.4 mRNA expression in BMDM and BMDC

I also investigated the effect of stimulation of BMDM and BMDC with LPS and ATP on mRNA for NLRP3, caspase-1, IL-1β, IL-18 and P2X7. Both P2X7 KO and WKY WT BMDM had significant up-regulation of NLRP3, IL-1β and to a lesser degree IL-18 mRNA in response to stimulation with LPS with or without addition of ATP. Caspase-1 mRNA was not up-regulated in response to stimulation with either LPS, ATP or both. P2X7 KO and WKY WT BMDC also showed up-regulation of IL-1β although to a lesser extent than seen in BMDM, fold change in BMDM stimulated with LPS +/- ATP was of the magnitude 400-500 and in BMDC was 50-80. BMDC had some up-regulation of NLRP3 mRNA following stimulation with LPS +/- ATP but this was not statistically significant and again was much smaller than that seen in BMDM. There was no increase in IL-18 or caspase-1 mRNA in BMDC. In WKY BMDM and BMDC I also investigated P2X7A and P2X7K mRNA levels, there was no up-regulation in either cell type in response to stimulation with LPS, ATP or both (Figure 3.15).

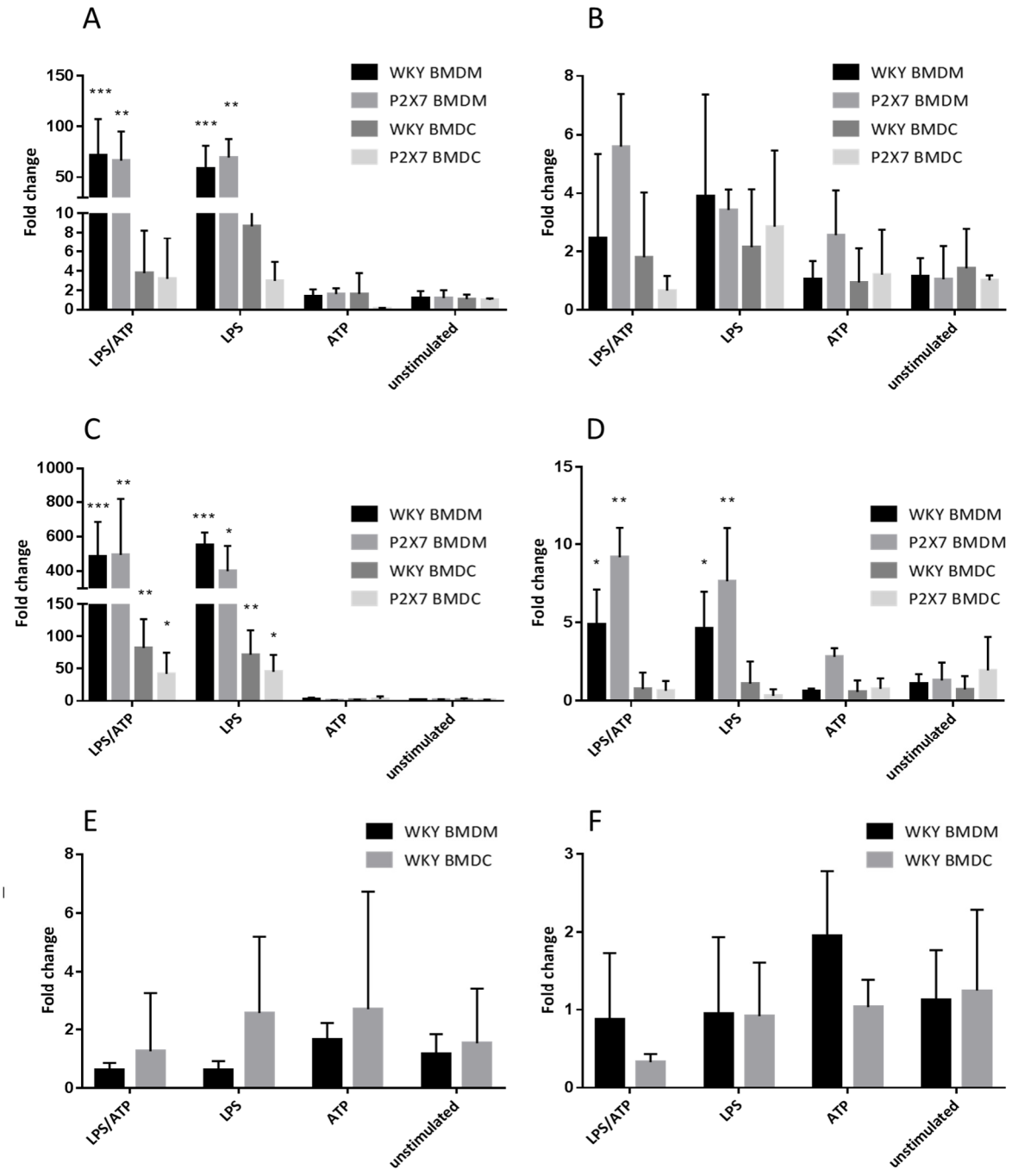

Figure 3.15 RT-qPCR analysis of mRNA expression levels of NLRP3, caspase-1, IL-1β, IL-18, P2X7A and P2X7K in BMDM and BMDC following stimulation with LPS and ATP

BMDM and BMDC from WKY WT and P2X7 KO rats were primed with LPS 1µg/ml for 4 hours followed by 5mM ATP for 30 minutes. (A) NLRP3, (B) Caspase-1, (C) IL-1β, (D) IL-18, (E)P2X7A, (F)P2X7K. ΔCT was normalised to housekeeping gene and fold change calculated using the $2^{-\Delta\Delta CT}$ method relative to unstimulated cells for each cell type. N≥3 cell culture for each condition. Data are shown as mean fold change with SEM. Statistical analysis was performed using 1-way ANOVA followed by Dunnetts post-hoc analysis. *p<0.05, **p<0.01 ***p<0.001

3.3 Discussion of results and future work

The results presented in this chapter show that the P2X7 KO rat seems to be a true knockout. I could not detect P2X7 protein in cells or tissue using either Western blotting or immunoprecipitation. A double band of protein was present in brain tissue from both P2X7 KO and WKY WT rats although it is not clear as to whether this represents P2X7 or not. Some studies have concluded that detection of P2X7 protein in the brain is actually a P2X7 like protein which is detected by the available antibodies.[51] Although P2X7 mRNA was still present in the P2X7 KO rat, sequencing has shown the presence of the 2 base pair insertion which results in mis-sense, a premature stop codon and should not be translated into protein. In addition to the lack of P2X7 protein, I was unable to detect any P2X7 function on bone marrow cells from the P2X7 KO rat differentiated into BMDM or BMDC. Cells were unable to form pores or secrete IL-1β in response to stimulation with ATP. There is the potential that there is an undescribed persistent splice variant which terminates before or lacks exon 10, and thus would escape mutation in the knockout, or that the mutated mRNA is translated into protein up to the premature stop codon at exon 10. However, I have not detected evidence of protein corresponding to this using an antibody directed against the extracellular portion of P2X7 (antibody binds to a region corresponding to the exon 4-5 junction – see Figure 1.4). Additionally, if this protein were present it would be missing the C terminus of the receptor which has been shown to be required for most P2X7 functions. P2X7J in humans which terminates at exon 8 has been shown to be non-functional when expressed alone.[152]

In order to definitively prove the presence or absence of persistent splice variants in the P2X7 KO rat it would be possible to use an RNASeq approach to detect mRNA. However this approach does not necessarily mean that P2X7 protein is produced (either as functional P2X7 or as a non-functional subunit that can oligomerise with P2X7A). This is the case with some of the identified splice variants identified in mice and humans; they are not actually expressed in native cells and tissues. Detection of specific regions of the P2X7 protein to identify splice variant protein is limited

by the range of antibodies currently available. It is possible that a mass spectrometry approach to detect P2X7 protein could identify novel splice variants in the rat, however my own experiments using an antibody directed against the extra-cellular portion of P2X7 did not result in immunoprecipitation of protein.

The other novel finding in this chapter is that BMDC do not require a second signal via P2X7 in order to produce active IL-1β. The mechanism of IL-1β production in response to LPS stimulation alone is caspase-1 dependent and independent of K+ efflux from the cell. It may be that the mechanism in rat BMDC is similar to that described by Gaidt et al in human monocytes, and LPS stimulation causes activation of an alternative inflammasome via a TRIF-RIPK1-FADD-caspase-8 dependent pathway. I would like to investigate whether caspase-8 is activated in response to LPS stimulation in my experiments, although I have been unable to identify a successful rat caspase-8 antibody for Western blotting. In human monocytes it has been reported that the 'alternative' inflammasome pathway and release of IL-1β occurs independently of pyroptosis despite the pathway involving caspase-1 maturation.[126] I would plan to investigate this in rat BMDM and BMDC either using LDH assays or a bioluminescent assay under real time imaging.

One surprising finding was that BMDC up-regulate IL-1β and NLRP3 mRNA after LPS stimulation to a much lesser degree than BMDM. This could potentially be explained by the fact that BMDC are a more heterogeneous population than BMDM as a consequence of growing and collecting all non-adherent cells. It would be useful to use a cell sorting approach to isolate a pure population of BMDC to fully investigate transcriptional differences between BMDM and BMDC following stimulation with LPS.

The ability for cells to dispense with the requirement for a second signal to produce active IL-1β could potentially be an important mechanism in the development of inflammatory diseases. It is interesting that identical bone marrow precursors can be differentiated both into cells which require a second signal and those which do not. Further work investigating the mechanism by which

P2X7/ATP independent pathways are up-regulated would be useful. Potentially this could be due to the influence of GMCSF as it has been described to be pro-inflammatory and some studies report it as interacting with the IL-1β axis.[397]

3.4 Summary of key findings

1. The P2X7 KO rat does not have detectable P2X7 protein and detected mRNA contains the 2 base pair insertion site
2. Cells from the P2X7 KO rat are unable to form pores or produce IL-1β in response to stimulation with ATP
3. BMDM require a second signal from ATP acting at P2X7 in order to cleave IL-1β
4. BMDC are able to cleave IL-1β in response to stimulation with LPS alone. This pathway is dependent on caspase-1 but independent of P2X7, ATP and K+ efflux from the cell.

Chapter 4: The effect of P2X7 knockout on severity of in vivo models of GN

4.1 Introduction

In this chapter I set out to define a role for P2X7 in rodent models of GN using the P2X7 knockout rat. Three models of in vivo glomerulonephritis were used in this thesis, NTN, EAG and EAV and are discussed in detail in 1.4.1, 1.4.2 and 1.6.2 respectively.

NTN is a passive model of crescentic anti-GBM antibody mediated GN induced by injection of nephrotoxic serum. Use of this model allows investigation of the effect of treatment or genetic modification on end organ damage and downstream effects of anti-GBM antibody while eliminating the effect interventions may have on antibody production.[267] For experiments using the knockout rat, day 28 after induction of disease was chosen as the end point of the experiment.

EAG is a rat model of anti-GBM disease which closely mirrors human disease and is induced by immunising rats with recombinant rat α3(IV)NC1. Circulating anti-GBM antibodies develop with antibody deposition in glomeruli resulting in T cell and macrophage infiltration, and necrotizing GN with crescent formation. Animals also develop pulmonary haemorrhage. Onset of proteinuria and haematuria is typically at day 18 and there are significant numbers of severely abnormal glomeruli from week 3 onwards. Day 28 was selected as the end point for experiments using this model as by this time point animals will have developed crescentic GN and lung haemorrhage but should not be at risk of developing severe renal impairment which generally occurs from around week 6 onwards and could impact on animal welfare and risk exceeding the limits of the home office license.[294]

EAV is a rat model of AAV developed in our laboratory and is induced by immunising rats with purified human MPO. Rats develop circulating anti-MPO antibodies and by week 4 after immunisation will have developed some proteinuria and haematuria. By week 6 urinary abnormalities and glomerular injury are maximal and by week 8 these findings typically begin to resolve hence day 42 was selected as the end point for this experiment. EAV is a much milder

model of renal injury than NTN and EAG with less severe glomerular injury and very infrequent crescent formation. Most animals will develop some degree of lung haemorrhage.[341]

Control animals were not routinely included in experiments to compare disease in WKY WT to P2X7 KO rats as these models are well characterised in our laboratory. Historical healthy control animals have been shown to have no urinary abnormalities, normal glomeruli by light microscopy, negative ED-1 staining and animals of the age and size included in my experiments would be expected to have a serum creatinine within the range of 40-80μmol/L.

4.2 mRNA in kidney cortex from NTN, EAG and EAV

To investigate whether P2X7, the inflammasome and downstream cytokines are up-regulated in rodent models of GN, kidney cortex from animals sacrificed at day 28 after NTN, day 28 after EAG, day 42 after EAV and from control animals was used for RNA extraction and RT-qPCR. This showed that there was up-regulation of P2X7, NLRP3, IL-1β and IL-18 mRNA which was greatest in EAG and NTN. There was a trend to up-regulation of caspase-1 mRNA although this was not significant in any of the disease models (Figure 4.1).

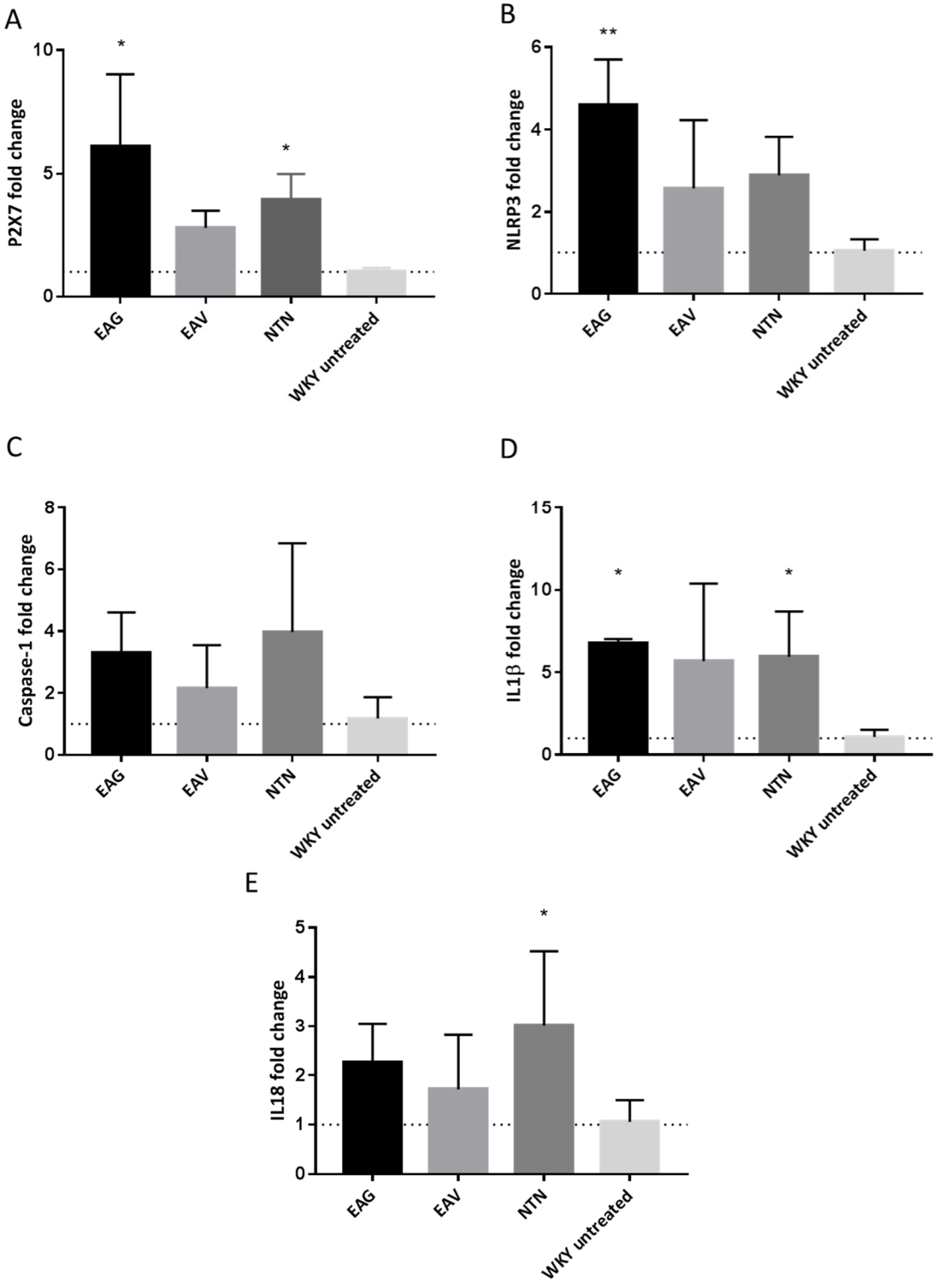

Figure 4.1 Renal cortical mRNA for P2X7 and downstream pathway. RT-qPCR of RNA extracted from renal cortex from rat GN/vasculitis models.

ΔCT was normalised to housekeeping gene and expressed relative to normal WKY rats using $2^{-\Delta\Delta CT}$ method Graphs show mean fold change with SEM for (A) P2X7, (B) NLRP3, (C) Caspase-1, (D) IL-1β and (E) IL-18. Data are shown as mean fold change with SEM. Statistical analysis was performed using 1-way ANOVA followed by Dunnetts post-hoc analysis. *p<0.05, **p<0.01 ***p<0.001

4.3 The effect of P2X7 deficiency on day 28 nephrotoxic nephritis: Experiment 1

Five 8-9 week old male P2X7 KO rats and 6 age matched male WKY WT controls were induced with NTN as described previously. When matched for age the P2X7 deficient rats were slightly smaller by weight than the controls (mean 209 g vs. 251 g). Rats were sacrificed at day 28 with weekly urine collection undertaken from day 7 onwards. Severity of glomerular injury was assessed by urinary abnormalities, histological injury, infiltrating glomerular leucocytes and renal function.

4.3.1 Haematuria and proteinuria

Proteinuria was quantified as total proteinuria in mg per day and for the end of the experiment when a urinary creatinine result was obtained as urinary protein:creatinine ratio (uPCR). uPCR corrects the total urinary protein excretion for differences in urine volume and concentration. Haematuria was assessed on urine dipstick. By day 7 animals already had significant proteinuria and this remained at stable levels throughout the time course of the experiment. Haematuria was maximal by day 14 and remained at this level for the remainder of the time course. There was no difference in either time to development or degree of severity at any time point of proteinuria and haematuria between P2X7 knockout rats and WKY WT controls. At day 28 urine protein creatinine ratio (uPCR) was also the same in both groups (Figure 4.2).

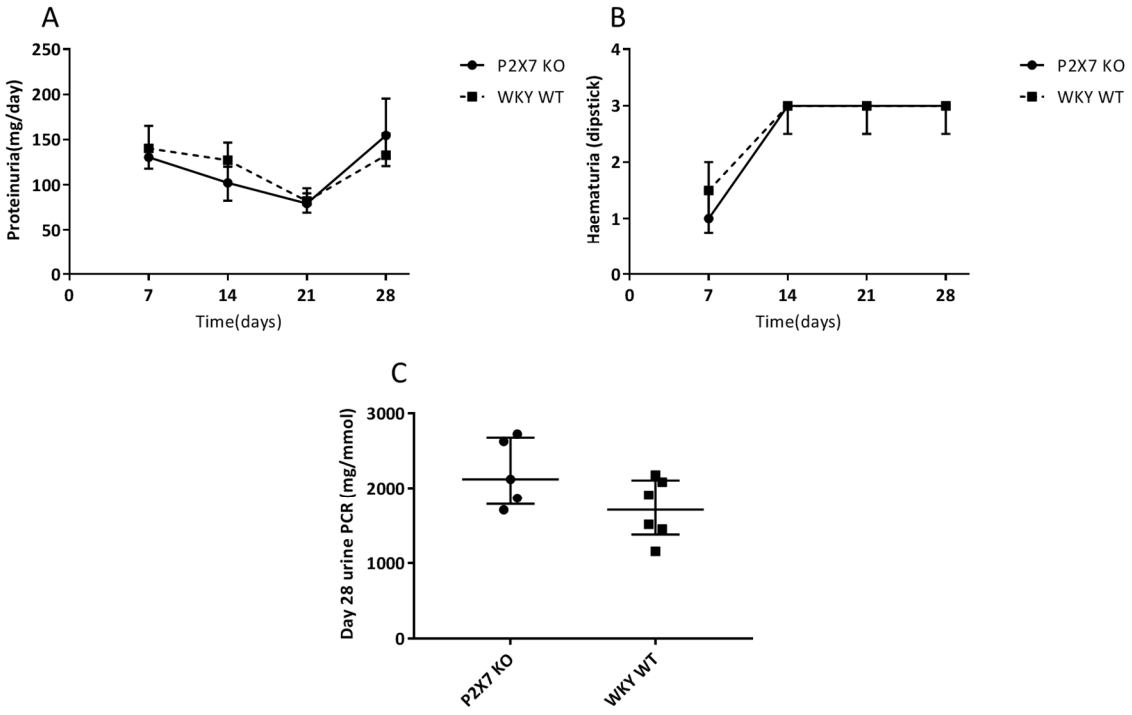

Figure 4.2 Urinary abnormalities in NTN experiment 1 in WKY WT and P2X7 KO rats
(A) Proteinuria, (B) Haematuria and (C) day 28 uPCR. Data shown as median with IQR

4.3.2 Histological injury and infiltrating leucocytes

By day 28 both groups of animals had significantly abnormal renal pathology with a high percentage of crescent formation. As this was a late time point of disease crescents were mainly fibrous and fibrocellular; significant glomerular obsolescence, tubular atrophy and interstitial fibrosis were also observed but not formally quantified (Figure 4.3).

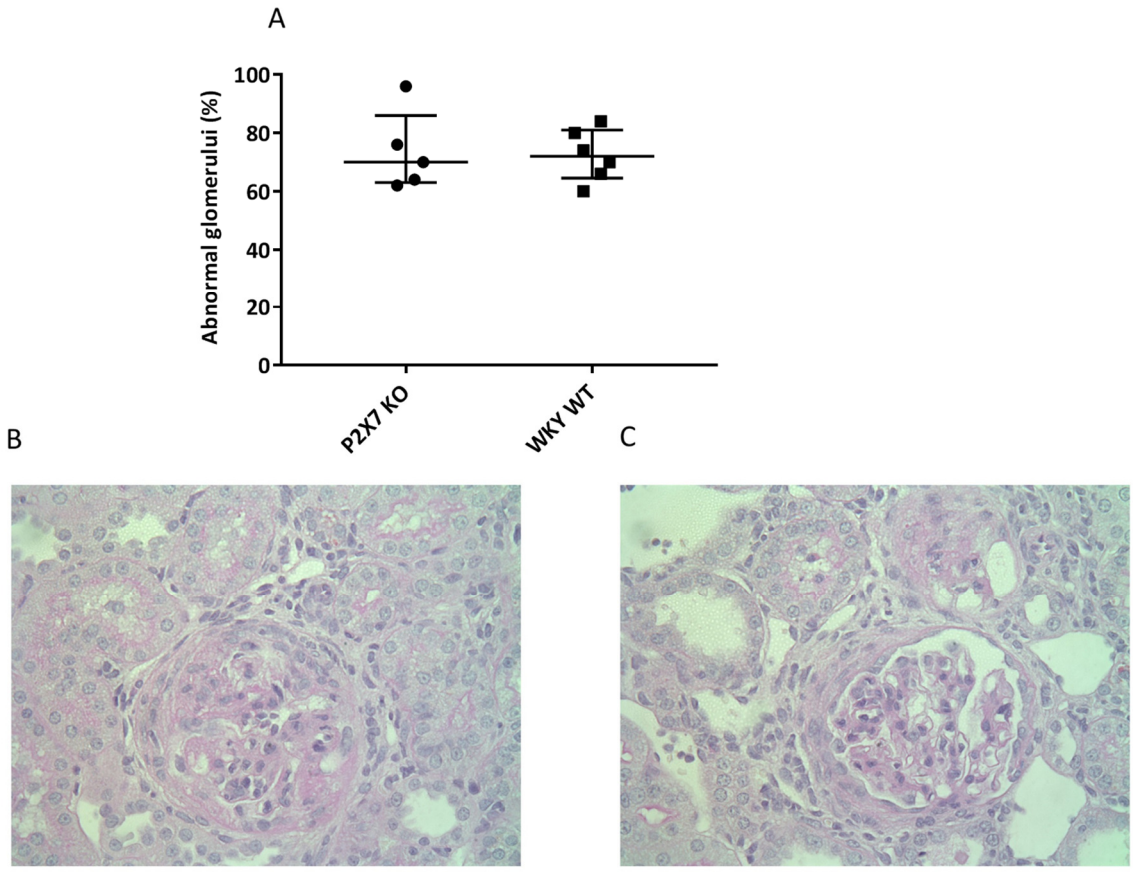

Figure 4.3 Renal histology in NTN experiment 1 in WKY WT and P2X7 KO rats
(A) Proportion of abnormal glomeruli in each group. Data shown as median with IQR. Photomicrographs showing representative histology in (C) P2X7 KO and (D) WKY WT. H+E stain, x400 magnification.

The degree of inflammatory cell infiltration into glomeruli was assessed using immunohistochemical staining for a rat macrophage marker, ED-1. Levels of infiltrating ED-1 cells were similar between the two groups although, again due to the late time point of disease the degree of cellular infiltration was not high in either group (Figure 4.4).

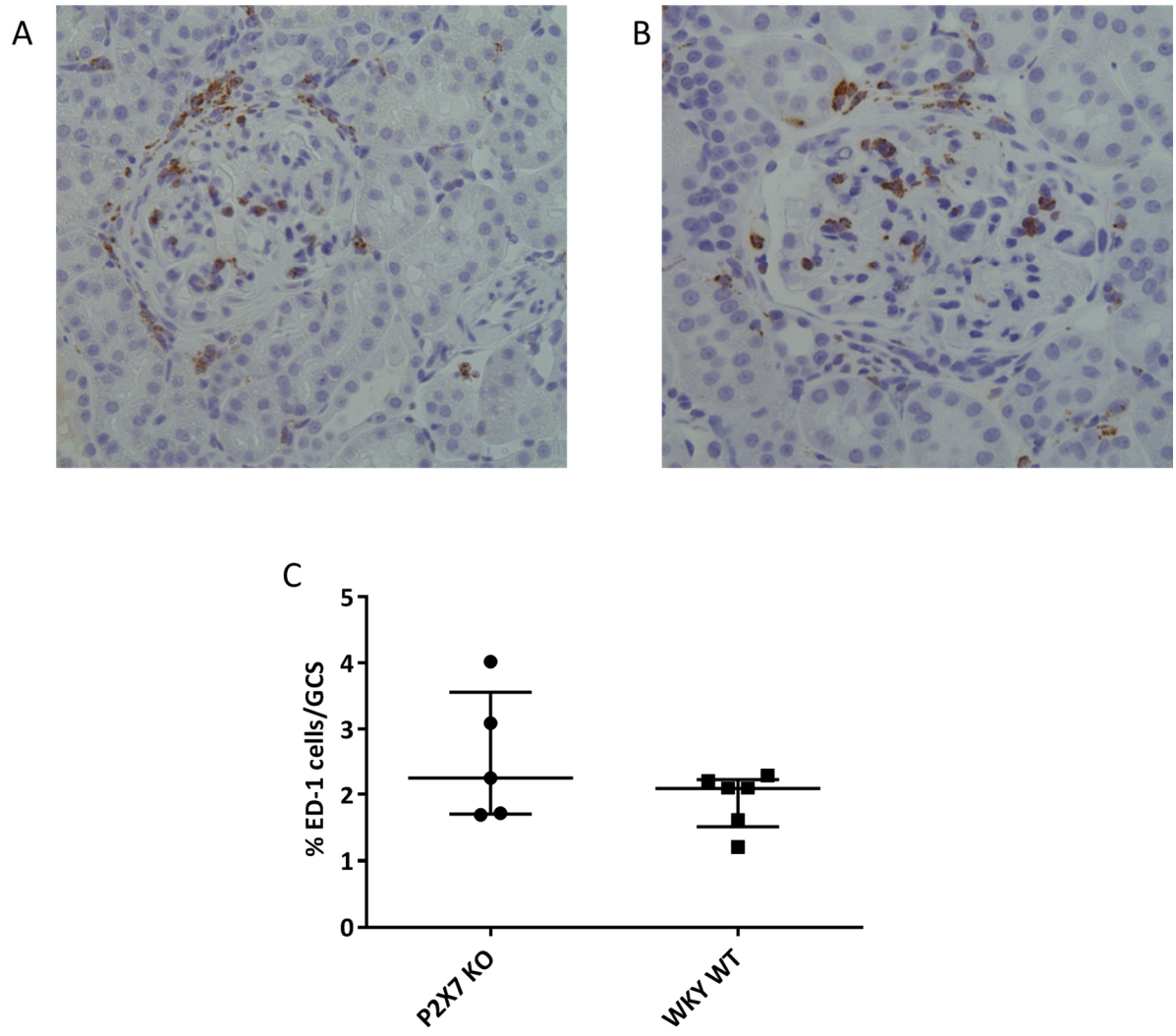

Figure 4.4 Glomerular macrophage infiltration in NTN experiment 1 in WKY WT and P2X7 KO rats

Photomicrographs showing representative immunoperoxidase staining for ED-1+ cells in (A) WKY WT and (B) P2X7 KO rat. (C) Macrophage infiltration quantified as mean % of ED-1 cells per glomerular cross section (GCS). Data shown as median with IQR.

4.3.3 Deposited autologous antibody

Degree of deposited autologous rat IgG was similar between the two groups (Figure 4.5). There was also similar degree of deposited (heterologous) rabbit IgG between the two groups although in all animals it was weaker than deposited rat IgG (Median IF 2 in both groups).

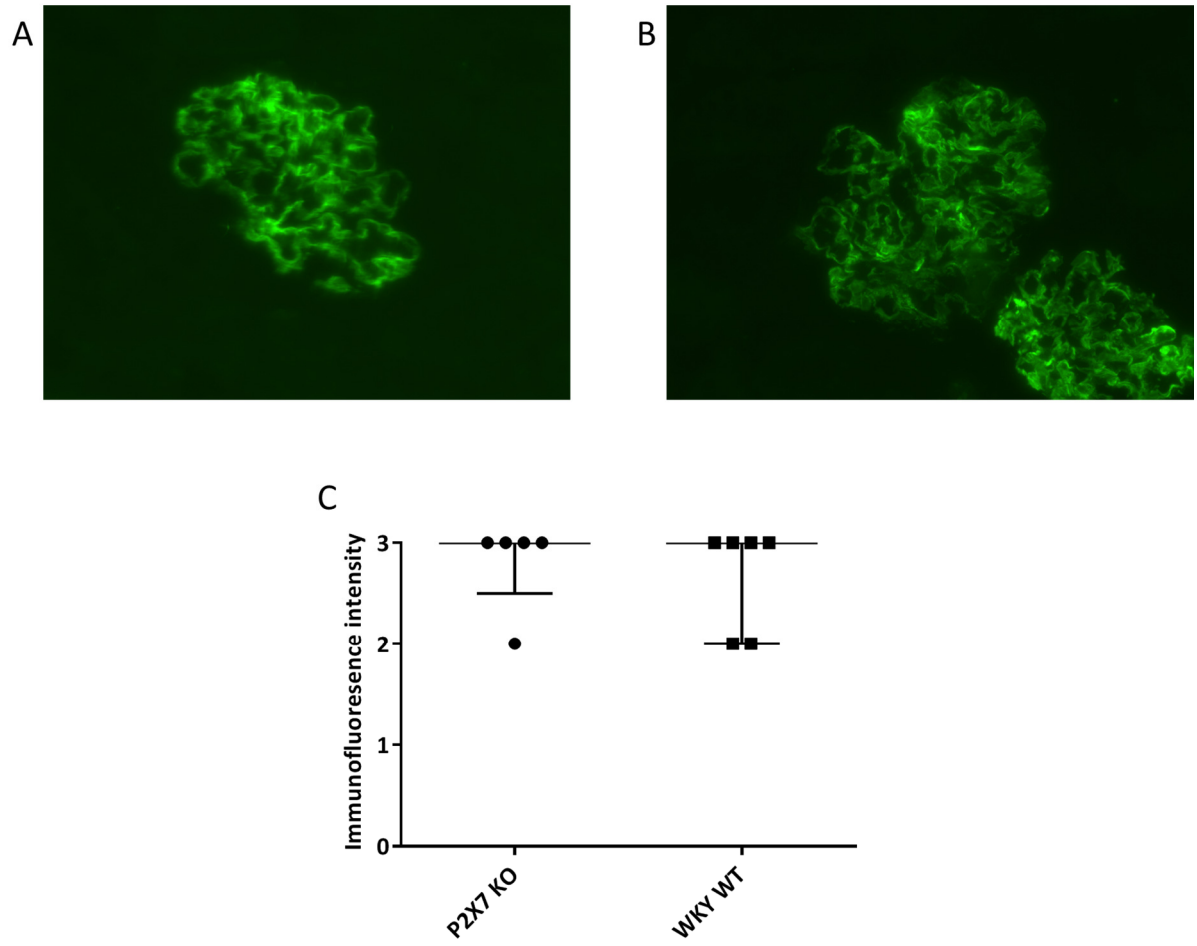

Figure 4.5 Deposited rat IgG in NTN experiment 1 in WKY WT and P2X7 KO rats
Photomicrographs showing representative fluorescence images in (A) WKY WT and (B) P2X7 KO rats of direct immunofluorescence for rat IgG. Anti-rat IgG FITC X400 magnification (C) Quantification of direct immunofluorescence for deposited rat IgG. Data shown as median with IQR.

4.3.4 Renal function

Renal function was assessed by measuring serum and urine creatinine at day 28 and calculating creatinine clearance. As shown in Figure 4.6, there was a trend towards higher serum creatinine and lower creatinine clearance in WKY WT rats compared to P2X7 knockout rats at day 28 although this was not significant and there was considerable overlap between the two groups. This could have been a result of the size disparity between the two groups, at time of culling the WKY WT rats remained nearly 10% larger than the P2X7 KO (Figure 4.6).

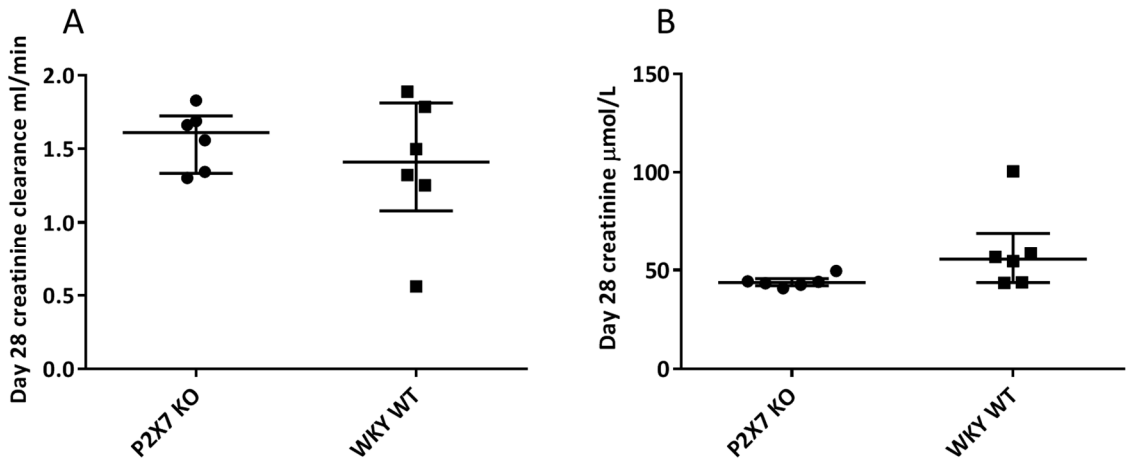

Figure 4.6 Renal function in NTN experiment 1 in WKY WT and P2X7 KO rats
(A) Creatinine clearance and (B) serum creatinine in WKY WT and P2X7 KO rats at day 28. Data shown as median with IQR.

4.4 The effect of P2X7 deficiency on day 28 nephrotoxic nephritis: Experiment 2

As there was a size difference between the rats in experiment one which could have led to elevated creatinine in the larger WKY WT rats compared to P2X7 KO, a further experiment was undertaken whereby rats were matched for size rather than age. The P2X7 rats were now more closely matched although still slightly smaller, mean weight 192.7g vs. 209.2g. This experiment confirmed the results of experiment 1, P2X7 deficiency did not protect against NTN. There was no difference in urinary abnormalities, glomerular macrophage infiltration, degree of intensity of immunofluorescence of deposited glomerular rat IgG or creatinine clearance. Again there was a trend towards higher creatinine and lower creatinine clearance in the WKY WT rats despite better size matching- at time of cull the two groups were well matched for body weight. All of the P2X7 KO rats had preserved renal function whereas one of the WKY WT rats had developed moderately severe renal failure (but appeared well prior to culling) (Figure 4.7).

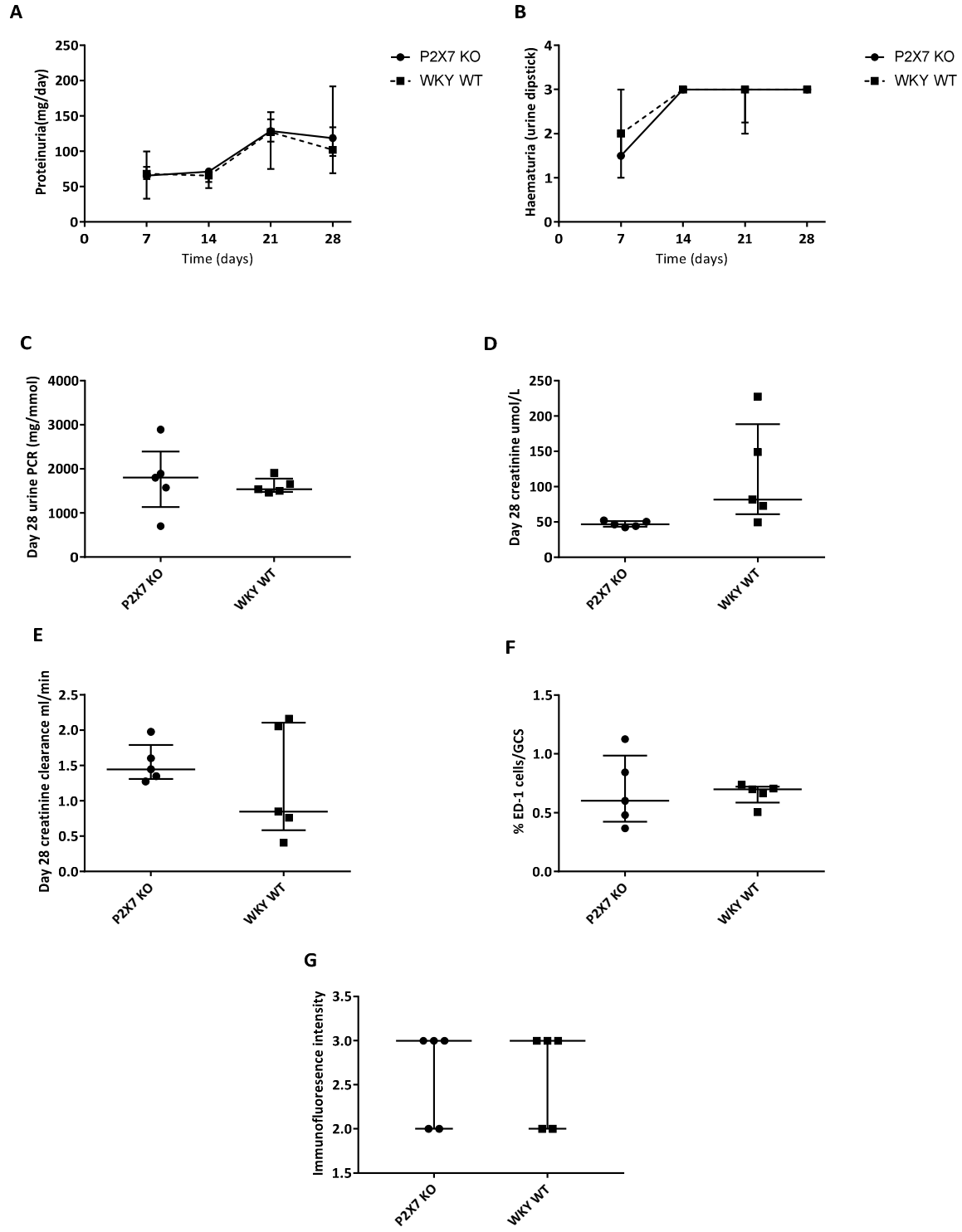

Figure 4.7 Summary of renal function, urinary abnormalities and glomerular macrophage infiltration in NTN experiment 2

In this experiment rats in the two groups were more closely matched for weight. (A) Proteinuria, (B) Haematuria, (C) urine PCR at day 28, (D) Creatinine at day 28, (E) Creatinine clearance at day 28, (F) % ED-1 positive cells per glomerular cross section (GCS), (G) Quantification of direct immunofluorescence for deposited rat IgG. Data are shown as median with IQR

4.5 The effect of P2X7 deficiency on day 28 EAG: Experiment 1

Six 6-7 week old female P2X7 KO rats and 6 age and sex matched WKY WT controls were induced with EAG as described. Again the P2X7 deficient rats were smaller with mean weight 111.5g vs 141.2g on day of immunisation. Rats were sacrificed at day 28 with serum and urine collections weekly from day 14. Severity of glomerular injury was assessed using the same parameters as in NTN and humoral immune response was assessed by measurement of circulating anti-α3(IV)NC1 antibodies and by glomerular antibody deposition.

4.5.1 Haematuria and proteinuria

Animals had developed haematuria and proteinuria by day 14 and this was maximal by day 21. Daily proteinuria, dipstick haematuria were comparable between the two groups at all-time points up to sacrifice as was uPCR at day 28.

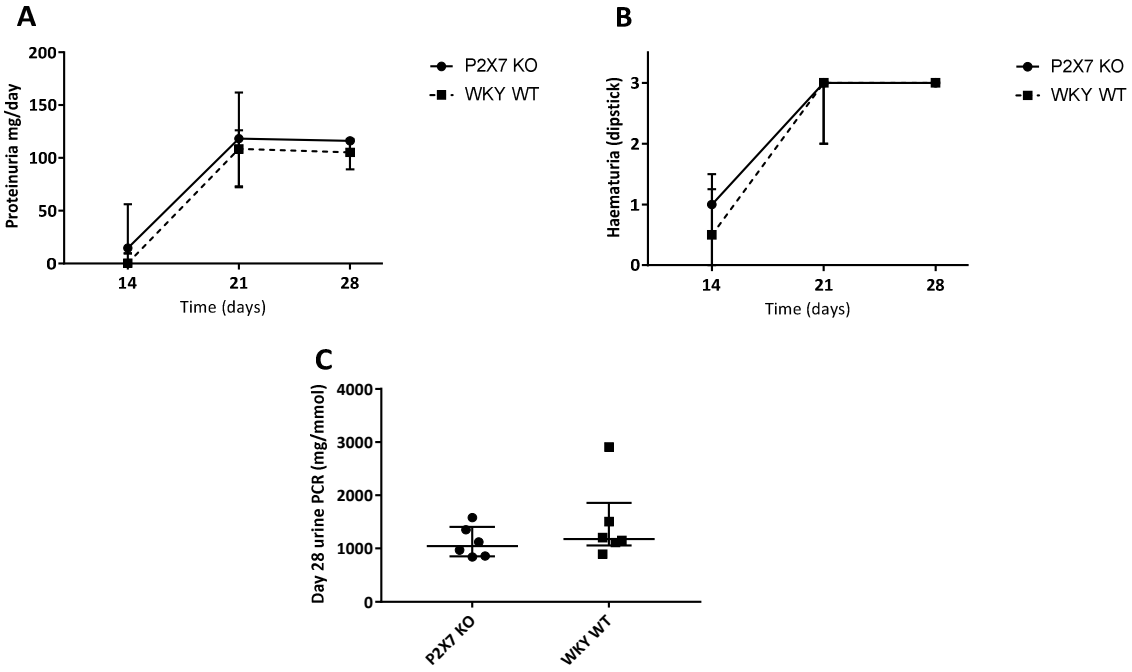

Figure 4.8 Urinary abnormalities in EAG experiment 1 in WKY WT and P2X7 KO rats
(A) Proteinuria, (B) Haematuria and (C) day 28 uPCR. Data shown as median with IQR

4.5.2 Histological injury and infiltrating leucocytes

At day 28 animals in both groups had comparable histology with severe abnormalities, approximately 60-70% of glomeruli were severely affected by crescent formation or necrosis and almost no normal glomeruli were seen (Figure 4.9).

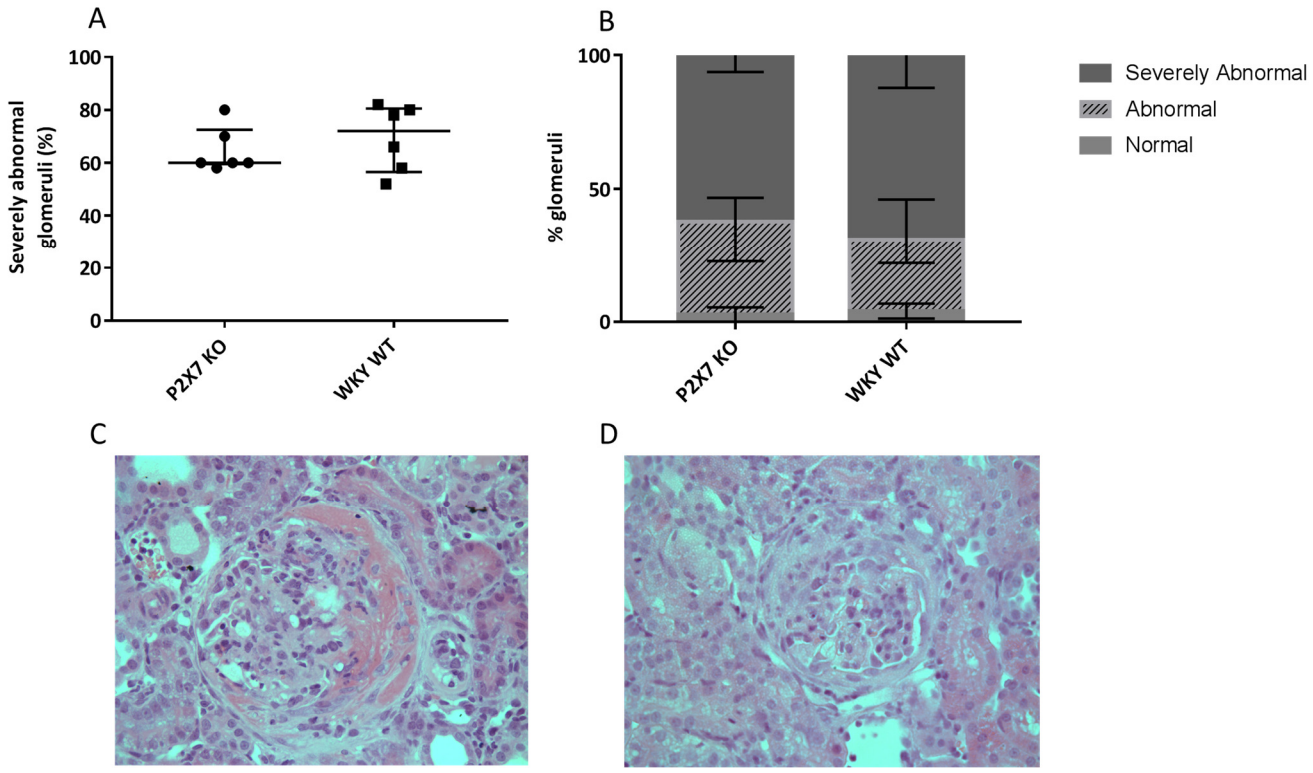

Figure 4.9 Renal histology in EAG experiment 1 in WKY WT and P2X7 KO rats
(A) Proportion of severely abnormal glomeruli. Data shown as median with IQR (B) Range of glomerular abnormalities (normal, abnormal or severely abnormal) in each group. Data shown as mean with SEM, Photomicrographs showing representative histology in (C) P2X7 KO and (D) WKY WT. H+E stain, x400 magnification.

Inflammatory cell infiltrate was assessed using immunohistochemical staining for ED-1, a rat macrophage marker. Both groups of animals had marked ED-1 positive infiltrate reflecting the natural history of this model with peak inflammatory infiltrate occurring at around day 28 (Figure 4.10).

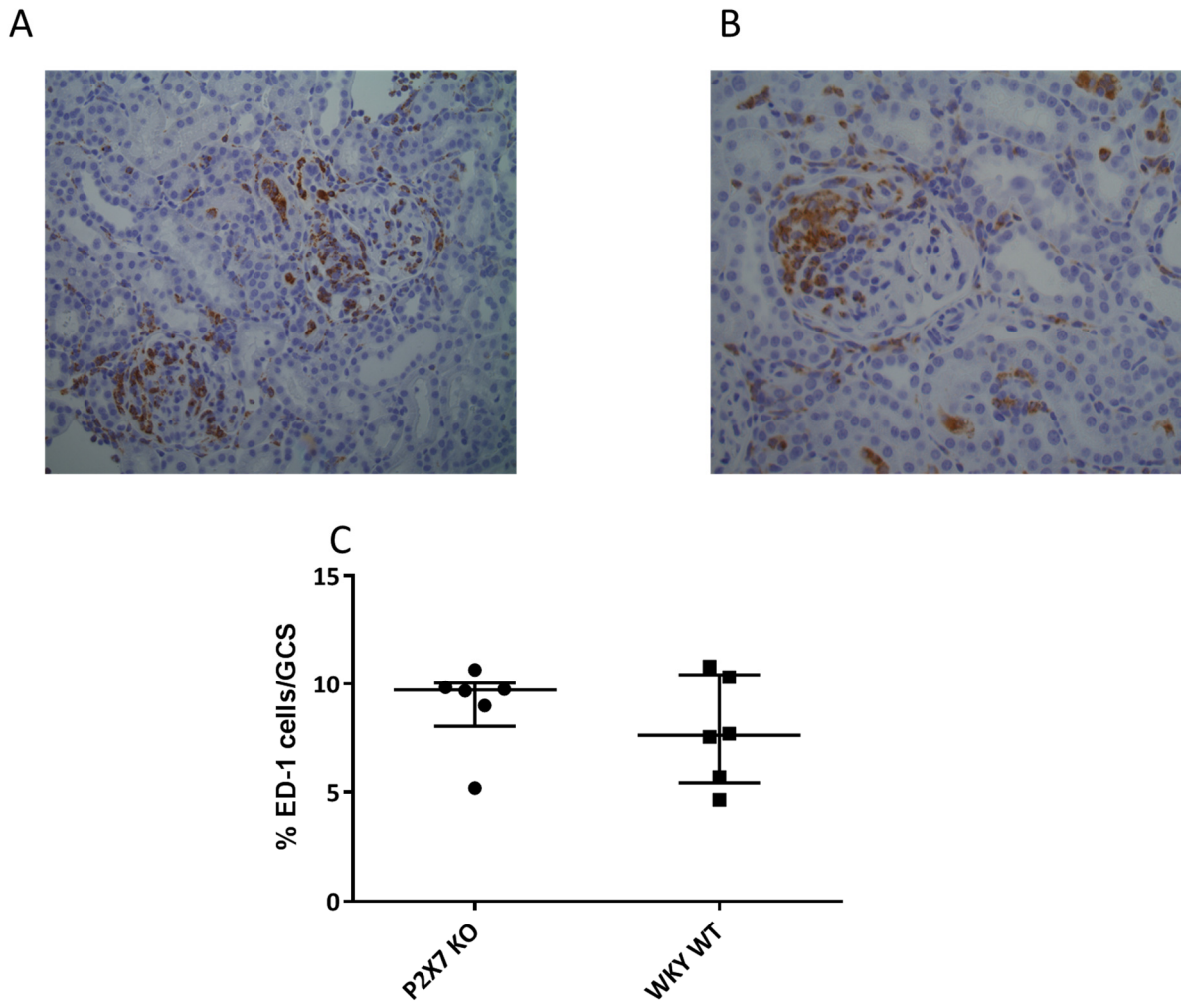

Figure 4.10 Glomerular inflammatory cell infiltrate in EAG experiment 1 in WKY WT and P2X7 KO rats

Photomicrographs showing representative immunoperoxidase staining for ED-1+ cells in (A) WKY WT and (B) P2X7 KO rat. x200 magnification (C) Macrophage infiltration quantified as mean % of ED-1 cells per glomerular cross section (GCS). Data shown as median with IQR.

4.5.3 Renal function

Renal function was assessed by absolute values for serum creatinine and by calculating creatinine clearance from serum and urine values. Animals had evidence of only mildly deranged renal function at this time point and there was no difference between the two groups (Figure 4.11).

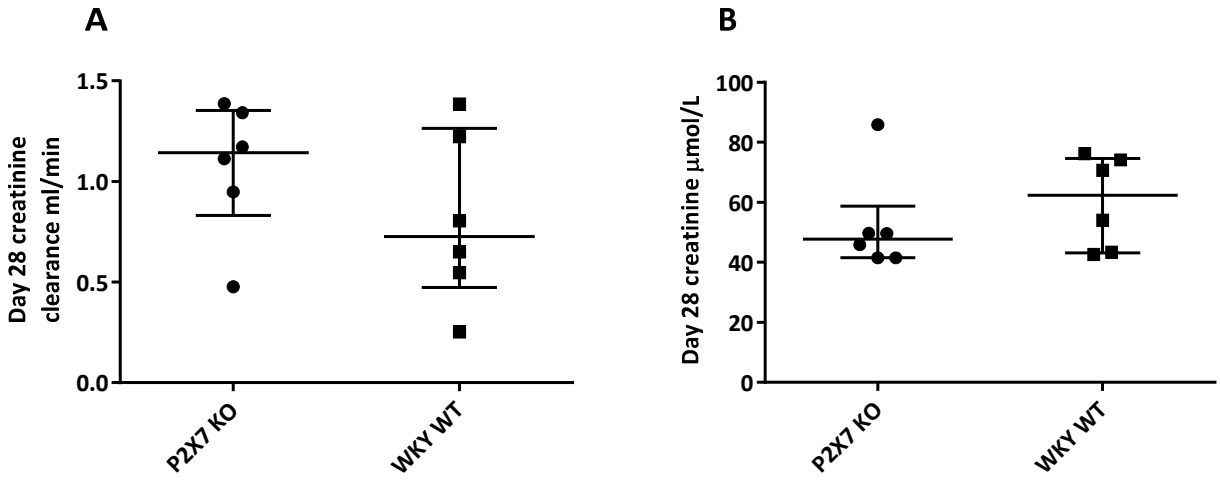

Figure 4.11 Renal function in EAG experiment 1 in WKY WT and P2X7 KO rats
(A) Creatinine clearance and (B) serum creatinine in WKY WT and P2X7 KO rats at day 28. Data shown as median with IQR

4.5.4 Lung haemorrhage

Lung haemorrhage was assessed using a semi-quantitative scoring system on visual inspection at time of culling and by microscopic inspection for haemosiderin-laden cells stained with Perls Prussian Blue stain. There was a non-significant trend towards more severe lung haemorrhage in the P2X7 KO group when assessed by both of these measures. In this age group of rats there was significant size disparity between the WKY WT and P2X7 KO. Anecdotally, I and others working with this disease model in our group have observed that smaller animals are more prone to lung disease which could account for this difference (Figure 4.12).

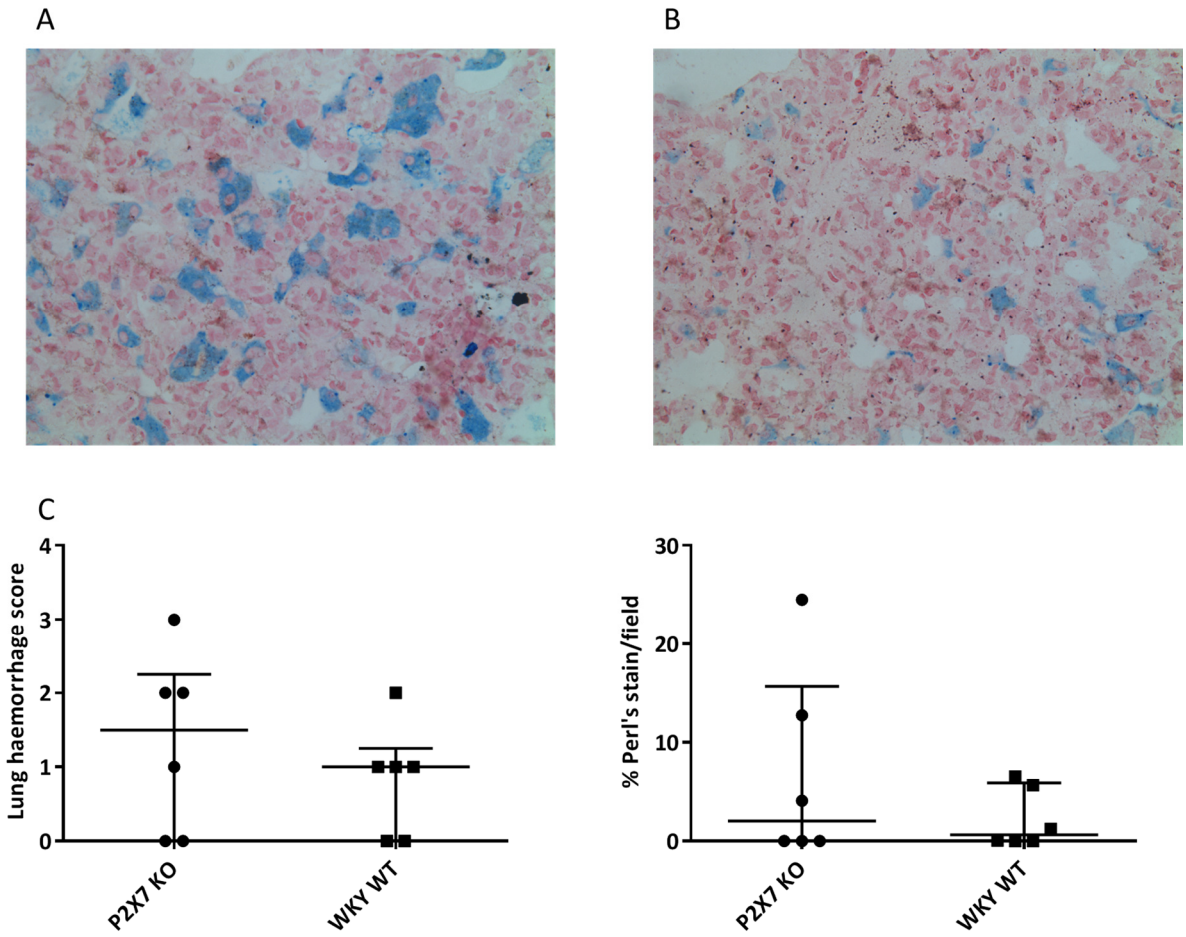

Figure 4.12 Lung haemorrhage in EAG experiment 1 in WKY WT and P2X7 KO rats
Photomicrographs showing representative staining for haemosiderin laden macrophages in the lung using Perls' Prussian Blue in (A) P2X7 KO and (B) WKY WT x200 magnification, (C) Macroscopic lung haemorrhage score and (D) Quantification of haemosiderin laden cells in lung tissue. Data are shown as median with IQR

4.5.5 Humoral autoimmune response

Animals had detectable circulating antibodies against α3(IV)NC1 by day 14 and titres continued to rise until time of sacrifice at day 28. On direct immunofluorescence all animals had strong linear staining of IgG deposited along the GBM. There was no difference in titre of circulating antibodies or of degree of deposited antibodies between the two groups (Figure 4.13).

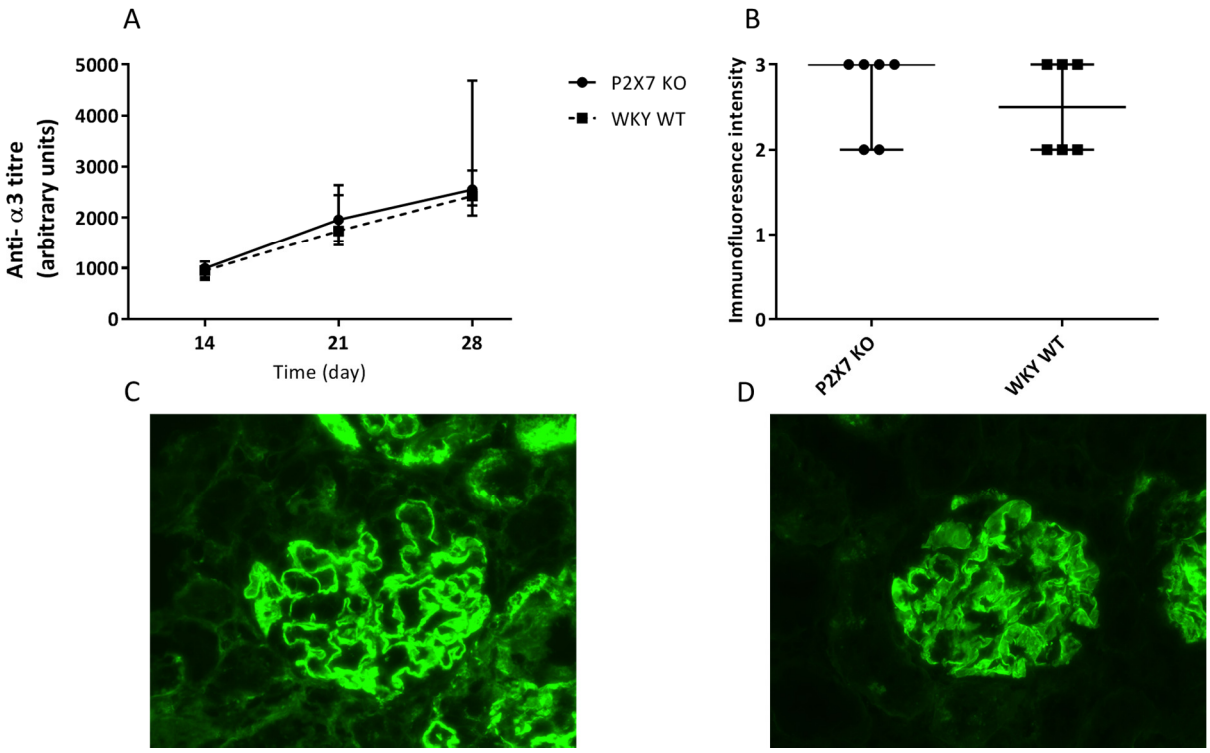

Figure 4.13 Circulating and deposited α3(IV)NC1 antibodies in EAG experiment 1 in WKY WT and P2X7 KO rats

(**A**) Circulating anti- α3(IV)NC1 antibody levels, (B) Quantification of direct immunofluorescence for deposited rat IgG. Data are shown as median with IQR. Representative photomicrographs of direct immunofluorescence for deposited rat IgG in (C) P2X7 KO and (D) WKY WT animals. Anti-rat IgG FITC, x400 magnification

4.6 The effect of P2X7 deficiency on day 28 EAG: Experiment 2

As there was a trend to increased lung haemorrhage in P2X7 KO rats which could be accounted for by differences in animal body weight between the two groups a further experiment was undertaken in which rats were matched for body weight rather than age. Six P2X7 KO and 6 WKY WT were induced with EAG as previously described. Mean weights at induction of disease were more comparable (120.3g vs. 130.8g). Again, P2X7 deficiency did not protect from disease with similar degree of proteinuria, haematuria, creatinine clearance and glomerular abnormalities and no difference in antibody production or deposition within the glomerulus. The trend for more severe lung haemorrhage in the P2X7 KO rats was no longer observed. There was less severe lung

haemorrhage in both groups of animals in this experiment which could be explained by their larger size. Urinary abnormalities, histological injury, infiltrating leucocytes and renal function in this experiment are summarised in Figure 4.14. Lung haemorrhage and humoral responses are summarised in Figure 4.15.

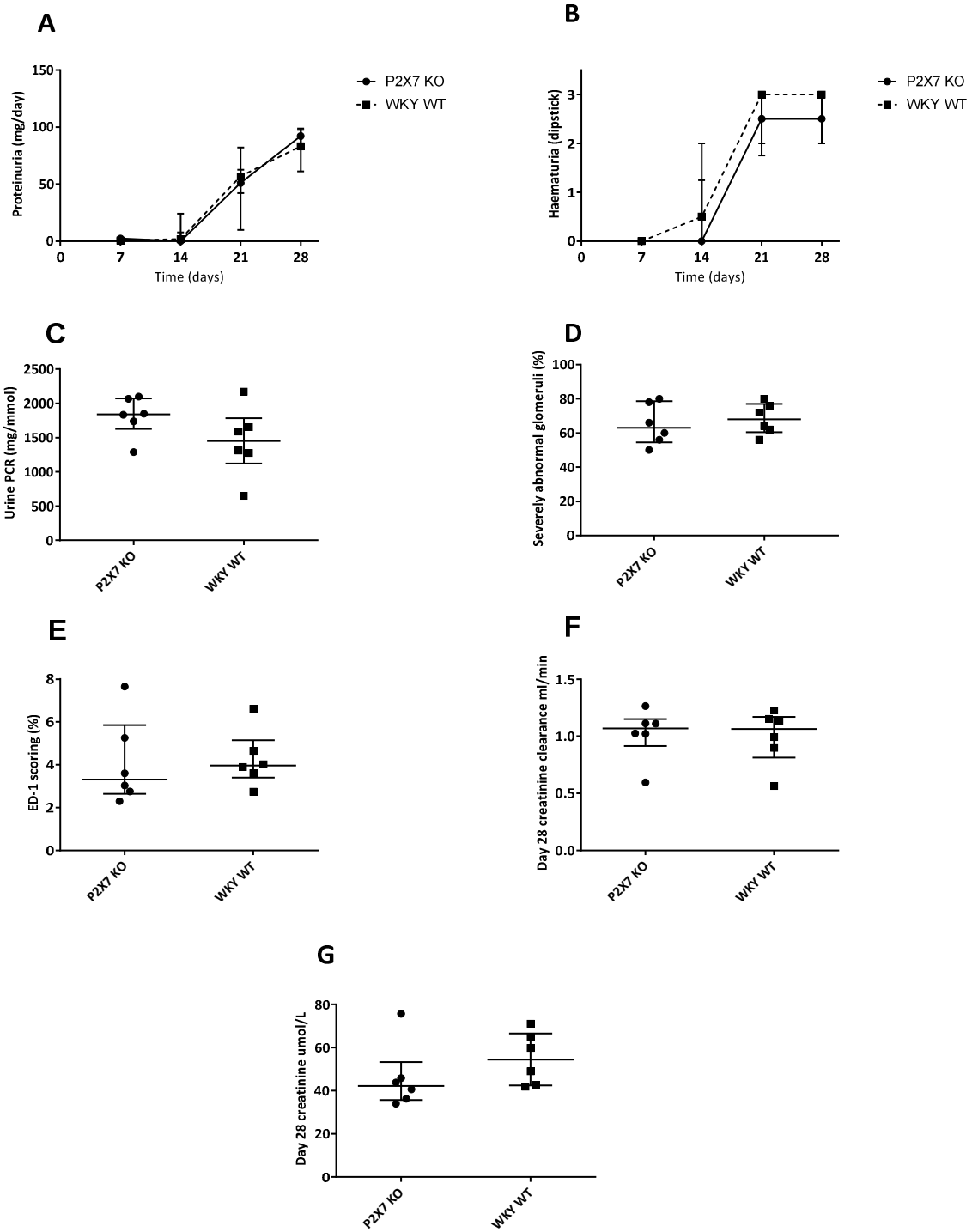

Figure 4.14 Summary of renal function, urinary abnormalities and glomerular abnormalities in EAG experiment 2

In this experiment rats in the two groups were more closely matched for weight. (A) Proteinuria, (B) Haematuria, (C) urine PCR, (D) % of severely abnormal glomeruli (E) Creatinine at day 28, (F) Creatinine clearance at day 28, (G) % ED-1 positive cells per glomerular cross section (GCS). Data are shown as median with IQR.

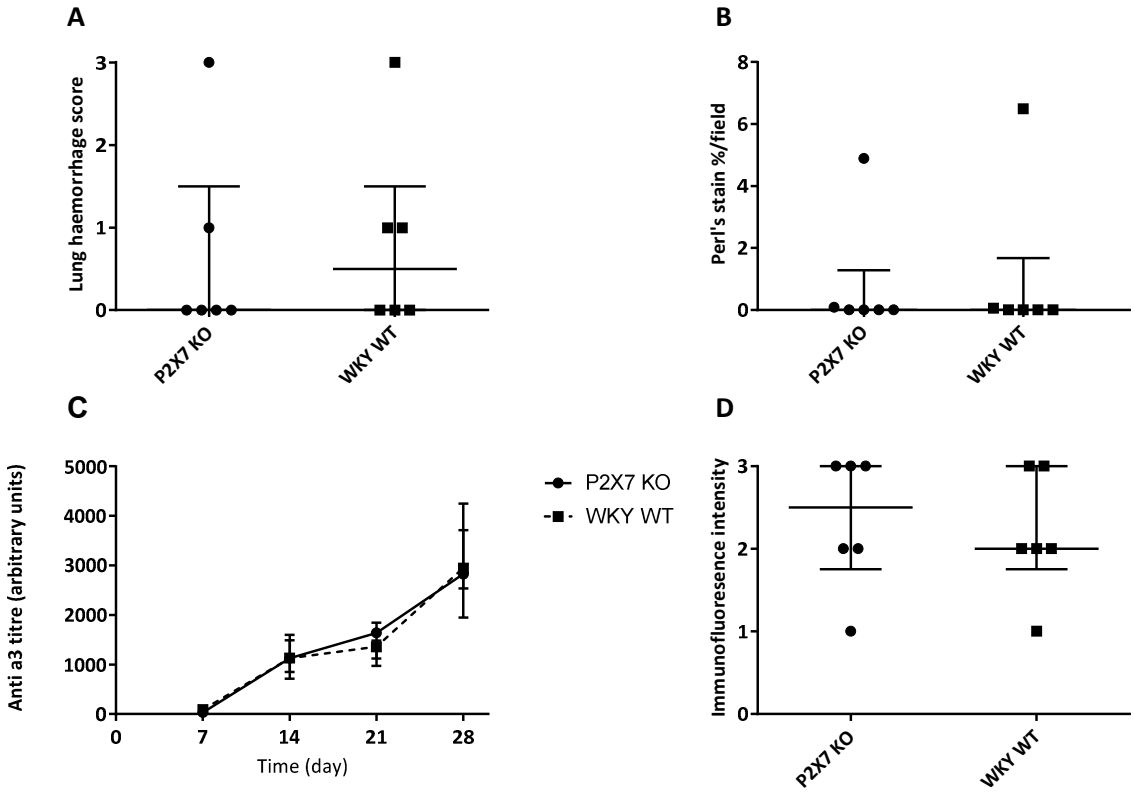

Figure 4.15 Summary of humoral abnormalities and lung injury in EAG experiment 2
(A) Macroscopic lung haemorrhage score, (B) Quantification of haemosiderin laden cells in lung tissue, (C) Circulating anti- α3(IV)NC1 antibody levels, (D) Quantification of direct immunofluorescence for deposited rat IgG. Data are shown as median with IQR.

4.7 The effect of P2X7 deficiency on glomerular cytokine production: EAG experiments 3 and 4

As P2X7 deficiency had no effect on disease severity in either NTN or EAG despite up-regulation of P2X7, the inflammasome and IL-1β RNA in renal cortex tissue from these models when compared to rats without disease, I undertook experiments to investigate glomerular cytokine production ex vivo to assess whether P2X7 dependent cytokines were being produced. I carried out an initial experiment, EAG 3 to determine the time of peak cytokine production from nephritic glomeruli in WKY WT rats and a subsequent experiment, EAG 4 to investigate differences in cytokine production between WKY WT, P2X7 KO and control rats.

4.7.1 EAG experiment 3

Twelve 6-7 week old female WKY rats were immunised with α3(IV)NC1 in order to induce EAG. Three rats were sacrificed at weekly time points from day 14-28 with an additional 3 rats at day 18 as this is the approximate time of onset of disease in this model. No control group was included in this experiment as its aim was to choose an appropriate time point for a further comparison experiment, control animals were included in the experiments described in section 4.8. Weekly urine collection was undertaken to assess development of disease and circulating antibodies were measured at time of sacrifice. As described previously, animals began to develop urinary abnormalities and auto-antibodies by day 18 with progressively increasing titre until day 28 (Figure 4.16).

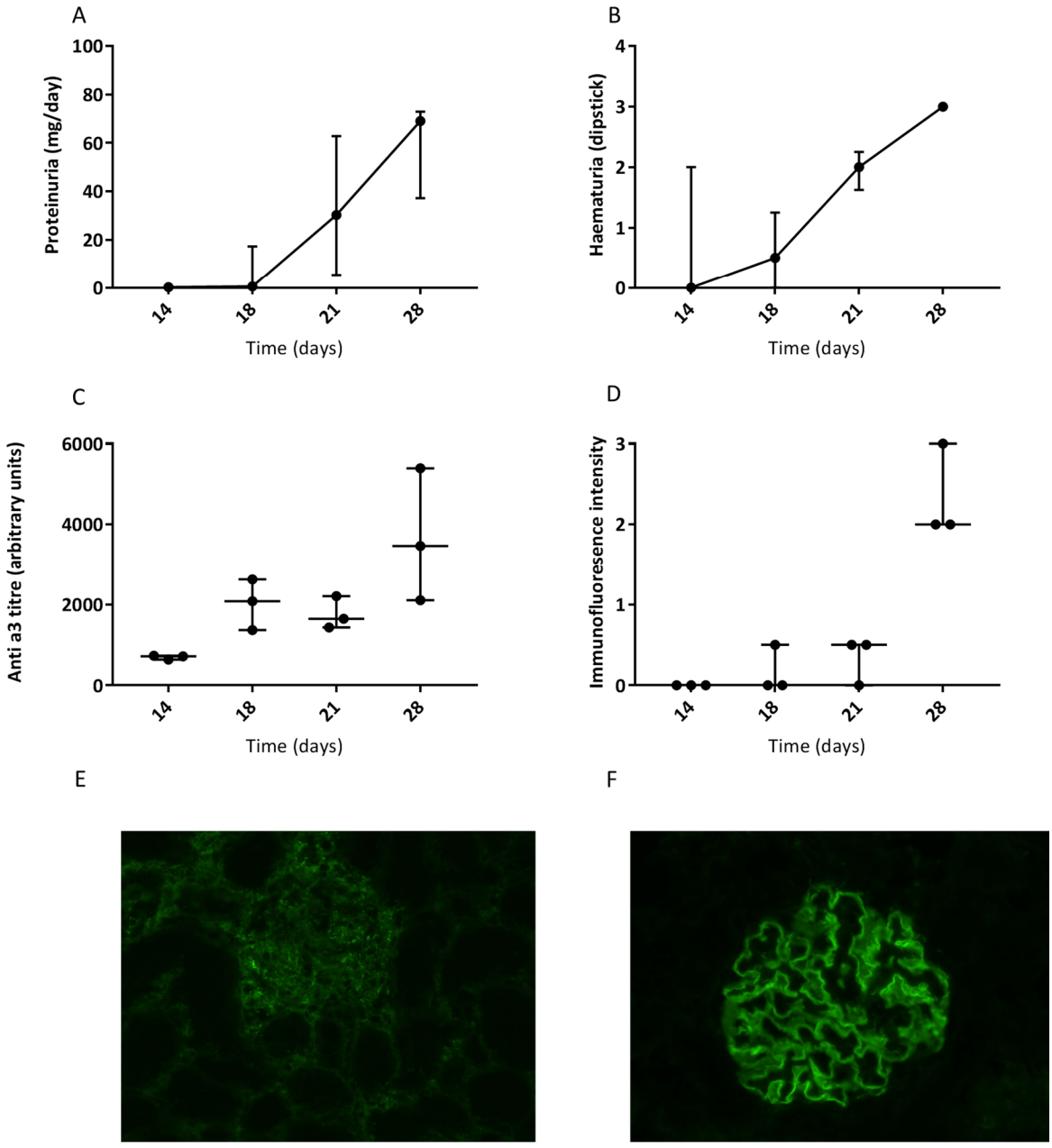

Figure 4.16 Urinary abnormalities and humoral responses in EAG 3

(A) Proteinuria, (B) Haematuria, (C) Circulating anti- α3(IV)NC1 antibody levels, (D) Quantification of direct immunofluorescence for deposited rat IgG. Data shown as median with IQR. Representative photomicrographs of direct immunofluorescence for deposited rat IgG at (E) day 14 and (F) day 28. Anti-rat IgG FITC, x400 magnification

Glomerular macrophage infiltration as characterised by ED-1 immunohistochemistry began to occur from day 18 onwards and glomerular abnormalities were also apparent from this time point onwards. Despite this there was only significant deposited glomerular antibody in those animals

sacrificed at day 28 point (Figure 4.17). Interestingly, one of the group of rats culled on day 14 had already developed mild lung haemorrhage despite only low levels of circulating autoantibodies present at this time

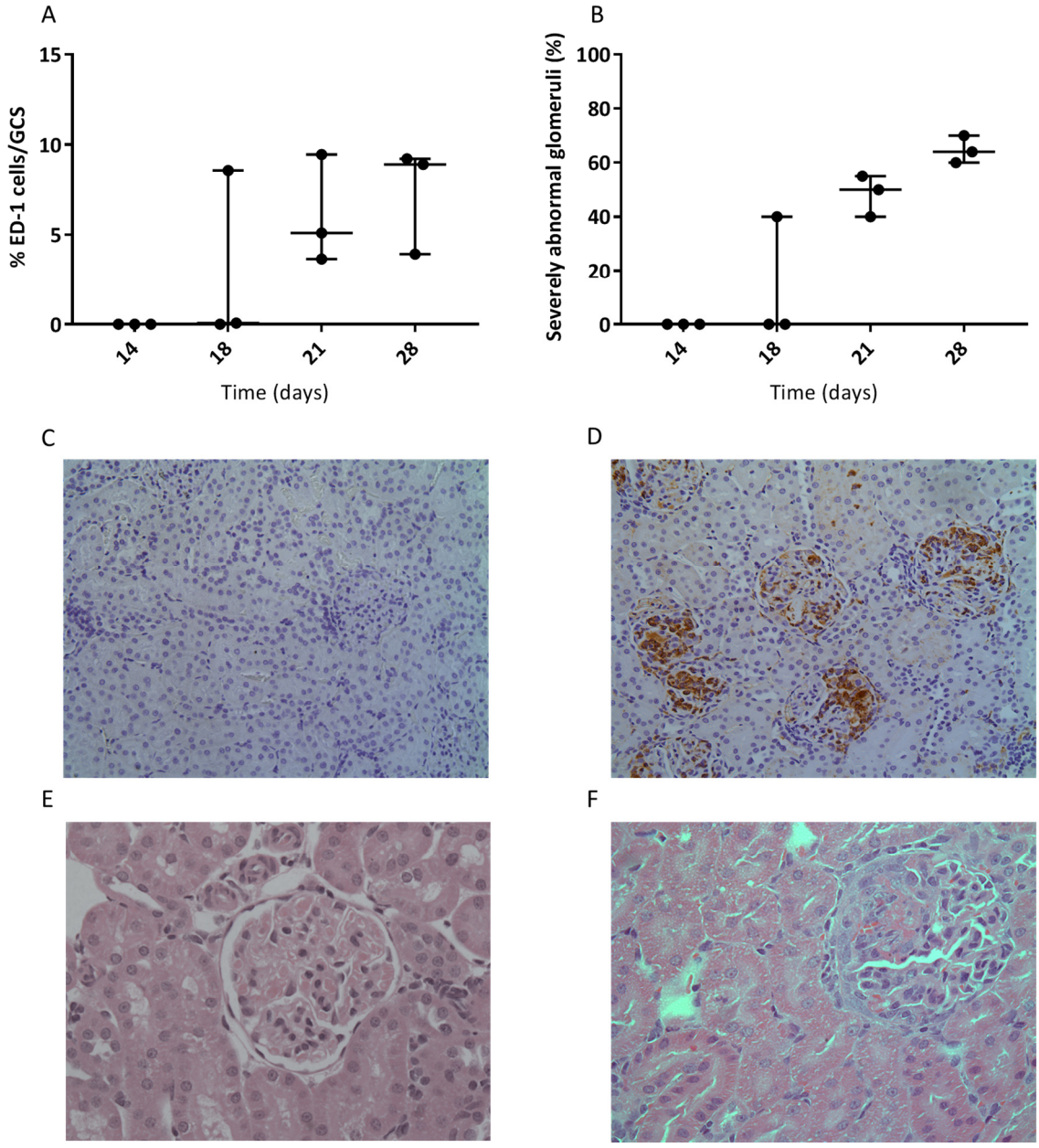

Figure 4.17 Glomerular leucocyte infiltration and severity of glomerular injury in EAG 3
(A) Macrophage infiltration quantified as mean % of ED-1 cells per glomerular cross section (GCS). Data shown as median with IQR. (B) Proportion of severely abnormal glomeruli. Data shown as median with IQR. Photomicrographs showing representative immunoperoxidase staining for ED-1+ cells at (C) Day 14 and (D) Day 28 x200 magnification, Photomicrographs showing representative histology at (E) Day 14 and (F) Day 28. H+E stain, x400 magnification.

4.7.1.1 Spontaneous cytokine production from nephritic glomeruli cultured ex vivo

I isolated nephritic glomeruli at each of the time points after disease initiation and measured spontaneous cytokine production ex vivo over a 48 hour period. Levels of IL-1β in supernatant were raised at all of the time points studied as was IL-6. Despite the fact that there was significant glomerular macrophage infiltration seen on ED-1 staining at both day 21 and 28, there was not significant MCP-1 release into supernatant until day 28 (Figure 4.18). Other inflammatory mediators were not measured.

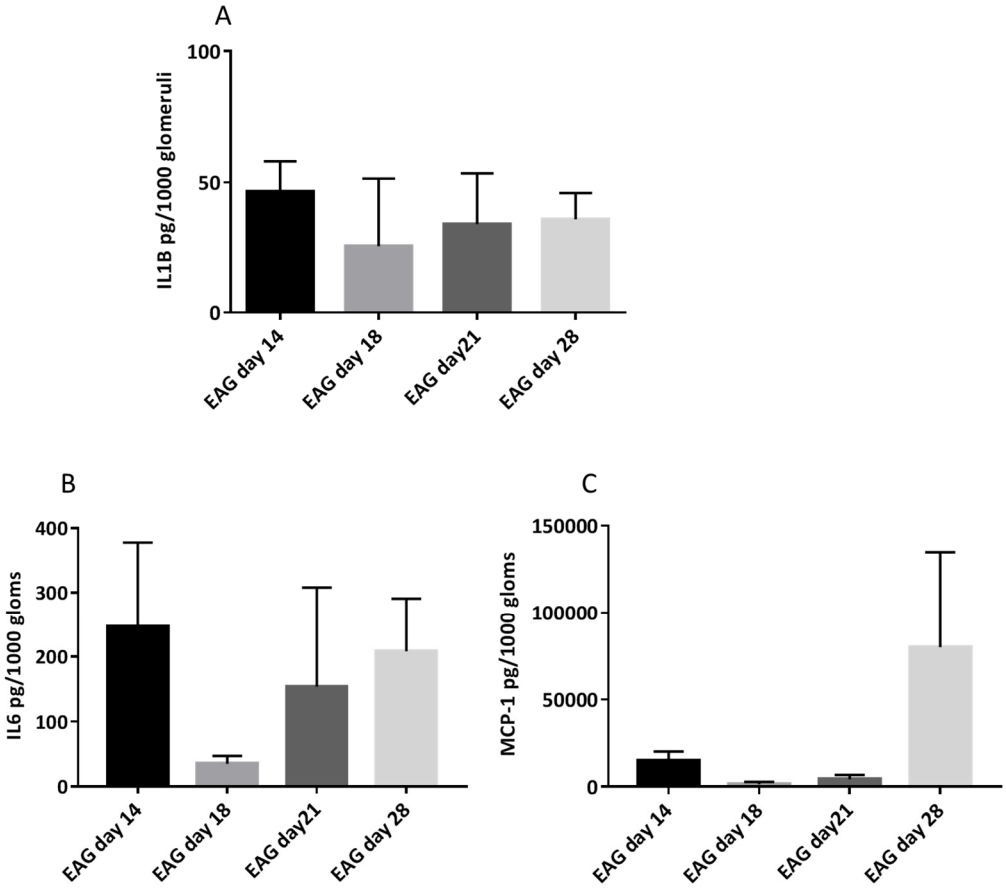

Figure 4.18 Spontaneous cytokine production by nephritic glomeruli *ex vivo*
Production of pro-inflammatory cytokines by nephritic glomeruli over 48 hours (A) IL-1β, (B) IL-6, (C) MCP-1. As the yield of sieved glomeruli was variable for each replicate, cytokine production was normalised to 1000 glomeruli cultured. For each time point there were biological triplicates with technical duplicates. Data shown are mean with SEM.

4.7.2 EAG experiment 4

Although IL-1β and IL-6 production were relatively consistent throughout the time course of EAG, MCP-1 production did not occur until day 28 so this was the time point I selected to compare cytokine production between P2X7 KO, WKY WT and control animals. Four 6-7 week old female WKY rats and 4 weight and sex matched P2X7 KO rats were immunised with α3(IV)NC1 in order to induce EAG. Four further matched WKY WT rats received vehicle alone (CFA) to serve as control animals. To assess development of disease, weekly urine collections were undertaken and circulating and deposited glomerular antibodies were measured at day 28. As expected, there was no difference in urinary abnormalities or antibody between P2X7 KO and WKY WT animals, control animals which were immunised with CFA alone did not develop disease (Figure 4.19).

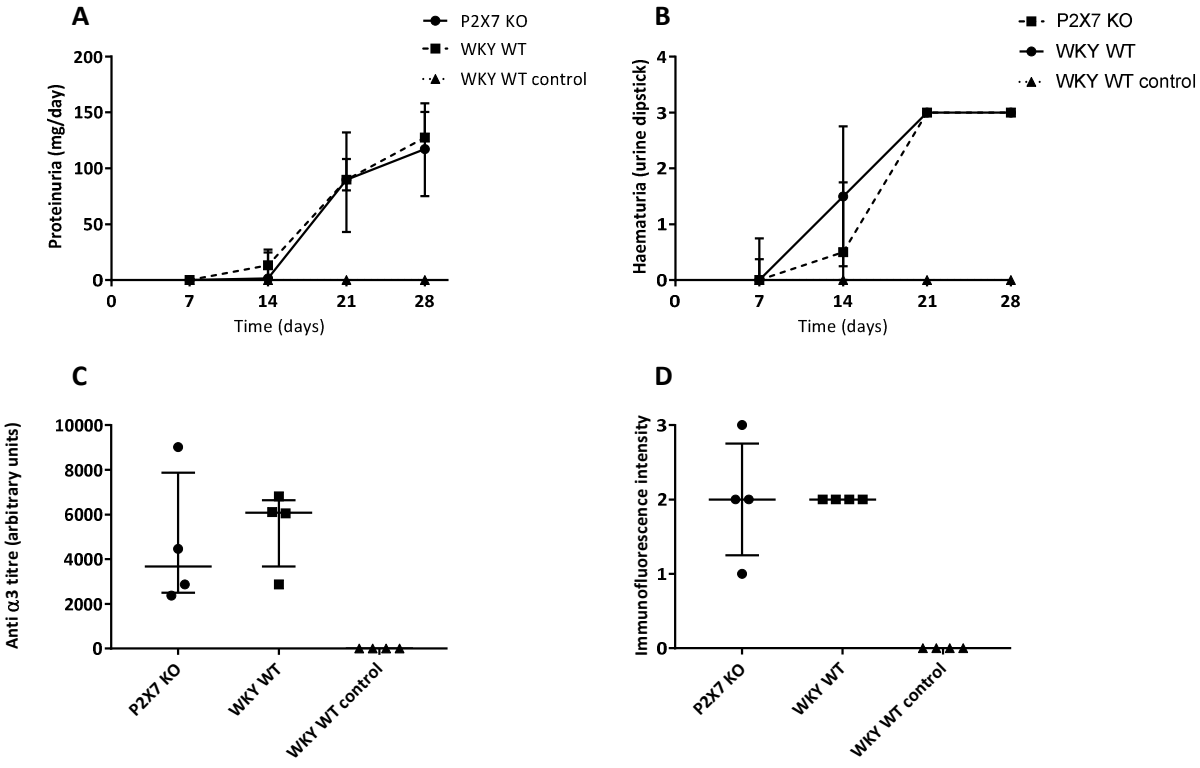

Figure 4.19 Urinary abnormalities and humoral responses in EAG 4
(A) Proteinuria, (B) Haematuria, (C) Circulating anti- α3(IV)NC1 antibody levels at day 28, (D) Quantification of direct immunofluorescence for deposited rat IgG. Data shown are median with IQR

4.7.2.2 Spontaneous cytokine production from nephritic glomeruli cultured ex vivo

As in the previous experiment nephritic glomeruli were isolated from each of the animals, cultured ex vivo for 48 hours and spontaneous cytokine production measured. There was significant amount of IL-1β detected in supernatant from both P2X7 KO and WKY WT glomeruli and none detected in supernatant from glomeruli from animals immunised with CFA alone. Given that macrophages from P2X7 deficient rats cannot produce IL-1β this result implies that another cell type than renal macrophages are the source of this cytokine. There was also detectable IL-6 and MCP-1 in supernatant from P2X7 KO and WKY WT glomeruli and none or minimal from control animals. There was a small increase in the amount of both of these cytokines released from WKY WT glomeruli compared to P2X7 KO but there was considerable overlap and this was not significant (Figure 4.20).

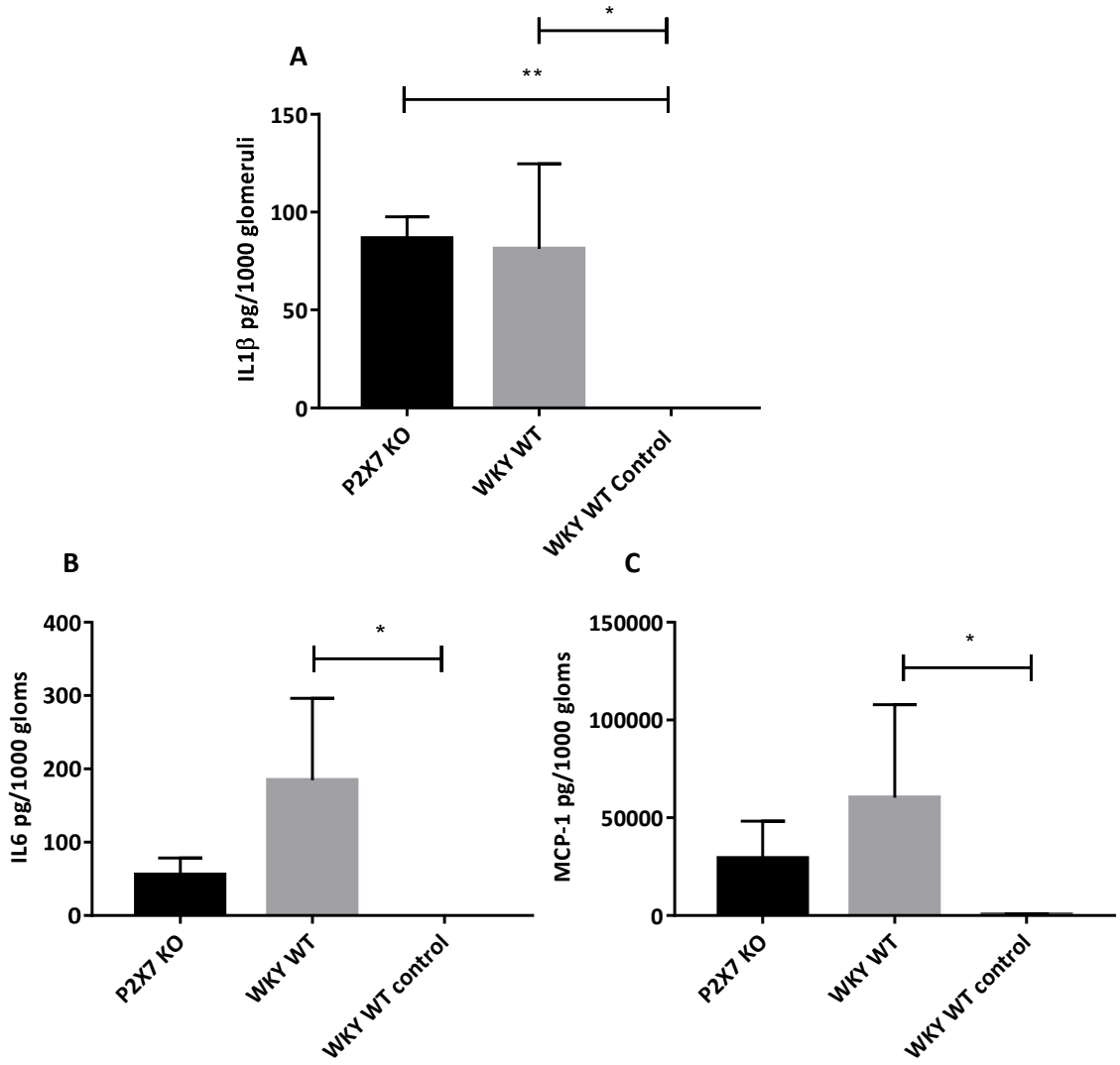

Figure 4.20 Spontaneous cytokine production by nephritic glomeruli *ex vivo* in WKY WT, P2X7 KO and control animals in EAG day 28

Production of pro-inflammatory cytokines by nephritic glomeruli over 48 hours (A) IL-1β, (B) IL-6, (C) MCP-1. As the yield of sieved glomeruli was variable for each replicate, cytokine production was normalised to 1000 glomeruli cultured. Data shown are median with IQR. Statistical analysis was performed using Kruskall-Wallis test with Dunn's post-test comparison to WKY WT control group. *p<0.05, **p<0.01

4.8 The effect of P2X7 deficiency on day 42 EAV

Although there was no difference in the severity of NTN and EAG between P2X7 KO and WKY WT rats, EAV is a distinct model with different pathogenic mechanisms and so a role for P2X7 in this model was investigated. Six female P2X7 KO rats aged 6-7 weeks and 6 age and sex matched WKY WT controls were immunised with human MPO in CFA, animals also received 500 ng of pertussis toxin IP as an immune adjuvant on day 0 and day 2. Rats were sacrificed at day 42 with weekly urine collections and fortnightly serum collection from day 14 onwards.

4.8.1 Haematuria and proteinuria

By day 28 after immunisation all animals had developed urinary abnormalities. The degree of proteinuria in this model is very mild and haematuria is the predominant abnormality. Onset of microscopic haematuria was at day 28 and this progressed in severity until day 42. There was no difference in the degree of urinary abnormalities observed between the two groups (Figure 4.21).

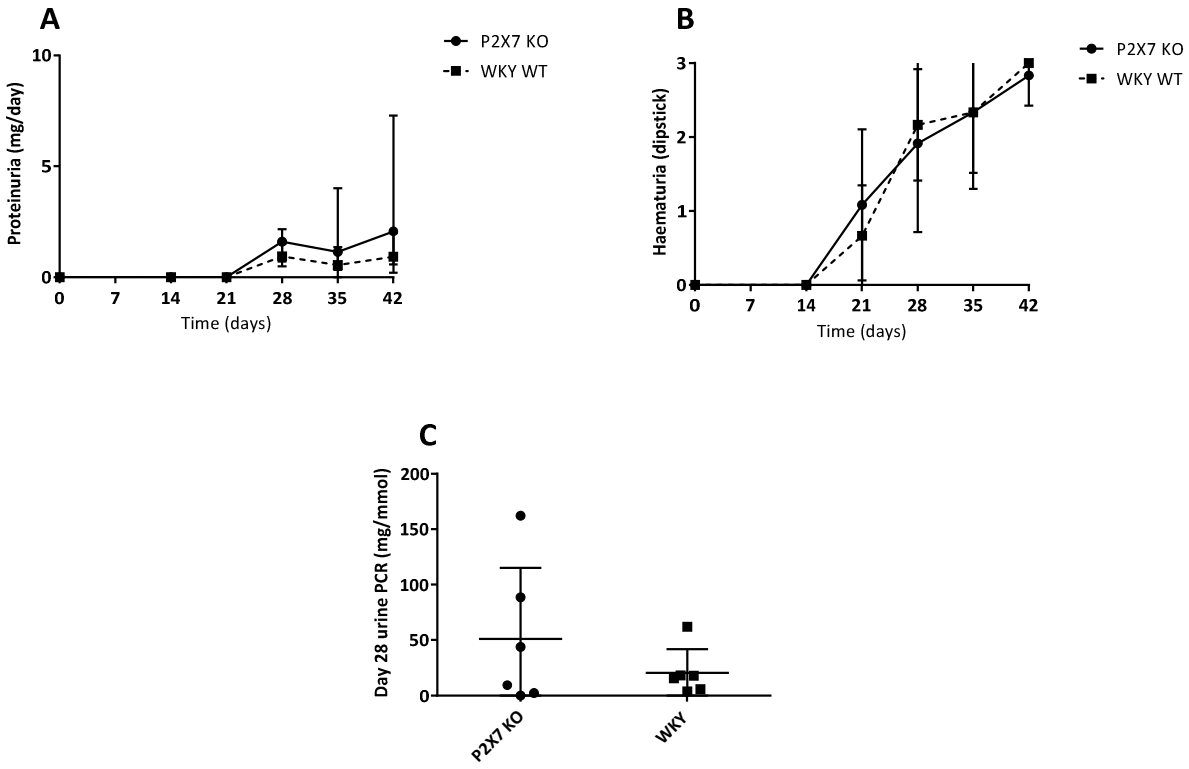

Figure 4.21 Urinary abnormalities in EAV in WKY WT and P2X7 KO rats
(A) Proteinuria, (B) Haematuria and (C) day 28 uPCR. Data shown are median with IQR

4.8.2 Histological injury and infiltrating leucocytes

Assessment of histology at day 42 revealed mild glomerular abnormalities. The most common abnormalities seen were minor proliferation and segmental necrosis; crescent formation was infrequent. Histological abnormalities were similar between the two groups. The degree of inflammatory cell infiltration into glomeruli was assessed using immunohistochemical staining for a rat macrophage marker, ED-1. Levels of infiltrating ED-1 cells were similar between the two groups although, again the degree of cellular infiltration was not high in either group (Figure 4.22).

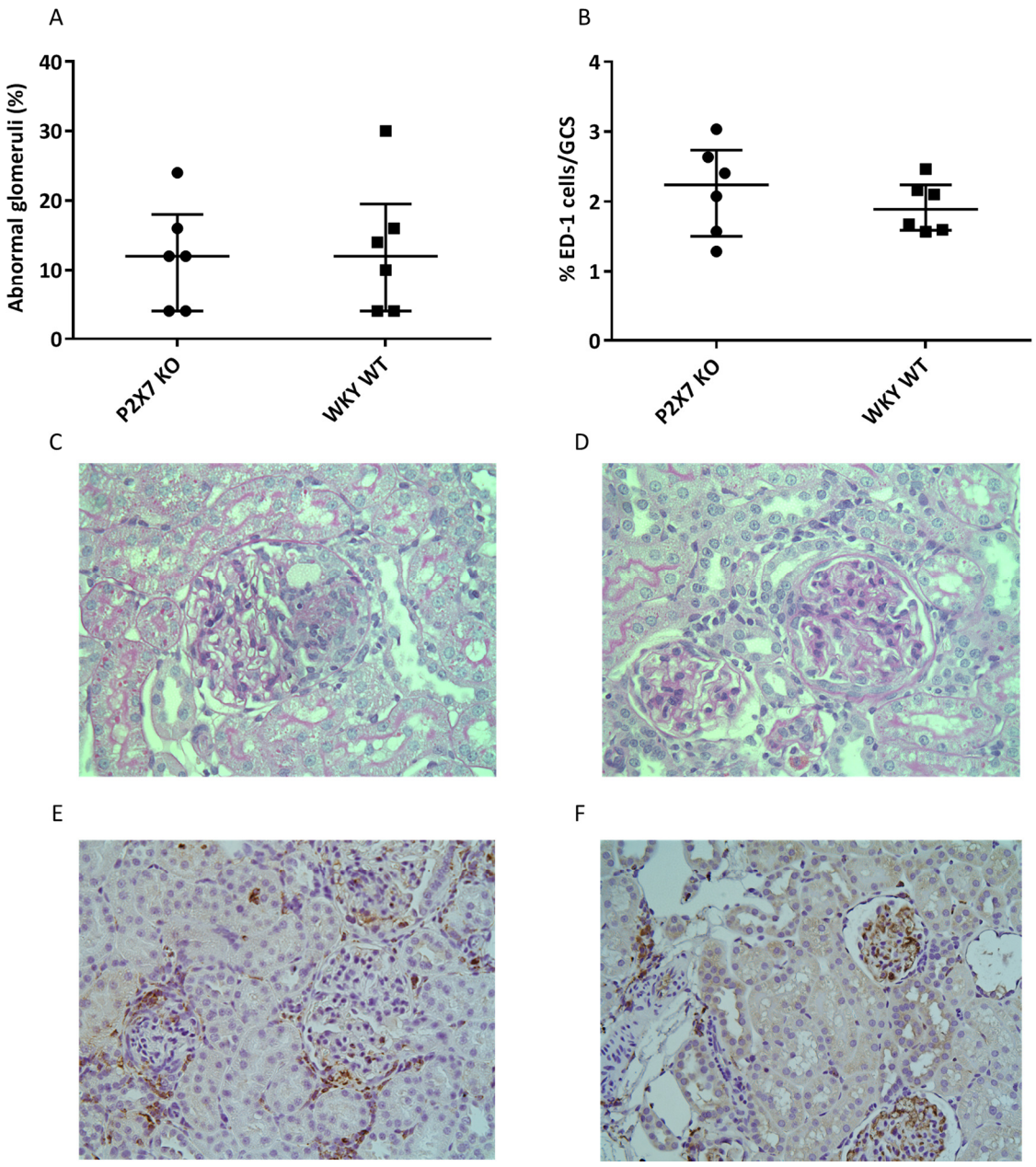

Figure 4.22 Severity of glomerular injury and glomerular leucocyte infiltration in EAV in WKY WT and P2X7 KO rats

(A) Proportion of abnormal glomeruli, (B) Macrophage infiltration quantified as mean % of ED-1 cells per glomerular cross section (GCS). Data shown are median with IQR. Photomicrographs showing representative histology in (C) P2X7 KO and (D) WKY WT. PAS stain, x400 magnification. Photomicrographs showing representative immunoperoxidase staining for ED-1+ cells in (E) P2X7 KO and (F) WKY WT x200 magnification.

4.8.3 Renal function

In keeping with the mild histological abnormalities seen in the model, renal function was well preserved at day 42 after disease induction and there was no difference between the two groups in either absolute values for serum urea and creatinine or in urea or creatinine clearance (Figure 4.23).

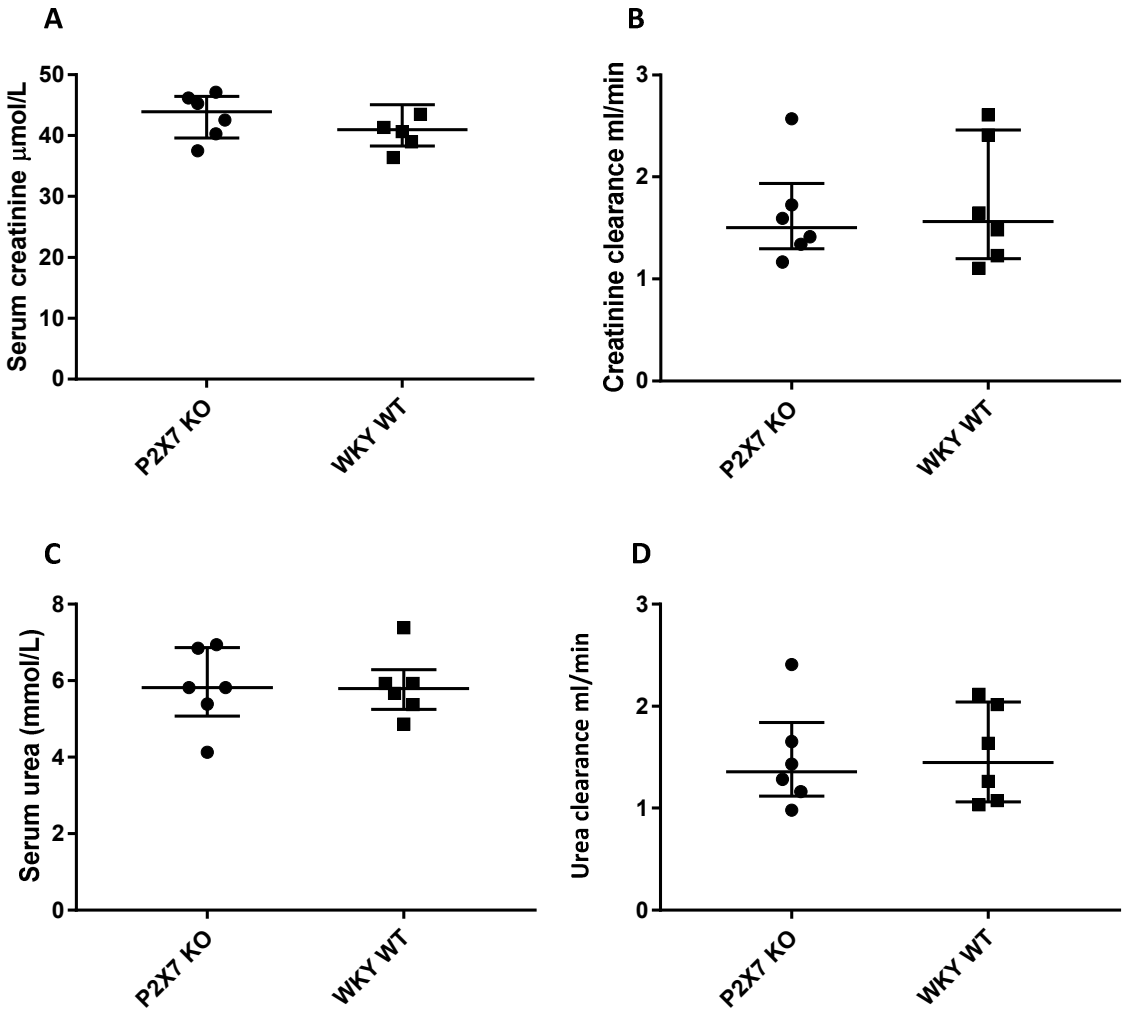

Figure 4.23 Renal function in EAV in WKY WT and P2X7 KO rats
(A) Serum creatinine, (B) Creatinine clearance, (C) Serum urea and (D) Urea clearance in WKY WT and P2X7 KO rats at day 42. Data shown as median with IQR.

4.8.4 Lung haemorrhage

At time of sacrifice all animals but one had macroscopic evidence of some degree of lung haemorrhage and there was corresponding haemosiderin laden macrophages on microscopic examination. Degree of lung haemorrhage was similar in P2X7 KO and WKY WT animals (figure 4.24).

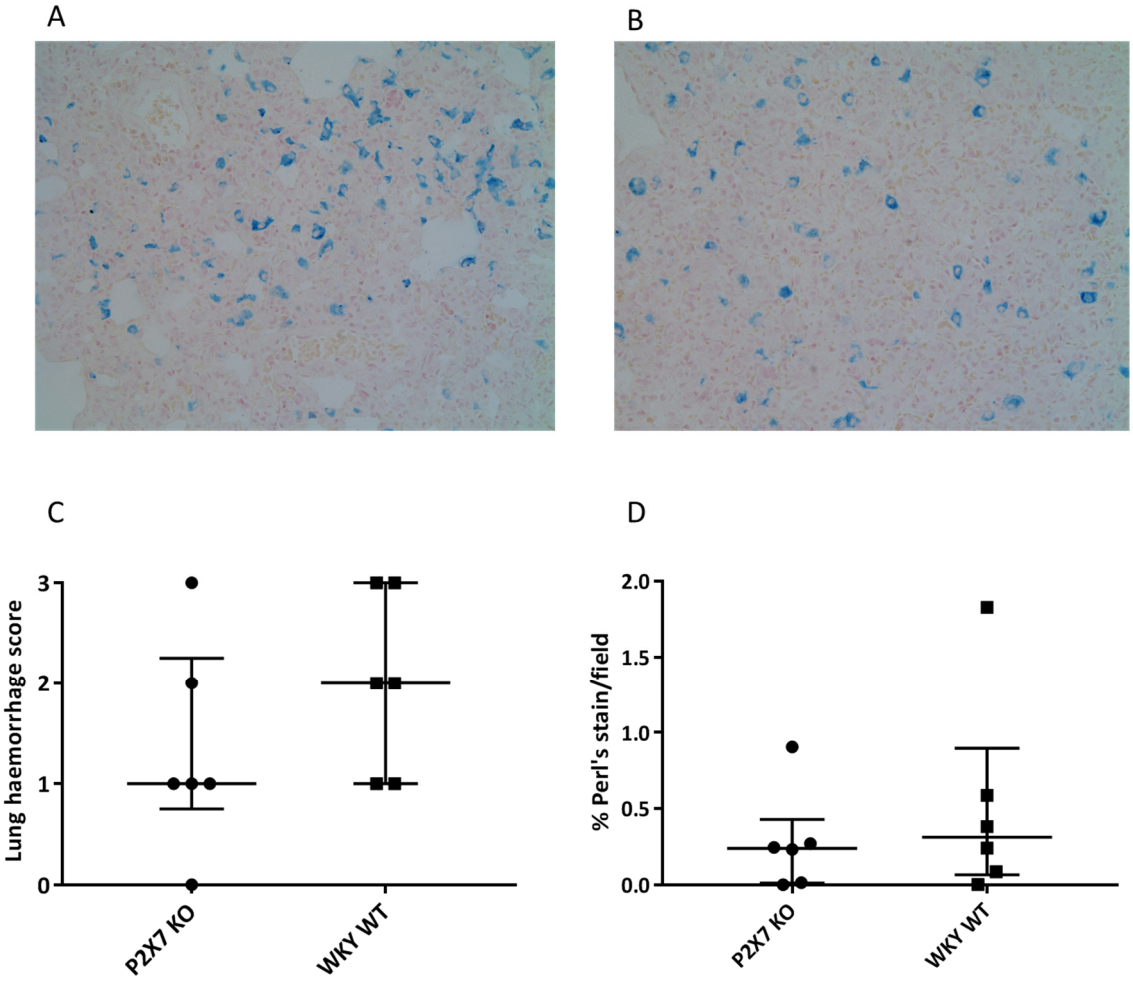

Figure 4.24 Lung haemorrhage in EAV in WKY WT and P2X7 KO rats
Photomicrographs showing representative staining for haemosiderin laden macrophages in the lung using Perls' Prussian Blue in (A) P2X7 KO and (B) WKY WT x200 magnification, (C) Macroscopic lung haemorrhage score and (D) Quantification of haemosiderin laden cells in lung tissue. Data shown as median with IQR.

4.8.5 Humoral responses

4.8.5.1 Deposited and circulating anti-MPO antibodies

Anti-MPO antibodies developed by day 28 in all animals and levels were similar in both P2X7 KO and WKY WT rats. Direct immunofluorescence for deposited IgG was negative in keeping with the pauci-immune pattern of renal disease which has previously been described in this model. There was no difference in observed glomerular immunofluorescence intensity between the two groups (Figure 4.25)

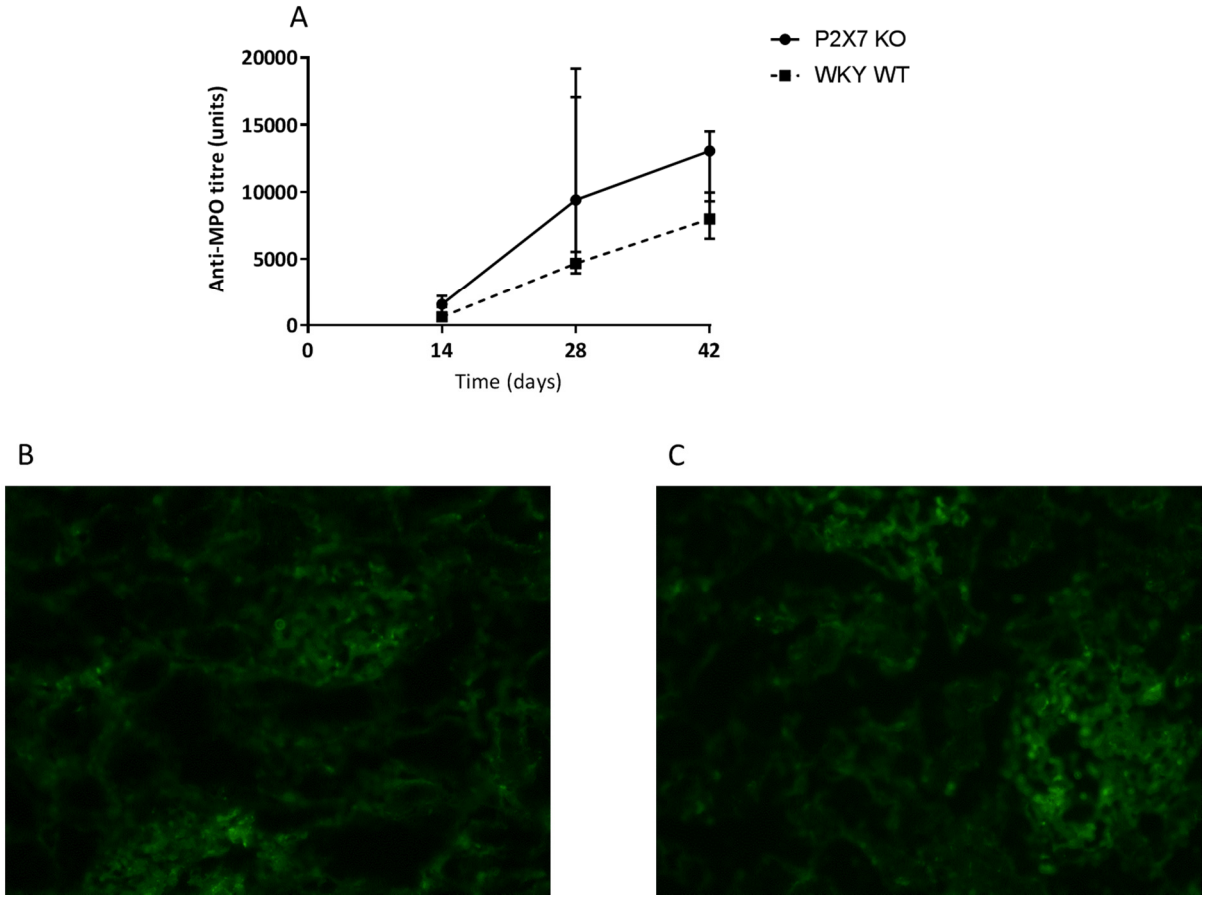

Figure 4.25 Humoral responses in EAV in WKY WT and P2X7 KO rats
(A) Circulating anti-MPO antibody as measured by ELISA. Data shown are median with IQR. Photomicrographs showing direct immunofluorescence for rat IgG in (B) P2X7 KO and (C) WKY WT. anti-rat IgG FITC x200 magnification.

4.8.5.2 Indirect immunofluorescence using rat anti-MPO IgG

In this model rats are immunised with human MPO so to ensure antibodies produced reacted with rat MPO on leucocytes I used IgG purified from the serum of rats with EAV for indirect immunofluorescence on acetone fixed bone marrow cell cytospins. This showed binding of the antibody to rat leucocyte cytoplasm in a perinuclear pattern particularly to neutrophils. Control IgG isolated from serum of control rats did not show reactivity (Figure 4.26).

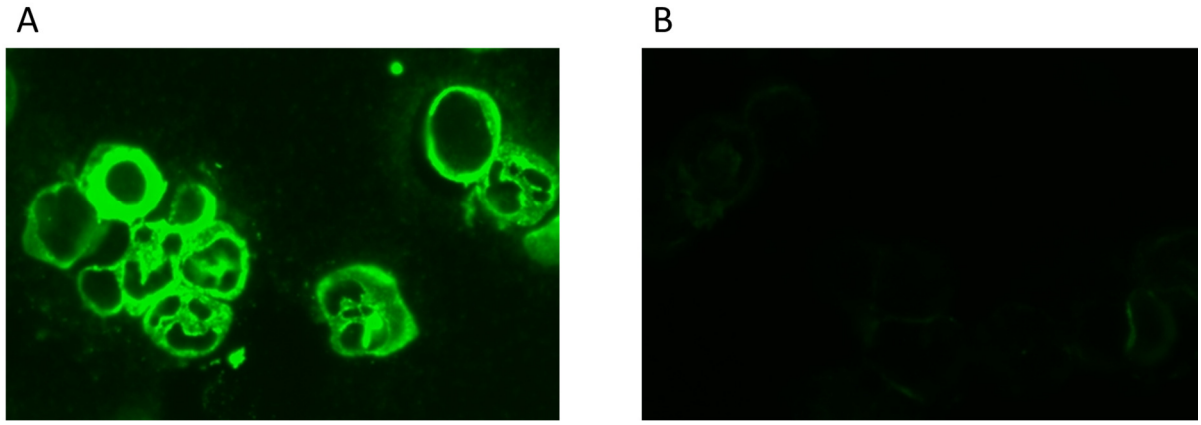

Figure 4.26 Indirect immunofluorescence on acetone fixed rat bone marrow
Indirect immunofluorescence using (A) anti-MPO IgG isolated from serum of rats with EAV and (B) IgG from serum of control rats. Antibodies are directed against rat cytoplasm with a perinuclear patter. Anti- rat IgG FITC x400 magnification.

4.8.5.3 B Cell ELISpot in EAV

I used a B cell ELISpot technique to determine if there were differences in antigen-specific B cell numbers between P2X7 KO and WKY WT rats with EAV. Both P2X7 KO and WKY WT rats had similar numbers of specific B cells whereas control splenocytes generated a weaker B cell response against MPO (Figure 4.27)

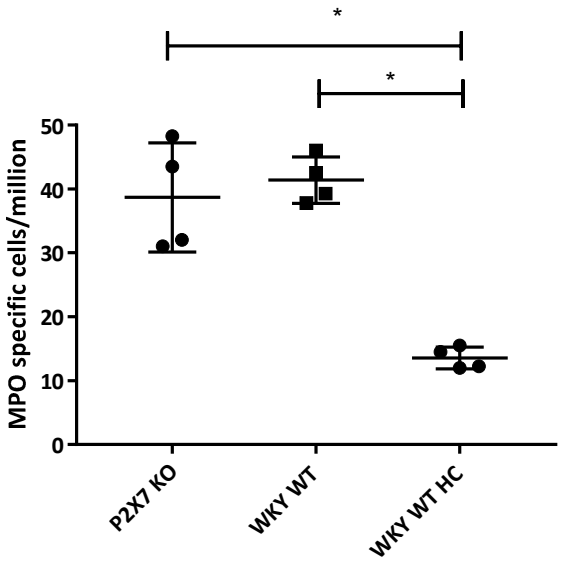

Figure 4.27: MPO-specific splenic B cells in WKY WT and P2X7 KO rats with EAV and WKY WT control rats

MPO-specific B cells identified by B cell ELISpot. Results are from 4 biological replicates which were each performed with 4 technical replicates. Each data point is the mean of 4 technical replicates with median with IQR. Statistical analysis was performed using Kruskall-Wallis test with Dunn's multiple comparison test to healthy control (HC) rats. *$p<0.05$

4.9 Discussion and future work

The results presented in this chapter show that the P2X7 KO rat is not protected from experimental GN or vasculitis. There are equivalent degrees of renal injury, lung injury and humoral responses in all 3 models of disease studied. Three distinct in vivo models were used: NTN a passive model of glomerular injury due to anti-GBM antibodies; EAG an auto-immune model of anti-GBM disease with crescentic GN and lung haemorrhage and; EAV an auto-immune model of AAV with lung haemorrhage and milder glomerular injury.

The three main hypotheses to account for these results were;

1. There is a persistent splice variant in the P2X7 deficient rat which is able to mediate disease

2. Knockout of P2X7 in utero results in over-development of other pathways which are able to mediate disease despite P2X7 deficiency

3. P2X7 is not sufficient to mediate disease alone and other pathways predominate in development of autoimmunity and glomerular injury in rats.

As described in chapter 3 I could find no evidence of a persistent splice variant at the protein level and bone marrow derived cells behave in a functionally P2X7 deficient way in terms of both cytokine production and pore formation. As discussed in Chapter 3 it is possible that a previously unknown splice variant which terminates before exon 10 could have escaped deletion. However, such a splice variant would be missing the C terminus of P2X7 and therefore unlikely to be functional. Given this it would seem unlikely that a persistent splice variant is mediating disease in the animal models.

In order to differentiate between hypothesis 2 and 3 I planned an experiment using the NTN model of GN with the administration of P2X7 antagonist to both P2X7 KO and WKY WT rats. These results are described in chapter 5.

4.10 Summary of key findings

1. NLRP3, IL-1β and P2X7 are up-regulated at the RNA level in renal cortex from rats with experimental glomerulonephritis and vasculitis

2. P2X7 deficient rats are not protected from NTN, EAG or EAV

3. Nephritic glomeruli cultured ex vivo from rats with EAG secrete IL-1β and this occurs to a similar degree in both P2X7 deficient and WKY WT rats

Chapter 5: P2X7 antagonist in nephrotoxic nephritis

5.1 Introduction

My results described in chapter 4 have shown no difference in severity in NTN, EAG and EAV between P2X7 deficient and WKY WT rats. These results were somewhat surprising given work previously published by our group showing that P2X7 deficiency in mice and use of a P2X7 antagonist in rats resulted in decreased severity of NTN. My results presented in chapter 3 suggest that this rat strain truly is deficient in P2X7; I could detect no P2X7 protein in tissues and no functional P2X7 in bone marrow derived cells. The likelihood that persistence of such a splice variant is mediating P2X7 signalling sufficiently to explain preserved disease severity in these models seems small, leaving 2 main hypotheses;

1. P2X7 is not a critical pathway for development of experimental GN or,

2. Up-regulation of alternative pathways due to global knockout of P2X7 in utero is mediating disease in the P2X7 KO (but not WKY WT) rat,

In order to differentiate between these two hypotheses and also to confirm I could replicate our earlier results using the P2X7 antagonist in NTN, I administered P2X7 antagonist to both WKY WT and P2X7 KO rats. The experimental design is summarised in Figure 5.1.

Rats were immunised with NTS on day 0 and started treatment with P2X7 antagonist (A438079) 12 hours later on day 1. Antagonist was administered twice daily by IP injection for 6 days at a dose of 275 µmol/kg. This dose was selected as the maximum tolerable dose, and as in our published study 300 µmol/kg was effective but 100 µmol/kg was not. Animals were sacrificed on day 7 (12 hours after the last dose of antagonist). Day 7 was selected as this was the maximum length of time I could administer the antagonist IP twice daily within the limits set in our home office license. The antagonist needs to be given by IP injection, although unpublished PK data does show some oral bioavailability. C_{max} was 0.45 mg/ml at 15 minutes after an IP dose of 10 µmol/kg and 0.12 mg/ml at 20 minutes after the same dose given orally but there was greater variation

between animals in response to oral dosing. At day 7 after induction of NTN all animals will have significant haematuria and proteinuria with extensive glomerular leucocyte infiltration and histological abnormalities making this a suitable time point to study the effects of P2X7 antagonist.[267]

Nine 8-9 week old P2X7 KO rats and 10 age and sex matched WKY WT controls were immunised with NTS. In the two groups 4 or 5 animals respectively received P2X7 antagonist and 5 received vehicle (sterile water).

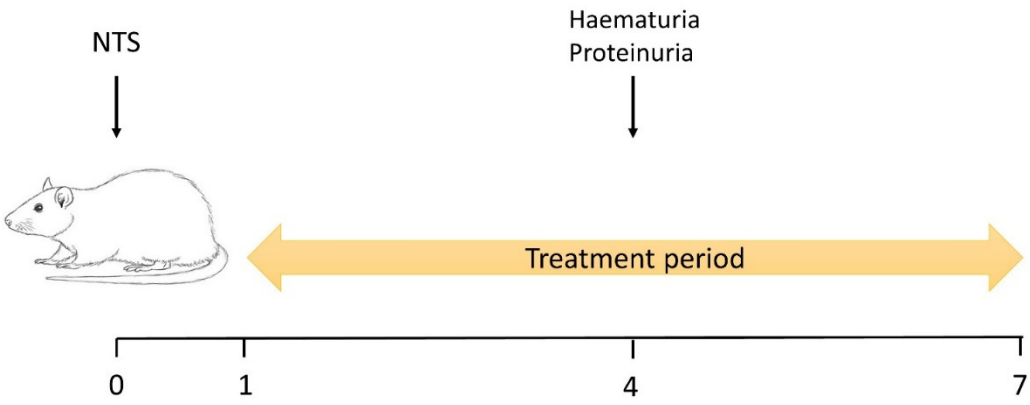

Figure 5.1 Experimental design for P2X7 antagonist in nephrotoxic nephritis
This experiment aimed to prevent development of NTN using P2X7 antagonist. Rats were immunised with NTS on day 0 and received antagonist from days 1-7.

5.2 Haematuria and proteinuria

At day 7 animals in both vehicle treated groups had significant amounts of haematuria and proteinuria whereas animals receiving P2X7 antagonist were protected (Figure 5.2).

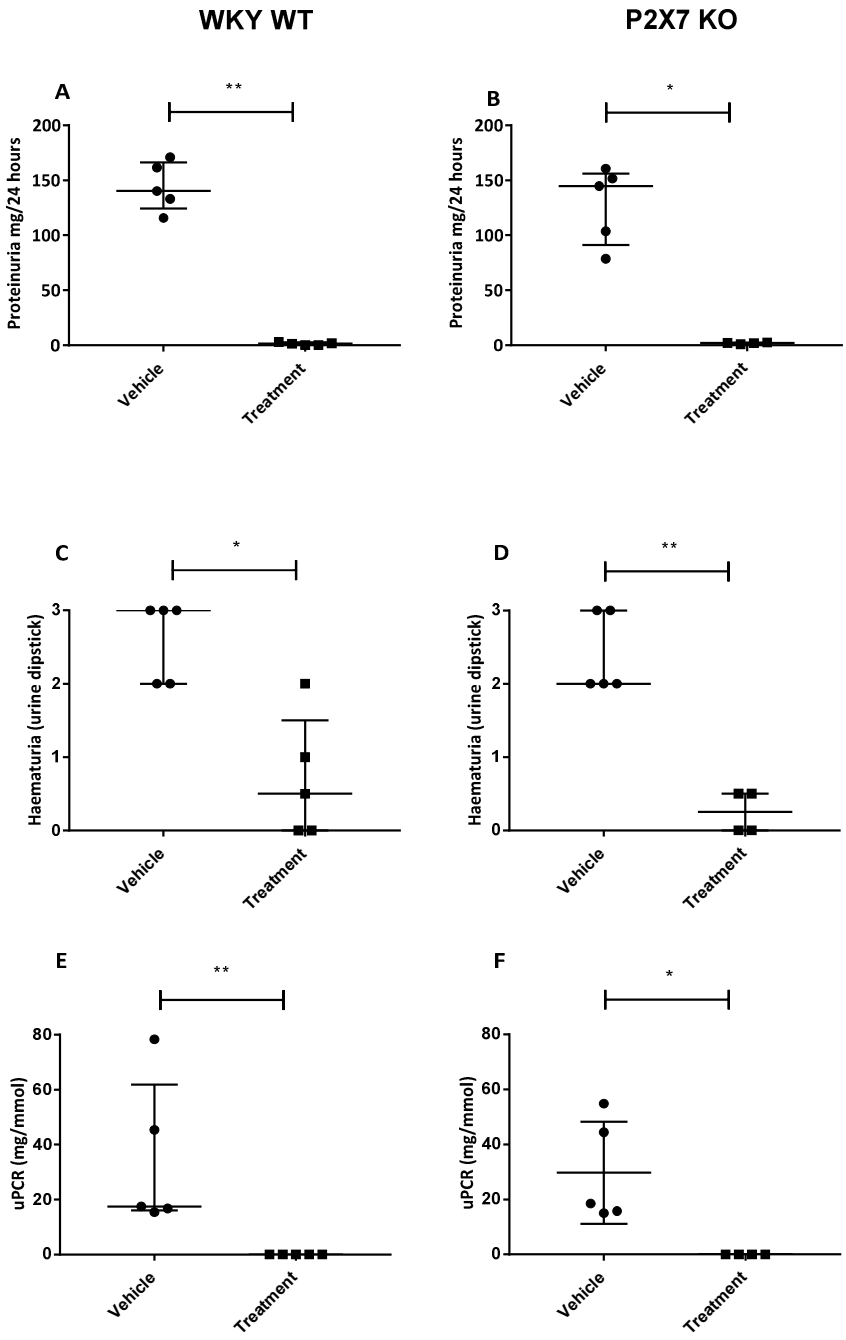

Figure 5.2 Urinary abnormalities in NTN disease prevention

(A) and (B) 24 hour proteinuria at day 7, (C) and (D) Dipstick haematuria at day 7 and (E) and (F) uPCR at day 7 in WKY WT (A, C, E) and P2X7 KO (B, D, F). Data are shown as median with IQR Statistical analysis was performed using Mann-Whitney U test. *p<0.05, **p<0.01

5.3 Histological injury and infiltrating leucocytes

At day 7 there were marked glomerular abnormalities in vehicle treated animals with profound hypercellularity, segmental necrosis and the development of some cellular crescents. Animals receiving P2X7 antagonist were protected from injury and glomeruli were either normal or hypercellular but no severe abnormalities were seen (Figure 5.3).

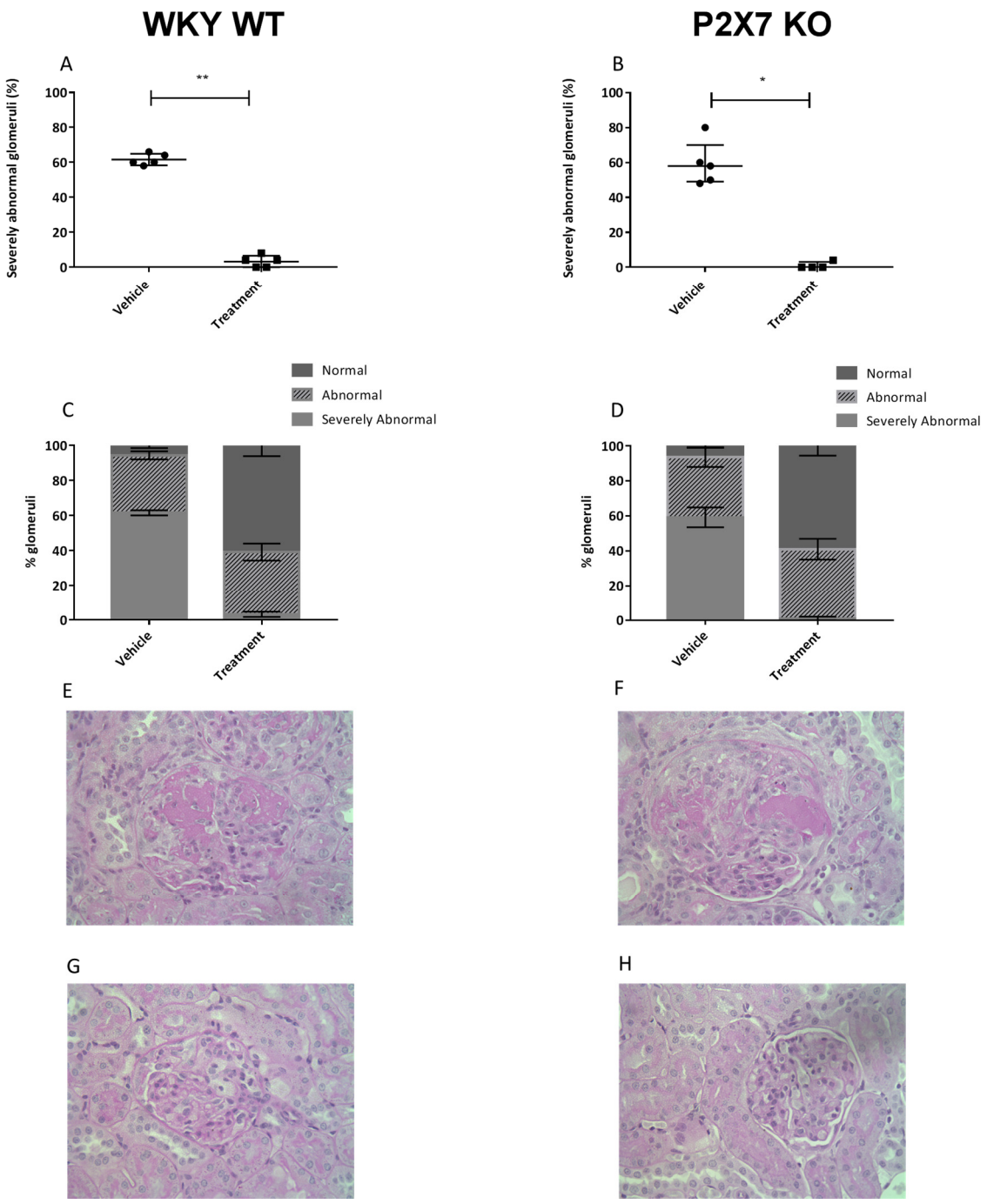

Figure 5.3 Renal histology in NTN disease prevention

Proportion of severely abnormal glomeruli, shown as median with IQR in (A) WKY WT and (B) P2X7 KO rats. Range of glomerular abnormalities (normal, abnormal or severely abnormal) in (C) WKY WT and (D) P2X7 KO rats shown as mean with SEM, Photomicrographs showing representative histology in vehicle treated animals in (E) WKY WT and (F) P2X7 KO and in antagonist treated animals in (G) WKY WT and (H) P2X7 KO. PAS stain, x400 magnification. Statistical analysis was performed using Mann-Whitney U test. *$p<0.05$, **$p<0.01$

In vehicle treated animals there was widespread, massive ED-1 positive cellular infiltrate in all glomeruli. In both groups receiving antagonist there was a significant reduction in cellular infiltrate (Figure 5.4).

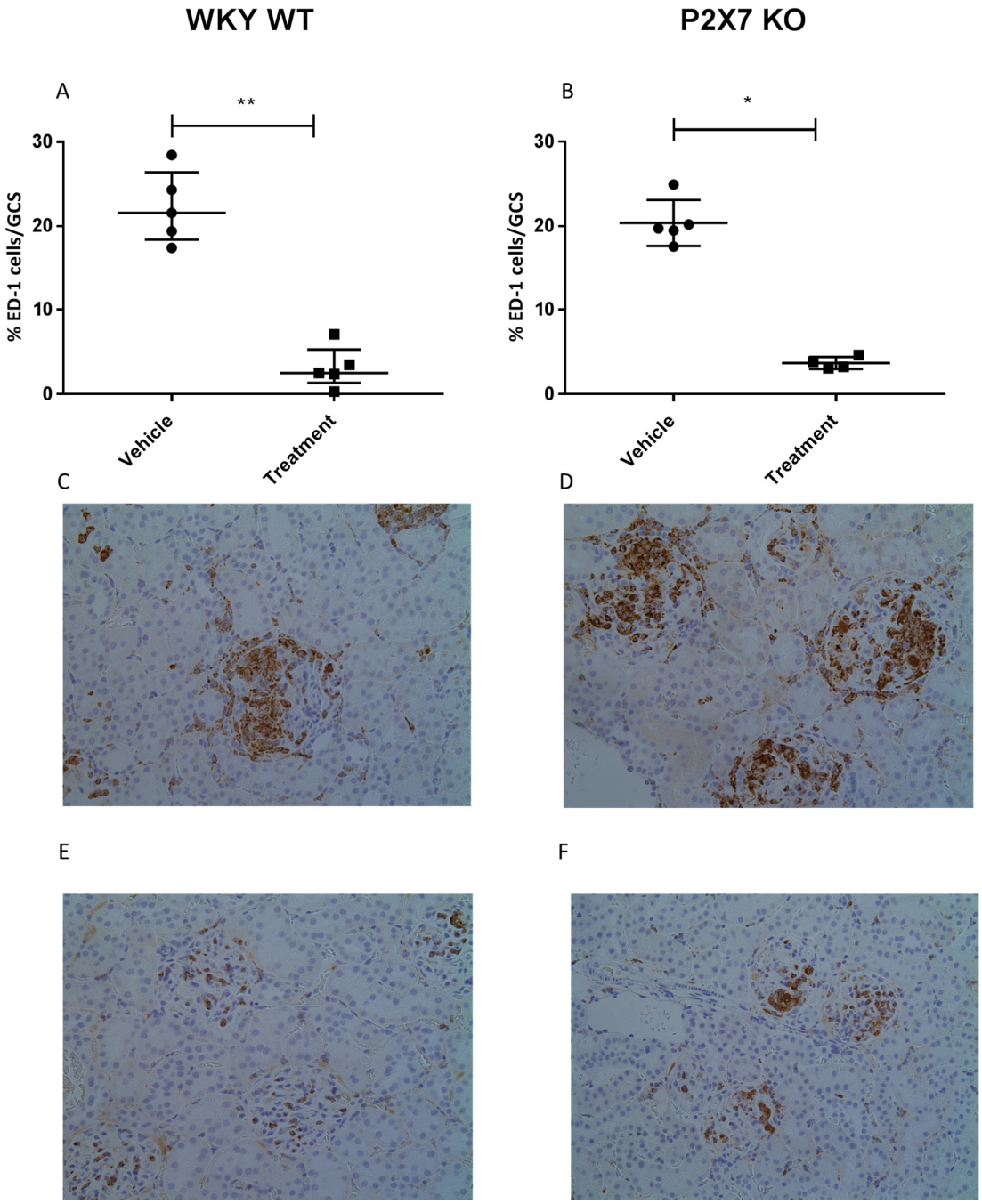

Figure 5.4 Leucocyte infiltration in NTN disease prevention

Macrophage infiltration quantified as mean % of ED-1 cells per glomerular cross section (GCS) in (A) WKY WT and (B) P2X7 KO rats. Data shown as median with IQR. Photomicrographs showing representative immunoperoxidase staining for ED-1+ cells in vehicle treated animals in (C) WKY WT and (D) P2X7 KO and in antagonist treated animals in (E) WKY WT and (F) P2X7 KO. X200 magnification. Statistical analysis was performed using Mann-Whitney U test. *p<0.05, **p<0.01

5.4 Deposited heterologous antibody

At this time point of NTN the immune response is still predominantly in the heterologous phase. Deposited IgG along the glomerular basement membrane was rabbit IgG with largely negative deposited rat IgG. There was no difference between vehicle and antagonist treated rats in either the WKY WT or P2X7 KO groups (Figure 5.5).

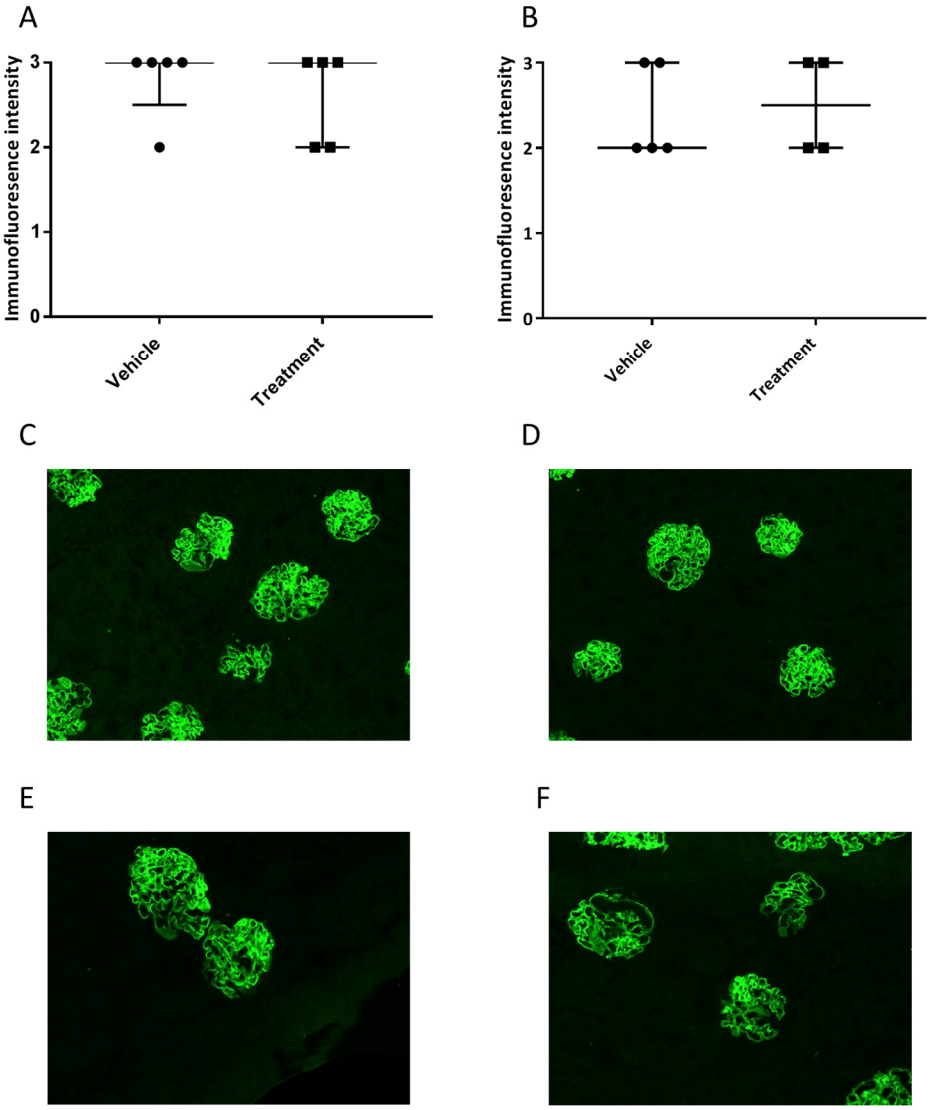

Figure 5.5 Deposited rabbit IgG in NTN disease prevention
Quantification of direct immunofluorescence for deposited rabbit IgG in (A) WKY WT and (B) P2X7 KO rats. Data are shown as median with IQR. Representative photomicrographs from vehicle treated animals are shown in (C) WKY WT and (D) P2X7 KO, antagonist treated animals are shown in (E) WKY WT and (F) P2X7 KO. Anti-rabbit IgG FITC, 200x objective.

5.5 Renal function

Animals in both vehicle treated groups had derangement of renal function with increased urea and decreased urea clearance. In both the group of WKY WT and of P2X7 KO rats treated with P2X7 antagonist there was improvement in these parameters. (Figure 5.6).

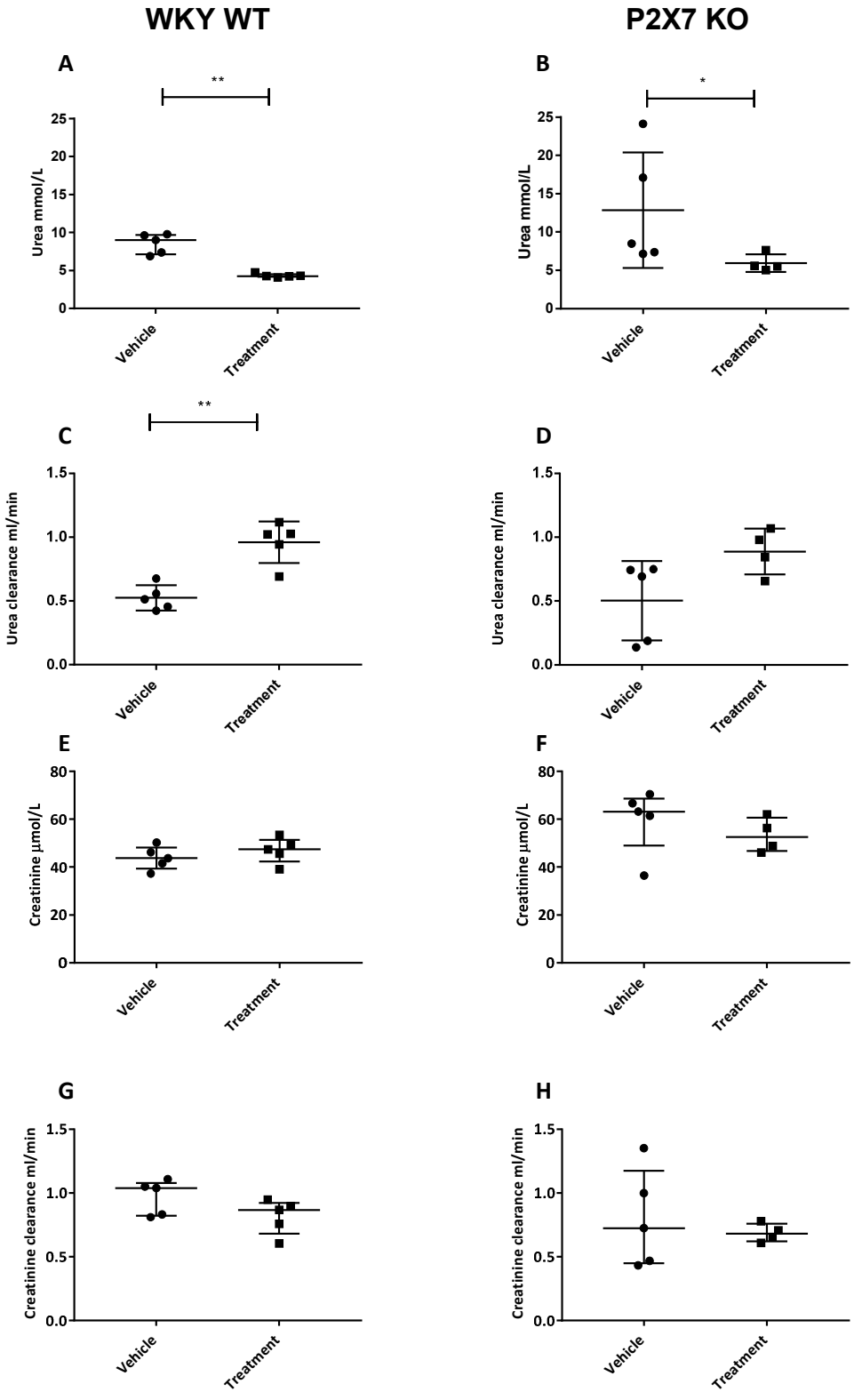

Figure 5.6 Renal function in NTN prevention study

(A) and (B) Serum urea, (C) and (D) Urea clearance, (E) and (F) Serum creatinine and (G) and (H) Creatinine clearance in WKY WT and P2X7 KO rats at day 7. Data shown as median with IQR. Statistical analysis was performed using Mann-Whitney U test. *p<0.05, **p<0.01

5.6 Discussion of results and future work

Both WKY WT and P2X7 KO rats treated with P2X7 antagonist from 12 hours after induction of disease for 6 days were protected from developing NTN. Proteinuria was almost completely abolished in treated rats and there was improvement in renal function as measured by urea or urea clearance. Severity of glomerular injury as assessed by light microscopy was much improved, glomeruli in vehicle treated rats were markedly abnormal with huge cellular infiltrates and extensive fibrinoid necrosis, in P2X7 antagonist treated rats glomeruli were normal or had mild abnormalities such as mild to moderate hypercellularity.

As the P2X7 antagonist is equally as effective in P2X7 KO rats as it is in WKY WT, I suggest that it may be acting via off-target non-P2X7 pathways. Initial PK studies showed that this antagonist was selective for P2X7 compared to other P2X and P2Y receptors in cell culture up to doses of 100µM. At a variety of GPCR, enzymes and kinases in a cell free system it was selective with an ED_{50} >5µM at all tested. Following an IP dose of 10 µmol/kg in rats C_{max} was 0.45 µg/ml (1.3 µM) at 15 minutes after injection and plasma concentration was 0.2 µg/ml (0.59 µM)) at 30 minutes after injection.[187] Based on the available in vitro data these concentrations would be expected to be selective for P2X7. However, the dose used in this experiment (and in many other published in vivo studies) is nearly 30 times higher than this and no PK data is available for this dose. It is reported that a dose of 80 µmol/kg given intravenously results in peak plasma concentrations of 32 µg/ml (93 µM) which is approaching the reported limit of selectivity against other P2 receptors in vitro.[187] It would be useful to perform at least some limited PK studies with this IP dose to determine what the peak plasma concentration is. This concentration of drug could then be used to assess selectivity in vitro, both using a cell culture system for other P2X and P2Y receptors and a cell free microarray to investigate a range of targets. As this antagonist is a small molecule it is plausible that it may be mediating its actions via an intracellular target.

My experiments using the P2X7 antagonist suggest that my results in chapter 4 showing no difference in disease severity between P2X7 KO and WKY WT rats is unlikely to be explained by over development of alternative pathways in P2X7 KO rats. One possibility is that P2X7 is not a critical pathway for development of disease in these experimental models. If this is the case, this leads to questions regarding the relative importance of IL-1β in these models with two main possibilities:

1. The source of IL-1β is cells which can produce bioactive IL-1β via a P2X7 independent mechanism or,

2. IL-1β is not required to mediate renal injury.

There is extensive evidence of a role for IL-1β in mouse models of GN including NTN and anti-MPO AAV. In rats, infusion of IL-1β has been shown to worsen severity of NTN and use of a recombinant human IL1R antagonist (IL1Ra) decreased severity of an accelerated NTN model.[398] My results in chapter 4 also suggest that IL-1β may be important in these models; there is up-regulation of IL-1β mRNA in the kidney cortex of animals with disease and nephritic glomeruli cultured ex vivo from rats with EAG produce IL-1β whereas control glomeruli do not. Interestingly the amount of IL-1β in glomerular supernatant was the same between P2X7 KO and WKY WT glomeruli.

As shown in chapter 3, macrophages produce IL-1β in a P2X7 dependent manner and as expected P2X7 KO cells did not secrete IL-1β. This may imply that cells other than macrophages are the predominant source of IL-1β in the kidney in GN. My results have shown that dendritic cells are able to secrete IL-1β via a P2X7 independent, caspase-1 dependent mechanism and preliminary results (not shown in this thesis) suggest that rat monocytes may also utilise this pathway. Possibly these cell types have greater effect at mediating disease than macrophages. Available rat cell surface markers to distinguish between macrophages, monocytes and dendritic cells are limited,

ED-1 (CD68) and Cd11b are expressed by all 3 cell types. Previous studies therefore may not have differentiated between the roles of monocytes and macrophages in mediating disease.

There is evidence however, in both rat and mouse models of GN that macrophages can mediate glomerular injury. An adoptive transfer study of bone marrow derived macrophages administered to rats pre-treated with cyclophosphamide showed that macrophages were sufficient to induce proteinuria and mesangial cell proliferation in the first 24-48 hours after administration of NTS.[399] However this model was short-lived with disappearance of macrophages from the glomerulus 3-24 hours after transfer. Pharmacological macrophage depletion has been shown in several studies to result in decreased severity of glomerulonephritis however techniques used to deplete cells may be non-specific. Many older studies have used depleting agents such as liposomal clodronate which is non-specific and may also deplete not only myeloid cells but neutrophils too.[400 401] Several more recent studies have used inhibitors of M-CSF[402 403] which is more specific but could possibly also have an effect on circulating monocytes as there is evidence that M-CSF can act to modulate monocyte survival and chemotaxis.[404] A recent study using a multiphoton imaging technique has identified a role for non-classical monocytes in mediating experimental glomerulonephritis, perhaps by promoting neutrophil dependent injury.[405] Future work defining the differential roles for macrophages, monocytes and dendritic cells in rat NTN would help in understanding the mechanisms of disease but may be limited by difficulties distinguishing between these cells using available rat antibodies.

5.7 Summary of key findings

1. A P2X7 antagonist protects rats from developing NTN with decreased urinary abnormalities, severity of glomerular abnormalities, glomerular leucocyte infiltration and improved renal function in treated rats.
2. Both WKY WT and P2X7 KO rats were protected from disease suggesting the antagonist may be having off target effects.

Chapter 6. P2X7 and human neutrophils and PBMC

6.1 Introduction

Thus far my results have focussed on in vivo work using rodent models of GN in the P2X7 knockout rat and using a P2X7 antagonist. In this chapter I set out to define a role for P2X7 on human immune cells both in healthy controls and from patients with AAV. The presence of P2X7 on immune cells such as PBMC and monocytes is well known but there is conflicting evidence as to whether neutrophils have functional P2X7, cytoplasmic receptors only or no P2X7 at all.[36 41 44]

In this chapter I have sought to demonstrate that human neutrophils express cell surface P2X7, using flow cytometry and Western blotting, and to show that the receptors are functional in terms of pore formation and cytokine production. I have then investigated differences in cell surface P2X7 on both neutrophils and PBMC between patients with AAV and healthy controls, and investigated whether stimulation of these cells with MPO-ANCA can result in production of IL-1β by a P2X7 dependent mechanism. I have investigated P2X7 mRNA expression in renal biopsy tissue from patients with AAV using RNAscope.

6.2 Neutrophils

6.2.1 Neutrophil purification

The expression of P2X7 on human neutrophils is a controversial area with conflicting reports as to whether it is expressed as a functional cell surface receptor, as an intracellular receptor, or not at all. Some of this disparity may be related to the difficulties of isolating a population of highly purified but quiescent neutrophils. Therefore, I initially optimised a protocol for isolation of neutrophils using a dextran sedimentation and Percoll gradient technique with water lysis to remove contaminating red blood cells. It is reported in several studies that Percoll gradient results in less

ex vivo activation of cells and greater cell yields when compared to Histopaque.[406] The full isolation protocol is detailed in methods, chapter 2.14.2. Purity of neutrophil preparations was assessed using flow cytometry and cytospins. Neutrophils have uniquely high levels of side scatter making the population easily identifiable on flow cytometry, cell surface staining confirms that these cells express typical neutrophil markers with high levels of CD15 and no expression of CD14 (Figure 6.1).

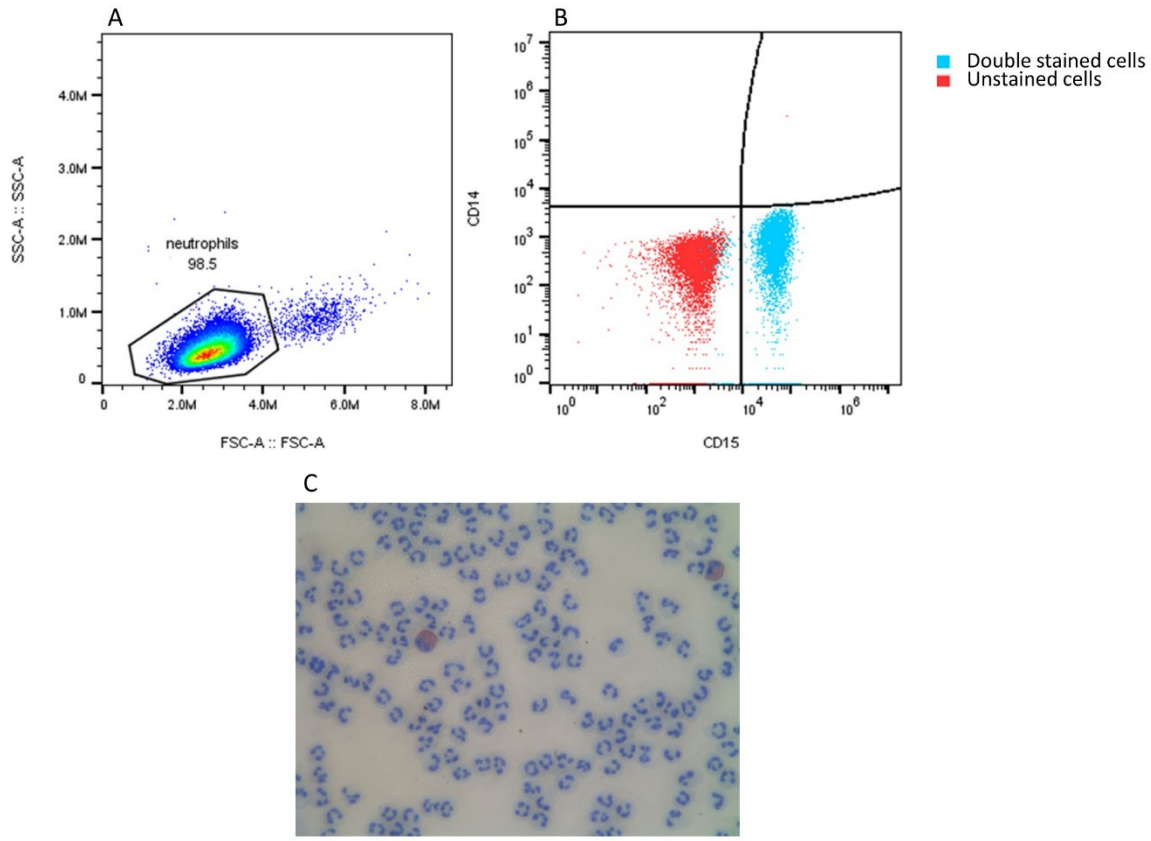

Figure 6.1 Neutrophil purification

(A) FACS plot of forward scatter (FSC-A) and side scatter (SSC-A) of neutrophil preparation showing a population with high side scatter, (B) Cells stain positively for CD15 but do not express CD14, (C) Cytospin of granulocyte layer stained with Kwikdiff™ showing characteristic neutrophil morphology of multilobed nucleus (one eosinophil is seen with red cytoplasm). No contaminating PBMC are seen. 20x magnification.

6.2.2 Neutrophil cell surface P2X7 expression

Neutrophils were isolated from 15 healthy controls and cell surface staining carried out on non-permeabilised cells using an antibody directed against the extracellular domain of P2X7. Analysis using flow cytometry showed that all donors had constitutive expression of cell surface P2X7. Representative staining from 2 patients is shown in Figure 5.2. To confirm this result, cell lysates were used for Western blotting with an antibody directed against the C terminus of P2X7 (Figure 6.2).

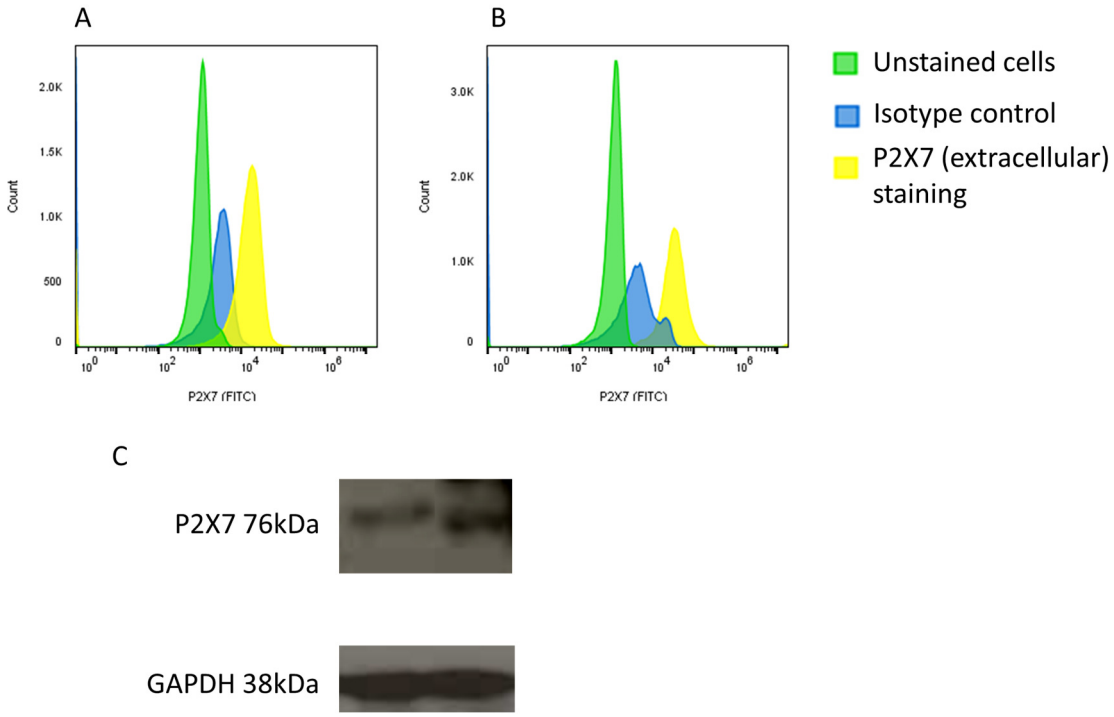

Figure 6.2 Neutrophil P2X7 expression

(A) and (B) Flow cytometry detection of cell surface staining for P2X7 using a FITC conjugated antibody directed at the extracellular domain. Images are representative from 2 of 15 different healthy donors. Granulocytes were gated on FSC and SSC. (C) Western blot analysis of P2X7 (C terminus antibody) neutrophil lysates from 2 healthy donors.

6.2.3 P2X7 functional responses on human neutrophils

To determine whether P2X7 receptors on neutrophils were functional I investigated their ability to form pores and produce cytokine in response to stimulation with LPS and ATP. Neutrophils did not tolerate live cell flow cytometry well, so an end point study looking at dye uptake in response to ATP was used rather than real time imaging. Neutrophils were primed with and without LPS 100ng/ml for 4 hours then media removed and To-pro-3 dye added with or without ATP. After 30 minutes pore formation was inhibited with excess magnesium and cells fixed prior to analysis. Stimulation with ATP induced pore formation and dye uptake into cells and priming with LPS did not significantly alter the amount of dye uptake (Figure 6.3).

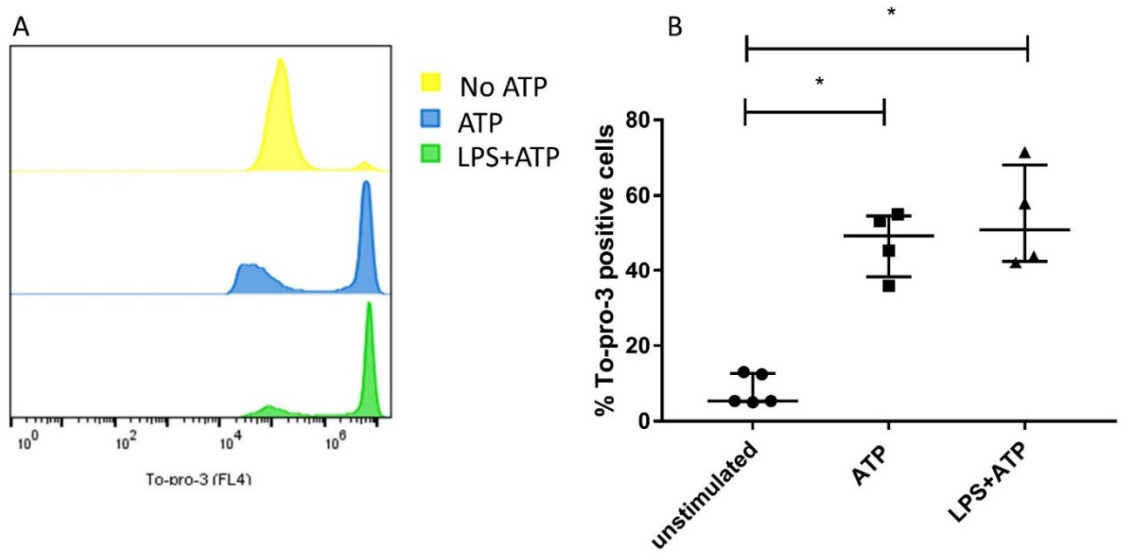

Figure 6.3 Neutrophil pore formation
(A) Representative flow cytometry analysis showing uptake of To-pro-3 by neutrophils in response to stimulation with 5mM ATP with or without 4 hours of LPS 100ng/ml priming, (B) Percentage To-pro-3 positive cells following stimulation with ATP in unprimed and LPS primed cells. Data shown as median with IQR. Statistical analysis was performed using Kruskall-Wallis test with Dunn's post-test comparison to unstimulated cells. *p<0.05.

Neutrophils could also produce IL-1β in a P2X7 dependent manner. In response to stimulation with LPS 100ng/ml for 4 hours and ATP 5mM for 30 minutes neutrophils produced significant IL-1β when compared to unstimulated cells or cells stimulated with LPS or ATP alone. This release was inhibited by use of the P2X7 antagonist A438079 (Figure 6.4).

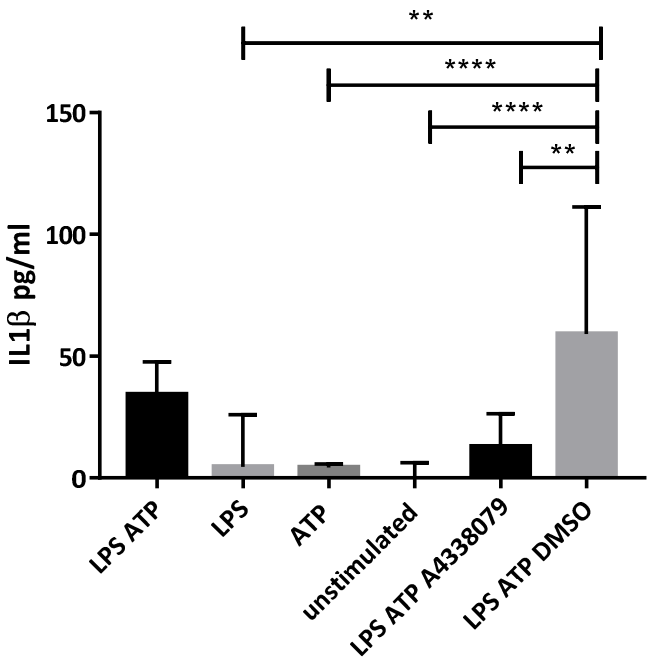

Figure 6.4 Neutrophil cytokine production following stimulation with LPS and ATP
(A) IL-1β production from neutrophils stimulated with LPS 100ng/ml for 4 hours and ATP 5mM for 30 mins with 10μM P2X7 antagonist (A438079) or vehicle (DMSO) prior to addition of ATP. Data shown as mean with SEM. Statistical analysis was performed using one way ANOVA with Dunnett's multiple comparisons post test. **p<0.01, ****p<0.0001. Results are from 5 biological replicates with technical duplicates.

6.2.4 Neutrophil cell surface P2X7 expression in patients with AAV

I next investigated whether neutrophils from patients with AAV had differences in expression to healthy controls. I collected samples from 40 patients with AAV. Nineteen patients had active disease and this was their first presentation of disease, 5 patients had active, relapsing disease and 16 patients were in remission. Patients with an acute presentation of AAV (either new presentation

or relapse) had sometimes received either oral or IV steroids and in the group with relapse one patient was receiving MMF but no patients were receiving other immunosuppression such as cytotoxics or rituximab at the time the sample was taken. The majority of patients had evidence of renal involvement as part of their vasculitis although not all were biopsied due to a need to start urgent treatment. Demographic characteristics of acute and remission patients is summarised in Table 6.1. The healthy control group used had a similar male:female split to the patient group but were of significantly younger age.

	Active (n=24)	Remission (n=16)
Age (years)	67.5 (31.3-85.3)	70.3 (32.8-81.5)
Sex (M/F)	12/12	9/7
MPO/PR3/ANCA negative	12/9/3	7/9/0
Steroids/No steroids	11/13	14/2

Table 6.1 Characteristics of AAV patients included in neutrophil isolation

Patients with active AAV had higher levels of cell surface P2X7 than healthy controls when analysed by flow cytometry. To confirm these results I carried out Western blot which showed higher amounts of P2X7 protein in cell lysates from patients with AAV (Figure 6.5).

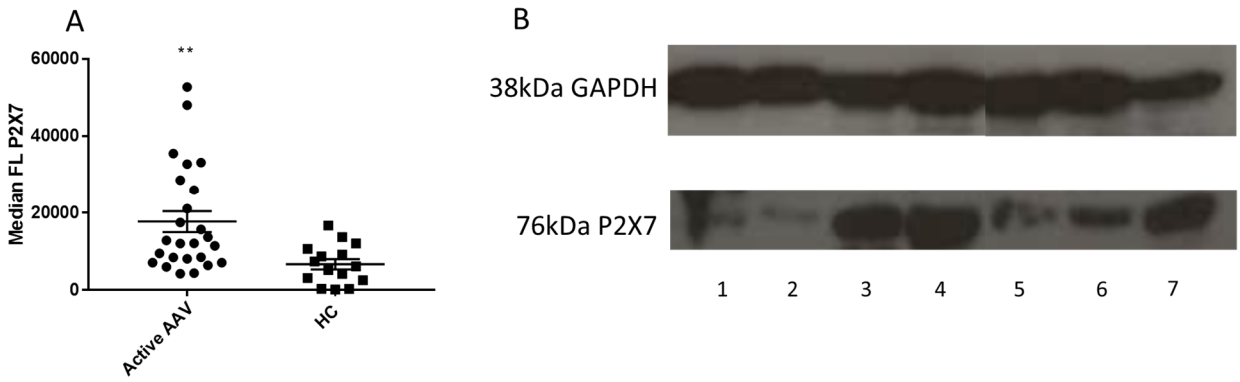

Figure 6.5 Neutrophil cell surface P2X7 expression in patients with AAV and Healthy controls
(A) Cell surface P2X7 analysed by flow cytometry in patients with active AAV and healthy controls (HC), (B) Representative Western blot analysis of P2X7 (C terminus antibody) of neutrophil lysates, 1 and 2: HC, 3-7: AAV patients. Data shown as mean with SEM. Statistical analysis performed using unpaired t test. **p<0.01.

Patients with a new presentation of AAV or with relapse had higher levels of cell surface P2X7 and those in remission had levels which were close to those seen in healthy controls. For 6 patients cell surface P2X7 staining was available both at acute presentation and at remission; in 5 of the 6 cell surface P2X7 expression had fallen in the remission sample. Within the group of patients with active disease (both first presentation and relapse) there were similar levels of cell surface P2X7 on neutrophils from those with MPO-ANCA and PR3-ANCA specificity (Figure 6.6)

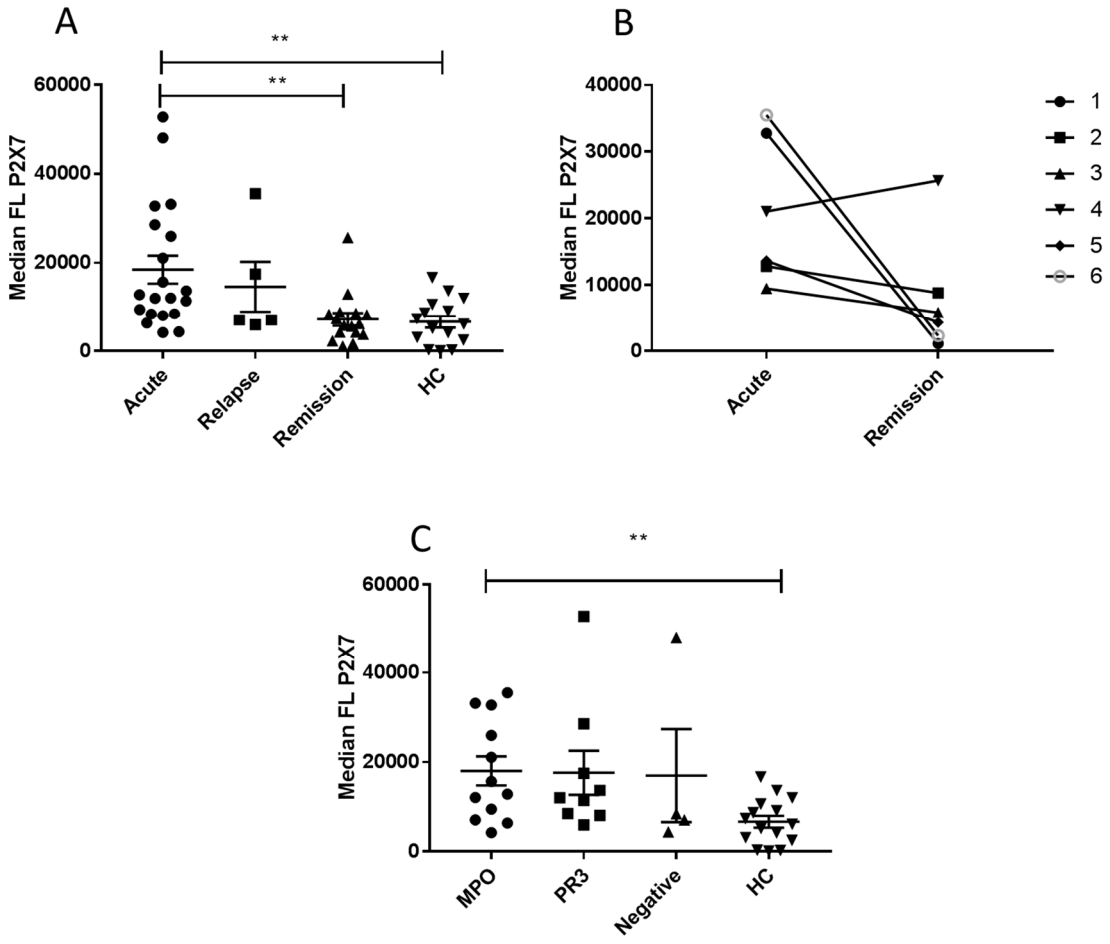

Figure 6.6 Neutrophil cell surface P2X7 expression in patients with active and remission AAV
(A) Cell surface P2X7 analysed by flow cytometry in patients with acute presentation of AAV, relapse of AAV, remission patients and HC, (B) Cell surface P2X7 for individual patients at acute presentation and in remission, (C) Cell surface P2X7 levels by ANCA specificity. Data shown as mean with SEM. Statistical analysis performed using one way ANOVA with Dunnett's multiple comparisons post test. **p<0.01 *p<0.05

When the group of patients with active disease was analysed there was no correlation between cell surface P2X7 and CRP or creatinine at the time the sample was taken (Figure 6.7). There was also no difference between patients with active disease who had received treatment with steroids prior to cell isolation (n=11) and those who had received no immunosuppression (n=13) (mean MFI 17919 and 18553 respectively).

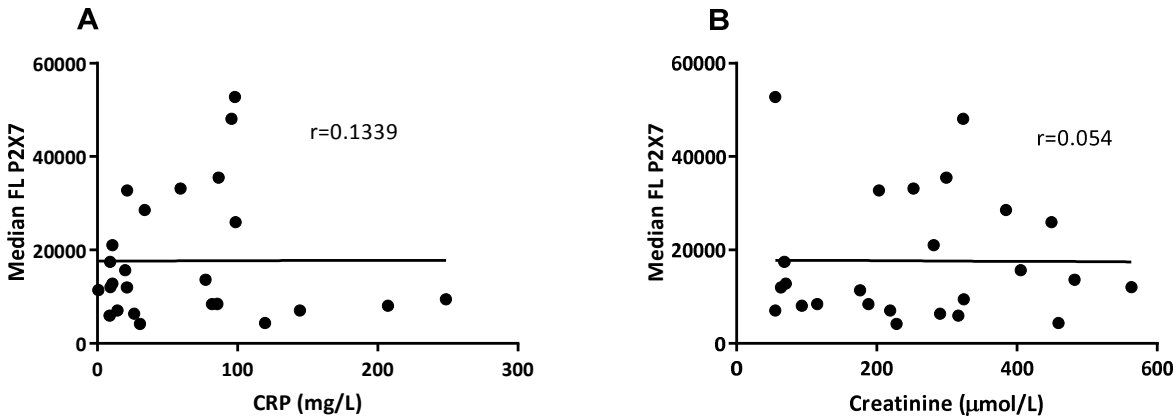

Figure 6.7 Correlation between neutrophil cell surface P2X7 expression and CRP or creatinine in patients with active AAV

(A) Correlation between P2X7 cell surface staining and CRP, (B) Correlation between P2X7 cell surface staining and creatinine. Statistical analysis carried out using Pearson correlation coefficient.

6.2.5 Neutrophil stimulation with MPO-ANCA IgG

6.2.5.1 Purification of MPO-ANCA IgG

MPO-ANCA IgG was isolated from the plasma exchange fluid of patients with anti-MPO AAV using a protein G sepharose column as detailed in 2.14.5. Eluate from the column was collected as 1ml aliquots and protein quantified using a spectrophotometer to measure OD at 280 nm. A representative elution is shown in Figure 6.8.

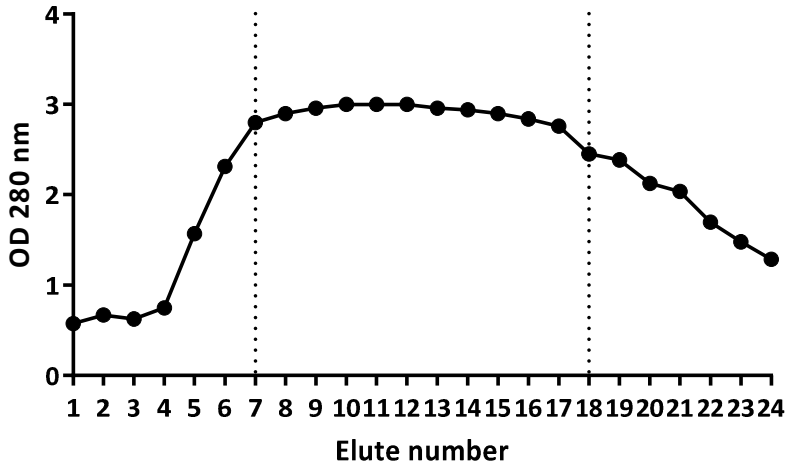

Figure 6.8: Representative elution of MPO-ANCA IgG from protein G column.
Protein content measured at 280nm in serial elutions purified from plasma exchange fluid from a patient with anti-MPO AAV. Fractions between the dotted lines were pooled.

Pooled fractions were dialysed and protein concentration re-quantified. For cell stimulation the amount of MPO-ANCA IgG used was standardised to IgG concentration rather than ANCA titres; however it was necessary to demonstrate that the IgG preparations contained MPO-ANCA IgG. Dialysed IgG from several patients was used on an anti-MPO ELISA along with IgG from a patient with anti-PR3 AAV and a healthy subject as a control. Amount of sample used for ELISA was standardised so the same amount of IgG was used for each patient/control. ELISA results are shown in Figure 6.9.

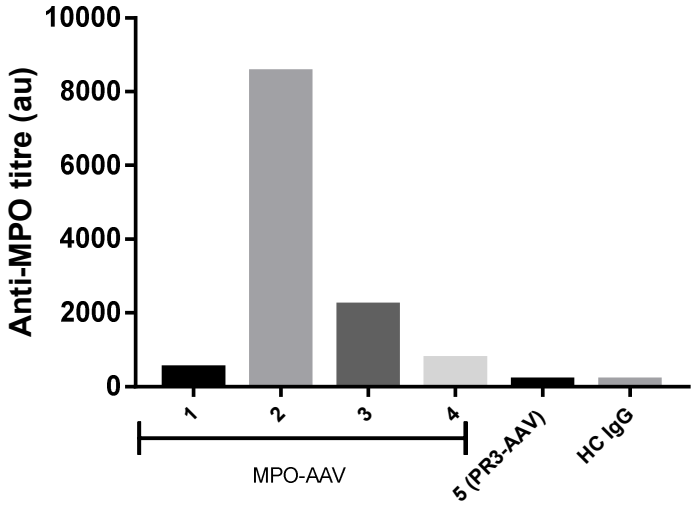

Figure 6.9 Anti-MPO ELISA

Anti-MPO ELISA results using a standardised amount of IgG purified from plasma exchange fluid from patients with anti-MPO AAV (1-4), a patient with anti-PR3 AAV (5) and from serum from a healthy control (HC).

6.2.5.2 Neutrophil stimulation with MPO-ANCA IgG

To test if the MPO-ANCA IgG was pathogenic and could induce neutrophil cytokine production, neutrophils were primed with 2ng/ml of TNFα then stimulated with 100µg/ml of MPO-ANCA IgG or healthy control IgG. Cell culture supernatants were collected and analysed for production of IL-8 and IL-1β. For IL-8 release priming of cells with TNFα was required; however TNFα priming had little effect on increasing the amount of IL-1β released. (Figure 6.10)

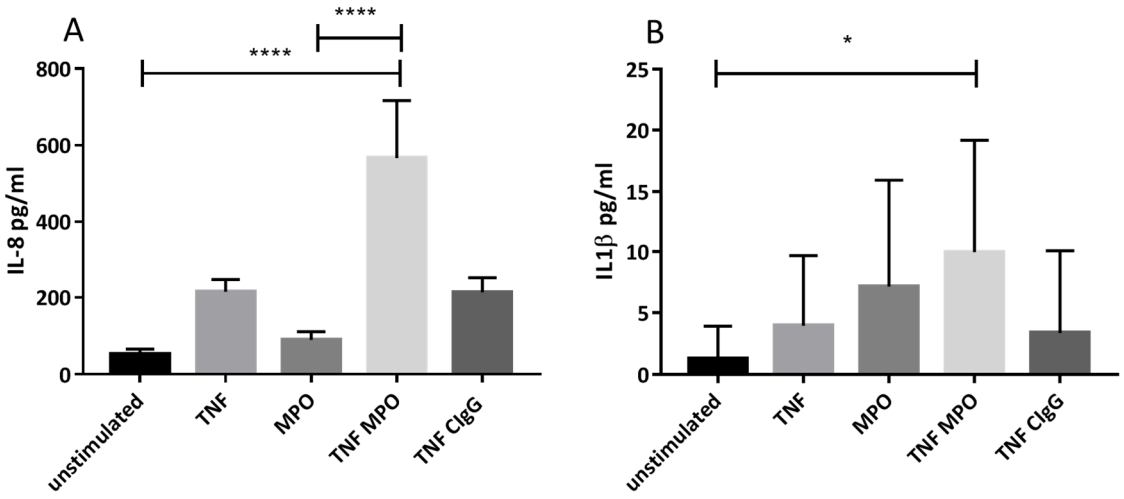

Figure 6.10 Pro-inflammatory cytokine production by human neutrophils following stimulation with TNFα and MPO-ANCA IgG

(A) Neutrophils primed with TNFα and stimulated with MPO-ANCA IgG (MPO) produced significant amounts of IL-8 whereas (B) IL-1β production was similar between neutrophils stimulated with MPO-ANCA IgG alone or TNFα priming followed by MPO-ANCA IgG. Results pooled from 5 biological replicates with technical duplicates. Data shown as mean with SD. Statistical analysis performed using one way ANOVA with Dunnett's multiple comparisons post test. ****p<0.0001, *p<0.05

To investigate whether ATP could enhance cytokine production I added 5mM ATP for 30 mins following stimulation with MPO-ANCA IgG (in TNFα primed and un-primed cells). ATP enhanced IL-1β release to the same degree in cells primed with TNFα and from unprimed cells whereas, as expected, IL-8 release was not enhanced by the addition of ATP. This experiment was to assess the requirement for TNFα priming of cells on IL-1β release so control IgG was not used; following identification of optimum conditions control IgG was used as a control for MPO-ANCA IgG in further experiments. Incubation of cells with 10μM of P2X7 antagonist (A438079) after stimulation with MPO-ANCA IgG and prior to addition of ATP resulted in a significant decrease in IL-1β production. As there was some variation in the amount of IL-1β produced, each experiment was normalised to cytokine production in response to stimulation with MPO-ANCA IgG and ATP. The range of IL-1β produced in response to this stimulus was 9-75 pg/ml (mean 32 pg/ml) (Figure 6.11). Cell viability after stimulation was assessed by 7AAD staining and analysed by flow cytometry. Cell survival was not affected by any of the conditions used (data not shown).

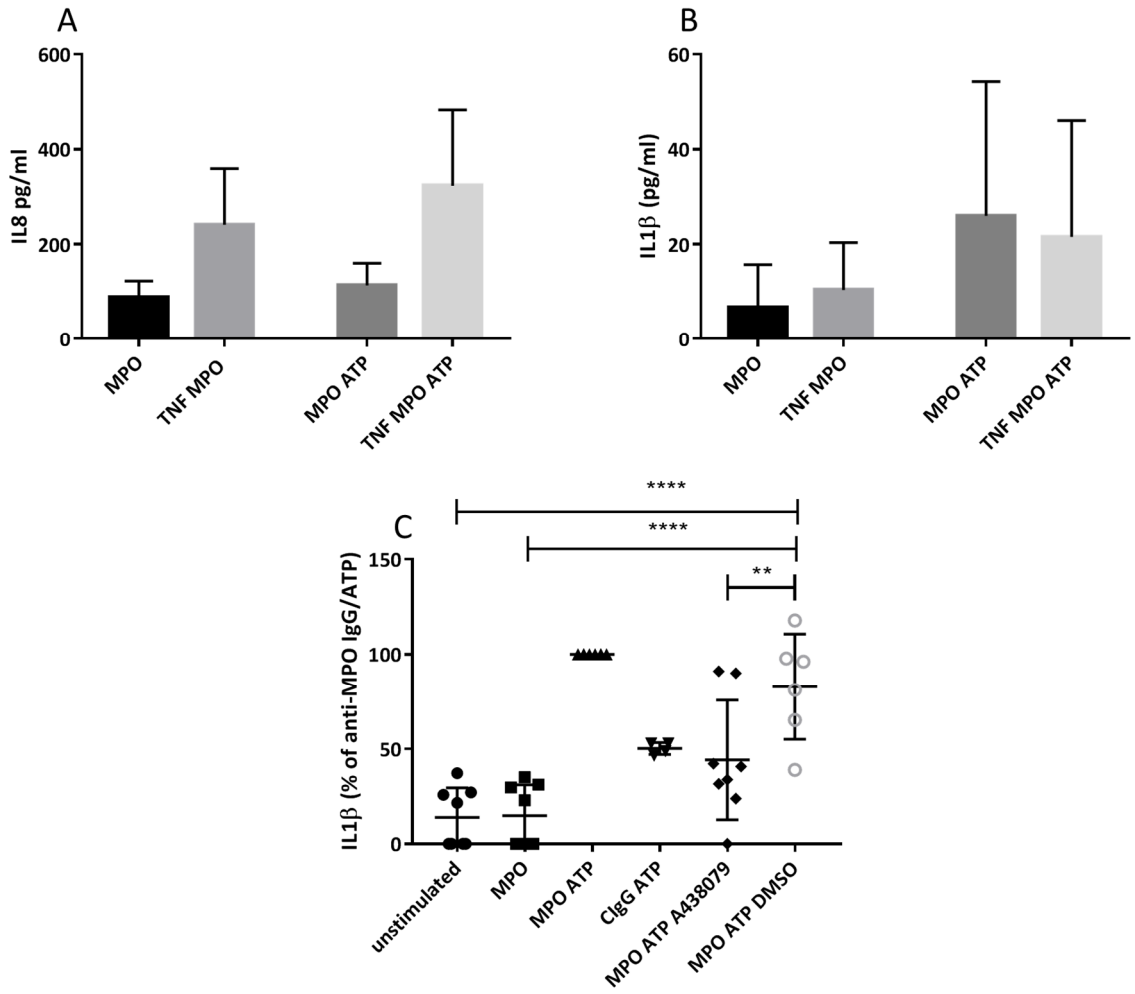

Figure 6.11 Pro-inflammatory cytokine production by human neutrophils following stimulation with TNFα, MPO-ANCA IgG and ATP

(A) IL-8 production was not significantly enhanced by the addition of 5mM ATP after stimulation with MPO-ANCA IgG (MPO), (B) IL-1β release was increased by the addition of 5mM ATP after stimulation with MPO-ANCA IgG. Results pooled from 5 biological replicates with technical duplicates. Data shown as mean with SEM. (C) IL-1β release following stimulation with MPO-ANCA IgG and ATP was significantly reduced by addition of 10μM P2X7 antagonist (A438079). Results are expressed as % IL-1β of that produced by cells stimulated with MPO-ANCA IgG and ATP and each data point represents a biological replicate. Statistical analysis performed using one way ANOVA with Dunnett's multiple comparisons post test. ****p<0.0001, **p<0.01

My results so far show that neutrophils express functional, cell-surface P2X7 and are able to form pores and produce IL-1β in response to stimulation with LPS and extracellular ATP. Although

neutrophils released some IL-1β following stimulation with MPO-ANCA IgG the amount was very small and on some occasions fell below the lower limit of detection of the ELISA used, suggesting that MPO-ANCA IgG mediated IL-1β production by neutrophils is not a major pathway for pro-inflammatory cytokine mediated damage in AAV. I therefore also studied P2X7 expression and cytokine production from PBMC.

6.3 PBMC

6.3.1 PBMC P2X7 expression

PBMC were isolated from patients with AAV and healthy controls using the same isolation protocol as for neutrophils. Cells were isolated from 8 healthy controls, 15 patients with active AAV and 12 patients with AAV but in remission. Characteristics of the patients with AAV used for PBMC isolation are shown in Table 6.2.

	Active (n=15)	Remission (n=12)
Age (years)	62.7 (31.3-83.4)	66.0 (32.9-81.53)
Sex (M/F)	7/8	5/7
MPO/PR3/ANCA negative	6/7/2	5/6/1
Steroids/No steroids	6/9	10/2

Table 6.2 Characteristics of AAV patients included in PBMC isolation

To investigate P2X7 function on PBMC I investigated the cells ability to form pores and produce cytokine in response to stimulation with LPS and ATP. PBMC were cultured with and without LPS 1μg/ml for 4 hours and then used for live cell flow cytometry to assess Yo-pro-1 dye uptake. Cells

were incubated with Yo-pro-1, baseline fluorescence measured, 150µM BzATP added and uptake of dye measured. PBMC were able to form pores and take up dye in response to stimulation with extracellular ATP and as with other cell types, LPS priming does not augment dye uptake in response to ATP (Figure 6.12).

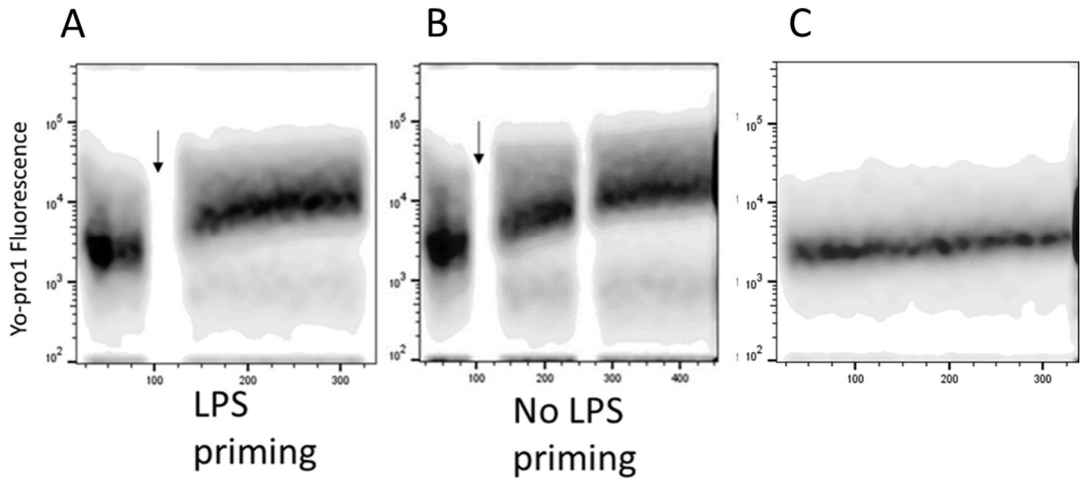

Figure 6.12 Yo-pro-1 uptake by PBMC
Cells were incubated with a final concentration of 10µM Yo-pro-1 fluorescent dye and baseline fluorescence measured over 1 minute. 150µM BzATP was added at the arrow and dye uptake in response to this is seen as an increase in cell fluorescence. (A) PBMC primed with 100ng/ml LPS for 4 hours, (B) No LPS priming, (C) No BzATP added. Images are representative of 3 biological replicates.

PBMC can produce significant amounts of IL-1β in response to stimulation with LPS 100ng/ml for 4 hours and ATP 5mM for 30 minutes. There was some IL-1β produced in response to stimulation with LPS alone but this was 4 fold lower than the amount produced with the addition of ATP (mean production with LPS 808.5 pg/ml, with LPS and ATP 3263 pg/ml). Production of IL-1β in response to stimulation with LPS and ATP was P2X7 dependent; addition of 10µM P2X7 antagonist (A438079) prior to ATP resulted in a reduction in amount of IL-1β produced to a level similar to stimulation with LPS alone (mean 902.6 pg/ml) (Figure 6.13).

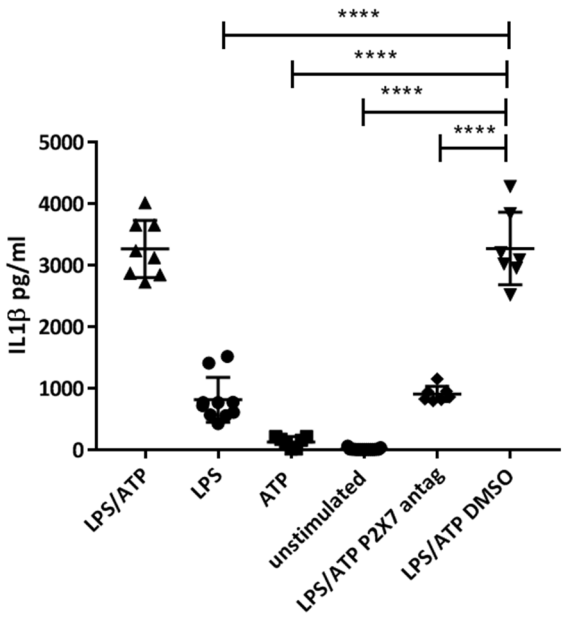

Figure 6.13 PBMC IL-1β production following stimulation with LPS and ATP
IL-1β production from PBMC stimulated with LPS 100ng/ml for 4 hours and ATP 5mM for 30 mins with 10μM P2X7 antagonist (A438079) or vehicle (DMSO) prior to addition of ATP. Results are from 4 biological replicates with technical duplicates. Data shown as mean with SEM. Statistical analysis performed using one way ANOVA with Dunnett's multiple comparisons post test. ****p<0.0001.

Patients with active AAV had a trend towards higher cell surface expression of P2X7 than on PBMC from healthy controls or patients with AAV and in remission, although this was not statistically significant and there was some overlap between the groups. There was no difference in cell surface expression of P2X7 between patients who are MPO ANCA positive and PR3 ANCA positive (Figure 6.14). This may represent the fact that PBMC are a mixed population of cells; the proportion of monocytes and lymphocytes in each cell preparation was not quantified. It is reported in several studies that P2X7 expression is higher on monocytes than on T and B lymphocytes and so results may be skewed towards higher MFI for cell surface P2X7 in samples which have greater proportion of monocytes.

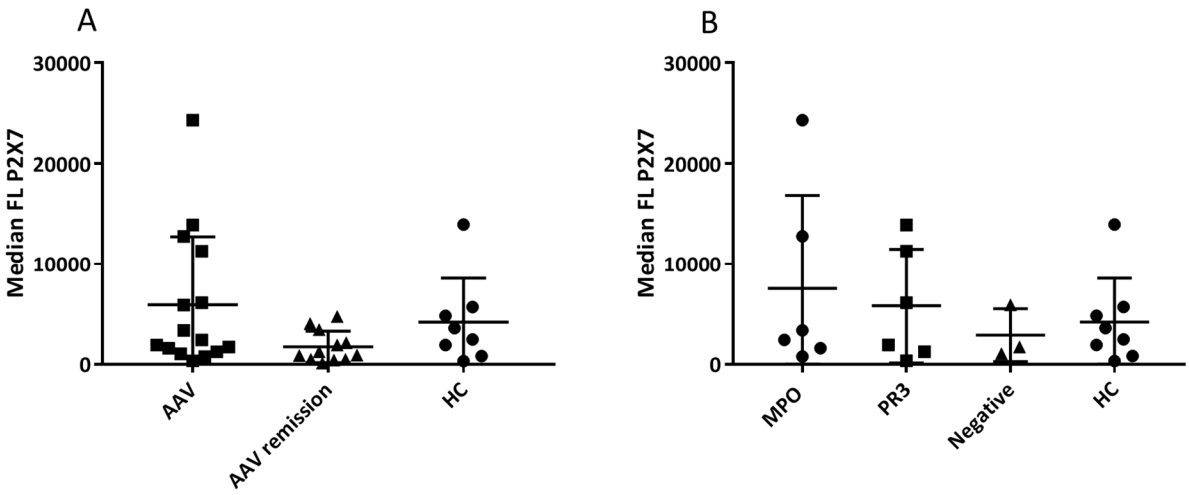

Figure 6.14 PBMC cell surface P2X7 expression in patients with active and remission AAV
(A) Cell surface P2X7 analysed by flow cytometry in patients with active AAV, remission AAV patients and healthy controls (HC), (B) Cell surface P2X7 levels by ANCA specificity.

PBMC surface P2X7 expression (as quantified by median fluorescence) was compared with levels of CRP or creatinine at the time the sample was taken within the group of patients with active AAV. There was a trend towards a weak positive correlation between cell surface P2X7 expression and CRP with a correlation coefficient of 0.32, although this was not statistically significant (p=0.28) (Figure 6.15). This could potentially reflect the differential contribution of different cell populations to the PBMC fraction between patients with more or less inflammation.

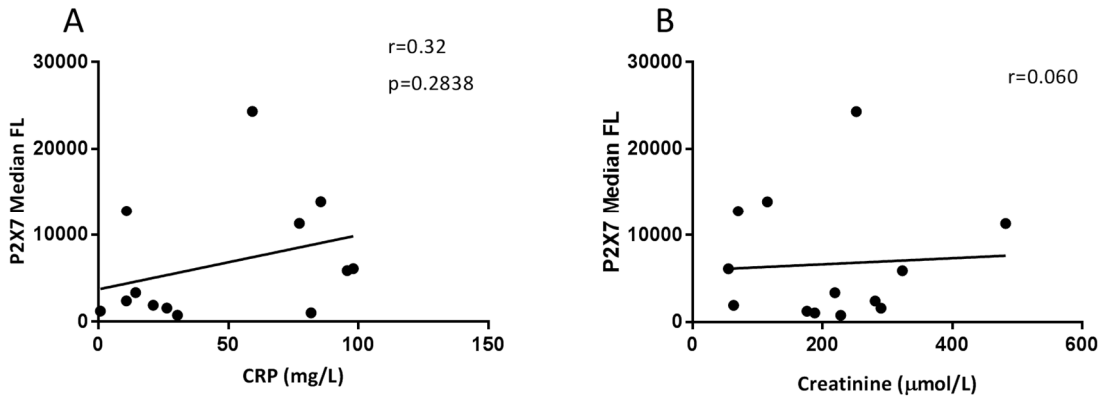

Figure 6.15 Correlation between PBMC surface P2X7 expression and CRP or creatinine in patients with active AAV

(A) Correlation between P2X7 cell surface staining and CRP, (B) Correlation between P2X7 cell surface staining and creatinine. Statistical analysis carried out using Pearson correlation coefficient.

6.3.2 PBMC mRNA expression

RT-qPCR for P2X7, NLRP3, caspase-1, IL-1β and IL-18 was carried out on PBMC from patients with active AAV (both first presentation and relapse) and from healthy controls. There was a trend towards up-regulation of mRNA for P2X7, Caspase-1, IL-1β and IL-18 in PBMC from patients with active AAV when compared to healthy controls, although this was not significant. There was no difference in NLRP3 mRNA levels. The lack of statistical significance may be due to the variation in expression of the target genes of interest between patients. This could represent the mixed population of cells used for this experiment or be due to the differences in severity of disease or inflammatory state of the fairly heterogeneous group of patients included- for example one patient presented with an ENT limited relapse whereas another had severe RPGN and pulmonary haemorrhage requiring plasma exchange. Expanding the number of patients included in this analysis may enable identification of trends between clinical information and mRNA expression (Figure 6.16).

A

	AAV patients (n=8)
Age (years)	58.9 (33.5-83.4)
Sex (M/F)	4/4
MPO/PR3/ANCA negative	3/4/1
Steroids/No steroids	5/3

B

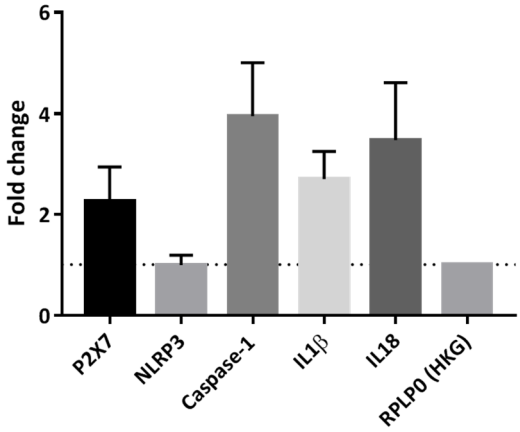

Figure 6.16 RT-qPCR analysis of expression levels of mRNA of P2X7, NLRP3, caspase-1, IL-1β and IL-18 in PBMC from patients with active AAV

(A) Characteristics of patients with active AAV whose PBMC were used for RT-qPCR, (B) Fold change for target genes in patients with active AAV, ΔCT was normalised to housekeeping gene (RPLP0, HKG) and expressed relative to healthy controls (n=7) using $2^{-\Delta\Delta CT}$ method.

6.3.3 PBMC stimulation with MPO-ANCA IgG

PBMC were primed with TNFα 2ng/ml for 30 minutes followed by MPO-ANCA IgG 100µg/ml for 4 hours and then ATP 5mM for 30 minutes. IL-8 production was maximal from cells stimulated with TNFα and MPO-ANCA IgG. Addition of ATP did not enhance IL-8 secretion further. In contrast, priming of cells with TNFα did not affect IL-1β production, but the addition of ATP after MPO-ANCA IgG did have a synergistic effect (Figure 6.17).

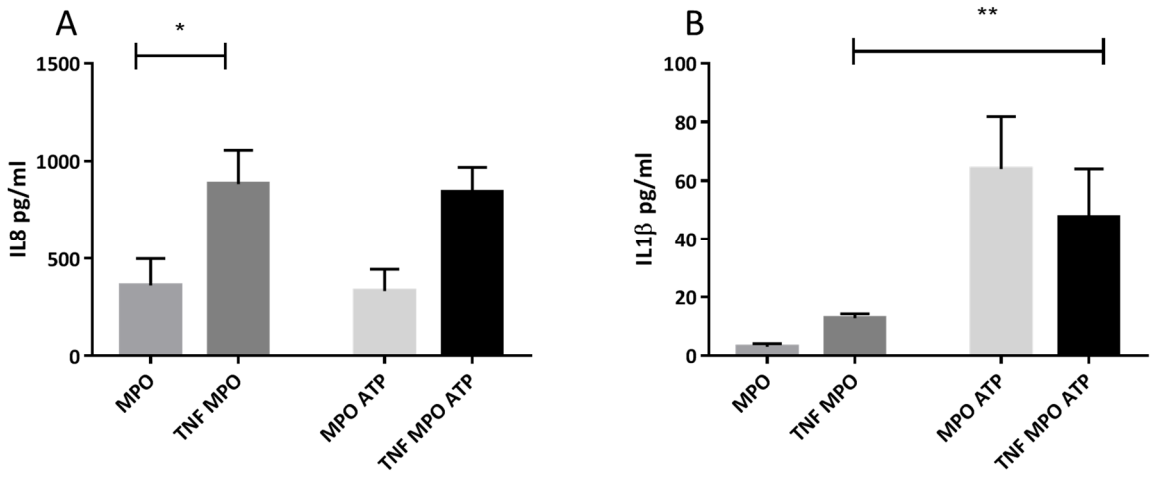

Figure 6.17 Pro-inflammatory cytokine production by human PBMC following stimulation with TNFα, MPO-ANCA IgG and ATP

(A) IL-8 production was not significantly enhanced by the addition of 5mM ATP after stimulation with MPO-ANCA IgG (MPO), (B) IL-1β release was increased by the addition of 5mM ATP after stimulation with MPO-ANCA IgG. Results pooled from 4 biological replicates with technical duplicates. Data shown as mean with SEM. Statistical analysis performed using one way ANOVA with Bonnferroni multiple comparisons post test. *p<0.05, **p<0.01

IL-1β production following stimulation with MPO-ANCA IgG and ATP was P2X7 dependent and could be inhibited by 10μM P2X7 antagonist (A438079) added prior to addition of ATP. As in my neutrophil experiments there was heterogeneity in the amount of IL-1β produced by PBMC following this stimulation and so each experiment was normalised to cytokine production in response to stimulation with MPO-ANCA IgG and ATP. The range of mean IL-1β produced following MPO-ANCA IgG and ATP was 49-623 pg/ml. There was also some release of IL-1β from cells stimulated with control IgG and ATP which could indicate that the mechanism of IL-1β production in response to both MPO-ANCA IgG and control IgG involves Fc receptors. This is further addressed in the discussion section of this chapter (Figure 6.18).

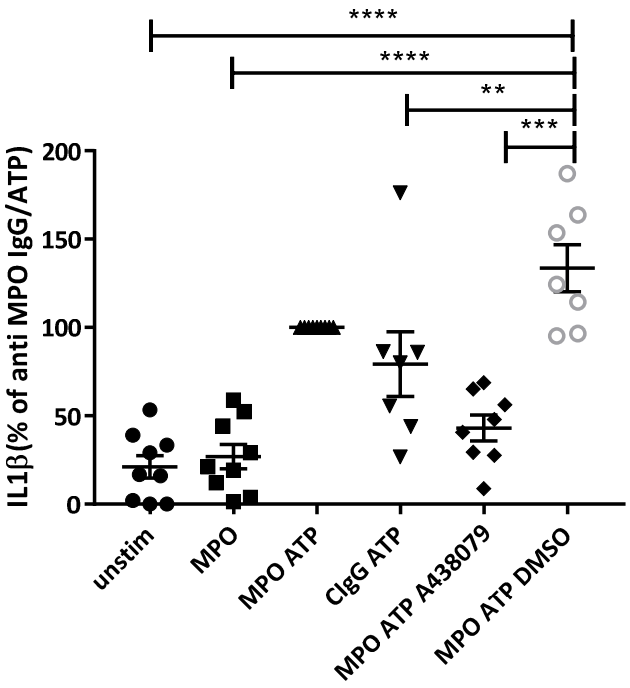

Figure 6.18 Effect of A438079 on IL1β production from human PBMC stimulated with MPO-ANCA IgG

IL-1β release following stimulation with MPO-ANCA IgG and ATP was significantly reduced by addition of 10μM P2X7 antagonist (A438079). Results are expressed as % mean IL-1β of that produced by cells stimulated with MPO-ANCA IgG and ATP and each data point represents a biological replicate. Statistical analysis performed using one way ANOVA with Dunnett's multiple comparisons post test. ****p<0.0001, **p<0.01

6.4 RNAscope for P2X7

I demonstrated that P2X7 was expressed on human neutrophils and PBMC and so next set out to demonstrate whether P2X7 was expressed in human glomerular disease. I initially tried using an immunohistochemistry technique on formalin fixed paraffin embedded tissue sections but despite testing a range of antibodies and techniques I was unable to optimise staining sufficiently. Several of the antibodies tested gave heavy tubular staining and it was difficult to conclude if this represented true staining or non-specific background staining. Within our laboratory we have often noticed tubular background staining with rabbit polyclonal antibodies. Other antibodies tested gave no IHC staining at all despite attempts to optimise antigen retrieval. I therefore opted to use RNAscope to detect P2X7 at the mRNA level.

Biopsies from 5 patients with crescentic AAV and 5 patients with sclerotic AAV were used for P2X7 RNAscope with PPIB used as a positive control probe to check RNA integrity. In patients with crescentic disease, P2X7 localised to areas of crescent formation and segmental inflammation with minimal P2X7 staining in sclerotic glomeruli. There was also P2X7 present within the tubulo-interstitium in patients who had evidence of tubulo-interstitial nephritis (Figure 6.19).

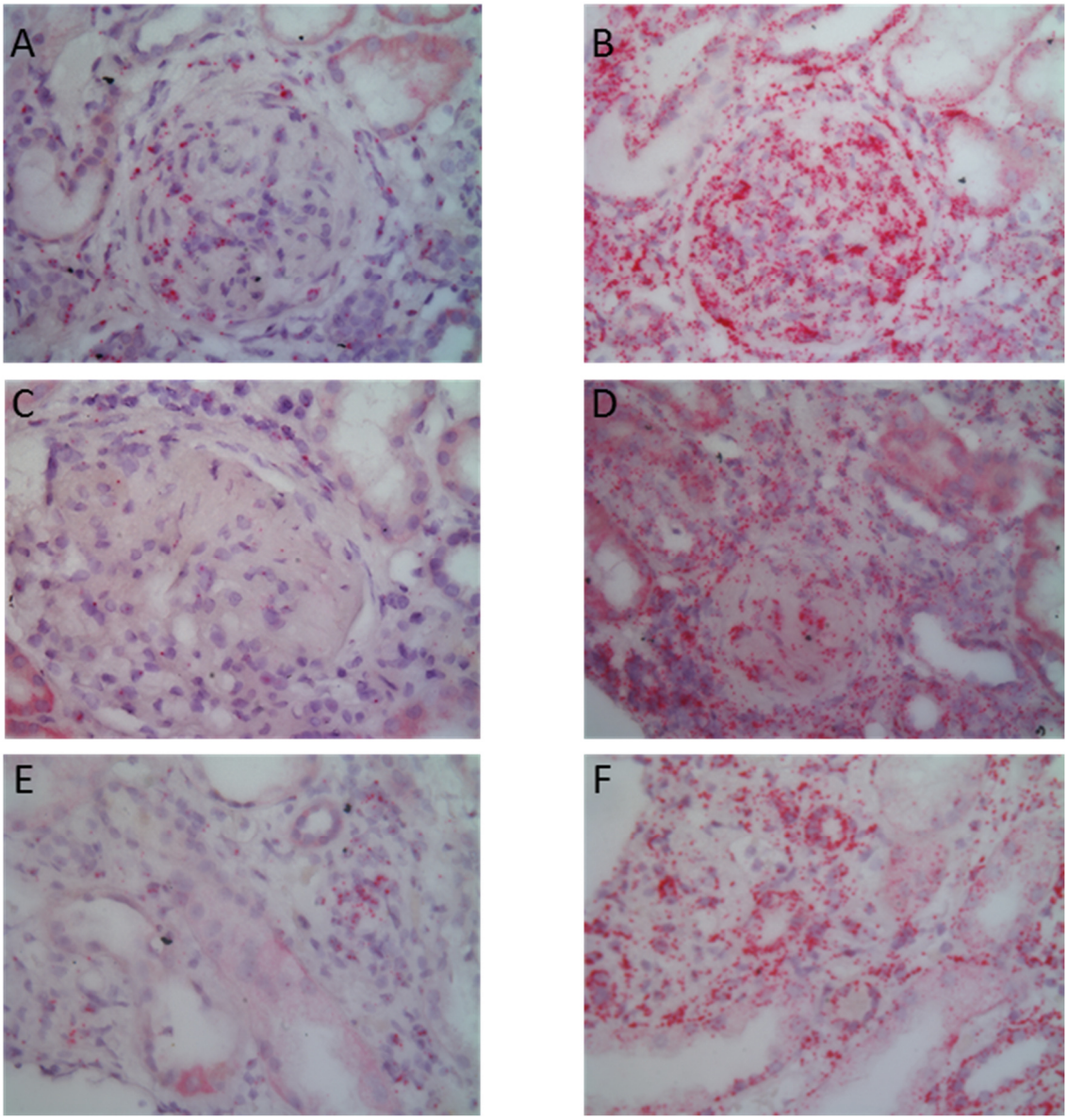

Figure 6.19 RNAscope for P2X7 in AAV

Representative RNAscope images showing the presence of P2X7 mRNA in glomeruli from (A) a patient with crescentic disease with corresponding control probe (PPIB) in (B), minimal P2X7 mRNA in glomeruli from (C) a patient with sclerotic disease with corresponding control probe (PPIB) in (D). (E) Positive P2X7 staining within tubule-interstitial infiltrate with corresponding control probe (PPIB) in (F). 400x magnification

6.5 Discussion of results and future work

The results presented in this chapter show that human neutrophils and PBMC express functional cell surface P2X7 receptors and these are up-regulated in patients with active AAV. P2X7 mRNA is present on cells in glomeruli in patients with crescentic AAV and also in tubulointerstitial infiltrates. There has previously been conflicting evidence as to the presence of cell surface, functional P2X7 on neutrophils. I have shown that neutrophils do express cell surface P2X7 using 2 different techniques FACS analysis and Western blot- and using 2 antibodies each directed at different P2X7 epitopes. Additionally neutrophils can form pores in response to extracellular ATP and produce IL-1β in a P2X7 dependent manner. There was some variation in IL-1β production in response to ATP following LPS priming from neutrophils isolated from different donors which may represent polymorphisms in P2X7 between individuals or differences in cell surface expression. This is in keeping with a recent study by Karmakar et al who identified that there was differences in Ca^{2+} current elicited by ATP between neutrophil donors.[44] It would be interesting to sequence P2X7 mRNA from neutrophils to look for presence of splice variants or SNPs such as the C terminus substitution of glutamate to alanine at position 496, which results in preserved receptor cell surface expression but has been shown to decrease P2X7 responsiveness to ATP in mononuclear cells.[137]

The up-regulation of P2X7 on neutrophils from patients with active AAV was more pronounced in neutrophils than on PBMC; mean MFI on neutrophils from patients with AAV was 2.6x that of healthy controls and for PBMC was only 1.5x higher. This could represent the mixed population of cells within PBMC; P2X7 expression is known to be higher on monocytes than lymphocytes and it may be that PBMC preparations with a higher percentage of lymphocytes have apparently lower P2X7 cell surface expression. In future, it would be useful to characterise each PBMC preparation using cell surface staining and correlate this with P2X7 cell-surface expression. Alternatively either cell sorting or magnetic bead based separation kits could be used to separate

the PBMC fraction into lymphocytes, classical and non-classical monocytes and determine relative P2X7 expression between cell types in healthy controls and patients with AAV.

A novel finding in this chapter is that MPO-ANCA IgG and ATP seem act synergistically to result in release of IL-1β from PBMC. In keeping with another published study the amount of IL-1β released from neutrophils in response to MPO-ANCA IgG stimulation was small compared to that released from monocytes/PBMC.[385] It would be interesting to also study other neutrophil functions such as NETosis or ROS production in response to MPO-ANCA IgG stimulation and whether P2X7 plays a role in these pathways.

Several mechanisms have been proposed for how stimulation of monocytes with either antibody or immune complexes can result in production of IL-1β and this mechanism may be different depending on whether it is immune complexes or pathogenic antibodies which are inducing cytokine release. One study by O'Brien et al showed that TNFα primed monocytes produced significant amounts of IL-1β in response to stimulation with MPO-ANCA IgG, the main source of this was intermediate monocytes and it was not dependent on Fc receptor engagement. Pre-incubation of cells with Fc block did not alter cytokine production.[407] Other studies using immune complexes rather than ANCA to stimulate monocytes or other myeloid cells have shown that interaction of immune complexes with FcγRIIa can result in IL-1β production.[385 408-410] Several studies have shown evidence for ANCA binding to FcγRIIa mediating neutrophil activation so this could also be a potential mechanism by which ANCA can induce release of IL-1β and other cytokines.

In one study, when monocytes were stimulated with immune complexes formed of dsDNA antibodies and dsDNA, IL-1β production was shown to be dependent on NLRP3 and caspase-1 and required K+ efflux from the cell.[410] Another study showed evidence for both caspase-1 dependent and independent mechanism for IL-1β production from monocytes after stimulation with anti-MPO monoclonal antibodies. In this study IL-1β release was diminished but not completely abolished by

caspase-1 inhibition and caspase independent release was via IL-1β cleavage by neutrophil serine proteases.[385] There are also studies in human dendritic cells and macrophages reporting synergy between subtherapeutic TLR stimulation and immune complexes acting at FcγRIIa to induce IL-1β release. In one study on human DCs, FcγR stimulation alone was sufficient to induce upregulation of caspase mRNA and activation of the inflammasome. Cross talk between FcγRIIa and TLR4 resulted in accumulation of pro-IL1β within the cell.[408] This mechanism has not been shown using ANCA or other pathogenic antibodies, rather than immune complexes, and so I would like to compare the effect of stimulation with low dose LPS and MPO-ANCA IgG to my stimulation protocol using MPO-ANCA IgG and ATP in future experiments.

Further investigation of the mechanism of MPO-ANCA IgG and receptor interactions on PBMC or monocytes in my protocol would be useful. There is evidence that anti-MPO IgG can act via both Fc receptor binding and Fab binding to the ANCA antigen on the cell surface to stimulate neutrophils and monocytes. However, whether both of these interactions are important in mediating IL-1β production is unknown and my results could provide evidence for both. In my experiments the combination of control IgG and ATP resulted in some release of cytokine but this was 20% lower than that released from PBMC stimulated with MPO-ANCA IgG and ATP. As there was some cytokine release in response to the combination of control IgG and ATP, presumably some activity is mediated via Fc receptor engagement but the additional cytokine release by anti-MPO IgG over control IgG may be mediated by antigen specific Fab binding. If Fab binding to MPO on cells is a mechanism in this pathway it is surprising that TNFα priming of cells did not enhance IL-1β production as this has been shown in other studies to up-regulate the MPO antigen on the cell surface.[324] Performing a digest of the isolated antibody to see if F(ab)2 fragments alone can result in cytokine release would be useful to elucidate this mechanism.

There was variation in the amount of cytokine produced by PBMC in response to stimulation with anti-MPO ANCA IgG and ATP, both in cells isolated from healthy controls and from patients with AAV. As discussed previously, this could be due to P2X7 polymorphisms but could also be due to

polymorphisms in Fc receptors as ANCA mediated neutrophil activation has been shown to be affected by allelic variants of FcγRIIa.

6.6 Summary of key findings

1. Human neutrophils express functional P2X7 and can form pores and release IL-1β in response to extracellular ATP
2. Neutrophils from patients with active AAV have higher cell surface P2X7 than healthy controls or patients with AAV in remission
3. Neutrophils produce significant IL-8 in response to priming with TNFα and stimulation with MPO-ANCA IgG. They can produce IL-1β following stimulation with MPO-ANCA IgG and ATP although the amount is small
4. There is a trend to up-regulation of cell surface P2X7 on PBMC from patients with active AAV compared to healthy controls and remission patients
5. PBMC stimulated with MPO-ANCA IgG and ATP produce IL-1β and this can be inhibited by use of a P2X7 antagonist
6. P2X7 mRNA can be detected in the glomeruli of patients with AAV and crescentic GN and in the tubulo-interstitium where co-existing tubulointerstitial nephritis is present

Chapter 7: Discussion and Future Work

7.1 Discussion

In this project I aimed to determine a role for P2X7 in the pathogenesis of GN and vasculitis and to investigate its importance at a cellular level in inflammatory responses of neutrophils and monocytes. Using a novel P2X7 KO rat I studied the role of P2X7 in cytokine production from bone marrow derived cells. I defined a role for P2X7 in experimental GN and vasculitis using both the KO rat and a pharmacological inhibitor. I have studied the role of P2X7 in AAV by investigating a potential role for P2X7 in ANCA induced cytokine production and the expression of P2X7 mRNA in renal biopsy sections from patients with AAV.

Key findings from my thesis include:

1. The first description of a novel P2X7 knockout rat developed using zinc finger nuclease technology
2. Bone marrow derived cells have a differential requirement for P2X7 to cleave active IL-1β; BMDM require P2X7/ATP stimulation to produce active IL-1β and BMDC are able to cleave IL-1β via ATP/P2X7 independent pathways in response to stimulation with LPS alone
3. P2X7 deficient rats are not protected from disease in experimental glomerulonephritis or vasculitis
4. Use of a P2X7 antagonist protects both WKY WT and P2X7 KO rats from disease suggesting it may be mediating its actions via off target effects

5. Human neutrophils express functional cell surface P2X7 and this is up-regulated in patients with active AAV

6. PBMC stimulated with MPO-ANCA IgG and ATP produce IL-1β and this can be inhibited using a P2X7 antagonist

7. P2X7 mRNA is present in glomeruli and interstitium in renal biopsy tissue from patients with active AAV

My *in vivo* work using the P2X7 knockout rat shows that this rat does seem to be a true knockout with no functional P2X7 detected. It was therefore surprising that the rats were not protected from in vivo models of GN and vasculitis, particularly as previous work undertaken in our laboratory showed that P2X7 KO mice and rats treated with P2X7 antagonist were protected from NTN.[194] There are several possibilities as to why mice should be protected from disease whereas rats are not. Firstly, the model of NTN in mice differs from that in rats; mice immunised with nephrotoxic serum alone do not develop severe disease and require pre-immunisation with sheep IgG (as in the study by Taylor et al) or co-administration of LPS.[411] There are also some differences in P2X7 between rats and mice; although there is 85% sequence homology, BzATP is 10 times more potent at rat (and human) P2X7 than at mouse P2X7.[163] The background strain on which P2X7 KO mice are based, C57BL/6, express a naturally occurring low sensitivity P2X7 allele P451L.[135]

My results using the P2X7 antagonist A438079 in rats with NTN confirm our earlier published results.[194] However, as discussed in Chapter 5, a limitation of this work is the lack of PK data for the antagonist at this dose. Given that the drug was equally as effective in WKY WT and P2X7 KO rats it is possible that it is mediating its actions via off target effects. The dose of A438079 used was comparable with that used in several other published studies including other in vivo models of kidney disease.[194 196 197] However doses of drug used for in vitro experiments (including my experiments in this thesis) are much lower and more in keeping with published doses used to assess

selectivity. In mice it was not possible to administer a sufficient dose to inhibit NTN without toxic neurological side effects (Simon Taylor, PhD thesis), which again may imply that the drug is having off-target effects. Additionally, the published in vivo PK data in rats (using lower doses) was undertaken in Sprague-Dawley rats and it is not known whether this would be applicable to WKY rats, particularly following induction of GN or vasculitis when animals may have impaired renal function.[187] An experiment is planned to determine C_{max} following administration of the antagonist at the dose used in my studies. I also plan to collect tissue samples to investigate the relative concentration of drug in the plasma, kidney and brain. I will then use this concentration of drug to assess selectivity using cell and non-cell based approaches. An *in silico* approach may also be useful to predict potential drug actions. The drug's potential 'off-target' effects do not necessarily preclude its use in treatment of patients but need to be understood.

IL-1β release is a key function of P2X7 but my in vitro experiments using the P2X7 KO rat show a differential requirement for ATP and P2X7 between BMDM and BMDC. In both the WKY WT and P2X7 KO BMDC IL-1β release can occur in response to stimulation with LPS alone and occurs via a caspase-1 dependent, P2X7 independent pathway. I plan to further define the mechanism of this pathway, particularly looking at a role for caspase-8. Other than some preliminary data suggesting that rat blood monocytes are also able to utilise P2X7 independent pathways I have not yet investigated the different roles of P2X7 dependent and independent cytokine production using the P2X7 KO rat in other cell types such as neutrophils. Given that P2X7 KO rats were not protected from experimental GN it may be that cell types which are able to produce cytokine by P2X7 independent pathways play a relatively greater role than those which cannot utilise this mechanism. It is possible that in the disease state P2X7 independent pathways for activation of the inflammasome and IL-1β secretion can become up-regulated.

My results using cells and biopsy tissue from patients with AAV suggest a role for P2X7 in AAV. I have shown that P2X7 is up-regulated on neutrophils in patients with active disease, and P2X7 mRNA is present on infiltrating cells in glomeruli of patients with crescentic AAV and in tubulo-

interstitial infiltrates. In response to stimulation with MPO-ANCA IgG and ATP, PBMC produce IL-1β via a P2X7 dependent pathway. However, my results in experimental models of disease would suggest that P2X7 is not a key pathway in mediating disease. Even if P2X7 is up-regulated in AAV, but is not a critical pathway for pathogenesis, there may be a role for targeting P2X7 as an adjunctive treatment in AAV such as using it as a steroid sparing agent. There are, however, significant differences between rodent and human immune systems and the mechanisms of in vivo models are well known to differ from human disease. Therapeutic targets which had initially seemed promising in experimental models often do not translate to use in clinical practise. EAV in particular has a less severe phenotype than the crescentic GN seen in AAV in humans and over time will spontaneously resolve. It is possible therefore, that due to differing mechanisms between human and rodent GN, P2X7 could play a greater role in human disease than it does in rat models of GN and vasculitis.

There have been negative clinical trials using P2X7 antagonists in inflammatory conditions such as rheumatoid arthritis and Crohn's disease.[200] However the P2X7 antagonist used in this thesis, both in vivo and in vitro, is different to the ones used in clinical trials. My work has demonstrated some paradoxical results; the P2X7 KO rats still develop experimental disease but the P2X7 antagonist was effective in decreasing renal injury in both WKY WT and P2X7 KO rats. Further investigation of how the antagonist is mediating its effects may lead to further understanding of the pathogenesis of disease and the identification of novel therapeutic targets for treatment of AAV.

7.2 Future Work

I plan several experiments to further investigate the results presented in this thesis and these are discussed in more detail in the discussion sections of each chapter. I will investigate the mechanisms of P2X7 dependent and independent IL-1β production in both bone marrow derived cells and other cell types such as monocytes and lymphocytes. I plan PK studies using the dose of A438079 used in my in vivo experiments and once I have determined the peak plasma concentration of the drug I will use this to investigate its potential targets. In human neutrophils and PBMC I will further investigate the mechanisms of P2X7 dependent cytokine production in response to stimulation with MPO-ANCA IgG and ATP.

Aside from the role of P2X7 in glomerulonephritis and vasculitis investigated in this project, P2X7 also plays a role in other diseases and signalling pathways and it would be useful to investigate these using the P2X7 knockout rat particularly in areas where results from P2X7 knockout mice have been conflicting.

1. Bone metabolism

Osteoblasts and osteoclasts express P2X7 and Pfizer P2X7 deficient mice have reduced total and cortical bone volume with decreased periosteal bone formation in one study.[50] However the other P2X7 deficient mouse (GSK) did not have an overt bone phenotype.[412] In vitro, P2X7 activation in osteoblasts has been shown to enhance bone formation and differentiation whereas in osteoclasts it leads to apoptosis.[413] The P2X7 KO rat described here has smaller body weight than WKY WT controls, and preliminary results using CT scanning of the long bones have suggested there may be decreased cortical bone and periosteal diameter at 12 but not 6 weeks of age. This would be in keeping with the study of bone phenotype of Pfizer P2X7 KO mice in which the phenotype was

most apparent in adult (9 months of age) mice compared to those which were rapidly growing (2 months of age).[50]

2. Neuropsychiatric disorders

There is much conflicting evidence regarding the role of P2X7 in the brain. It has been definitively shown to be expressed on microglial cells and these cells can produce IL-1β.[414] However the expression of P2X7 on neurones either at the mRNA or protein level is controversial.[415] P2X7 has been implicated in several neuropsychiatric disorders including depression, bipolar disease and schizophrenia.[416] The P2X7 KO rat was noted by myself and colleagues to display some behavioural differences when compared to WKY WT rats, although no formal behavioural testing was carried out. It would be interesting to collaborate with a group in this field to complete a more comprehensive behavioural phenotype of the rat including models of neuropsychiatric conditions.

3. Atherosclerotic disease

There is substantial evidence that atheroma and thrombosis are closely linked to inflammation. A recent, large clinical trial has concluded that canakinumab, a monoclonal antibody targeting IL-1β, is effective in secondary prevention of cardiovascular events.[417] P2X7 has also been shown to play a role in thrombosis, and stimulation of P2X7 on human dendritic cells has been shown to lead to release of microparticles containing tissue factor, a potent pro-coagulant.[418] P2X7 deficient mice have been shown to be protected from thrombosis in a tissue factor dependent model, and to have reduced atherosclerosis in a high cholesterol diet model.[419] [420] P2X7 may well be a potential therapeutic target in atheromatous disease, warranting further investigation.

7.3 Conclusions

The findings reported in this thesis describe a novel P2X7 KO rat and suggest that this rat is not protected from experimental models of glomerulonephritis. Interestingly, the P2X7 antagonist protected both P2X7 KO and WKY WT rats from developing NTN, suggesting it may be mediating its actions via off target effects. My findings suggest a role for P2X7 in human AAV although given my in vivo results it may not be a critical pathway. Further understanding of the mechanisms by which the antagonist is mediating its effects in vivo may further our understanding of AAV and experimental GN and could lead to the identification of novel therapeutic targets.

References

1. Drury AN, Szent-Györgyi A. The physiological activity of adenine compounds with especial reference to their action upon the mammalian heart. *The Journal of Physiology* 1929;68(3):213-37.
2. Burnstock G, Campbell G, Satchell D, et al. Evidence that adenosine triphosphate or a related nucleotide is the transmitter substance released by non-adrenergic inhibitory nerves in the gut. *British Journal of Pharmacology* 1970;40(4):668-88.
3. Burnstock G. Purinergic nerves. *Pharmacol Rev* 1972;24(3):509-81.
4. G B. A basis for distinguishing two types of purinergic receptor. New York: Raven Press 1978:107-18.
5. Burnstock G, Kennedy C. Is there a basis for distinguishing two types of P2-purinoceptor? *Gen Pharmacol* 1985;16(5):433-40.
6. O'Connor SE, Dainty IA, Leff P. Further subclassification of ATP receptors based on agonist studies. *Trends Pharmacol Sci* 1991;12(4):137-41.
7. Gordon JL. Extracellular ATP: effects, sources and fate. *Biochem J* 1986;233(2):309-19.
8. Barnard EA, Burnstock G, Webb TE. G protein-coupled receptors for ATP and other nucleotides: a new receptor family. *Trends Pharmacol Sci* 1994;15(3):67-70.
9. Abbracchio MP, Burnstock G. Purinoceptors: are there families of P2X and P2Y purinoceptors? *Pharmacol Ther* 1994;64(3):445-75.
10. Surprenant A, Rassendren F, Kawashima E, et al. The cytolytic P2Z receptor for extracellular ATP identified as a P2X receptor (P2X7). *Science* 1996;272(5262):735-8.
11. Burnstock G. Purinergic signalling: Its unpopular beginning, its acceptance and its exciting future. *Bioessays* 2012;34(3):218-25.
12. Valera S, Hussy N, Evans RJ, et al. A new class of ligand-gated ion channel defined by P2x receptor for extracellular ATP. *Nature* 1994;371(6497):516-9.
13. Brake AJ, Wagenbach MJ, Julius D. New structural motif for ligand-gated ion channels defined by an ionotropic ATP receptor. *Nature* 1994;371(6497):519-23.
14. North RA. Molecular physiology of P2X receptors. *Physiol Rev* 2002;82(4):1013-67.
15. Ennion SJ, Evans RJ. Conserved cysteine residues in the extracellular loop of the human P2X(1) receptor form disulfide bonds and are involved in receptor trafficking to the cell surface. *Mol Pharmacol* 2002;61(2):303-11.
16. Nicke A, Bäumert HG, Rettinger J, et al. P2X1 and P2X3 receptors form stable trimers: a novel structural motif of ligand-gated ion channels. *Embo j* 1998;17(11):3016-28.
17. Jiang LH, Kim M, Spelta V, et al. Subunit arrangement in P2X receptors. *J Neurosci* 2003;23(26):8903-10.
18. Ding S, Sachs F. Single channel properties of P2X2 purinoceptors. *J Gen Physiol* 1999;113(5):695-720.

19. Stoop R, Thomas S, Rassendren F, et al. Contribution of individual subunits to the multimeric P2X(2) receptor: estimates based on methanethiosulfonate block at T336C. *Mol Pharmacol* 1999;56(5):973-81.
20. Kawate T, Michel JC, Birdsong WT, et al. Crystal structure of the ATP-gated P2X(4) ion channel in the closed state. *Nature* 2009;460(7255):592-8.
21. Marquez-Klaka B, Rettinger J, Bhargava Y, et al. Identification of an intersubunit cross-link between substituted cysteine residues located in the putative ATP binding site of the P2X1 receptor. *J Neurosci* 2007;27(6):1456-66.
22. Torres GE, Egan TM, Voigt MM. Hetero-oligomeric assembly of P2X receptor subunits. Specificities exist with regard to possible partners. *J Biol Chem* 1999;274(10):6653-9.
23. Barrera NP, Ormond SJ, Henderson RM, et al. Atomic force microscopy imaging demonstrates that P2X2 receptors are trimers but that P2X6 receptor subunits do not oligomerize. *J Biol Chem* 2005;280(11):10759-65.
24. Aschrafi A, Sadtler S, Niculescu C, et al. Trimeric architecture of homomeric P2X2 and heteromeric P2X1+2 receptor subtypes. *J Mol Biol* 2004;342(1):333-43.
25. Lewis C, Neidhart S, Holy C, et al. Coexpression of P2X2 and P2X3 receptor subunits can account for ATP-gated currents in sensory neurons. *Nature* 1995;377(6548):432-5.
26. Lalo U, Pankratov Y, Wichert SP, et al. P2X1 and P2X5 subunits form the functional P2X receptor in mouse cortical astrocytes. *J Neurosci* 2008;28(21):5473-80.
27. Guo C, Masin M, Qureshi OS, et al. Evidence for functional P2X4/P2X7 heteromeric receptors. *Mol Pharmacol* 2007;72(6):1447-56.
28. Perez-Flores G, Levesque SA, Pacheco J, et al. The P2X7/P2X4 interaction shapes the purinergic response in murine macrophages. *Biochem Biophys Res Commun* 2015;467(3):484-90.
29. Casas-Pruneda G, Reyes JP, Pérez-Flores G, et al. Functional interactions between P2X4 and P2X7 receptors from mouse salivary epithelia. *J Physiol* 2009;587(Pt 12):2887-901.
30. Boumechache M, Masin M, Edwardson JM, et al. Analysis of assembly and trafficking of native P2X4 and P2X7 receptor complexes in rodent immune cells. *J Biol Chem* 2009;284(20):13446-54.
31. Nicke A. Homotrimeric complexes are the dominant assembly state of native P2X7 subunits. *Biochem Biophys Res Commun* 2008;377(3):803-8.
32. Antonio LS, Stewart AP, Xu XJ, et al. P2X4 receptors interact with both P2X2 and P2X7 receptors in the form of homotrimers. *Br J Pharmacol* 2011;163(5):1069-77.
33. Kawano A, Tsukimoto M, Mori D, et al. Regulation of P2X7-dependent inflammatory functions by P2X4 receptor in mouse macrophages. *Biochem Biophys Res Commun* 2012;420(1):102-7.
34. Sakaki H, Fujiwaki T, Tsukimoto M, et al. P2X4 receptor regulates P2X7 receptor-dependent IL-1beta and IL-18 release in mouse bone marrow-derived dendritic cells. *Biochem Biophys Res Commun* 2013;432(3):406-11.

35. North RA, Surprenant A. Pharmacology of cloned P2X receptors. *Annu Rev Pharmacol Toxicol* 2000;40:563-80.
36. Gu BJ, Zhang WY, Bendall LJ, et al. Expression of P2X(7) purinoceptors on human lymphocytes and monocytes: evidence for nonfunctional P2X(7) receptors. *Am J Physiol Cell Physiol* 2000;279(4):C1189-97.
37. Gu BJ, Sluyter R, Skarratt KK, et al. An Arg307 to Gln polymorphism within the ATP-binding site causes loss of function of the human P2X7 receptor. *J Biol Chem* 2004;279(30):31287-95.
38. Perez-Figueroa E, Torres J, Sanchez-Zauco N, et al. Activation of NLRP3 inflammasome in human neutrophils by Helicobacter pylori infection. *Innate Immun* 2016;22(2):103-12.
39. Karmakar M, Sun Y, Hise AG, et al. Cutting edge: IL-1beta processing during Pseudomonas aeruginosa infection is mediated by neutrophil serine proteases and is independent of NLRC4 and caspase-1. *J Immunol* 2012;189(9):4231-5.
40. Guma M, Ronacher L, Liu-Bryan R, et al. Caspase 1-independent activation of interleukin-1beta in neutrophil-predominant inflammation. *Arthritis Rheum* 2009;60(12):3642-50.
41. Martel-Gallegos G, Rosales-Saavedra MT, Reyes JP, et al. Human neutrophils do not express purinergic P2X7 receptors. *Purinergic Signal* 2010;6(3):297-306.
42. Mohanty JG, Raible DG, McDermott LJ, et al. Effects of purine and pyrimidine nucleotides on intracellular Ca2+ in human eosinophils: activation of purinergic P2Y receptors. *J Allergy Clin Immunol* 2001;107(5):849-55.
43. Suh BC, Kim JS, Namgung U, et al. P2X7 nucleotide receptor mediation of membrane pore formation and superoxide generation in human promyelocytes and neutrophils. *J Immunol* 2001;166(11):6754-63.
44. Karmakar M, Katsnelson MA, Dubyak GR, et al. Neutrophil P2X7 receptors mediate NLRP3 inflammasome-dependent IL-1β secretion in response to ATP. *Nat Commun* 2016;7:10555.
45. Turner CM, Tam FW, Lai PC, et al. Increased expression of the pro-apoptotic ATP-sensitive P2X7 receptor in experimental and human glomerulonephritis. *Nephrol Dial Transplant* 2007;22(2):386-95.
46. Menzies RI, Booth JWR, Mullins JJ, et al. Hyperglycemia-induced Renal P2X7 Receptor Activation Enhances Diabetes-related Injury. *EBioMedicine* 2017;19:73-83.
47. Harada H, Chan CM, Loesch A, et al. Induction of proliferation and apoptotic cell death via P2Y and P2X receptors, respectively, in rat glomerular mesangial cells. *Kidney International* 2000;57(3):949-58.
48. Orriss I, Syberg S, Wang N, et al. Bone phenotypes of P2 receptor knockout mice. *Front Biosci (Schol Ed)* 2011;3:1038-46.

49. Orriss IR, Key ML, Brandao-Burch A, et al. The regulation of osteoblast function and bone mineralisation by extracellular nucleotides: The role of p2x receptors. *Bone* 2012;51(3):389-400.
50. Ke HZ, Qi H, Weidema AF, et al. Deletion of the P2X7 nucleotide receptor reveals its regulatory roles in bone formation and resorption. *Mol Endocrinol* 2003;17(7):1356-67.
51. Sim JA, Young MT, Sung HY, et al. Reanalysis of P2X7 receptor expression in rodent brain. *J Neurosci* 2004;24(28):6307-14.
52. Collo G, Neidhart S, Kawashima E, et al. Tissue distribution of the P2X7 receptor. *Neuropharmacology* 1997;36(9):1277-83.
53. Masin M, Young C, Lim K, et al. Expression, assembly and function of novel C-terminal truncated variants of the mouse P2X7 receptor: re-evaluation of P2X7 knockouts. *Br J Pharmacol* 2012;165(4):978-93.
54. Burnstock G, Knight GE. Cellular distribution and functions of P2 receptor subtypes in different systems. *Int Rev Cytol* 2004;240:31-304.
55. Virginio C, MacKenzie A, North RA, et al. Kinetics of cell lysis, dye uptake and permeability changes in cells expressing the rat P2X7 receptor. *J Physiol* 1999;519 Pt 2:335-46.
56. Jiang LH, Rassendren F, Mackenzie A, et al. N-methyl-D-glucamine and propidium dyes utilize different permeation pathways at rat P2X(7) receptors. *Am J Physiol Cell Physiol* 2005;289(5):C1295-302.
57. Virginio C, Church D, North RA, et al. Effects of divalent cations, protons and calmidazolium at the rat P2X7 receptor. *Neuropharmacology* 1997;36(9):1285-94.
58. Pelegrin P, Surprenant A. Pannexin-1 mediates large pore formation and interleukin-1beta release by the ATP-gated P2X7 receptor. *Embo j* 2006;25(21):5071-82.
59. Beyer EC, Steinberg TH. Evidence that the gap junction protein connexin-43 is the ATP-induced pore of mouse macrophages. *J Biol Chem* 1991;266(13):7971-4.
60. Steinberg TH, Di Virgilio F. Cell-mediated cytotoxicity: ATP as an effector and the role of target cells. *Curr Opin Immunol* 1991;3(1):71-5.
61. Sandilos JK, Bayliss DA. Physiological mechanisms for the modulation of pannexin 1 channel activity. *J Physiol* 2012;590(24):6257-66.
62. Qu Y, Misaghi S, Newton K, et al. Pannexin-1 is required for ATP release during apoptosis but not for inflammasome activation. *J Immunol* 2011;186(11):6553-61.
63. Alberto AV, Faria RX, Couto CG, et al. Is pannexin the pore associated with the P2X7 receptor? *Naunyn Schmiedebergs Arch Pharmacol* 2013;386(9):775-87.
64. Ousingsawat J, Wanitchakool P, Kmit A, et al. Anoctamin 6 mediates effects essential for innate immunity downstream of P2X7 receptors in macrophages. *Nat Commun* 2015;6:6245.
65. Li M, Chang TH, Silberberg SD, et al. Gating the pore of P2X receptor channels. *Nat Neurosci* 2008;11(8):883-7.

66. Egan TM, Khakh BS. Contribution of calcium ions to P2X channel responses. *J Neurosci* 2004;24(13):3413-20.

67. Kim M, Jiang LH, Wilson HL, et al. Proteomic and functional evidence for a P2X7 receptor signalling complex. *Embo j* 2001;20(22):6347-58.

68. Pfeiffer ZA, Aga M, Prabhu U, et al. The nucleotide receptor P2X7 mediates actin reorganization and membrane blebbing in RAW 264.7 macrophages via p38 MAP kinase and Rho. *J Leukoc Biol* 2004;75(6):1173-82.

69. Ferrari D, La Sala A, Chiozzi P, et al. The P2 purinergic receptors of human dendritic cells: identification and coupling to cytokine release. *Faseb j* 2000;14(15):2466-76.

70. Verhoef PA, Estacion M, Schilling W, et al. P2X7 receptor-dependent blebbing and the activation of Rho-effector kinases, caspases, and IL-1 beta release. *J Immunol* 2003;170(11):5728-38.

71. Wilson HL, Wilson SA, Surprenant A, et al. Epithelial membrane proteins induce membrane blebbing and interact with the P2X7 receptor C terminus. *J Biol Chem* 2002;277(37):34017-23.

72. Charras GT. A short history of blebbing. *J Microsc* 2008;231(3):466-78.

73. Tedder TF, Steeber DA, Chen A, et al. The selectins: vascular adhesion molecules. *Faseb j* 1995;9(10):866-73.

74. Scheuplein F, Schwarz N, Adriouch S, et al. NAD+ and ATP released from injured cells induce P2X7-dependent shedding of CD62L and externalization of phosphatidylserine by murine T cells. *J Immunol* 2009;182(5):2898-908.

75. Elliott JI, Surprenant A, Marelli-Berg FM, et al. Membrane phosphatidylserine distribution as a non-apoptotic signalling mechanism in lymphocytes. *Nat Cell Biol* 2005;7(8):808-16.

76. Bevers EM, Comfurius P, Dekkers DW, et al. Lipid translocation across the plasma membrane of mammalian cells. *Biochim Biophys Acta* 1999;1439(3):317-30.

77. Devaux PF. Static and dynamic lipid asymmetry in cell membranes. *Biochemistry* 1991;30(5):1163-73.

78. Fadok VA, Bratton DL, Rose DM, et al. A receptor for phosphatidylserine-specific clearance of apoptotic cells. *Nature* 2000;405(6782):85-90.

79. Mackenzie AB, Young MT, Adinolfi E, et al. Pseudoapoptosis induced by brief activation of ATP-gated P2X7 receptors. *J Biol Chem* 2005;280(40):33968-76.

80. Frasch SC, Henson PM, Nagaosa K, et al. Phospholipid flip-flop and phospholipid scramblase 1 (PLSCR1) co-localize to uropod rafts in formylated Met-Leu-Phe-stimulated neutrophils. *J Biol Chem* 2004;279(17):17625-33.

81. van den Eijnde SM, van den Hoff MJ, Reutelingsperger CP, et al. Transient expression of phosphatidylserine at cell-cell contact areas is required for myotube formation. *J Cell Sci* 2001;114(Pt 20):3631-42.

82. Bratton DL, Fadok VA, Richter DA, et al. Appearance of phosphatidylserine on apoptotic cells requires calcium-mediated nonspecific flip-flop and is enhanced by loss of the aminophospholipid translocase. *J Biol Chem* 1997;272(42):26159-65.
83. Sluyter R, Shemon AN, Wiley JS. P2X(7) receptor activation causes phosphatidylserine exposure in human erythrocytes. *Biochem Biophys Res Commun* 2007;355(1):169-73.
84. Zheng LM, Zychlinsky A, Liu CC, et al. Extracellular ATP as a trigger for apoptosis or programmed cell death. *J Cell Biol* 1991;112(2):279-88.
85. Molloy A, Laochumroonvorapong P, Kaplan G. Apoptosis, but not necrosis, of infected monocytes is coupled with killing of intracellular bacillus Calmette-Guerin. *J Exp Med* 1994;180(4):1499-509.
86. Ferrari D, Los M, Bauer MK, et al. P2Z purinoreceptor ligation induces activation of caspases with distinct roles in apoptotic and necrotic alterations of cell death. *FEBS Lett* 1999;447(1):71-5.
87. Rissiek B, Haag F, Boyer O, et al. P2X7 on Mouse T Cells: One Channel, Many Functions. *Front Immunol* 2015;6:204.
88. Schulze-Lohoff E, Hugo C, Rost S, et al. Extracellular ATP causes apoptosis and necrosis of cultured mesangial cells via P2Z/P2X7 receptors. *Am J Physiol* 1998;275(6 Pt 2):F962-71.
89. Taylor SR, Gonzalez-Begne M, Dewhurst S, et al. Sequential shrinkage and swelling underlie P2X7-stimulated lymphocyte phosphatidylserine exposure and death. *J Immunol* 2008;180(1):300-8.
90. Yuan J, Shaham S, Ledoux S, et al. The C. elegans cell death gene ced-3 encodes a protein similar to mammalian interleukin-1 beta-converting enzyme. *Cell* 1993;75(4):641-52.
91. Xue D, Horvitz HR. Caenorhabditis elegans CED-9 protein is a bifunctional cell-death inhibitor. *Nature* 1997;390(6657):305-8.
92. Orth K, Chinnaiyan AM, Garg M, et al. The CED-3/ICE-like protease Mch2 is activated during apoptosis and cleaves the death substrate lamin A. *J Biol Chem* 1996;271(28):16443-6.
93. Rudel T, Bokoch GM. Membrane and morphological changes in apoptotic cells regulated by caspase-mediated activation of PAK2. *Science* 1997;276(5318):1571-4.
94. Abe J, Morrell C. Pyroptosis as a Regulated Form of Necrosis: PI+/Annexin V-/High Caspase 1/Low Caspase 9 Activity in Cells = Pyroptosis? *Circ Res* 2016;118(10):1457-60.
95. Hanley PJ, Kronlage M, Kirschning C, et al. Transient P2X7 receptor activation triggers macrophage death independent of Toll-like receptors 2 and 4, caspase-1, and pannexin-1 proteins. *J Biol Chem* 2012;287(13):10650-63.
96. Laliberte RE, Eggler J, Gabel CA. ATP treatment of human monocytes promotes caspase-1 maturation and externalization. *J Biol Chem* 1999;274(52):36944-51.
97. Li P, Allen H, Banerjee S, et al. Mice deficient in IL-1 beta-converting enzyme are defective in production of mature IL-1 beta and resistant to endotoxic shock. *Cell* 1995;80(3):401-11.

98. Le Feuvre RA, Brough D, Iwakura Y, et al. Priming of macrophages with lipopolysaccharide potentiates P2X7-mediated cell death via a caspase-1-dependent mechanism, independently of cytokine production. *J Biol Chem* 2002;277(5):3210-8.

99. Yip L, Woehrle T, Corriden R, et al. Autocrine regulation of T-cell activation by ATP release and P2X7 receptors. *Faseb j* 2009;23(6):1685-93.

100. Loomis WH, Namiki S, Ostrom RS, et al. Hypertonic stress increases T cell interleukin-2 expression through a mechanism that involves ATP release, P2 receptor, and p38 MAPK activation. *J Biol Chem* 2003;278(7):4590-6.

101. Graves LM, Guy HI, Kozlowski P, et al. Regulation of carbamoyl phosphate synthetase by MAP kinase. *Nature* 2000;403(6767):328-32.

102. Bradford MD, Soltoff SP. P2X7 receptors activate protein kinase D and p42/p44 mitogen-activated protein kinase (MAPK) downstream of protein kinase C. *Biochem J* 2002;366(Pt 3):745-55.

103. Adinolfi E, Melchiorri L, Falzoni S, et al. P2X7 receptor expression in evolutive and indolent forms of chronic B lymphocytic leukemia. *Blood* 2002;99(2):706-8.

104. Greig AV, Linge C, Healy V, et al. Expression of purinergic receptors in non-melanoma skin cancers and their functional roles in A431 cells. *J Invest Dermatol* 2003;121(2):315-27.

105. Slater M, Danieletto S, Gidley-Baird A, et al. Early prostate cancer detected using expression of non-functional cytolytic P2X7 receptors. *Histopathology* 2004;44(3):206-15.

106. Ferrari D, Pizzirani C, Adinolfi E, et al. The P2X7 receptor: a key player in IL-1 processing and release. *J Immunol* 2006;176(7):3877-83.

107. Cogswell JP, Godlevski MM, Wisely GB, et al. NF-kappa B regulates IL-1 beta transcription through a consensus NF-kappa B binding site and a nonconsensus CRE-like site. *J Immunol* 1994;153(2):712-23.

108. Howard AD, Kostura MJ, Thornberry N, et al. IL-1-converting enzyme requires aspartic acid residues for processing of the IL-1 beta precursor at two distinct sites and does not cleave 31-kDa IL-1 alpha. *J Immunol* 1991;147(9):2964-9.

109. Thornberry NA, Bull HG, Calaycay JR, et al. A novel heterodimeric cysteine protease is required for interleukin-1βprocessing in monocytes. *Nature* 1992;356:768.

110. Schmidt J.A. TMJ. Interleukin-1. In: Sporn M.B. RAB, ed. Peptide Growth Factors and Their Receptors I Handbook of Experimental Pharmacology. Berlin, Heidelberg: Springer 1990:473-521.

111. Gracie JA, Robertson SE, McInnes IB. Interleukin-18. *J Leukoc Biol* 2003;73(2):213-24.

112. Schmitz J, Owyang A, Oldham E, et al. IL-33, an interleukin-1-like cytokine that signals via the IL-1 receptor-related protein ST2 and induces T helper type 2-associated cytokines. *Immunity* 2005;23(5):479-90.

113. Cayrol C, Girard JP. Interleukin-33 (IL-33): A nuclear cytokine from the IL-1 family. *Immunol Rev* 2018;281(1):154-68.

114. Kaplanski G. Interleukin-18: Biological properties and role in disease pathogenesis. *Immunol Rev* 2018;281(1):138-53.

115. Martinon F, Burns K, Tschopp J. The inflammasome: a molecular platform triggering activation of inflammatory caspases and processing of proIL-beta. *Mol Cell* 2002;10(2):417-26.

116. Ruland J. Inflammasome: Putting the Pieces Together. *Cell* 2014;156(6):1127-29.

117. Perregaux D, Gabel CA. Interleukin-1 beta maturation and release in response to ATP and nigericin. Evidence that potassium depletion mediated by these agents is a necessary and common feature of their activity. *J Biol Chem* 1994;269(21):15195-203.

118. Solle M, Labasi J, Perregaux DG, et al. Altered cytokine production in mice lacking P2X(7) receptors. *J Biol Chem* 2001;276(1):125-32.

119. Ferrari D, Chiozzi P, Falzoni S, et al. Extracellular ATP triggers IL-1 beta release by activating the purinergic P2Z receptor of human macrophages. *J Immunol* 1997;159(3):1451-8.

120. Sluyter R, Shemon AN, Wiley JS. Glu496 to Ala polymorphism in the P2X7 receptor impairs ATP-induced IL-1 beta release from human monocytes. *J Immunol* 2004;172(6):3399-405.

121. Perregaux DG, Gabel CA. Human monocyte stimulus-coupled IL-1beta posttranslational processing: modulation via monovalent cations. *Am J Physiol* 1998;275(6 Pt 1):C1538-47.

122. de Torre-Minguela C, Mesa del Castillo P, Pelegrín P. The NLRP3 and Pyrin Inflammasomes: Implications in the Pathophysiology of Autoinflammatory Diseases. *Front Immunol* 2017;8(43)

123. Viganò E, Diamond CE, Spreafico R, et al. Human caspase-4 and caspase-5 regulate the one-step non-canonical inflammasome activation in monocytes. *Nature Communications* 2015;6:8761.

124. Parzych K, Zetterqvist AV, Wright WR, et al. Differential role of pannexin-1/ATP/P2X7 axis in IL-1beta release by human monocytes. *Faseb j* 2017;31(6):2439-45.

125. Netea MG, Nold-Petry CA, Nold MF, et al. Differential requirement for the activation of the inflammasome for processing and release of IL-1beta in monocytes and macrophages. *Blood* 2009;113(10):2324-35.

126. Gaidt MM, Ebert TS, Chauhan D, et al. Human Monocytes Engage an Alternative Inflammasome Pathway. *Immunity* 2016;44(4):833-46.

127. He Y, Franchi L, Núñez G. Toll-like Receptor Agonists Stimulate Nlrp3-dependent IL-1β Production Independently of the purinergic P2X7 Receptor in Dendritic Cells and in Vivo. *J Immunol* 2013;190(1):334-39.

128. Ferrari D, Wesselborg S, Bauer MK, et al. Extracellular ATP activates transcription factor NF-kappaB through the P2Z purinoreceptor by selectively targeting NF-kappaB p65. *J Cell Biol* 1997;139(7):1635-43.

129. Korcok J, Raimundo LN, Ke HZ, et al. Extracellular nucleotides act through P2X7 receptors to activate NF-kappaB in osteoclasts. *J Bone Miner Res* 2004;19(4):642-51.

130. Liu Y, Xiao Y, Li Z. P2X7 receptor positively regulates MyD88-dependent NF-kappaB activation. *Cytokine* 2011;55(2):229-36.

131. Coutinho-Silva R, Stahl L, Raymond MN, et al. Inhibition of chlamydial infectious activity due to P2X7R-dependent phospholipase D activation. *Immunity* 2003;19(3):403-12.

132. Alzola E, Perez-Etxebarria A, Kabre E, et al. Activation by P2X7 agonists of two phospholipases A2 (PLA2) in ductal cells of rat submandibular gland. Coupling of the calcium-independent PLA2 with kallikrein secretion. *J Biol Chem* 1998;273(46):30208-17.

133. Denlinger LC, Sommer JA, Parker K, et al. Mutation of a dibasic amino acid motif within the C terminus of the P2X7 nucleotide receptor results in trafficking defects and impaired function. *J Immunol* 2003;171(3):1304-11.

134. Denlinger LC, Fisette PL, Sommer JA, et al. Cutting edge: the nucleotide receptor P2X7 contains multiple protein- and lipid-interaction motifs including a potential binding site for bacterial lipopolysaccharide. *J Immunol* 2001;167(4):1871-6.

135. Adriouch S, Dox C, Welge V, et al. Cutting edge: a natural P451L mutation in the cytoplasmic domain impairs the function of the mouse P2X7 receptor. *J Immunol* 2002;169(8):4108-12.

136. Young MT, Pelegrin P, Surprenant A. Identification of Thr283 as a key determinant of P2X7 receptor function. *Br J Pharmacol* 2006;149(3):261-8.

137. Gu BJ, Zhang W, Worthington RA, et al. A Glu-496 to Ala polymorphism leads to loss of function of the human P2X7 receptor. *J Biol Chem* 2001;276(14):11135-42.

138. Shemon AN, Sluyter R, Fernando SL, et al. A Thr357 to Ser polymorphism in homozygous and compound heterozygous subjects causes absent or reduced P2X7 function and impairs ATP-induced mycobacterial killing by macrophages. *J Biol Chem* 2006;281(4):2079-86.

139. Wiley JS, Dao-Ung LP, Gu BJ, et al. A loss-of-function polymorphic mutation in the cytolytic P2X7 receptor gene and chronic lymphocytic leukaemia: a molecular study. *Lancet* 2002;359(9312):1114-9.

140. Bartlett R, Stokes L, Sluyter R. The P2X7 receptor channel: recent developments and the use of P2X7 antagonists in models of disease. *Pharmacol Rev* 2014;66(3):638-75.

141. Cabrini G, Falzoni S, Forchap SL, et al. A His-155 to Tyr polymorphism confers gain-of-function to the human P2X7 receptor of human leukemic lymphocytes. *J Immunol* 2005;175(1):82-9.

142. Stokes L, Fuller SJ, Sluyter R, et al. Two haplotypes of the P2X(7) receptor containing the Ala-348 to Thr polymorphism exhibit a gain-of-function effect and enhanced interleukin-1beta secretion. *Faseb j* 2010;24(8):2916-27.

143. Wu G, Zhao M, Gu X, et al. The effect of P2X7 receptor 1513 polymorphism on susceptibility to tuberculosis: A meta-analysis. *Infect Genet Evol* 2014;24:82-91.

144. Haas SL, Ruether A, Singer MV, et al. Functional P2X7 receptor polymorphisms (His155Tyr, Arg307Gln, Glu496Ala) in patients with Crohn's disease. *Scand J Immunol* 2007;65(2):166-70.

145. Starczynski J, Pepper C, Pratt G, et al. The P2X7 receptor gene polymorphism 1513 A-->C has no effect on clinical prognostic markers, in vitro sensitivity to fludarabine, Bcl-2 family protein expression or survival in B-cell chronic lymphocytic leukaemia. *Br J Haematol* 2003;123(1):66-71.

146. Roger S, Mei ZZ, Baldwin JM, et al. Single nucleotide polymorphisms that were identified in affective mood disorders affect ATP-activated P2X7 receptor functions. *J Psychiatr Res* 2010;44(6):347-55.

147. Gu BJ, Baird PN, Vessey KA, et al. A rare functional haplotype of the P2RX4 and P2RX7 genes leads to loss of innate phagocytosis and confers increased risk of age-related macular degeneration. *Faseb j* 2013;27(4):1479-87.

148. Gartland A, Skarratt KK, Hocking LJ, et al. Polymorphisms in the P2X7 receptor gene are associated with low lumbar spine bone mineral density and accelerated bone loss in post-menopausal women. *Eur J Hum Genet* 2012;20(5):559-64.

149. Jamieson SE, Peixoto-Rangel AL, Hargrave AC, et al. Evidence for associations between the purinergic receptor P2X(7) (P2RX7) and toxoplasmosis. *Genes Immun* 2010;11(5):374-83.

150. Cheewatrakoolpong B, Gilchrest H, Anthes JC, et al. Identification and characterization of splice variants of the human P2X7 ATP channel. *Biochem Biophys Res Commun* 2005;332(1):17-27.

151. Skarratt KK, Fuller SJ, Sluyter R, et al. A 5' intronic splice site polymorphism leads to a null allele of the P2X7 gene in 1-2% of the Caucasian population. *FEBS Lett* 2005;579(12):2675-8.

152. Feng YH, Li X, Wang L, et al. A truncated P2X7 receptor variant (P2X7-j) endogenously expressed in cervical cancer cells antagonizes the full-length P2X7 receptor through hetero-oligomerization. *J Biol Chem* 2006;281(25):17228-37.

153. Sluyter R, Stokes L. Significance of P2X7 receptor variants to human health and disease. *Recent Pat DNA Gene Seq* 2011;5(1):41-54.

154. Adinolfi E, Cirillo M, Woltersdorf R, et al. Trophic activity of a naturally occurring truncated isoform of the P2X7 receptor. *Faseb j* 2010;24(9):3393-404.

155. Giuliani AL, Colognesi D, Ricco T, et al. Trophic activity of human P2X7 receptor isoforms A and B in osteosarcoma. *PLOS ONE* 2014;9(9):e107224.

156. Nicke A, Kuan YH, Masin M, et al. A functional P2X7 splice variant with an alternative transmembrane domain 1 escapes gene inactivation in P2X7 knock-out mice. *J Biol Chem* 2009;284(38):25813-22.

157. Xu XJ, Boumechache M, Robinson LE, et al. Splice variants of the P2X7 receptor reveal differential agonist dependence and functional coupling with pannexin-1. *J Cell Sci* 2012;125(Pt 16):3776-89.
158. Kido Y, Kawahara C, Terai Y, et al. Regulation of activity of P2X7 receptor by its splice variants in cultured mouse astrocytes. *Glia* 2014;62(3):440-51.
159. Chessell IP, Hatcher JP, Bountra C, et al. Disruption of the P2X7 purinoceptor gene abolishes chronic inflammatory and neuropathic pain. *Pain* 2005;114(3):386-96.
160. Taylor SR, Gonzalez-Begne M, Sojka DK, et al. Lymphocytes from P2X7-deficient mice exhibit enhanced P2X7 responses. *J Leukoc Biol* 2009;85(6):978-86.
161. Sharp AJ, Polak PE, Simonini V, et al. P2x7 deficiency suppresses development of experimental autoimmune encephalomyelitis. *J Neuroinflammation* 2008;5:33.
162. Chen L, Brosnan CF. Exacerbation of experimental autoimmune encephalomyelitis in P2X7R-/- mice: evidence for loss of apoptotic activity in lymphocytes. *J Immunol* 2006;176(5):3115-26.
163. Donnelly-Roberts DL, Namovic MT, Han P, et al. Mammalian P2X7 receptor pharmacology: comparison of recombinant mouse, rat and human P2X7 receptors. *Br J Pharmacol* 2009;157(7):1203-14.
164. Hibell AD, Kidd EJ, Chessell IP, et al. Apparent species differences in the kinetic properties of P2X(7) receptors. *Br J Pharmacol* 2000;130(1):167-73.
165. Chakfe Y, Seguin R, Antel JP, et al. ADP and AMP induce interleukin-1beta release from microglial cells through activation of ATP-primed P2X7 receptor channels. *J Neurosci* 2002;22(8):3061-9.
166. Young MT, Pelegrin P, Surprenant A. Amino acid residues in the P2X7 receptor that mediate differential sensitivity to ATP and BzATP. *Mol Pharmacol* 2007;71(1):92-100.
167. Sanz JM, Chiozzi P, Di Virgilio F. Tenidap enhances P2Z/P2X7 receptor signalling in macrophages. *Eur J Pharmacol* 1998;355(2-3):235-44.
168. Adinolfi E, Kim M, Young MT, et al. Tyrosine phosphorylation of HSP90 within the P2X7 receptor complex negatively regulates P2X7 receptors. *J Biol Chem* 2003;278(39):37344-51.
169. Ferrari D, Pizzirani C, Adinolfi E, et al. The antibiotic polymyxin B modulates P2X7 receptor function. *J Immunol* 2004;173(7):4652-60.
170. Elssner A, Duncan M, Gavrilin M, et al. A novel P2X7 receptor activator, the human cathelicidin-derived peptide LL37, induces IL-1 beta processing and release. *J Immunol* 2004;172(8):4987-94.
171. Tomasinsig L, Pizzirani C, Skerlavaj B, et al. The human cathelicidin LL-37 modulates the activities of the P2X7 receptor in a structure-dependent manner. *J Biol Chem* 2008;283(45):30471-81.

172. Perregaux DG, Bhavsar K, Contillo L, et al. Antimicrobial peptides initiate IL-1 beta posttranslational processing: a novel role beyond innate immunity. *J Immunol* 2002;168(6):3024-32.
173. Di Virgilio F, Pinton P, Falzoni S. Assessing Extracellular ATP as Danger Signal In Vivo: The pmeLuc System. *Methods Mol Biol* 2016;1417:115-29.
174. Morciano G, Sarti AC, Marchi S, et al. Use of luciferase probes to measure ATP in living cells and animals. *Nature Protocols* 2017;12:1542.
175. Liu X, Surprenant A, Mao HJ, et al. Identification of key residues coordinating functional inhibition of P2X7 receptors by zinc and copper. *Mol Pharmacol* 2008;73(1):252-9.
176. Jiang LH. Inhibition of P2X(7) receptors by divalent cations: old action and new insight. *Eur Biophys J* 2009;38(3):339-46.
177. Jiang LH, Mackenzie AB, North RA, et al. Brilliant blue G selectively blocks ATP-gated rat P2X(7) receptors. *Mol Pharmacol* 2000;58(1):82-8.
178. Murgia M, Hanau S, Pizzo P, et al. Oxidized ATP. An irreversible inhibitor of the macrophage purinergic P2Z receptor. *J Biol Chem* 1993;268(11):8199-203.
179. Gargett CE, Wiley JS. The isoquinoline derivative KN-62 a potent antagonist of the P2Z-receptor of human lymphocytes. *Br J Pharmacol* 1997;120(8):1483-90.
180. Humphreys BD, Virginio C, Surprenant A, et al. Isoquinolines as antagonists of the P2X7 nucleotide receptor: high selectivity for the human versus rat receptor homologues. *Mol Pharmacol* 1998;54(1):22-32.
181. Cario-Toumaniantz C, Loirand G, Ferrier L, et al. Non-genomic inhibition of human P2X7 purinoceptor by 17beta-oestradiol. *J Physiol* 1998;508 (Pt 3):659-66.
182. Buell G, Chessell IP, Michel AD, et al. Blockade of human P2X7 receptor function with a monoclonal antibody. *Blood* 1998;92(10):3521-8.
183. Alcaraz L, Baxter A, Bent J, et al. Novel P2X7 receptor antagonists. *Bioorg Med Chem Lett* 2003;13(22):4043-6.
184. Baxter A, Bent J, Bowers K, et al. Hit-to-Lead studies: the discovery of potent adamantane amide P2X7 receptor antagonists. *Bioorg Med Chem Lett* 2003;13(22):4047-50.
185. Honore P, Donnelly-Roberts D, Namovic MT, et al. A-740003 [N-(1-{[(cyanoimino)(5-quinolinylamino) methyl]amino}-2,2-dimethylpropyl)-2-(3,4-dimethoxyphenyl)acetamide], a novel and selective P2X7 receptor antagonist, dose-dependently reduces neuropathic pain in the rat. *J Pharmacol Exp Ther* 2006;319(3):1376-85.
186. Nelson DW, Gregg RJ, Kort ME, et al. Structure-activity relationship studies on a series of novel, substituted 1-benzyl-5-phenyltetrazole P2X7 antagonists. *J Med Chem* 2006;49(12):3659-66.
187. McGaraughty S, Chu KL, Namovic MT, et al. P2X7-related modulation of pathological nociception in rats. *Neuroscience* 2007;146(4):1817-28.

188. Danquah W, Meyer-Schwesinger C, Rissiek B, et al. Nanobodies that block gating of the P2X7 ion channel ameliorate inflammation. *Science Translational Medicine* 2016;8(366):366ra162-366ra162.

189. Kim JE, Kang TC. The P2X7 receptor-pannexin-1 complex decreases muscarinic acetylcholine receptor-mediated seizure susceptibility in mice. *J Clin Invest* 2011;121(5):2037-47.

190. Jimenez-Pacheco A, Mesuret G, Sanz-Rodriguez A, et al. Increased neocortical expression of the P2X7 receptor after status epilepticus and anticonvulsant effect of P2X7 receptor antagonist A-438079. *Epilepsia* 2013;54(9):1551-61.

191. Rodriguez-Alvarez N, Jimenez-Mateos EM, Engel T, et al. Effects of P2X7 receptor antagonists on hypoxia-induced neonatal seizures in mice. *Neuropharmacology* 2017;116:351-63.

192. Eltom S, Stevenson CS, Rastrick J, et al. P2X7 receptor and caspase 1 activation are central to airway inflammation observed after exposure to tobacco smoke. *PLOS ONE* 2011;6(9):e24097.

193. Wang S, Zhao J, Wang H, et al. Blockage of P2X7 attenuates acute lung injury in mice by inhibiting NLRP3 inflammasome. *Int Immunopharmacol* 2015;27(1):38-45.

194. Taylor SR, Turner CM, Elliott JI, et al. P2X7 deficiency attenuates renal injury in experimental glomerulonephritis. *J Am Soc Nephrol* 2009;20(6):1275-81.

195. Yan Y, Bai J, Zhou X, et al. P2X7 receptor inhibition protects against ischemic acute kidney injury in mice. *Am J Physiol Cell Physiol* 2015;308(6):C463-72.

196. Franco M, Bautista-Perez R, Cano-Martinez A, et al. Physiopathological implications of P2X1 and P2X7 receptors in regulation of glomerular hemodynamics in angiotensin II-induced hypertension. *Am J Physiol Renal Physiol* 2017;313(1):F9-f19.

197. Ji X, Naito Y, Hirokawa G, et al. P2X(7) receptor antagonism attenuates the hypertension and renal injury in Dahl salt-sensitive rats. *Hypertens Res* 2012;35(2):173-9.

198. Keystone EC, Wang MM, Layton M, et al. Clinical evaluation of the efficacy of the P2X7 purinergic receptor antagonist AZD9056 on the signs and symptoms of rheumatoid arthritis in patients with active disease despite treatment with methotrexate or sulphasalazine. *Ann Rheum Dis* 2012;71(10):1630-5.

199. Stock TC, Bloom BJ, Wei N, et al. Efficacy and safety of CE-224,535, an antagonist of P2X7 receptor, in treatment of patients with rheumatoid arthritis inadequately controlled by methotrexate. *J Rheumatol* 2012;39(4):720-7.

200. Eser A, Colombel JF, Rutgeerts P, et al. Safety and Efficacy of an Oral Inhibitor of the Purinergic Receptor P2X7 in Adult Patients with Moderately to Severely Active Crohn's Disease: A Randomized Placebo-controlled, Double-blind, Phase IIa Study. *Inflamm Bowel Dis* 2015;21(10):2247-53.

201. Gilbert SM, Gidley Baird A, Glazer S, et al. A phase I clinical trial demonstrates that nfP2X7 - targeted antibodies provide a novel, safe and tolerable topical therapy for basal cell carcinoma. *Br J Dermatol* 2017;177(1):117-24.
202. Martins JP, Silva RB, Coutinho-Silva R, et al. The role of P2X7 purinergic receptors in inflammatory and nociceptive changes accompanying cyclophosphamide-induced haemorrhagic cystitis in mice. *Br J Pharmacol* 2012;165(1):183-96.
203. Zhang Y, Yuan F, Cao X, et al. P2X7 receptor blockade protects against cisplatin-induced nephrotoxicity in mice by decreasing the activities of inflammasome components, oxidative stress and caspase-3. *Toxicol Appl Pharmacol* 2014;281(1):1-10.
204. Rassendren F, Buell GN, Virginio C, et al. The permeabilizing ATP receptor, P2X7. Cloning and expression of a human cDNA. *J Biol Chem* 1997;272(9):5482-6.
205. Vonend O, Turner CM, Chan CM, et al. Glomerular expression of the ATP-sensitive P2X receptor in diabetic and hypertensive rat models. *Kidney Int* 2004;66(1):157-66.
206. Deetjen P, Thomas J, Lehrmann H, et al. The luminal P2Y receptor in the isolated perfused mouse cortical collecting duct. *J Am Soc Nephrol* 2000;11(10):1798-806.
207. Wu H, Nie Y, Xiong H, et al. P2X7 Receptor Expression in Peripheral Blood Monocytes Is Correlated With Plasma C-Reactive Protein and Cytokine Levels in Patients With Type 2 Diabetes Mellitus: a Preliminary Report. *Inflammation* 2015;38(6):2076-81.
208. Vieira FS, Nanini HF, Takiya CM, et al. P2X7 receptor knockout prevents streptozotocin-induced type 1 diabetes in mice. *Molecular and Cellular Endocrinology* 2016;419(Supplement C):148-57.
209. Solini A, Chiozzi P, Morelli A, et al. Enhanced P2X7 activity in human fibroblasts from diabetic patients: a possible pathogenetic mechanism for vascular damage in diabetes. *Arterioscler Thromb Vasc Biol* 2004;24(7):1240-5.
210. Goncalves RG, Gabrich L, Rosario A, Jr., et al. The role of purinergic P2X7 receptors in the inflammation and fibrosis of unilateral ureteral obstruction in mice. *Kidney Int* 2006;70(9):1599-606.
211. Deplano S, Cook HT, Russell R, et al. P2X7 receptor-mediated Nlrp3-inflammasome activation is a genetic determinant of macrophage-dependent crescentic glomerulonephritis. *J Leukoc Biol* 2013;93(1):127-34.
212. Zhao J, Wang H, Dai C, et al. P2X7 blockade attenuates murine lupus nephritis by inhibiting activation of the NLRP3/ASC/caspase 1 pathway. *Arthritis Rheum* 2013;65(12):3176-85.
213. Matute C, Torre I, Perez-Cerda F, et al. P2X(7) receptor blockade prevents ATP excitotoxicity in oligodendrocytes and ameliorates experimental autoimmune encephalomyelitis. *J Neurosci* 2007;27(35):9525-33.
214. Stanton MC, Tange JD. Goodpasture's syndrome (pulmonary haemorrhage associated with glomerulonephritis). *Australas Ann Med* 1958;7(2):132-44.

215. Goodpasture EW. Landmark Publication from The American Journal of the Medical Sciences: The Significance Of Certain Pulmonary Lesions In Relation To The Etiology Of Influenza. *The American Journal of the Medical Sciences*;338(2):148-51.
216. Lerner RA, Glassock RJ, Dixon FJ. The role of anti-glomerular basement membrane antibody in the pathogenesis of human glomerulonephritis. *J Exp Med* 1967;126(6):989-1004.
217. Scheer RL, Grossman MA. IMmune aspects of the glomerulonephritis associated with pulmonary hemmorhage. *Ann Intern Med* 1964;60(6):1009-21.
218. Savage CO, Pusey CD, Bowman C, et al. Antiglomerular basement membrane antibody mediated disease in the British Isles 1980-4. *Br Med J (Clin Res Ed)* 1986;292(6516):301-4.
219. Taylor DM, Yehia M, Simpson IJ, et al. Anti-glomerular basement membrane disease in Auckland. *Intern Med J* 2012;42(6):672-6.
220. Canney M, O'Hara PV, McEvoy CM, et al. Spatial and Temporal Clustering of Anti-Glomerular Basement Membrane Disease. *Clin J Am Soc Nephrol* 2016;11(8):1392-9.
221. McAdoo SP, Pusey CD. Anti-Glomerular Basement Membrane Disease. *Clin J Am Soc Nephrol* 2017;12(7):1162-72.
222. Levy JB, Turner AN, Rees AJ, et al. Long-term outcome of anti-glomerular basement membrane antibody disease treated with plasma exchange and immunosuppression. *Ann Intern Med* 2001;134(11):1033-42.
223. Segelmark M, Hellmark T, Wieslander J. The prognostic significance in Goodpasture's disease of specificity, titre and affinity of anti-glomerular-basement-membrane antibodies. *Nephron Clin Pract* 2003;94(3):c59-68.
224. Fischer EG, Lager DJ. Anti-glomerular basement membrane glomerulonephritis: a morphologic study of 80 cases. *Am J Clin Pathol* 2006;125(3):445-50.
225. Huey B, McCormick K, Capper J, et al. Associations of HLA-DR and HLA-DQ types with anti-GBM nephritis by sequence-specific oligonucleotide probe hybridization. *Kidney Int* 1993;44(2):307-12.
226. Kitagawa W, Imai H, Komatsuda A, et al. The HLA-DRB1*1501 allele is prevalent among Japanese patients with anti-glomerular basement membrane antibody-mediated disease. *Nephrol Dial Transplant* 2008;23(10):3126-9.
227. Fisher M, Pusey CD, Vaughan RW, et al. Susceptibility to anti-glomerular basement membrane disease is strongly associated with HLA-DRB1 genes. *Kidney International* 1997;51(1):222-29.
228. Zhou XJ, Lv JC, Bu DF, et al. Copy number variation of FCGR3A rather than FCGR3B and FCGR2B is associated with susceptibility to anti-GBM disease. *Int Immunol* 2010;22(1):45-51.
229. Rees AJ, Lockwood CM, Peters DK. Enhanced allergic tissue injury in Goodpasture's syndrome by intercurrent bacterial infection. *British Medical Journal* 1977;2(6089):723-26.

230. Gu QH, Xie LJ, Jia XY, et al. Fever and prodromal infections in anti-glomerular basement membrane disease. *Nephrology (Carlton)* 2017

231. Karkar AM, Rees AJ. Influence of an established acute phase response on the severity of experimental nephritis. *Clin Exp Immunol* 1994;98(2):295-9.

232. Bombassei GJ, Kaplan AA. The association between hydrocarbon exposure and anti-glomerular basement membrane antibody-mediated disease (Goodpasture's syndrome). *Am J Ind Med* 1992;21(2):141-53.

233. Donaghy M, Rees AJ. Cigarette smoking and lung haemorrhage in glomerulonephritis caused by autoantibodies to glomerular basement membrane. *Lancet* 1983;2(8364):1390-3.

234. Jia XY, Hu SY, Chen JL, et al. The clinical and immunological features of patients with combined anti-glomerular basement membrane disease and membranous nephropathy. *Kidney Int* 2014;85(4):945-52.

235. Basford AW, Lewis J, Dwyer JP, et al. Membranous nephropathy with crescents. *J Am Soc Nephrol* 2011;22(10):1804-8.

236. Hudson BG, Tryggvason K, Sundaramoorthy M, et al. Alport's Syndrome, Goodpasture's Syndrome, and Type IV Collagen. *New England Journal of Medicine* 2003;348(25):2543-56.

237. Saus J, Wieslander J, Langeveld JP, et al. Identification of the Goodpasture antigen as the alpha 3(IV) chain of collagen IV. *J Biol Chem* 1988;263(26):13374-80.

238. Weber M, Köhler H, Manns M, et al. Identification of Goodpasture target antigens in basement membranes of human glomeruli, lung, and placenta. *Clin Exp Immunol* 1987;67(2):262-9.

239. Cashman SJ, Pusey CD, Evans DJ. Extraglomerular distribution of immunoreactive Goodpasture antigen. *J Pathol* 1988;155(1):61-70.

240. Netzer KO, Leinonen A, Boutaud A, et al. The goodpasture autoantigen. Mapping the major conformational epitope(s) of alpha3(IV) collagen to residues 17-31 and 127-141 of the NC1 domain. *J Biol Chem* 1999;274(16):11267-74.

241. Kalluri R, Cantley LG, Kerjaschki D, et al. Reactive oxygen species expose cryptic epitopes associated with autoimmune goodpasture syndrome. *J Biol Chem* 2000;275(26):20027-32.

242. Cui Z, Zhao MH. Avidity of anti-glomerular basement membrane autoantibodies was associated with disease severity. *Clin Immunol* 2005;116(1):77-82.

243. Choy BY, Chan TM, Lai KN. Recurrent glomerulonephritis after kidney transplantation. *Am J Transplant* 2006;6(11):2535-42.

244. Yang R, Cui Z, Hellmark T, et al. Natural anti-GBM antibodies from normal human sera recognize alpha3(IV)NC1 restrictively and recognize the same epitopes as anti-GBM antibodies from patients with anti-GBM disease. *Clin Immunol* 2007;124(2):207-12.

245. Bowman C, Ambrus K, Lockwood CM. Restriction of human IgG subclass expression in the population of auto-antibodies to glomerular basement membrane. *Clin Exp Immunol* 1987;69(2):341-49.

246. Cui Z, Wang HY, Zhao MH. Natural autoantibodies against glomerular basement membrane exist in normal human sera. *Kidney Int* 2006;69(5):894-9.

247. McAdoo SP, Pusey CD. Anti-glomerular Basement Membrane Disease. In: Mackay IR, Rose NR, Diamond B, et al., eds. Encyclopedia of Medical Immunology: Autoimmune Diseases. New York, NY: Springer New York 2014:50-56.

248. Wu J, Hicks J, Borillo J, et al. CD4(+) T cells specific to a glomerular basement membrane antigen mediate glomerulonephritis. *J Clin Invest* 2002;109(4):517-24.

249. Dean EG, Wilson GR, Li M, et al. Experimental autoimmune Goodpasture's disease: a pathogenetic role for both effector cells and antibody in injury. *Kidney Int* 2005;67(2):566-75.

250. Reynolds J, Tam FW, Chandraker A, et al. CD28-B7 blockade prevents the development of experimental autoimmune glomerulonephritis. *J Clin Invest* 2000;105(5):643-51.

251. Bolton WK, Innes DJ, Jr., Sturgill BC, et al. T-cells and macrophages in rapidly progressive glomerulonephritis: clinicopathologic correlations. *Kidney Int* 1987;32(6):869-76.

252. Derry CJ, Ross CN, Lombardi G, et al. Analysis of T cell responses to the autoantigen in Goodpasture's disease. *Clin Exp Immunol* 1995;100(2):262-8.

253. Segelmark M, Butkowski R, Wieslander J. Antigen restriction and IgG subclasses among anti-GBM autoantibodies. *Nephrol Dial Transplant* 1990;5(12):991-6.

254. Salama AD, Chaudhry AN, Ryan JJ, et al. In Goodpasture's disease, CD4(+) T cells escape thymic deletion and are reactive with the autoantigen alpha3(IV)NC1. *J Am Soc Nephrol* 2001;12(9):1908-15.

255. Zou J, Hannier S, Cairns LS, et al. Healthy individuals have Goodpasture autoantigen-reactive T cells. *J Am Soc Nephrol* 2008;19(2):396-404.

256. Hellmark T, Brunmark C, Trojnar J, et al. Epitope mapping of anti-glomerular basement membrane (GBM) antibodies with synthetic peptides. *Clin Exp Immunol* 1996;105(3):504-10.

257. Arends J, Wu J, Borillo J, et al. T cell epitope mimicry in antiglomerular basement membrane disease. *J Immunol* 2006;176(2):1252-8.

258. Phelps RG, Jones VL, Coughlan M, et al. Presentation of the Goodpasture autoantigen to CD4 T cells is influenced more by processing constraints than by HLA class II peptide binding preferences. *J Biol Chem* 1998;273(19):11440-7.

259. Serisier DJ, Wong RCW, Armstrong JG. Alveolar haemorrhage in anti-glomerular basement membrane disease without detectable antibodies by conventional assays. *Thorax* 2006;61(7):636-39.

260. Harrity P, Gilbert-Barness E, Cabalka A, et al. Isolated pulmonary Goodpasture syndrome. *Pediatr Pathol* 1991;11(4):635-46.

261. Moulis G, Huart A, Guitard J, et al. IgA-mediated anti-glomerular basement membrane disease: an uncommon mechanism of Goodpasture's syndrome. *Clin Kidney J* 2012;5(6):545-8.

262. Ohlsson S, Herlitz H, Lundberg S, et al. Circulating anti-glomerular basement membrane antibodies with predominance of subclass IgG4 and false-negative immunoassay test results in anti-glomerular basement membrane disease. *Am J Kidney Dis* 2014;63(2):289-93.
263. Jennette JC. Rapidly progressive crescentic glomerulonephritis. *Kidney Int* 2003;63(3):1164-77.
264. Lockwood CM, Rees AJ, Pearson TA, et al. Immunosuppression and plasma-exchange in the treatment of Goodpasture's syndrome. *Lancet* 1976;1(7962):711-5.
265. Lindemann W. Sur le mode d'action de certain poisons renaux. *Ann Inst Pasteur* 1900;14:49-59.
266. Sato T, Kawachi H, Morioka T, et al. Nephrotoxic serum nephritis in nude rats: the roles of host immune reactions in the accelerated type. *Clin Exp Immunol* 1993;91(1):131-4.
267. Tam FW, Smith J, Morel D, et al. Development of scarring and renal failure in a rat model of crescentic glomerulonephritis. *Nephrology Dialysis Transplantation* 1999;14(7):1658-66.
268. Aitman TJ, Dong R, Vyse TJ, et al. Copy number polymorphism in Fcgr3 predisposes to glomerulonephritis in rats and humans. *Nature* 2006;439(7078):851-5.
269. Behmoaras J, Smith J, D'Souza Z, et al. Genetic loci modulate macrophage activity and glomerular damage in experimental glomerulonephritis. *J Am Soc Nephrol* 2010;21(7):1136-44.
270. Huang XR, Tipping PG, Shuo L, et al. Th1 responsiveness to nephritogenic antigens determines susceptibility to crescentic glomerulonephritis in mice. *Kidney Int* 1997;51(1):94-103.
271. Cook HT, Singh SJ, Wembridge DE, et al. Interleukin-4 ameliorates crescentic glomerulonephritis in Wistar Kyoto rats. *Kidney Int* 1999;55(4):1319-26.
272. Lai PC, Cook HT, Smith J, et al. Interleukin-11 attenuates nephrotoxic nephritis in Wistar Kyoto rats. *J Am Soc Nephrol* 2001;12(11):2310-20.
273. Khan SB, Cook HT, Bhangal G, et al. Antibody blockade of TNF-alpha reduces inflammation and scarring in experimental crescentic glomerulonephritis. *Kidney Int* 2005;67(5):1812-20.
274. Lai PC, Smith J, Bhangal G, et al. Interleukin-11 reduces renal injury and glomerular NF-kappa B activity in murine experimental glomerulonephritis. *Nephron Exp Nephrol* 2005;101(4):e146-54.
275. Sakurai H, Hisada Y, Ueno M, et al. Activation of transcription factor NF-kappa B in experimental glomerulonephritis in rats. *Biochim Biophys Acta* 1996;1316(2):132-8.
276. Li S, Holdsworth SR, Tipping PG. Antibody independent crescentic glomerulonephritis in mu chain deficient mice. *Kidney Int* 1997;51(3):672-8.
277. Tipping PG, Huang XR, Qi M, et al. Crescentic glomerulonephritis in CD4- and CD8-deficient mice. Requirement for CD4 but not CD8 cells. *Am J Pathol* 1998;152(6):1541-8.
278. Wolf D, Hochegger K, Wolf AM, et al. CD4+CD25+ regulatory T cells inhibit experimental anti-glomerular basement membrane glomerulonephritis in mice. *J Am Soc Nephrol* 2005;16(5):1360-70.

279. Paust HJ, Turner JE, Steinmetz OM, et al. The IL-23/Th17 axis contributes to renal injury in experimental glomerulonephritis. *J Am Soc Nephrol* 2009;20(5):969-79.

280. Hamour S, Gan PY, Pepper R, et al. Local IL-17 Production Exerts a Protective Role in Murine Experimental Glomerulonephritis. *PLOS ONE* 2015;10(8):e0136238.

281. Tomosugi NI, Cashman SJ, Hay H, et al. Modulation of antibody-mediated glomerular injury in vivo by bacterial lipopolysaccharide, tumor necrosis factor, and IL-1. *J Immunol* 1989;142(9):3083-90.

282. Timoshanko JR, Kitching AR, Iwakura Y, et al. Contributions of IL-1β and IL-1α to Crescentic Glomerulonephritis in Mice. *Journal of the American Society of Nephrology* 2004;15(4):910-18.

283. Timoshanko JR, Kitching AR, Iwakura Y, et al. Leukocyte-derived interleukin-1beta interacts with renal interleukin-1 receptor I to promote renal tumor necrosis factor and glomerular injury in murine crescentic glomerulonephritis. *Am J Pathol* 2004;164(6):1967-77.

284. Lichtnekert J, Kulkarni OP, Mulay SR, et al. Anti-GBM Glomerulonephritis Involves IL-1 but Is Independent of NLRP3/ASC Inflammasome-Mediated Activation of Caspase-1. *PLOS ONE* 2011;6(10):e26778.

285. Andersen K, Eltrich N, Lichtnekert J, et al. The NLRP3/ASC inflammasome promotes T-cell-dependent immune complex glomerulonephritis by canonical and noncanonical mechanisms. *Kidney International* 2014;86(5):965-78.

286. Hochheiser K, Engel DR, Hammerich L, et al. Kidney Dendritic Cells Become Pathogenic during Crescentic Glomerulonephritis with Proteinuria. *Journal of the American Society of Nephrology* 2011;22(2):306-16.

287. Giorgini A, Brown HJ, Sacks SH, et al. Toll-like receptor 4 stimulation triggers crescentic glomerulonephritis by multiple mechanisms including a direct effect on renal cells. *Am J Pathol* 2010;177(2):644-53.

288. Steblay RW. Glomerulonephritis induced in sheep by injections of heterologous glomerular basement membrane and Freund's complete adjuvant. *J Exp Med* 1962;116:253-72.

289. Pusey CD, Holland MJ, Cashman SJ, et al. Experimental autoimmune glomerulonephritis induced by homologous and isologous glomerular basement membrane in Brown-Norway rats. *Nephrol Dial Transplant* 1991;6(7):457-65.

290. Reynolds J, Mavromatidis K, Cashman SJ, et al. Experimental autoimmune glomerulonephritis (EAG) induced by homologous and heterologous glomerular basement membrane in two substrains of Wistar-Kyoto rat. *Nephrol Dial Transplant* 1998;13(1):44-52.

291. Ryan JJ, Reynolds J, Norgan VA, et al. Expression and characterization of recombinant rat alpha 3(IV)NC1 and its use in induction of experimental autoimmune glomerulonephritis. *Nephrol Dial Transplant* 2001;16(2):253-61.

292. Reynolds J, Albouainain A, Duda MA, et al. Strain susceptibility to active induction and passive transfer of experimental autoimmune glomerulonephritis in the rat. *Nephrol Dial Transplant* 2006;21(12):3398-408.

293. Sado Y, Naito I, Okigaki T. Transfer of anti-glomerular basement membrane antibody-induced glomerulonephritis in inbred rats with isologous antibodies from the urine of nephritic rats. *J Pathol* 1989;158(4):325-32.

294. Reynolds J, Moss J, Duda MA, et al. The evolution of crescentic nephritis and alveolar haemorrhage following induction of autoimmunity to glomerular basement membrane in an experimental model of Goodpasture's disease. *J Pathol* 2003;200(1):118-29.

295. Wu J, Hicks J, Ou C, et al. Glomerulonephritis induced by recombinant collagen IV alpha 3 chain noncollagen domain 1 is not associated with glomerular basement membrane antibody: a potential T cell-mediated mechanism. *J Immunol* 2001;167(4):2388-95.

296. Kalluri R, Danoff TM, Okada H, et al. Susceptibility to anti-glomerular basement membrane disease and Goodpasture syndrome is linked to MHC class II genes and the emergence of T cell-mediated immunity in mice. *J Clin Invest* 1997;100(9):2263-75.

297. Reynolds J, Norgan VA, Bhambra U, et al. Anti-CD8 monoclonal antibody therapy is effective in the prevention and treatment of experimental autoimmune glomerulonephritis. *J Am Soc Nephrol* 2002;13(2):359-69.

298. Reynolds J, Pusey CD. In vivo treatment with a monoclonal antibody to T helper cells in experimental autoimmune glomerulonephritis in the BN rat. *Clin Exp Immunol* 1994;95(1):122-7.

299. Reynolds J, Abbott DS, Karegli J, et al. Mucosal tolerance induced by an immunodominant peptide from rat alpha3(IV)NC1 in established experimental autoimmune glomerulonephritis. *Am J Pathol* 2009;174(6):2202-10.

300. Reynolds J, Prodromidi EI, Juggapah JK, et al. Nasal administration of recombinant rat alpha3(IV)NC1 prevents the development of experimental autoimmune glomerulonephritis in the WKY rat. *J Am Soc Nephrol* 2005;16(5):1350-9.

301. Hunemorder S, Treder J, Ahrens S, et al. TH1 and TH17 cells promote crescent formation in experimental autoimmune glomerulonephritis. *J Pathol* 2015;237(1):62-71.

302. Wiik A. Granulocyte-specific antinuclear antibodies. Possible significance for the pathogenesis, clinical features and diagnosis of rheumatoid arthritis. *Allergy* 1980;35(4):263-89.

303. Eisenberger U, Fakhouri F, Vanhille P, et al. ANCA-negative pauci-immune renal vasculitis: histology and outcome. *Nephrol Dial Transplant* 2005;20(7):1392-9.

304. Watts RA, Mahr A, Mohammad AJ, et al. Classification, epidemiology and clinical subgrouping of antineutrophil cytoplasmic antibody (ANCA)-associated vasculitis. *Nephrol Dial Transplant* 2015;30 Suppl 1:i14-22.

305. Watts RA, Lane SE, Bentham G, et al. Epidemiology of systemic vasculitis: a ten-year study in the United Kingdom. *Arthritis Rheum* 2000;43(2):414-9.

306. Gonzalez-Gay MA, Garcia-Porrua C, Guerrero J, et al. The epidemiology of the primary systemic vasculitides in northwest Spain: implications of the Chapel Hill Consensus Conference definitions. *Arthritis Rheum* 2003;49(3):388-93.

307. Mohammad AJ, Jacobsson LT, Westman KW, et al. Incidence and survival rates in Wegener's granulomatosis, microscopic polyangiitis, Churg-Strauss syndrome and polyarteritis nodosa. *Rheumatology (Oxford)* 2009;48(12):1560-5.

308. Fujimoto S, Watts RA, Kobayashi S, et al. Comparison of the epidemiology of anti-neutrophil cytoplasmic antibody-associated vasculitis between Japan and the U.K. *Rheumatology (Oxford)* 2011;50(10):1916-20.

309. Lyons PA, Rayner TF, Trivedi S, et al. Genetically distinct subsets within ANCA-associated vasculitis. *N Engl J Med* 2012;367(3):214-23.

310. Cao Y, Schmitz JL, Yang J, et al. DRB1*15 allele is a risk factor for PR3-ANCA disease in African Americans. *J Am Soc Nephrol* 2011;22(6):1161-7.

311. Popa ER, Stegeman CA, Abdulahad WH, et al. Staphylococcal toxic-shock-syndrome-toxin-1 as a risk factor for disease relapse in Wegener's granulomatosis. *Rheumatology (Oxford)* 2007;46(6):1029-33.

312. Kain R, Exner M, Brandes R, et al. Molecular mimicry in pauci-immune focal necrotizing glomerulonephritis. *Nat Med* 2008;14(10):1088-96.

313. Roth AJ, Brown MC, Smith RN, et al. Anti-LAMP-2 antibodies are not prevalent in patients with antineutrophil cytoplasmic autoantibody glomerulonephritis. *J Am Soc Nephrol* 2012;23(3):545-55.

314. Pendergraft Iii WF, Preston GA, Shah RR, et al. Autoimmunity is triggered by cPR-3(105–201), a protein complementary to human autoantigen proteinase-3. *Nat Med* 2003;10:72.

315. Summers SA, van der Veen BS, O'Sullivan KM, et al. Intrinsic renal cell and leukocyte-derived TLR4 aggravate experimental anti-MPO glomerulonephritis. *Kidney Int* 2010;78(12):1263-74.

316. Pendergraft WF, 3rd, Herlitz LC, Thornley-Brown D, et al. Nephrotoxic effects of common and emerging drugs of abuse. *Clin J Am Soc Nephrol* 2014;9(11):1996-2005.

317. de Lind van Wijngaarden RA, van Rijn L, Hagen EC, et al. Hypotheses on the etiology of antineutrophil cytoplasmic autoantibody associated vasculitis: the cause is hidden, but the result is known. *Clin J Am Soc Nephrol* 2008;3(1):237-52.

318. Yu F, Chen M, Gao Y, et al. Clinical and pathological features of renal involvement in propylthiouracil-associated ANCA-positive vasculitis. *Am J Kidney Dis* 2007;49(5):607-14.

319. Furuta S, Jayne DRW. Antineutrophil cytoplasm antibody–associated vasculitis: recent developments. *Kidney International* 2013;84(2):244-49.

320. Bansal PJ, Tobin MC. Neonatal microscopic polyangiitis secondary to transfer of maternal myeloperoxidase-antineutrophil cytoplasmic antibody resulting in neonatal pulmonary hemorrhage and renal involvement. *Ann Allergy Asthma Immunol* 2004;93(4):398-401.
321. Silva F, Specks U, Sethi S, et al. Successful pregnancy and delivery of a healthy newborn despite transplacental transfer of antimyeloperoxidase antibodies from a mother with microscopic polyangiitis. *Am J Kidney Dis* 2009;54(3):542-5.
322. Jayne DR, Gaskin G, Rasmussen N, et al. Randomized trial of plasma exchange or high-dosage methylprednisolone as adjunctive therapy for severe renal vasculitis. *J Am Soc Nephrol* 2007;18(7):2180-8.
323. Jones RB, Tervaert JW, Hauser T, et al. Rituximab versus cyclophosphamide in ANCA-associated renal vasculitis. *N Engl J Med* 2010;363(3):211-20.
324. Falk RJ, Terrell RS, Charles LA, et al. Anti-neutrophil cytoplasmic autoantibodies induce neutrophils to degranulate and produce oxygen radicals in vitro. *Proc Natl Acad Sci U S A* 1990;87(11):4115-9.
325. Savage CO, Gaskin G, Pusey CD, et al. Anti-neutrophil cytoplasm antibodies can recognize vascular endothelial cell-bound anti-neutrophil cytoplasm antibody-associated autoantigens. *Exp Nephrol* 1993;1(3):190-5.
326. Schreiber A, Xiao H, Jennette JC, et al. C5a receptor mediates neutrophil activation and ANCA-induced glomerulonephritis. *J Am Soc Nephrol* 2009;20(2):289-98.
327. Radford DJ, Luu NT, Hewins P, et al. Antineutrophil cytoplasmic antibodies stabilize adhesion and promote migration of flowing neutrophils on endothelial cells. *Arthritis Rheum* 2001;44(12):2851-61.
328. Kettritz R, Jennette JC, Falk RJ. Crosslinking of ANCA-antigens stimulates superoxide release by human neutrophils. *J Am Soc Nephrol* 1997;8(3):386-94.
329. Weidner S, Neupert W, Goppelt-Struebe M, et al. Antineutrophil cytoplasmic antibodies induce human monocytes to produce oxygen radicals in vitro. *Arthritis Rheum* 2001;44(7):1698-706.
330. Mulder AH, Heeringa P, Brouwer E, et al. Activation of granulocytes by anti-neutrophil cytoplasmic antibodies (ANCA): a Fc gamma RII-dependent process. *Clin Exp Immunol* 1994;98(2):270-8.
331. Porges AJ, Redecha PB, Kimberly WT, et al. Anti-neutrophil cytoplasmic antibodies engage and activate human neutrophils via Fc gamma RIIa. *J Immunol* 1994;153(3):1271-80.
332. Hulett MD, Hogarth PM. Molecular Basis of Fc Receptor Function. In: Dixon FJ, ed. Advances in Immunology: Academic Press 1994:1-127.
333. Kimberly JCEKCJWJESRP. FcγRIIIb alleles predict renal dysfunction in Wegener's granulomatosis. *Arthritis Rheum* 1996;39:S210.
334. Kocher M, Edberg JC, Fleit HB, et al. Antineutrophil cytoplasmic antibodies preferentially engage Fc gammaRIIIb on human neutrophils. *J Immunol* 1998;161(12):6909-14.

335. Fuchs TA, Abed U, Goosmann C, et al. Novel cell death program leads to neutrophil extracellular traps. *J Cell Biol* 2007;176(2):231-41.

336. Kessenbrock K, Krumbholz M, Schonermarck U, et al. Netting neutrophils in autoimmune small-vessel vasculitis. *Nat Med* 2009;15(6):623-5.

337. Villanueva E, Yalavarthi S, Berthier CC, et al. Netting neutrophils induce endothelial damage, infiltrate tissues, and expose immunostimulatory molecules in systemic lupus erythematosus. *J Immunol* 2011;187(1):538-52.

338. Wang H, Wang C, Zhao MH, et al. Neutrophil extracellular traps can activate alternative complement pathways. *Clin Exp Immunol* 2015;181(3):518-27.

339. Sangaletti S, Tripodo C, Chiodoni C, et al. Neutrophil extracellular traps mediate transfer of cytoplasmic neutrophil antigens to myeloid dendritic cells toward ANCA induction and associated autoimmunity. *Blood* 2012;120(15):3007-18.

340. Xiao H, Heeringa P, Hu P, et al. Antineutrophil cytoplasmic autoantibodies specific for myeloperoxidase cause glomerulonephritis and vasculitis in mice. *J Clin Invest* 2002;110(7):955-63.

341. Little MA, Smyth CL, Yadav R, et al. Antineutrophil cytoplasm antibodies directed against myeloperoxidase augment leukocyte-microvascular interactions in vivo. *Blood* 2005;106(6):2050-8.

342. Xu PC, Cui Z, Chen M, et al. Comparison of characteristics of natural autoantibodies against myeloperoxidase and anti-myeloperoxidase autoantibodies from patients with microscopic polyangiitis. *Rheumatology (Oxford)* 2011;50(7):1236-43.

343. Nowack R, Grab I, Flores-Suarez LF, et al. ANCA titres, even of IgG subclasses, and soluble CD14 fail to predict relapses in patients with ANCA-associated vasculitis. *Nephrol Dial Transplant* 2001;16(8):1631-7.

344. Roth AJ, Ooi JD, Hess JJ, et al. Epitope specificity determines pathogenicity and detectability in ANCA-associated vasculitis. *J Clin Invest* 2013;123(4):1773-83.

345. Brouwer E, Huitema MG, Mulder AH, et al. Neutrophil activation in vitro and in vivo in Wegener's granulomatosis. *Kidney Int* 1994;45(4):1120-31.

346. Xiao H, Heeringa P, Liu Z, et al. The role of neutrophils in the induction of glomerulonephritis by anti-myeloperoxidase antibodies. *Am J Pathol* 2005;167(1):39-45.

347. Jennette JC, Falk RJ. ANCAs are also antimonocyte cytoplasmic autoantibodies. *Clin J Am Soc Nephrol* 2015;10(1):4-6.

348. Tarzi RM, Liu J, Schneiter S, et al. CD14 expression is increased on monocytes in patients with anti-neutrophil cytoplasm antibody (ANCA)-associated vasculitis and correlates with the expression of ANCA autoantigens. *Clin Exp Immunol* 2015;181(1):65-75.

349. Haller H, Eichhorn J, Pieper K, et al. Circulating leukocyte integrin expression in Wegener's granulomatosis. *J Am Soc Nephrol* 1996;7(1):40-8.

350. Weidner S, Carl M, Riess R, et al. Histologic analysis of renal leukocyte infiltration in antineutrophil cytoplasmic antibody-associated vasculitis: importance of monocyte and neutrophil infiltration in tissue damage. *Arthritis Rheum* 2004;50(11):3651-7.
351. Zhao L, David MZ, Hyjek E, et al. M2 Macrophage Infiltrates in the Early Stages of ANCA-Associated Pauci-Immune Necrotizing GN. *Clinical Journal of the American Society of Nephrology* 2015;10(1):54-62.
352. Rousselle A, Kettritz R, Schreiber A. Monocytes Promote Crescent Formation in Anti-Myeloperoxidase Antibody-Induced Glomerulonephritis. *Am J Pathol* 2017;187(9):1908-15.
353. Xiao H, Schreiber A, Heeringa P, et al. Alternative complement pathway in the pathogenesis of disease mediated by anti-neutrophil cytoplasmic autoantibodies. *Am J Pathol* 2007;170(1):52-64.
354. Huugen D, van Esch A, Xiao H, et al. Inhibition of complement factor C5 protects against anti-myeloperoxidase antibody-mediated glomerulonephritis in mice. *Kidney Int* 2007;71(7):646-54.
355. Xiao H, Dairaghi DJ, Powers JP, et al. C5a receptor (CD88) blockade protects against MPO-ANCA GN. *J Am Soc Nephrol* 2014;25(2):225-31.
356. Xing GQ, Chen M, Liu G, et al. Complement activation is involved in renal damage in human antineutrophil cytoplasmic autoantibody associated pauci-immune vasculitis. *J Clin Immunol* 2009;29(3):282-91.
357. Gou SJ, Yuan J, Wang C, et al. Alternative complement pathway activation products in urine and kidneys of patients with ANCA-associated GN. *Clin J Am Soc Nephrol* 2013;8(11):1884-91.
358. Augusto JF, Langs V, Demiselle J, et al. Low Serum Complement C3 Levels at Diagnosis of Renal ANCA-Associated Vasculitis Is Associated with Poor Prognosis. *PLOS ONE* 2016;11(7):e0158871.
359. Huang YM, Wang H, Wang C, et al. Promotion of hypercoagulability in antineutrophil cytoplasmic antibody-associated vasculitis by C5a-induced tissue factor-expressing microparticles and neutrophil extracellular traps. *Arthritis Rheumatol* 2015;67(10):2780-90.
360. Hao J, Wang C, Yuan J, et al. A pro-inflammatory role of C5L2 in C5a-primed neutrophils for ANCA-induced activation. *PLOS ONE* 2013;8(6):e66305.
361. Popa ER, Stegeman CA, Bos NA, et al. Differential B- and T-cell activation in Wegener's granulomatosis. *J Allergy Clin Immunol* 1999;103(5 Pt 1):885-94.
362. Stone JH, Merkel PA, Spiera R, et al. Rituximab versus cyclophosphamide for ANCA-associated vasculitis. *N Engl J Med* 2010;363(3):221-32.
363. Culton DA, Nicholas MW, Bunch DO, et al. Similar CD19 dysregulation in two autoantibody-associated autoimmune diseases suggests a shared mechanism of B-cell tolerance loss. *J Clin Immunol* 2007;27(1):53-68.

364. Jennette JC, Falk RJ. B-Cell Mediated Pathogenesis of ANCA-Mediated Vasculitis. *Seminars in immunopathology* 2014;36(3):327-38.

365. Todd SK, Pepper RJ, Draibe J, et al. Regulatory B cells are numerically but not functionally deficient in anti-neutrophil cytoplasm antibody-associated vasculitis. *Rheumatology* 2014;53(9):1693-703.

366. Wilde B, Thewissen M, Damoiseaux J, et al. Regulatory B cells in ANCA-associated vasculitis. *Ann Rheum Dis* 2013;72(8):1416.

367. Holden NJ, Williams JM, Morgan MD, et al. ANCA-stimulated neutrophils release BLyS and promote B cell survival: a clinically relevant cellular process. *Ann Rheum Dis* 2011;70(12):2229-33.

368. Sanders JS, Huitma MG, Kallenberg CG, et al. Plasma levels of soluble interleukin 2 receptor, soluble CD30, interleukin 10 and B cell activator of the tumour necrosis factor family during follow-up in vasculitis associated with proteinase 3-antineutrophil cytoplasmic antibodies: associations with disease activity and relapse. *Ann Rheum Dis* 2006;65(11):1484-9.

369. Krumbholz M, Specks U, Wick M, et al. BAFF is elevated in serum of patients with Wegener's granulomatosis. *J Autoimmun* 2005;25(4):298-302.

370. Pollard RP, Abdulahad WH, Vissink A, et al. Serum levels of BAFF, but not APRIL, are increased after rituximab treatment in patients with primary Sjogren's syndrome: data from a placebo-controlled clinical trial. *Ann Rheum Dis* 2013;72(1):146-8.

371. Free ME, Bunch DO, McGregor JA, et al. Patients with antineutrophil cytoplasmic antibody-associated vasculitis have defective Treg cell function exacerbated by the presence of a suppression-resistant effector cell population. *Arthritis Rheum* 2013;65(7):1922-33.

372. Schmitt WH, Hagen EC, Neumann I, et al. Treatment of refractory Wegener's granulomatosis with antithymocyte globulin (ATG): an open study in 15 patients. *Kidney Int* 2004;65(4):1440-8.

373. Schonermarck U, Csernok E, Trabandt A, et al. Circulating cytokines and soluble CD23, CD26 and CD30 in ANCA-associated vasculitides. *Clinical and Experimental Rheumatology* 2000;18(4):457-63.

374. Ruth AJ, Kitching AR, Kwan RY, et al. Anti-neutrophil cytoplasmic antibodies and effector CD4+ cells play nonredundant roles in anti-myeloperoxidase crescentic glomerulonephritis. *J Am Soc Nephrol* 2006;17(7):1940-9.

375. Gan PY, Steinmetz OM, Tan DS, et al. Th17 cells promote autoimmune anti-myeloperoxidase glomerulonephritis. *J Am Soc Nephrol* 2010;21(6):925-31.

376. Hoshino A, Nagao T, Nagi-Miura N, et al. MPO-ANCA induces IL-17 production by activated neutrophils in vitro via classical complement pathway-dependent manner. *J Autoimmun* 2008;31(1):79-89.

377. Yates M, Watts RA, Bajema IM, et al. EULAR/ERA-EDTA recommendations for the management of ANCA-associated vasculitis. *Ann Rheum Dis* 2016;75(9):1583-94.
378. Little MA, Nightingale P, Verburgh CA, et al. Early mortality in systemic vasculitis: relative contribution of adverse events and active vasculitis. *Ann Rheum Dis* 2010;69(6):1036-43.
379. Xiao H, Ciavatta D, Aylor DL, et al. Genetically determined severity of anti-myeloperoxidase glomerulonephritis. *Am J Pathol* 2013;182(4):1219-26.
380. Gan PY, Holdsworth SR, Kitching AR, et al. Myeloperoxidase (MPO)-specific CD4+ T cells contribute to MPO-anti-neutrophil cytoplasmic antibody (ANCA) associated glomerulonephritis. *Cell Immunol* 2013;282(1):21-7.
381. Ooi JD, Gan PY, Odobasic D, et al. T cell mediated autoimmune glomerular disease in mice. *Curr Protoc Immunol* 2014;107:15.27.1-19.
382. Chang J, Eggenhuizen P, O'Sullivan KM, et al. CD8+ T Cells Effect Glomerular Injury in Experimental Anti-Myeloperoxidase GN. *J Am Soc Nephrol* 2017;28(1):47-55.
383. Ooi JD, Chang J, Hickey MJ, et al. The immunodominant myeloperoxidase T-cell epitope induces local cell-mediated injury in antimyeloperoxidase glomerulonephritis. *Proc Natl Acad Sci U S A* 2012;109(39):E2615-24.
384. Schreiber A, Xiao H, Falk RJ, et al. Bone marrow-derived cells are sufficient and necessary targets to mediate glomerulonephritis and vasculitis induced by anti-myeloperoxidase antibodies. *J Am Soc Nephrol* 2006;17(12):3355-64.
385. Schreiber A, Pham CT, Hu Y, et al. Neutrophil serine proteases promote IL-1beta generation and injury in necrotizing crescentic glomerulonephritis. *J Am Soc Nephrol* 2012;23(3):470-82.
386. Little MA, Smyth L, Salama AD, et al. Experimental autoimmune vasculitis: an animal model of anti-neutrophil cytoplasmic autoantibody-associated systemic vasculitis. *Am J Pathol* 2009;174(4):1212-20.
387. Little MA, Bhangal G, Smyth CL, et al. Therapeutic effect of anti-TNF-alpha antibodies in an experimental model of anti-neutrophil cytoplasm antibody-associated systemic vasculitis. *J Am Soc Nephrol* 2006;17(1):160-9.
388. Pfister H, Ollert M, Frohlich LF, et al. Antineutrophil cytoplasmic autoantibodies against the murine homolog of proteinase 3 (Wegener autoantigen) are pathogenic in vivo. *Blood* 2004;104(5):1411-8.
389. Little MA. L7. Animal models of PR3-ANCA vasculitis: approaches and controversies. *Presse Med* 2013;42(4 Pt 2):512-5.
390. van der Geld YM, Hellmark T, Selga D, et al. Rats and mice immunised with chimeric human/mouse proteinase 3 produce autoantibodies to mouse Pr3 and rat granulocytes. *Ann Rheum Dis* 2007;66(12):1679-82.
391. Primo VC, Marusic S, Franklin CC, et al. Anti-PR3 immune responses induce segmental and necrotizing glomerulonephritis. *Clin Exp Immunol* 2010;159(3):327-37.

392. Little MA, Al-Ani B, Ren S, et al. Anti-proteinase 3 anti-neutrophil cytoplasm autoantibodies recapitulate systemic vasculitis in mice with a humanized immune system. *PLOS ONE* 2012;7(1):e28626.

393. Langnaese K, John R, Schweizer H, et al. Selection of reference genes for quantitative real-time PCR in a rat asphyxial cardiac arrest model. *BMC Molecular Biology* 2008;9:53-53.

394. Chun J, Chung H, Wang X, et al. NLRP3 Localizes to the Tubular Epithelium in Human Kidney and Correlates With Outcome in IgA Nephropathy. *Scientific Reports* 2016;6:24667.

395. McAdoo SP, Reynolds J, Bhangal G, et al. Spleen Tyrosine Kinase Inhibition Attenuates Autoantibody Production and Reverses Experimental Autoimmune GN. *J Am Soc Nephrol* 2014;25(10):2291-302.

396. Rühl S, Broz P. Caspase-11 activates a canonical NLRP3 inflammasome by promoting K+ efflux. *European Journal of Immunology* 2015;45(10):2927-36.

397. Croxford AL, Lanzinger M, Hartmann FJ, et al. The Cytokine GM-CSF Drives the Inflammatory Signature of CCR2+ Monocytes and Licenses Autoimmunity. *Immunity* 2015;43(3):502-14.

398. Lan HY, Nikolic-Paterson DJ, Zarama M, et al. Suppression of experimental crescentic glomerulonephritis by the interleukin-1 receptor antagonist. *Kidney Int* 1993;43(2):479-85.

399. Ikezumi Y, Hurst LA, Masaki T, et al. Adoptive transfer studies demonstrate that macrophages can induce proteinuria and mesangial cell proliferation. *Kidney Int* 2003;63(1):83-95.

400. Holdsworth SR, Neale TJ, Wilson CB. Abrogation of macrophage-dependent injury in experimental glomerulonephritis in the rabbit. Use of an antimacrophage serum. *J Clin Invest* 1981;68(3):686-98.

401. Isome M, Fujinaka H, Adhikary LP, et al. Important role for macrophages in induction of crescentic anti-GBM glomerulonephritis in WKY rats. *Nephrol Dial Transplant* 2004;19(12):2997-3004.

402. Han Y, Ma FY, Tesch GH, et al. c-fms blockade reverses glomerular macrophage infiltration and halts development of crescentic anti-GBM glomerulonephritis in the rat. *Lab Invest* 2011;91(7):978-91.

403. Chalmers SA, Chitu V, Herlitz LC, et al. Macrophage depletion ameliorates nephritis induced by pathogenic antibodies. *J Autoimmun* 2015;57:42-52.

404. Wang JM, Griffin JD, Rambaldi A, et al. Induction of monocyte migration by recombinant macrophage colony-stimulating factor. *J Immunol* 1988;141(2):575-9.

405. Finsterbusch M, Hall P, Li A, et al. Patrolling monocytes promote intravascular neutrophil activation and glomerular injury in the acutely inflamed glomerulus. *Proc Natl Acad Sci U S A* 2016;113(35):E5172-81.

406. Pember SO, Barnes KC, Brandt SJ, et al. Density heterogeneity of neutrophilic polymorphonuclear leukocytes: gradient fractionation and relationship to chemotactic stimulation. *Blood* 1983;61(6):1105-15.

407. O'Brien EC, Abdulahad WH, Rutgers A, et al. Intermediate monocytes in ANCA vasculitis: increased surface expression of ANCA autoantigens and IL-1β secretion in response to anti-MPO antibodies. *Scientific Reports* 2015;5:11888.

408. den Dunnen J, Vogelpoel LT, Wypych T, et al. IgG opsonization of bacteria promotes Th17 responses via synergy between TLRs and FcgammaRIIa in human dendritic cells. *Blood* 2012;120(1):112-21.

409. Vogelpoel LT, Hansen IS, Rispens T, et al. Fc gamma receptor-TLR cross-talk elicits pro-inflammatory cytokine production by human M2 macrophages. *Nat Commun* 2014;5:5444.

410. Shin MS, Kang Y, Lee N, et al. Self dsDNA induces IL-1β production from human monocytes by activating NLRP3 inflammasome in the presence of anti-dsDNA antibodies. *J Immunol* 2013;190(4):1407-15.

411. Robson MG, Cook HT, Pusey CD, et al. Antibody-mediated glomerulonephritis in mice: the role of endotoxin, complement and genetic background. *Clin Exp Immunol* 2003;133(3):326-33.

412. Gartland A, Buckley KA, Hipskind RA, et al. Multinucleated osteoclast formation in vivo and in vitro by P2X7 receptor-deficient mice. *Crit Rev Eukaryot Gene Expr* 2003;13(2-4):243-53.

413. Grol MW, Panupinthu N, Korcok J, et al. Expression, signaling, and function of P2X7 receptors in bone. *Purinergic Signalling* 2009;5(2):205.

414. Bhattacharya A, Biber K. The microglial ATP-gated ion channel P2X7 as a CNS drug target. *Glia* 2016;64(10):1772-87.

415. Illes P, Khan TM, Rubini P. Neuronal P2X7 Receptors Revisited: Do They Really Exist? *The Journal of Neuroscience* 2017;37(30):7049.

416. Bhattacharya A. Recent Advances in CNS P2X7 Physiology and Pharmacology: Focus on Neuropsychiatric Disorders. *Frontiers in Pharmacology* 2018;9(30)

417. Ridker PM, Everett BM, Thuren T, et al. Antiinflammatory Therapy with Canakinumab for Atherosclerotic Disease. *New England Journal of Medicine* 2017;377(12):1119-31.

418. Baroni M, Pizzirani C, Pinotti M, et al. Stimulation of P2 (P2X7) receptors in human dendritic cells induces the release of tissue factor-bearing microparticles. *Faseb j* 2007;21(8):1926-33.

419. Furlan-Freguia C, Marchese P, Gruber A, et al. P2X7 receptor signaling contributes to tissue factor-dependent thrombosis in mice. *J Clin Invest* 2011;121(7):2932-44.

420. Stachon P, Heidenreich A, Merz J, et al. P2X7 Deficiency Blocks Lesional Inflammasome Activity and Ameliorates Atherosclerosis in Mice. *Circulation* 2017;135(25):2524-33.